Development of Peptidase-Resistant Peptide Substrates for Measurement of Protein Kinase B and Bcr-Abl Kinase Activity

Angela Proctor

A dissertation submitted to the faculty of the University of North Carolina at Chapel Hill in partial fulfillment of the requirements for the degree of Doctor of Philosophy in the Department of Chemistry.

Chapel Hill
2012

Approved by:

Nancy L. Allbritton

James W. Jorgenson

Royce W. Murray

David S. Lawrence

Kevin M. Weeks

ABSTRACT

ANGELA PROCTOR: Development of Peptidase-Resistant Peptide Substrates for Measurement of Protein Kinase B and Bcr-Abl Kinase Activity
(Under the direction of Nancy L. Allbritton)

Synthetic peptides are widely used by the biomedical research community as kinase substrates for purified kinases, in cell lysates, and sometimes in intact single cells. Peptides are relatively straightforward to construct, they have a long shelf-life, and they are easily derivatized with labels to facilitate detection. However, despite the benefits of peptides, they suffer from susceptibility to degradation by intracellular peptidases. Peptidolysis is often extremely rapid, yielding peptide fragmentation within minutes of introduction into a cell lysate or single cell. While protease inhibitors can be used to slow degradation, they do not entirely eliminate protease activity and they are difficult to use with intact cells. In order to render peptides more suitable as substrates in *in vivo* settings, proteolytic degradation needs to be dramatically slowed or halted.

The work described in this dissertation develops an iterative strategy to screen rationally designed peptides for their suitability as kinase substrates in cell lysates and single cells. Peptide bonds susceptible to peptidolysis were identified and stabilized by replacement of native residues with non-native residues, which are poor substrates for peptidases. Modified peptides were screened for substrate suitability as well as for resistance to degradation by peptidases. Substrates were designed for two kinases, protein kinase B and Bcr-Abl kinase, because of their roles in cancer. Protein kinase B is involved in regulation of

multiple cellular functions, including stress response and programmed cell death, and is upregulated in many cancers, including pancreatic, breast, and prostate tumors. Bcr-Abl is the primary driver of chronic myelogenous leukemia. This dissertation outlines the development of peptidase-resistant substrate reporters for these two kinases. Initial characterization and design was performed in cytosolic lysates. Once suitably designed peptide substrates were synthesized, they were incubated in single cells to characterize substrate metabolism and phosphorylation in the intracellular environment. Finally, protein kinase B activity was measured in single primary cells from a human pancreatic cancer xenograft. The design strategy presented in this dissertation should be applicable for future design of peptidase-resistant peptide substrates for alternative kinases.

This work is dedicated to my nephews,
Rigel Austin and Antonin Sirius.
May you always be curious about the universe around you.

And to those I lost along the way,
my uncle Larry R. Dipoma and my grandmother
Ruth Allred Dipoma. You are dearly missed.

Acknowledgements

There are so many individuals that I wish to thank for their assistance and encouragement throughout this process. This was not a task to be undertaken alone and I am grateful to those who accompanied me on my journey. I would like to thank my advisor, Dr. Nancy Allbritton, for her guidance throughout my graduate career. I appreciate the time and dedication you took to see me to the end. I also wish to thank past and present members of the Allbritton Lab, and specifically the CE team, for making each and every day in the lab enjoyable. Without you, I could not have thrived and accomplished what I have. Dr. Chris Sims, for your patience and assistance whenever something went wrong. Dr. Sumith Kottegoda, you welcomed me into the lab from the first day and you taught me the ropes of CE and how to be a good lab citizen. I appreciate your help and your constant smile, and I still miss having you around. Dr. Rahul Dhopeshwarkar, Dr. Wei Xu, Dr. Michelle Kovarik, Dr. David Detwiler, Jazz Dickinson, Pavak Shah, and Nicholas Dobes, thanks for everyday laughs, fun, and scientific discussions. It would not have been the same without you.

I also wish to thank my collaborators, Dr. David Lawrence, Dr. Qunzhao Wang, and Dr. Weichen Xu for your help and scientific collaboration. I believe we had a fruitful collaboration and I appreciate your knowledge about peptide synthesis. My woeful peptide synthesis skills would have never seen me through this project, so I am glad you were there! Weichen, I found in you not only a collaborator, but a friend, and I am honored to have been

a part of your life. I also appreciate my fellow students who started and took this journey with me, particularly Jordan Stobaugh for your friendship and Derek Wolfe for your sense of humor and your assistance with my computer programming for my single cell system.

Dr. Shan Yang, you are the reason that I made it this far. I miss you every day and cannot wait to see you again. China is such a very long way from North Carolina and I am not quite sure how I finished this off without you here. To my original pod, Abby Turner, Colleen Phillips, and Ryan Phillips: thank you. I have never laughed so much as when I was with you, nor have I ever eaten so much ice cream. It was with you three that I realized there is nothing so bad that a little ice cream cannot fix, nor is there anything too small that is not worth celebrating with a trip to Ben and Jerry's. I cannot thank you enough. Colleen, your friendship outside the lab has been something I cherish, as you help to bring me into the real world when I need it most. Laura Blue and Emily Oblath, thank you for being there with me every step of the way. From the ritualistic study sessions in our first semester to the regular lunches just to catch up, I have enjoyed your friendship. Thank you for listening to my complaints and triumphs over the years, I am grateful to have shared this journey with you both.

Dr. Mari Diaz, I cannot fully explain just how grateful I am to you. You joined my path when I thought I could go no further, and you showed me the way through while giving me the skills I needed to continue on. Your assistance and expertise has seen me through some of my darkest times. Thank you for listening.

I also need to thank those who started me on the path to graduate school and who continue to support me all these years later. Dr. Andy Lippert in the Chemistry Department at Weber State University, without you I do not know where I would be now. It is singularly

because of you that I chose to go to graduate school. You gave me the confidence that I could do this and you gave me the tools I needed to succeed. I appreciate your continued friendship and I will never forget that one conversation we had the last day of summer semester. That moment changed my life forever. To Dr. Stacy Palen in the Physics Department at Weber State University: you are amazing. You have been a wonderful example for me and I appreciate your advice and your friendship. You have given me an entirely new perspective to see from and I thank you for being my friend and mentor. Thank you for your support!! And to the others back home who are cheering from afar: Dr. Sue Harley, Dr. John Armstrong, Dr. Adam Johnston, Heather Jorgensen, Pam Tryon, and Dañelle Sundell, thanks for the friendship!

And last, but certainly not the least, I wish to thank my family. Your encouragement from thousands of miles away has kept me going every day. My mom and dad have never held me back from anything I wanted to do, and I am forever grateful for their unwavering support. I cherish every moment I get to spend with my parents, my brothers and sister-in-law, Aaron, Ron, and Amy Jo Proctor, and my nephews Rigel and Antonin. Thank you for supporting me from a distance through this incredibly challenging and rewarding phase of my education.

Table of Contents

List of Tables

List of Figures

List of Abbreviations and Symbols

A	alanine
Abl	Abelson tyrosine kinase
AGC	Protein Kinase A, G, or C sub-family
A/D	analog to digital
Akt	Protein kinase B
Ala	alanine
amol	attomole
Arg	arginine
Arg(Me2)	N-ω,ω-dimethyl-L-arginine (symmetrical)
ATP	adenosine triphosphate
B	band-broadening due to longitudinal diffusion
β-Ala	beta-alanine
β-Arg	beta-arginine
bcr	breakpoint cluster region
Bcr-Abl	Bcr-Abl fusion protein
BNC	Bayonet Neill-Concelman
BSA	bovine serum albumin
^{o}C	degrees Celcius
c-Abl	chromosomal Abl kinase
$CaCl_2$	calcium chloride
CE	capillary electrophoresis
CE-LIF	capillary electrophoresis with laser-induced fluorescence detection

CH_2Cl_2	dichloromethane
cm	centimeter
CML	chronic myelogenous leukemia
CMOS	complementary metal oxide silicon
CO_2	carbon dioxide
C-terminus	carboxy terminus
CyTOF	cytometry by time-of-flight
2D	two-dimensional
d	diameter
Da	Daltons
D/A	digital to analog
D-Ala	D-alanine
DAQ	data acquisition
DIC	diisopropylcarbodiimide
DIPEA	N,N-diisopropylethylamine
DMEM	Dulbecco's Modified Eagle Medium
DMF	dimethylformamide
DNA	deoxyribonucleic acid
DPh	D-phenylalanine
DTT	dithiothreitol
E	glutamic acid
E	applied electric field
ECB	extracellular buffer

EDTA	ethylene diamine tetraacetic acid
e.g.	for example
EO	electroosmotic
eq	equivalents
F	phenylalanine
FAM	carboxyfluorescein
FBS	fetal bovine serum
Fmoc	9-fluorenylmethoxycarbonyl
FRET	Förster resonance energy transfer
G	glycine
g	acceleration due to gravity
H	theoretical plate height
h	hours
h	height
HCl	hydrochloric acid
HCTU	2-(6-chloro-1*H*-benzotriazole-1-yl)-1,1,3,3-tetramethylaminium hexafluorophosphate
He/Ne	Helium/Neon laser
HEPES	4-(2-Hydroxyethyl)piperazine-1-ethanesulfonic acid
HF	hydrofluoric acid
H_2O	water
HOBt	N-hydroxybenzotriazole
HPLC	high performance liquid chromatography

HPLC-MS	high performance liquid chromatography coupled with mass spectrometric detection
hPa	hectopascals
HV	high voltage
Hz	Hertz
I	isoleucine
ID	inner diameter
IMAP	immobilized metal ion affinity-based fluorescence polarization
IMDM	Iscove's Modified Dulbecco's Medium
K	lysine
KCl	potassium chloride
kDa	kiloDalton
kHz	kilohertz
KH_2PO_4	potassium phosphate
k_{cat}	turnover number
K_M	Michaelis-Menten constant
kV	kilovolt
L	length
LIF	laser-induced fluorescence
LOD	limit of detection
μ	electrophoretic mobility
μA	microamps
μ_{eo}	electroosmotic mobility

μ_{ep}	electrophoretic mobility
μg	microgram
μJ	microJoules
μL	microliter
μM	micromolar
μm	micrometers
M	molar
M	mass
m	meter
MAP	mitogen activated protein
MeAla	N-methyl alanine
MeArg	N-methyl arginine
MEM	Minimal Essential Medium
MePh	N-methyl phenylalanine
MePhe	N-methyl phenylalanine
mg	milligram
$MgCl_2$	magnesium chloride
min	minutes
mL	milliliter
MLCK	myosin light chain kinase
mM	millimolar
mm	millimeters
$MnCl_2$	manganese chloride

MOPS	3-(N-morpholino)propane sulfonic acid
MPh	N-methylphenylalanine
MePh	N-methylphenylalanine
mRNA	messenger ribonucleic acid
MS	mass spectrometry
ms	millisecond
MSNT	1-(mesitylene-2-sulfonyl)-3-nitro-1,2,4-triazole
mTOR	mammalian target of rapamycin
mTORC2	mammalian target of rapamycin complex 2
mW	milliwatt
η	viscosity
NA	numerical aperture
NaCl	sodium chloride
NaH_2PO_4	sodium phosphate
Nal	β-(2-Napthyl)-L-alanine
NaOH	sodium hydroxide
Nd:YAG	neodymium-doped yttrium aluminum garnet
nL	nanoliter
nM	nanomolar
nm	nanometer
NMP	N-methyl-2-pyrrolidone
NRTK	non-receptor tyrosine kinase
N-terminus	amino terminus

O	ornithine
OD	outer diameter
π	pi
^{32}P	radioactive isotope of phosphorus
P	proline
PBS	phosphate buffered saline
PDA	pancreatic ductal adenocarcinoma
PDK-1	phosphoinositide-dependent kinase-1
PDMS	poly(dimethyl)siloxane
PEG	poly-ethylene glycol
PH	pleckstrin homology domain
Phe	phenylalanine
Phe(F5)	pentafluorophenylalanine
PHLPP	PH-domain leucine-rich repeat protein phosphatase
PI3-K	phosphoinositide 3-kinase
PIP_2	phosphatidylinositol 4,5-bisphosphate
PIP_3	phosphatidylinositol 3,4,5-trisphosphate
PKB	protein kinase B
pg	picogram
pL	picoliter
pM	picomolar
pm	picometer
PMT	photomultiplier tube

Pro	proline
psi	pounds per square inch
PTEN	phosphatase and tensin homolog
PyBrop	bromo-tris-pyrrolidino phosphonium hexafluorophosphate
q	particle charge
ρ	density
R	arginine
R	resistance
r	Stoke's radius
RFU	relative fluorescence units
RNA	ribonucleic acid
RPMI	Roswell Park Memorial Institute
RTK	receptor tyrosine kinase
s	seconds
Sarc	sarcosine, N-methylglycine
SDS	sodium dodecyl sulfate
Ser	serine
Ser473	serine residue in position 473
SH2	Src homology 2 domain
SH3	Src homology 3 domain
S/N	signal to noise
SPA	scintillation proximity assay
SPPS	solid phase peptide synthesis

Src	sarcoma kinase
STI-571	Imatinib mesylate, Gleevec
T	threonine
t	time
$t_{1/2}$	half-life
$t_{50\% P}$	time to 50% phosphorylation
TFA	trifluoroacetic acid
Thr	threonine
Thr308	threonine residue in position 308
TIS	triisopropyl silane
TK	tyrosine kinase
Tris-HCl	trizma hydrochoride
Tyr(3-NO_2)	3-nitrotyrosine
u	linear velocity
UV	ultraviolet
V	volts
V	partial specific volume
v	velocity
W	tryptophan
X	times
Y	tyrosine
zmol	zeptomole

CHAPTER 1

INTRODUCTION

1.1 Kinase Pathways and Implications in Cancer

1.1.1 Kinases and Kinase Functions

Nearly all proteins undergo post-translational modification after synthesis. These modifications can be irreversible, such as proteolysis of peptide bonds in the degradation and reprocessing of substrates, or reversible, such as acylation or glycosylation used to modify protein properties.[1] One common form of reversible modification is phosphorylation by a kinase. A protein kinase catalyzes the transfer of the terminal phosphoryl group from adenosine triphosphate (ATP) to a serine, threonine, or tyrosine residue on a substrate. This reversible modification is often used as a switching mechanism to activate and deactivate proteins. Phosphorylation of a target protein alters its properties by addition of the negatively charged phosphoryl group. Addition of this phosphoryl group changes the local charge properties of the protein and can also induce a conformational change in the protein. Either of these properties alone or together can cause a protein to alter its activity and function. For example, phosphorylation of proteins can control a protein's location within the cell, its enzymatic activity, and any interactions with other proteins.[1] Removal of the phosphoryl group is catalyzed by a phosphatase, which reverts the protein back to its non-phosphorylated form. The balance of kinase and phosphatase activity within a cell regulates

many of the signal transduction pathways leading to growth, metabolism, transcription differentiation, behavior, and apoptosis.[1, 2] Kinases themselves are often regulated by phosphorylation and dephosphorylation.

There are over 500 known kinases in the human genome which have been grouped into eight different families based on their structure and function.[2] For example, the tyrosine kinase (TK) family of the human genome contains all of the receptor tyrosine kinases (RTKs) responsible for signal transduction from the extracellular environment to the cytoplasm of cells.[3] RTKs on the surface of cell membranes bind to ligands, resulting in propagation of signal transduction within the cell. Included in tasks accomplished by RTKs are roles in regulation of cell proliferation or differentiation, vital processes for organism growth and function.[3] The TK family also contains multiple non-receptor tyrosine kinases (NRTKs), critical members of signaling cascades within a cell. Among other tasks, the NRTKs are involved in glucose uptake and metabolism, as well as in regulation of the immune system. Another family in the human kinome is the AGC family (related to protein kinases A, G, and C), which contains approximately 60 kinases responsible for a variety of functions including, but not limited to, proliferation, metabolism, protein synthesis, cell shape, and motility.[4] As kinases are involved in modulation of multiple signal transduction pathways, dysregulation of TK, AGC or other family kinase activity is implicated in many diseases, including multiple cancers.[2-5] It is for this reason that kinases are prime targets for therapeutic modification, notably as chemotherapeutic targets leading toward individualized treatment.[5, 6] While multiple kinases are implicated in many different types of cancers, the work presented in this dissertation focuses on two kinases, protein kinase B and Abl kinase, each discussed in detail in the following sections.

1.1.2 Protein Kinase B

Protein kinase B (PKB, also known as Akt) has been implicated in many cellular functions such as insulin signaling, glucose metabolism, transcription, proliferation, stress response, and apoptosis.[7] PKB was first described in 1977 by Staal *et al.* in their work with a murine leukemia virus found to be linked to lymphoma formation.[8] It was not until 1991 that the genes encoding PKB were found, when three independent research groups published results regarding PKB.[9-11] Interest in PKB has steadily increased as it has been implicated in assisting cellular survival during stressful events, such as prevention of apoptosis in cells programmed for cell death.[12] Increased PKB activity has been found to enhance tumor progression and is present in multiple cancers, including pancreatic, breast and prostate tumors.[13, 14] Many reasons exist for high PKB activity and any of these can lead to tumor survival and progression: i) PKB can be constitutively activated;[15] ii) normal PKB can be over-expressed;[12, 16] or iii) regulatory feedback control of PKB can be impaired.[8, 17] While increased PKB activity may not be directly responsible for producing tumors, there is abundant evidence that increased PKB activity does enable tumors to survive and proliferate, making PKB an attractive candidate for targeted therapy.[13, 18, 19]

PKB is a serine/threonine kinase and a member of the AGC family of kinases.[2] There are three isoforms of PKB, termed PKBα, PKBβ, and PKBγ, each responsible for different functions within cells. All three isoforms are approximately 80% homologous and share similarities in three highly conserved functional domains (Figure 1.1). These domains are: i) a pleckstrin homology (PH) domain found on the N-terminus which is a region of approximately 100 amino acids that interacts with lipids, including the plasma membrane; ii) a central kinase domain, containing the catalytic active site where substrates are

phosphorylated; and iii) a C-terminal regulatory domain containing one of the phosphorylation sites for PKB regulation.[7, 14, 15, 17, 20]

PKB activity is controlled by phosphorylation on two residues, Thr308, located in the kinase domain, and Ser473, found in the regulatory domain. Phosphorylation of both residues leads to maximum PKB activity, while phosphorylation solely at Thr308 has been shown to decrease PKB activity to approximately 10% of maximum.[14, 17] When a cell is stimulated, PKB is recruited to the plasma membrane by PIP_3 (phosphatidylinositol-3,4,5-trisphosphate). The PH domain acts to localize PKB to the membrane, where Thr308 is phosphorylated by the membrane protein PDK-1. At this stage, uncertainty exists as to how the Ser473 residue is phosphorylated, with some evidence suggesting phosphorylation by mTORC2 and others implicating autophosphorylation by PKB itself or attributing it to members of the PI3-K kinase family.[16, 17] After dual phosphorylation, PKB detaches from the membrane and moves to the cytosol or the nucleus to phosphorylate its substrates (Figure 1.2). PKB is no longer actively phosphorylated by PDK-1 when PTEN (phosphatase and tensin homolog) dephosphorylates the lipid messenger PIP_3, leading to a decrease in the association of PKB to the membrane and a decrease in additional PKB activation[8, 17, 21] and PKB activity is effectively halted when the Ser473 residue is dephosphorylated by PHLPP1 or 2 (PH-domain leucine-rich repeat protein phosphatase).[13, 17, 21] Aberrant activity at any of these regulatory steps can be responsible for abnormal PKB signaling and can lead to tumor survival and proliferation, reiterating the possibility of targeting PKB for therapeutic drug design. Chapters 4 and 5 of this dissertation focus on measurements of PKB activity in single tissue cultured cell lines and in single cells obtained from mouse xenograft models.

1.1.3 Abelson Tyrosine Kinase

Abelson tyrosine kinase (Abl) is a member of the TK family of kinases as a non-receptor kinase and is normally encoded by a gene found on chromosome 9. Abl can be found in many locations within the cell and is known to be involved in many cellular processes such as cell migration, DNA damage responses, and even regulation of growth and survival.[22] Abl contains the same three core domains as other Src-family kinases—an SH3, SH2 and kinase domain (Figure 1.3).[22, 23] Normal chromosomal Abl (c-Abl) contains a region upstream of the SH3 domain that is myristoylated and is responsible for regulation of the kinase. c-Abl is tightly regulated both temporally and spatially by auto-inhibition involving this myristate tail, the SH2-SH3 connector and the SH2-kinase domain linker.[22-24]

In the early 1960s, it was discovered that many chronic myelogenous leukemia (CML) patients had a shortened version of chromosome 22 (termed the Philadelphia chromosome), but it was not until the 1970s that it was discovered that this was the result of a reciprocal translocation between chromosomes 9 and 22.[25, 26] Chromosome 9 is disrupted within the abl gene and chromosome 22 below the breakpoint cluster region (bcr) gene during the translocation event. This fuses the bcr gene to abl and encodes for synthesis of a fusion protein known as Bcr-Abl (Figure 1.4).[26, 27] Bcr-Abl does not have the autoinhibition of c-Abl and has been discovered to be the primary driver of formation of leukemic cells in greater than 90% of all CML patients.[26, 27] Because of its primary role in the formation of leukemic cells, Bcr-Abl was targeted for specific inhibitor design and became the first kinase for which targeted therapy was approved for patient use. Gleevec, marketed by Novartis, is also known as imatinib mesylate or STI-571. Gleevec was developed in the mid-1990s and approved for use in CML therapy in the early 2000s.[28] Gleevec is a small molecule inhibitor

that competes with ATP for the binding pocket in the catalytic domain of Bcr-Abl[29, 30] and prevents Bcr-Abl from phosphorylating its substrates. Treatment with Gleevec has proven useful for many CML patients, notably those still in the chronic phase of the disease.[31] The success of Gleevec has led to the development of 2nd and 3rd generation inhibitors of Bcr-Abl as well as investigation and development of alternative drug therapies aimed specifically at targeting aberrant kinase activity.

As successful as Gleevec treatment has been for treatment of chronic phase CML, it has not worked for all patients, especially those in advanced or blast-stage CML.[32-34] There is also a sub-population of CML patients that do not have the Philadelphia chromosome, so drugs targeting Bcr-Abl are useless as these patients do not express Bcr-Abl.[26] Direct measurement of Bcr-Abl kinase activity would allow for quantification of Bcr-Abl activity and investigation of the likely response and sensitivity to Gleevec or to its 2nd and 3rd generation relatives. Chapters 3 and 6 of this dissertation discuss development of a peptide substrate reporter for Bcr-Abl kinase activity.

1.2 Use of Peptides in Biomedical Research

Synthetic peptides are widely used in the biomedical research community as substrates for kinase activity. Peptides are easily synthesized via solid phase peptide synthesis (SPPS) and large libraries of peptides composed of native and non-native amino acids are straightforward to construct, allowing for relatively simple synthesis of a wide variety of substrates.[35] Peptides possess a long shelf-life and are easily derivatized with labels (such as fluorophores) or targeting elements (such as biotin). Based on these traits, peptides are often preferred over proteins in a variety of assays such as determining enzyme

activity *in vitro*, in cell lysates, or *in vivo*. In addition, peptides can be constructed to contain only the select kinase's consensus sequence, the short region of a handful of amino acids around the phosphoryl-accepting residue recognized by a specific kinase or kinase family. Sometimes, these short peptide regions can mimic a full-length substrate protein and large libraries of consensus sequences have been determined for many kinases and the preferred sequences are readily available for nearly all known kinases.[20, 36-38] For these reasons many peptides are available commercially for use as substrates to measure kinase activity.

1.2.1 Peptides as Substrates

1.2.1.1 Techniques for Measuring Peptide Phosphorylation

Peptides are frequently utilized by commercial companies and research laboratories to quantify kinase activity of purified kinases. These formats are relatively inexpensive ways to quickly assess kinase activity and specificity. Select methods frequently utilized to measure phosphorylation of a peptide substrate by a kinase are discussed below. Transfer of a radioactive phosphoryl group from [^{32}P]-γ-ATP to the substrate can be quantitatively determined by capturing the radioactive substrates on a negatively charged phosphocellulose membrane and measuring radioactivity.[35, 39] An alternative radioactive technique is a homogenous scintillation proximity assay (SPA) that measures incorporation of the radioactive phosphoryl group on a substrate. When the radiolabeled substrate binds to the SPA bead, the emitted radiation activates the scintillant, which produces light that can be measured with a scintillation counter.[40, 41] However, due to the cost of disposal of radioactive materials and concern over radioactive exposure in the laboratory, use of these methods have decreased as more non-radiometric techniques are developed.[39, 42] One non-radiometric assay utilized to monitor phosphorylation is Förster resonance energy transfer

(FRET).[42] For example, a substrate constructed with a donor and acceptor fluorophore emits no fluorescence when the target amino acid is not phosphorylated as the conformation of the substrate separates the two fluorophores from one another. A conformational change is induced upon phosphorylation, usually when a phosphoryl-recognition sequence binds to the phosphoryl-group, arranging the fluorophores in close proximity to one another. When the proper wavelength of light illuminates the substrate, FRET occurs as the donor fluorophore emits in the acceptor fluorophore excitation region. The emission of the acceptor fluorophore is measured over time and utilized to quantify phosphorylation. Additional techniques to measure phosphorylation include immobilization of biotin-labeled substrate peptides on a streptavidin-coated surface, where phosphorylation is detected via radioactivity, colorimetric changes, or fluorescence of a labeled antiphosphoserine, -threonine, or -tyrosine antibody.[43-45] Enzyme activity is inferred based on the amount of phosphorylated substrate relative to non-phosphorylated substrate. An alternative technique to monitor substrate phosphorylation measures fluorescence polarization in the presence of an appropriate antiphospho antibody or a metal nanoparticle.[46, 47] Fluorescence polarization is high when the phosphorylated substrate is bound by the relatively large antibody or nanoparticle because the bulky addition prevents free rotation of the molecule, resulting in highly polarized emitted light. This fluorescence polarization change upon substrate phosphorylation permits quantification of enzyme activity. Additionally, capillary electrophoresis can be used to monitor substrate phosphorylation over time, as the addition of the double negatively-charged phosphoryl group results in altered electrophoretic mobility between the substrate and its phosphorylated counterpart, allowing for separation and quantification of reactant and product.[48-51] This method can use UV or absorbance detection,

but most often utilizes fluorescence detection of fluorescently-labeled substrates because of the exquisite sensitivity offered by laser-induced fluorescence detection. These techniques, as well as others not mentioned, can all be used to measure kinase activity of purified kinases, for example, to determine substrate suitability or as validation of new technology to measure enzyme activity.[50, 52, 53]

1.2.1.2 Peptide Substrates in Cell Lysates

In addition to their usefulness in monitoring activity of purified kinases, peptides are also utilized *in vitro* to monitor kinase activity in a cytosolic lysate. Cytosolic lysates provide an environment in which many of the cofactors and regulatory elements are present, though minimally regulated, allowing for a simulation of kinase behavior in these environments. Cytosolic lysates are also attractive because they are less expensive to use than intact cells for many reasons. Lysates are generated via a freeze-thaw cycle or by adding a lysis buffer, neither of which require specialized or costly materials. Many different measurement techniques can be utilized to accommodate assays performed in a cytosolic lysate, eliminating the need for purchase or construction of specialized detection instruments. Cytosolic lysates are easy to prepare in large volumes and can be modified to match nearly any detection strategy. Lysates are easily amenable to addition of co-factors or inhibitors to monitor enzyme reaction to changes and the substrate can be directly mixed with the lysate *in vitro*. A search of the literature yields multiple examples of peptides utilized as substrates of kinases in cell lysates.[54-64]

1.2.1.3 Peptide Substrates in Intact Cells

While cell lysates are a straightforward and cost-effective way to measure kinase activity in a simulated cellular environment, they do not entirely mimic the environment

within an intact cell. Intracellular compartments exist within intact cells, which keeps cell components isolated from other components and localized to certain areas. When a lysate is generated, these subcellular compartments are ruptured, eliminating this separation and localization. Additionally, intracellular compartments also facilitate formation of local regions of high concentration of a specific analyte, also eliminated when the lysate is generated and diluted into a homogenous mixture.

However, despite the cost advantages of lysates over single cells, lysates cannot recapitulate the native environment of an intact cell and lysates eliminate the ability to detect heterogeneity within a cell population. To gain an understanding into protein behavior within a population of cells, peptides are also being increasingly used in single cells as substrates to measure protein activity at the single cell level, such as that of kinases, acyl transferases, and proteases.[49, 51, 65-67] In these examples, peptide substrates were introduced into tissue-cultured cell lines via endocytosis,[66] electroporation,[65] or microinjection[49, 51, 67] and measurements were made utilizing laser-induced fluorescence detection after capillary electrophoresis on custom-designed systems mounted on a microscope stage. These substrate loading and measurement strategies are also amenable for use with primary cells, an exciting new frontier for studying protein activity in a population of diseased and healthy cells.

1.2.2 Peptide Susceptibility to Degradation

Despite all of the advantages listed above and the widespread use of peptides as substrates both *in vitro* and *in vivo*, peptides suffer from a susceptibility to degradation by intracellular proteases and peptidases. Cleavage of peptide bonds by endo- and exo-peptidases can be extremely rapid as they are integral in the protein-recycling machinery of

cells, responsible for breaking proteins and peptides into their constituent amino acids.[68] While not a problem for use with purified kinases, this is a major concern when peptides are utilized in cell lysates or intact cells because of the prevalence of peptidases. Peptidolysis can be extremely rapid, yielding peptide fragmentation within minutes of introduction into a lysate or single cell.[51, 69, 70] This is true for peptide substrates and inhibitors and low bioavailability due to peptide hydrolysis is a major disadvantage for peptide-based therapeutics.[71-75]

While protease inhibitors can be used to slow degradation, several drawbacks exist to using these inhibitors. Protease inhibitors do not entirely eliminate protease activity, they are often poorly soluble in aqueous solutions, rendering them available only in organic solvents not compatible with enzymes. Most inhibitors cannot be used with intact cells since they are not membrane permeable. Once a peptide is cleaved, it is generally no longer an effective substrate for the desired kinase as it does not possess all of the elements required for kinase recognition. In order for peptides to become more useful in biomedical research, proteolytic degradation needs to be dramatically slowed or eliminated. Strategies for achieving proteolytic stability are discussed in the following sections.

1.2.3 Strategies to Stabilize Peptides Against Degradation

1.2.3.1 Cyclization

Two strategies that exist for cyclizing peptides are head-to-tail cyclization or cyclization via the amide backbone.[76] Cyclization affords excellent resistance to degradation by creating a fixed secondary structure that prevents protease access to the peptide bonds.[76-79] However, it simultaneously prevents access to the substrate binding region of the protein and diminishes substrate efficacy.[78] Peptide cyclization can be somewhat varied in the size of the

rings used and in the methods utilized for cyclization, offering a range of useful strategies for prolonging peptide lifetime. However, cyclization methods are very challenging synthetically, requiring excessive amounts of time and resources for a very low yield of substrate. While cyclization is a valid strategy for stabilization of peptides, it does not lend itself to rapid synthesis and screening of possible substrates because of its synthetic challenges, expense, and reduction of substrate efficacy.

1.2.3.2 PEGylation

Addition of a poly-ethylene glyocol moiety (PEGylation) has also been demonstrated to reduce proteolytic activity on peptides.[80-82] PEGylation is relatively straightforward to accomplish and is easily incorporated into regular SPPS methods. PEG groups of various sizes (with molecular weights ranging from 1 – 30 kDa) can be added to peptides, thus altering their properties depending on the PEG group added. Lower molecular weight PEGylated substrate peptides tend to have better substrate activity than higher molecular weight substrates, yet also demonstrate a diminished resistance to degradation when compared to their higher-molecular weight counterparts.[81] While PEGylation of peptides allows them to resist degradation, problems exist due to the size and polydispersity of PEG groups. The molecular weights of most PEG groups are dramatically larger than the substrate peptides, rendering the mass difference between substrate and its phosphorylated counterpart much less and making electrophoretic separations difficult to achieve. Additionally, PEG moieties exist in a polydispersity unacceptable for most capillary electrophoretic applications as the band broadening significantly diminishes the peak capacity generally afforded by capillary electrophoresis.

1.2.3.3 Terminal Modifications

Modifications to either or both the C- and N-terminus have also been shown to impart some stability to peptides.[80, 83, 84] These modifications are varied and include lipid conjugations, acetylation of the N-terminus and amidation of the C-terminus. All of these modifications are easily accomplished via standard SPPS techniques. Lipid conjugation of peptides serves the added benefit of making the reporter more lipophilic, allowing it to become more cell permeable while also increasing loading efficiency into cells. Terminal modifications provide added protection against carboxy- and amino-peptidases, but do not stabilize the peptide against endo-peptidase degradation. For this reason, terminal modifications are often used in combination with one or more alternative stabilization strategies.

1.2.3.4 Non-Native Amino Acids

A strategy frequently utilized in peptide substrate and inhibitor design for promotion of peptide stability is utilization of non-native amino acids within the peptide. These can include D-amino acids, where the stereochemistry of the α-carbon is mirror image to the natural L-amino acids;[85] N-methylated amino acids, where a methyl group is added to the backbone nitrogen;[86] β- or γ-amino acids, where the backbone nitrogen is on the β- or γ-carbon as opposed to the α-carbon;[87] or a modification of any sort to the side chain.[35] Many non-native amino acids are available and ready for synthesis using standard SPPS techniques, making their incorporation into a peptide straightforward. There are multiple examples of use of peptides constructed with non-native amino acids in the literature.[35, 51, 77, 85, 86, 88, 89] An added benefit is that these peptides can be degradation resistant while simultaneously retaining efficacy as kinase substrates. Based on this property and their ease in incorporation

in peptide synthesis, this is the strategy utilized to stabilize reporters chosen for the work described in this dissertation. A more thorough discussion of how this was accomplished is presented in Chapters 3 through 6 of this work.

1.3 Capillary Electrophoresis

Capillary electrophoresis (CE) was first described in the early 1980s by Jorgenson and Lukacs.[90] CE is a separation method utilizing small inner-diameter fused silica capillaries (on the order of 50 μm) filled with and immersed in a current-carrying buffer solution. Sample is introduced at the inlet and a high voltage (typically up to 30 kV) is applied across the capillary. A detector near the capillary outlet monitors the species as they move toward the column exit (Figure 1.5). The velocity and direction of electrophoretic migration is a property of the size, shape, and charge of the species. Overall migration is determined by a combination of the electrophoretic mobility of the analytes and the electroosmotic flow of the buffer. For a rigid sphere, electrophoretic mobility can be approximated as shown in equations 1.1 and 1.2 and velocity of a species in CE is defined in equation 1.3.[90, 91]

Equation 1.1:

$$\mu = \frac{q}{6\pi\eta r}$$

μ = electrophoretic mobility

q = particle charge

η = buffer viscosity

r = Stoke's radius (Eq 1.2)

Equation 1.2:

$$M = \frac{4\pi r^3 V}{3}$$

M = mass

r = Stoke's radius

V = partial specific volume

Equation 1.3:

$$v = (\mu_{ep} + \mu_{eo})E$$

v = velocity

μ_{ep} = electrophoretic mobility

μ_{eo} = electroosmotic mobility

E = applied electric field

Electroosmotic flow within a narrow bore capillary arises when an electric field is applied across the ends of a capillary with a charged inner surface. The amount of charge on the inner surface of the fused silica capillary varies depending on the capillary surface properties and the buffer utilized. For example, a neutral or basic buffer results in a higher negative charge on the capillary surface, causing a large proportion of the positively-charged ions in the buffer to remain at the capillary surface. This causes an electric double layer to form at the interface of the capillary surface with the buffer. When a voltage is applied across the capillary, the charged ions in the electric double layer migrate toward the opposite pole. These ions are associated with other buffer components via hydrogen bonds and electrostatic interactions. These interactions are strong enough within the narrow bore

capillary that bulk migration of all buffer contents occurs in one direction, as the double layer ions migrating in the electric field pull their associated components with them. This results in a nearly flat fluid profile as all capillary components migrate to one end of the capillary.[90, 92] This flow, termed electroosmotic flow (EO flow) can be quite significant and it is utilized in CE to sweep all species toward the detector (Figure 1.6). Electrophoresis separates the analytes into discrete bands based on electrophoretic mobility and EO flow sweeps all bands toward the detector, allowing for detection of all species, including those of opposite charges as well as neutral species.

In this dissertation, CE was used for the separation of phosphorylated and non-phosphorylated peptides as well as peptide fragments. Phosphorylation of a peptide sequence yields an addition of a relatively small amount of mass and two negative charges, altering the electrophoretic mobility of the peptide and causing it to migrate differently than its non-phosphorylated counterpart. A comparison of the integrated peak areas under the peaks corresponding to non-phosphorylated substrate and its phosphorylated counterpart can be used to measure phosphorylation over time and allow for an inference of kinase activity.[49, 67, 93, 94] Also, when a peptide undergoes proteolysis, the differences in electrophoretic mobility of each fragment can be exploited, allowing for separation of all possible fragments. The high resolving power of CE permits separation and quantification of peptide fragments differing by a single amino acid, with the area under each fragment peak correlating to the concentration of the peptide fragment in solution.[51] Coupling of CE with ultrasensitive laser-induced fluorescence detection (LIF) allows for work at extremely low peptide concentrations, as mass detection limits are routinely in the range of 10^{-20} moles.[95, 96] Other benefits of CE include the high resolution due to minimal band broadening, fast separations,

small sample volumes (less than 10 nL) and ease of automation, all amenable to work with single cells. Chapter 2 provides a more thorough description of the custom made CE system utilized in this work.

1.4 Chemical Cytometry

Classic cytometry refers to instrumental methods utilized in the characterization of individual cells, such as image and flow cytometry.[97] These techniques are often nondestructive and can process large numbers of cells in relatively short periods of time to provide a wealth of information about cell populations. Both image and flow cytometry rely on fluorescence detection and can simultaneously monitor multiple parameters. However, spectral overlap of fluorescence markers is an important limitation of classic cytometry techniques, as it limits the number of parameters that can be monitored simultaneously. As opposed to classical cytometry, the use of highly sensitive analytical tools to characterize single cells has been given the name "chemical cytometry." The infancy of chemical cytometry was initiated with a 1953 study that used a copper silk thread to isolate and quantify RNA levels in single cells. More modern chemical cytometry techniques emerged from the Jorgenson, Ewing, and Yeung labs in the 1980s.[98, 99] Some current chemical cytometry measurement techniques include capillary electrophoresis, mass spectrometry and electrochemistry.[99-101] Chemical cytometry techniques are usually low throughput and destructive, as the cell is often lysed prior to analysis. However, an abundance of information on the cell contents can be obtained for each cell analyzed. Chemical cytometry provides the analytical techniques sensitive enough to measure heterogeneity within cellular populations, including differences that arise from mutations at the nucleic acid level all the

way to those originating from post-translational modifications of proteins in a signaling pathway.[97, 99, 101-104]

Population averages measured when thousands or millions of cells are pooled masks the heterogeneity that no doubt exists and can give a skewed version of the events. For example, cell signaling within a population was often thought of as being a graded response, in that all cells partially responded to a stimulus. However, it was determined that cells actually can respond in an all-or-none fashion, such that only part of the population responds fully to the signal while other cells do not respond at all.[105, 106] This is also true when seeking to identify rare subsets within a population, such as what is found in a tumor. Tumors are heterogenous, with only a small portion of cells that may be abnormal.[104, 107, 108] A population average would not reveal the aberrant cells, whereas interrogation of each cell would indicate how many cells were functioning as expected and how many were not. Single cell analysis is the ultimate goal for the work developed in this dissertation as a means for identification of abnormal kinase signaling in single cells, with the future intent of probing primary cells from a patient to determine kinase activity.

1.5 Scope of the Dissertation

The work described in this dissertation focuses on designing peptidase-resistant peptide substrate reporters for probing kinase activity in single cells. Chapter 2 presents a detailed description of the design and construction of a CE instrument capable of analyzing single cells. In addition to hardware construction, the software program was written specifically for this new system design and is also outlined in Chapter 2. Chapters 3 and 4 focus on the first cycle of rational design and development of peptide substrate reporters

resistant to degradation by intracellular peptidases. Both chapters outline the strategy of identifying specific locations in the reporter most susceptible to degradation, the iterative redesign and testing of successive substrates, and the analysis of the reporters in single cells. Chapter 3 describes the first cycle in development of a reporter for Bcr-Abl kinase and has been published in the *Analyst*.[51] Chapter 4 details the strategy for design and construction of a reporter for PKB and a manuscript has been submitted to *Analytical Chemistry* on this work. Chapter 5 extends upon the work presented in Chapter 4 by utilizing the designed substrate to measure PKB activity in pancreatic cancer cell lines with and without kinase inhibitor and to measure PKB activity in single cells obtained from human pancreatic tumor xenografts grown in mice. This work is being prepared for manuscript submission in the near future. Chapter 6 presents preliminary work accomplished on further development of a Bcr-Abl kinase substrate based on the work presented in Chapter 3.

1.6 Figures

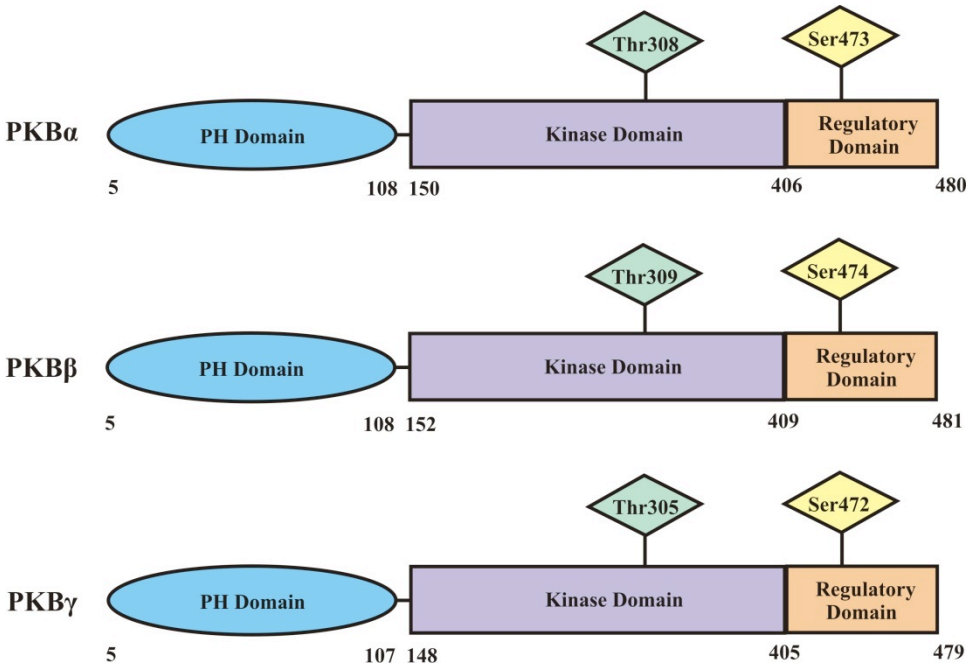

Figure 1.1: The domains of the three isoforms of PKB. Phosphorylation of the Thr and Ser residues leads to maximum activity of PKB.[14, 16]

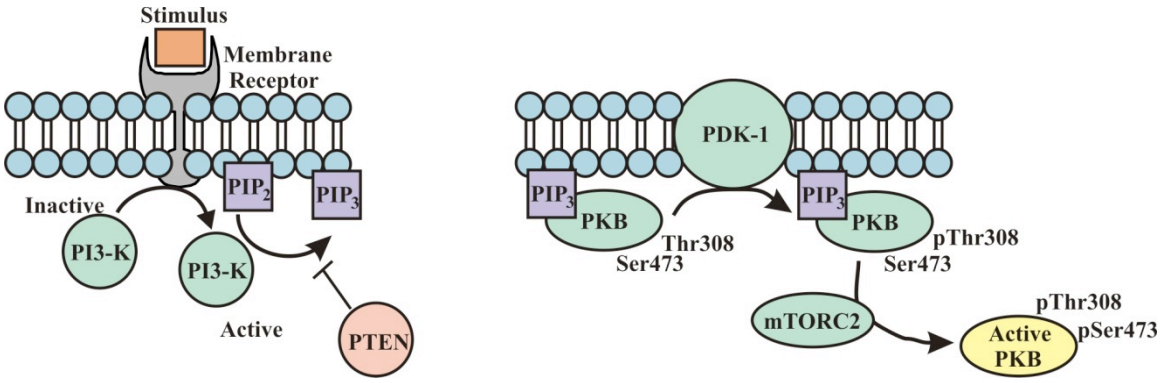

Figure 1.2: A simplified schematic of PKB activation. A stimulus (such as growth factor or insulin) activates a transmembrane receptor which activates PI3-K. PI3-K phosphorylates PIP_2 to PIP_3, which recruits inactive PKB to the membrane. At the membrane, Thr308 is phosphorylated by PDK-1, followed by phosphorylation of Ser473 (shown here by mTORC2). Once both residues are phosphorylated, active PKB moves to the cytosol or nucleus to regulate downstream effectors.[16, 17, 19, 21, 109, 110]

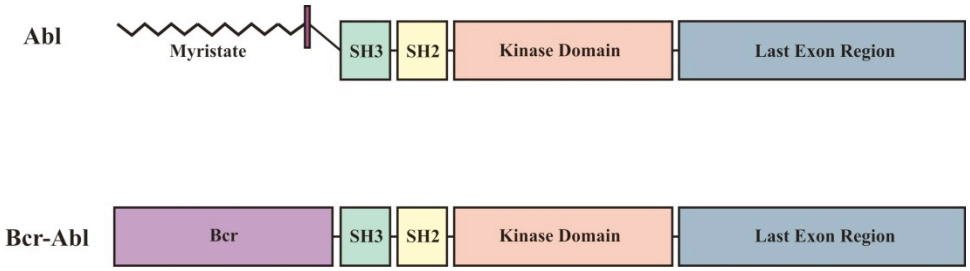

Figure 1.3: The domains of Abl and Bcr-Abl. Bcr-Abl does not include the myristate group, necessary for autoinhibition and tight regulation of Abl kinase activity.[22, 23]

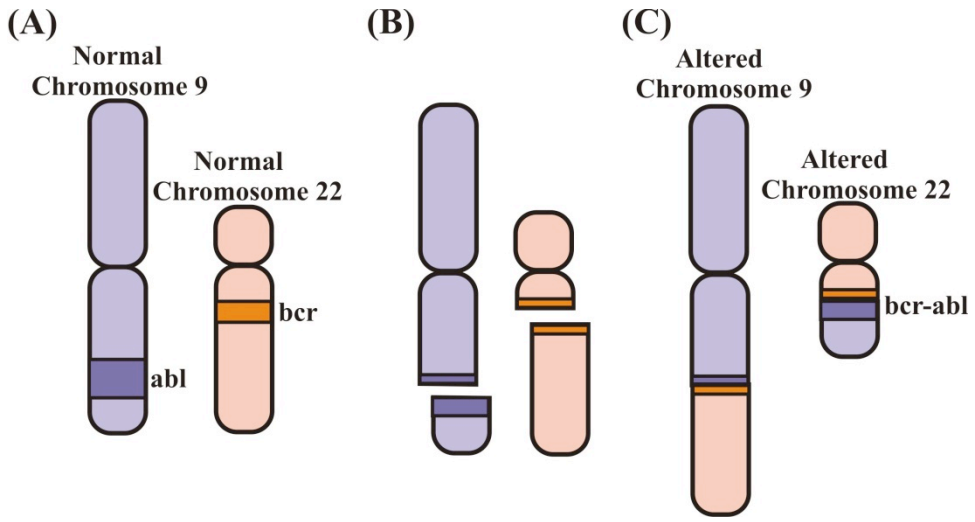

Figure 1.4: Formation of the Philadelphia chromosome. (A) The abl gene is on chromosome 9 and the bcr gene is on chromosome 22. (B) Chromosome 9 breaks just upstream of the SH3 domain in the abl gene and chromosome 22 breaks in the breakpoint cluster region. (C) Reciprocal translocation occurs when the bottom of chromosome 22 fuses to chromosome 9 and the bottom of chromosome 9 fuses to chromosome 22. Altered chromosome 22 is known as the Philadelphia chromosome. Translation of the Philadelphia chromosome leads to formation of Bcr-Abl fusion protein.[25-27]

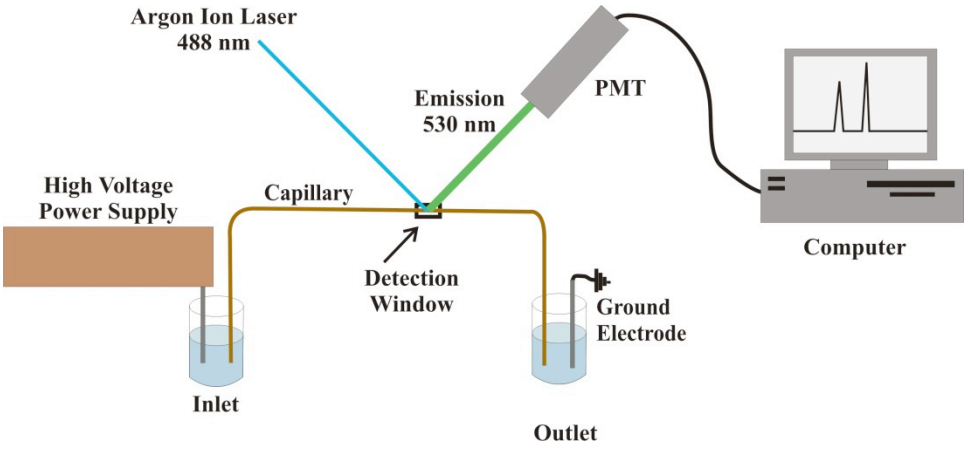

Figure 1.5: Diagram of a generic CE-LIF instrument. A high voltage power supply drives separation through a narrow-bore fused silica capillary. Detection via laser-induced fluorescence occurs through a window burned through the polyimide capillary coating. Data is collected and displayed on a computer.[90-92]

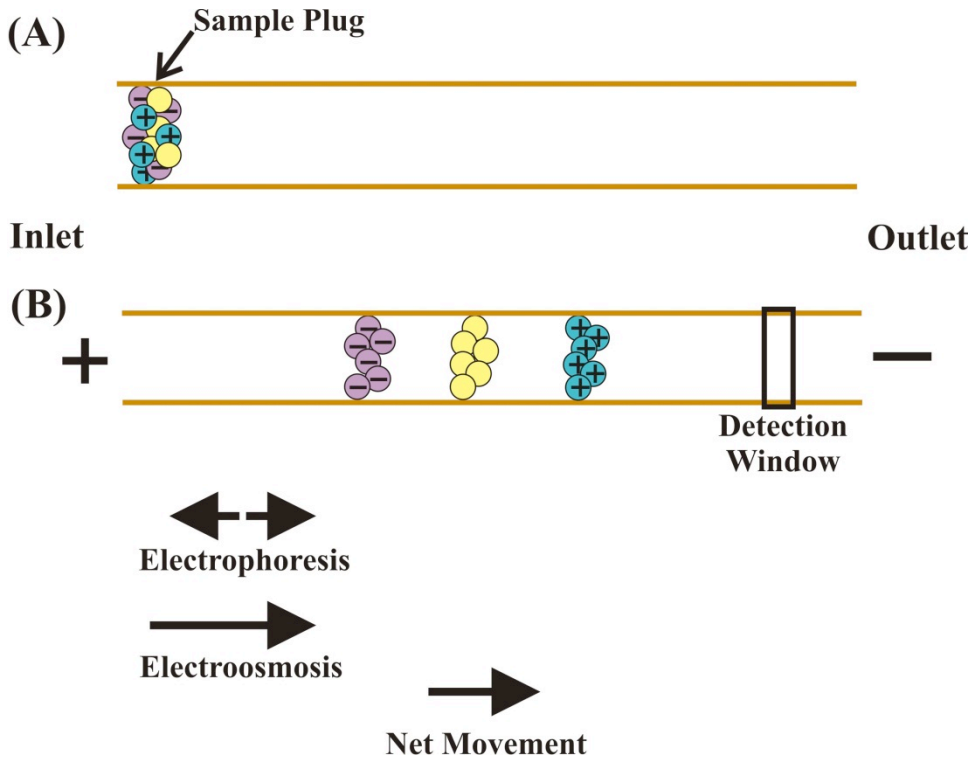

Figure 1.6: Movement of analytes through a capillary during CE. (A) A sample plug composed of ions and neutral species is injected into the capillary inlet. (B) When a voltage is applied across the capillary, the analytes separate into discrete bands based on electrophoretic mobility. In appropriate conditions, electroosmosis flows in one direction with a magnitude larger than electrophoresis and acts to sweep all species past the detection window at the capillary outlet.[90, 92]

1.7 References

1 G. A. Petsko and D. Ringe, *Protein Structure and Function*, New Science Press Ltd., London, 2004.

2 G. Manning, D. B. Whyte, R. Martinez, T. Hunter and S. Sudarsanam. "The Protein Kinase Complement of the Human Genome". *Science,* 2002, *298*, 1912-1934.

3 S. R. Hubbard and J. H. Till. "Protein Tyrosine Kinase Structure and Function". *Annu. Rev. Biochem.,* 2000, *69*, 373-398.

4 L. R. Pearce, D. Komander and D. R. Alessi. "The nuts and bolts of AGC protein kinases". *Nat. Rev. Mol. Cell Bio.,* 2010, *11*, 9-22.

5 G. Giamas, J. Stebbing, C. E. Vorgias and U. Knippschild. "Protein kinases as targets for cancer treatment". *Pharmacogenomics,* 2007, *8*, 1005-1016.

6 D. Hanahan and R. A. Weinberg. "Hallmarks of Cancer: The Next Generation". *Cell,* 2011, *144*, 646-674.

7 D. P. Brazil, J. Park and B. A. Hemmings. "PKB Binding Proteins: Getting in on the Akt". *Cell,* 2002, *111*, 293-303.

8 D. P. Brazil and B. A. Hemmings. "Ten years of protein kinase B signalling: a hard Akt to follow". *Trends Biochem. Sci.,* 2001, *26*, 657-664.

9 P. F. Jones, T. Jakubowicz, F. J. Pitossi, F. Maurer and B. A. Hemmings. "Molecular cloning and identification of a serine/threonine protein kinase of the second-messenger subfamily". *PNAS,* 1991, *88*, 4171-4175.

10 A. Bellacosa, J. Testa R., S. P. Staal and P. N. Tsichlis. "A Retroviral Oncogene, akt, Encoding a Serine-Threonine Kinase Containing an SH2-Like Region". *Science,* 1991, *254*, 274-277.

11 P. J. Coffer and J. R. Woodgett. "Molecular cloning and characterisation of a novel putative protein-serine kinase related to the cAMP-dependent and protein kinase C families". *Eur. J. Biochem.,* 1991, *201*, 475-481.

12 D. R. Alessi and P. Cohen. "Mechanism of activation and function of protein kinase B". *Curr. Opin. Genet. Dev.,* 1998, *8*, 55-62.

13 X. Chen, H. Thakkar, F. Tyan, S. Gim, H. Robinson, C. Lee, S. K. Pandey, C. Nwokorie, N. Onwudiew and R. K. Srivastava. "Constitutively active Akt is an important regulator of TRAIL sensitivity in prostate cancer". *Oncogene,* 2001, *20*, 6073-6083.

14 K. M. Nicholson and N. G. Anderson. "The protein kinase B/Akt signalling pathway in human malignancy". *Cell. Signal.,* 2002, *14*, 381-393.

15 D. Auguin, P. Barthe, M. Augé-Sénégas, M. Stern, M. Noguchi and C. Roumestand. "Solution structure and backbone dynamics of the pleckstrin homology domain of the human protein kinase B (PKB/Akt). Interaction with inositol phosphates". *J. Biomol. NMR,* 2004, *28*, 137-155.

16 E. Fayard, L. A. Tintignac, A. Baudry and B. A. Hemmings. "Protein kinase B/Akt at a glance". *J. Cell Science,* 2005, *118*, 5675-5678.

17 J. Brognard and A. C. Newton. "PHLiPPing the switch on Akt and protein kinase C signaling". *Trends Endocrin. Met.,* 2008, *19*, 223-230.

18 M. A. Lawlor and D. R. Alessi. "PKB/Akt: a key mediator of cell proliferation, survival and insulin responses?". *J. Cell Sci.,* 2001, *114*, 2903-2910.

19 C. Garcia-Echeverria and W. R. Sellers. "Drug discovery approaches targeting the PI3K/Akt pathway in cancer". *Oncogene,* 2008, *27*, 5511-5526.

20 D. R. Alessi, F. B. Caudwell, M. Andjelkovic, B. A. Hemmings and P. Cohen. "Molecular basis for the substrate specificity of protein kinase B; comparison with MAPKAP kinase-1 and p70 S6 kinase". *FEBS Lett.,* 1996, *399*, 333-338.

21 T. L. Yuan and L. C. Cantley. "PI3K pathway alterations in cancer: variations on a theme". *Oncogene,* 2008, *27*, 5497-5510.

22 O. Hantschel and G. Superti-Furga. "Regulation of the C-Abl and BCR-ABL Tyrosine Kinases". *Nat. Rev. Mol. Cell Bio.,* 2004, *5*, 33-44.

23 S. A. Courtneidge, "Escape from inhibition". *Nature,* 2003, *422*, 827-828.

24 S. C. Harrison, "Variation on a Src-like Theme". *Cell,* 2003, *112*, 737-740.

25 N. Heisterkamp, J. R. Stephenson, J. Groffen, P. F. Hansen, A. de Klien, C. Bartram and G. Grosveld. "Localization of the c-*abl* oncogene adjacent to a translocation break point in chronic myelocytic leukaemia". *Nature,* 1983, *306*, 239-242.

26 A. S. Advani and A. M. Pendergast. "*Bcr-Abl* variants: biological and clinical aspects". *Leukemia Res.,* 2002, *26*, 713-720.

27 C. R. Bartram, A. de Klein, A. Hagemeijer, T. van Agthoven, A. G. van Kessel, D. Bootsma, G. Grosveld, M. A. Ferguson-Smith, T. Davies, M. Stone, N. Heisterkamp, J. R. Stephenson and J. Groffen. "Translocation of c-*abl* oncogene correlates with the presence of a Philadelphia chromosome in chronic myelocytic leukemia". *Nature,* 1983, *306*, 277-280.

28 B. J. Druker, S. Tamura, E. Buchdunger, S. Ohno, Segal, Gerald M. Fanning, Shane, J. Zimmermann and N. B. Lydon. "Effects of a selective inhibitor of the Abl tyrosine kinase on the growth of Bcr-Abl positive cells". *Nat. Med.,* 1996, *2*, 561-566.

29 J. M. Goldman and J. V. Melo. "Targeting the BCR-ABL Tyrosine Kinase in Chronic Myeloid Leukemia". *New Engl. J. Med.,* 2001, *344*, 1084-1086.

30 D. G. Savage and K. H. Antman. "Imatinib Mesylate-A New Oral Targeted Therapy". *N. Engl. J. Med.,* 2002, *346*, 683-693.

31 C. A. Schiffer, "BCR-ABL Tyrosine Kinase Inhibitors for Chronic Myelogenous Leukemia". *N. Engl. J. Med.,* 2007, *357*, 258-265.

32 E. Weisberg, P. W. Manley, W. Breitenstein, J. Brüggen, S. W. Cowan-Jacob, A. Ray, B. Huntly, D. Fabbro, G. Fendrich, E. Hall-Meyers, A. L. Kung, J. Mestan, G. Q. Daley, L. Callahan, L. Catley, C. Cavazza, A. Mohammed, D. Neuberg, R. D. Wright, D. G. Gilliland and J. D. Griffin. "Characterization of AMN107, a selective inhibitor of native and mutant Bcr-Abl". *Cancer Cell,* 2005, *7*, 129-141.

33 E. Weisberg, P. Manley, J. Mestan, S. Cowan-Jacob, A. Ray and J. D. Griffin. "AMN107 (nilotinib): a novel and selective inhibitor of *BCR-ABL*". *Brit. J. Cancer,* 2006, *94*, 1765-1769.

34 E. Weisberg, P. W. Manley, S. W. Cowan-Jacob, A. Hochhaus and J. D. Griffin. "Second generation inhibitors of BCR-ABL for the treatment of imatinib-resistant chronic myeloid leukaemia". *Nat. Rev. Cancer,* 2007, *7*, 345-356.

35 J. H. Lee, S. K. Nandy and D. S. Lawrence. "A Highly Potent and Selective PKCα Inhibitor Generated via Combinatorial Modification of a Peptide Scaffold". *J. Am. Chem. Soc.,* 2004, *126*, 3395.

36 P. P. Pungaliya, Y. Bai, K. Lipinski, V. S. Anand, S. Sen, E. L. Brown, B. Bates, P. H. Reinhart, A. B. West, W. D. Hirst and S. P. Braithwaite. "Identification and CHaracterization of a Leucine-Rich Repeat Kinase 2 (LRRK2) Consensus Phosphorylation Motif". *PLoS ONE,* 2010, *5*, 1-13.

37 K. Nishikawa, A. Toker, F. Johannes, Z. Songyang and L. C. Cantley. "Determination of the Specific Substrate Sequence Motifs of Protein Kinase C Isozymes". *J. Biol. Chem.,* 1997, *272*, 952-960.

38 J. Wu J., D. E. H. Afar, H. Phan, O. Witte N. and K. S. Lam. "Recognition of Multiple Substrate Motifs by the c-ABL Protein Tyrosine Kinase". *Com. Chem. High T. Scr.,* 2002, *5*, 83-91.

39 C. J. Hastie, H. J. McLauchlan and P. Cohen. "Assay of protein kinases using radiolabeled ATP: a protocol". *Nat. Protoc.,* 2006, *1*, 968-971.

40 M. Beveridge, Y. Park, J. Hermes, A. Marenghi, G. Brophy and A. Santos. "Detection of $p56^{lck}$ Kinase Activity Using scintillation Proximity Assay in 384-Well Format and Imaging Proximity Assay in 384- and 1536-Well Format". *J. Biomol. Screen.,* 2000, *5*, 205-211.

41 O. B. McDonald, W. J. Chen, B. Ellis, C. Hoffman, L. Overton, M. Rink, A. Smith, C. J. Marshall and E. R. Wood. "A Scintillation Proximity Assay for the Raf/MEK/ERK Kinase Cascade: High-Throughput Screening and Identification of Selective Enzyme Inhibitors". *Anal. Biochem.,* 1999, *268*, 318-329.

42 S. M. Rodems, B. D. Hamman, C. Lin, J. Zhao, S. Shah, D. Heidary, L. Makings, J. H. Stack and B. A. Pollok. "A FRET-Based Assay Platform for Ultra-High Density Drug Screening of Protein Kinases and Phosphatases". *Assay Drug Dev. Tech.,* 2002, *1*, 9-19.

43 E. M. Schaefer and S. Guimond. "Detection of Protein Tyrosine Kinase Activity Using a High-Capacity Streptavidin-Coated Membrane and Optimized Biotinylated Peptide Substrates". *Anal. Biochem.,* 1998, *261*, 100-112.

44 M. Kim, Y. Park, D. Shin, J. Kim, B. Kim and Y. Lee. "Antibody-free peptide substrate screening of serine/threonine kinase (protein kinase A) with a biotinylated detection probe". *Anal. Biochem.,* 2011, *413*, 30-35.

45 T. Li, D. Liu and Z. Wang. "Screening Kinase Inhibitors with a Microarray-Based Fluorescent and Resonance Light Scattering Assay". *Anal. Chem.,* 2010, *82*, 3067-3072.

46 R. Seethala and R. Menzel. "A Fluorescence Polarization Competition Immunoassay for Tyrosine Kinases". *Anal. Biochem.,* 1998, *255*, 257-262.

47 E. A. Gaudet, K. Huang, Y. Zhang, W. Huang, D. Mark and J. R. Sportsman. "A Homogenous Fluorescence Polarization Assay Adaptable for a Range of Protein Serine/Threonine and Tyrosine Kinases". *J. Biomol. Screen.,* 2003, *8*, 164-175.

48 H. Li, H. Y. Wu, Y. Wang, C. E. Sims and N. L. Allbritton. "Improved capillary electrophoresis conditions for the separation of kinase substrates by the laser micropipet system". *J. Chromatogr. B,* 2001, *757*, 79-88.

49 H. Li, C. E. Sims, M. Kaluzova, E. J. Stanbridge and N. L. Allbritton. "A Quantitative Single-Cell Assay for Protein Kinase B Reveals Important Insights into the Biochemical Behavior of an Intracellular Substrate Peptide". *Biochemistry,* 2004, *43*, 1599-1608.

50 N. Fernandes, D. E. Bailey, D. L. VanVranken and N. L. Allbritton. "Use of Docking Peptides to Design Modular Substrates with High Efficiency for Mitogen-Activated

Protein Kinase Extracellular Signal-Regulated Kinase". *ACS Chem. Biol.,* 2007, *2*, 665-673.

51 A. Proctor, Q. Wang, D. S. Lawrence and N. L. Allbritton. "Metabolism of peptide reporters in cell lysates and single cells". *Analyst,* 2012, *137*, 3028-3038.

52 D. J. Bernsteel, D. L. Roman and R. R. Neubig. "In vitro protein kinase activity measurement by flow cytometry". *Anal. Biochem.,* 2008, *383*, 180-185.

53 L. L. Parker, S. B. Brueggemeier, W. J. Rhee, D. Wu, S. B. H. Kent, S. J. Kron and S. P. Palecek. "Photocleavable peptide hydrogel arrays for MALDI-TOF analysis of kinase activity". *Analyst,* 2006, *131*, 1097-1104.

54 Q. Wang, E. I. Zimmerman, A. Toutchkine, T. D. Martin, L. M. Graves and D. S. Lawrence. "Multicolor Monitoring of Dysregulated Protein Kinases in Chronic Myelogenous Leukemia". *ACS Chem. Biol.,* 2010, *5*, 887-895.

55 X. Xu, X. Liu, Z. Nie, Y. Pan, M. Guo and S. Yao. "Label-Free Fluorescent Detection of Protein Kinase Activity Based on the Aggregation Behavior of Unmodified Quantum Dots". *Anal. Chem.,* 2011, *83*, 52-59.

56 D. Wu, J. E. Sylvester, L. J. Parker, G. Zhou and S. J. Kron. "Peptide reporters of kinase activity in whole cell lysates". *Biopolymers,* 2010, *94*, 475-486.

57 V. Sharma, Q. Wang and D. S. Lawrence. "Peptide-based Fluorescent Sensors of Protein Kinase Activity: Design and Applications". *Biochim. Biophys. Acta,* 2008, *1784*, 94-99.

58 Z. Songyang, K. L. Carraway III, M. J. Eck, S. C. Harrison, R. A. Feldman, M. Mohammadi, J. Schlessinger, S. R. Hubbard, D. P. Smith, C. Eng, M. J. Lorenzo, B. A. J. Ponder, B. J. Mayer and L. C. Cantley. "Catalytic specificity of protein-tyrosine kinases is critical for selective signalling". *Nature,* 1995, *373*, 536-539.

59 D. Wu, M. R. Mand, D. R. Veach, L. L. Parker, B. Clarkson and S. J. Kron. "A solid-phase Bcr-Abl kinase assay in 96-well hydrogel plates". *Anal. Biochem.,* 2008, *375*, 18-26.

60 S. Bozinovski, B. E. Cristiano, N. Marmy-Conus and R. B. Pearson. "The Synthetic Peptide RPRAATF Allos Specific Assay of Akt Activity in Cell Lysates". *Anal. Biochem.,* 2002, *305*, 32-39.

61 D. Wu, E. Nair-Gill, D. A. Sher, L. L. Parker, J. M. Campbell, M. Siddiqui, W. Stock and S. J. Kron. "Assaying Bcr-Abl kinase activity and inhibition in whole cell extracts by phoshphorylation of substrates immobilized on agarose beads". *Anal. Biochem.,* 2005, *34*, 67-76.

62 J. E. Sylvester and S. J. Kron. "A bead-based activity screen for small-molecule inhibitors of signal transduction in chronic myelogenous leukemia cells". *Mol. Cancer Ther.,* 2010, *9*, 1469-1481.

63 M. D. Shults, K. A. Janes, D. A. Lauffenburger and B. Imperiali. "A multiplexed homogenous fluorescence-based assay for protein kinase activity in cell lysates". *Nat. Methods,* 2005, *2*, 277-283.

64 X. Han, G. Yamanouchi, T. Mori, J. Kang, T. Niidome and Y. Katayama. "Monitoring Protein Kinase Activity in Cell Lysates Using a High-Density Peptide Microarray". *J. Biomol. Screen,* 2009, *14*, 262.

65 R. B. Brown, J. A. Hewel, A. Emili and J. Audet. "Single Amino Acid Resolution of Proteolytic Fragments Generated in Individual Cells". *Cytom. Part A,* 2010, *77A*, 347-355.

66 S. N. Arkhipov, M. Berezovski, J. Jitkova and S. N. Krylov. "Chemical Cytometry for Monitoring Metabolism of a Ras-Mimicking Substrate in Single Cells". *Cytom. Part A,* 2005, *63A*, 41-47.

67 G. D. Meredith, C. E. Sims, J. S. Soughayer and N. L. Allbritton. "Measurement of kinase activation in single mammalian cells". *Nat. Biotechnol.,* 2000, *18*, 309-312.

68 E. Reits, A. Griekspoor, J. Neijssen, T. Groothuis, K. Jalink, P. van Veelen, H. Janssen, J. Calafat, J. W. Drijfhout and J. Neefjes. "Peptide Diffusion, Protection, and Degradation in Nuclear and Cytoplasmic Compartments before Antigen Presentation by MHC Class I". *Immunity,* 2003, *18*, 97-108.

69 M. K. Marshütz, W. Zauner, F. Mattner, A. Otava, M. Buschle and A. Bernkop-Schnürch. "Improvement of the enzymatic stability of a cytotoxic T-lymphocyte-epitope model peptide for its oral administration". *Peptides,* 2002, *23*, 1727-1733.

70 M. Stawikowski, R. Stowikowska, A. Jaśkiewicz, E. Zabłotna and K. Rolka. "Examples of Peptide-Peptoid Hybrid Serine Protease Inhibitors Based on the Trypsin Inhibitor SFTI-1 with Complete Protease Resistance at the P1-P1' Reactive Site". *ChemBioChem,* 2005, *6*, 1057-1061.

71 L. Pollaro and C. Heinis. "Strategies to prolong the plasma residence time of peptide drugs". *Med. Chem. Commun.,* 2010, *1*, 319-324.

72 V. Marx, "Watching Peptide Drugs Grow Up". *Chem. Eng. News,* 2005, *83*, 17-24.

73 B. Leader, Q. J. Baca and D. E. Golan. "Protein therapeutics: a summary and pharmacological classification". *Nat. Rev. Drug Discov.,* 2008, *7*, 21-39.

74 P. Vlieghe, V. Lisowski, J. Martinez and M. Khrestchatisky. "Synthetic therapeutic peptides: science and market". *Drug Discov. Today,* 2010, *15*, 40-56.

75 Z. Antosova, M. Mackova, V. Kral and T. Macek. "Therapeutic application of peptides and proteins: parenteral forever?". *Trend. Biotechnol.,* 2009, *27*, 629-635.

76 Y. Tal-Gan, M. Hurevich, S. Klein, A. Ben-Shimon, D. Rosenthal, C. Hazan, D. E. Shalev, M. Y. Niv, A. Levitzki and C. Gilon. "Backbone Cyclic Peptide Inhibitors of Protein Kinase B (PKB/Akt)". *J. Med. Chem.,* 2011, *54*, 5154-5164.

77 E. M. Molhoek, A. van Dijk, E. J. A. Veldhuizen, H. P. Haagsman and F. J. Bikker. "Improved proteolytic stability of chicken cathelicidin-2 derived peptides by D-amino acid substitutions and cyclization". *Peptides,* 2011, *32*, 875-880.

78 O. Ovadia, Y. Linde, C. Haskell-Leuvano, M. L. Dirain, T. Sheynis, R. Jelinek, C. Gilon and A. Hoffman. "The effect of backbone cyclization on PK/PD properties of bioactive peptide-peptoid hybrids: The melanocortin agonist paradigm". *Bioorgan. Med. Chem.,* 2010, *18*, 580-589.

79 L. T. Nguyen, J. K. Chau, N. A. Perry, L. de Boer, S. A. J. Zaat and H. J. Vogel. "Serum Stabilities of Short Tryptophan- and Arginine-Rich Antimicrobial Peptide Analogs". *PLoS ONE,* 2010, *5*, 1-8.

80 L. H. Brinckerhoff, V. V. Kalashnikov, L. W. Thompson, G. Yamshchikov, R. A. Pierce, H. S. Galavotti, V. H. Engelhard and C. L. Slingluff Jr. "Terminal Modifications Inhibit Proteolytic Degradation of an Immunogenic Mart-1_{27-35} Peptide: Implications for Peptide Vaccines". *Int. J. Cancer,* 1999, *83*, 326-334.

81 K. Bellmann-Sickert, C. E. Elling, A. N. Madsen, P. B. Little, K. Lundgren, L. Gerlach, R. Bergmann, B. Holst, T. W. Schwartz and A. G. Beck-Sickinger. "Long-Acting Lipidated Analogue of Human Pancreatic Polypeptide Is Slowly Released into Circulation". *J. Med. Chem.,* 2011, *54*, 2658-2667.

82 G. Pasut and F. M. Veronese. "PEG conjugates in clinical development or use as anticancer agents: An overview". *Adv. Drug Deliver. Rev.,* 2009, *61*, 1177-1188.

83 Y. Koda, M. T. Liang, J. T. Blanchfield and I. Toth. "*In vitro* stability and permeability studies of lipsomal delivery systems for a novel lipophilic endomorphin 1 analogue". *Int. J. Pharm.,* 2008, *356*, 37-43.

84 C. D. Cros, I. Toth and J. T. Blanchfield. "Lipophilic derivatives of leu-enkephalinamide: In vitro permeability, stability and in vivo nasal delivery". *Bioorgan. Med. Chem.,* 2011, *19*, 1528-1534.

85 R. Tugyi, K. Uray, D. Iván, E. Fellinger, A. Perkins and F. Hudecz. "Partial D-amino acid substitution: Improved enzymatic stability and preserved Ab recognition of a MUC2 epitope peptide". *PNAS,* 2005, *102*, 413-418.

86 E. V. Pappa, A. A. Zompra, Z. Spyranti, Z. Diamantopoulou, G. Pairas, F. N. Lamari, P. Katsoris, G. A. Spyroulias and P. Cordopatis. "Enzymatic Stability, Solution Structure, and Antiproliferative Effect on Prostate Cancer Cells of Leuprolide and New Gonadotropin-Releasing Hormone Peptide Analogs". *Biopolymers,* 2010, *96*, 260-272.

87 M. D. Disney, D. F. Hook, K. Namoto, P. H. Seeberger and D. Seebach. "*N*-Linked Glycosylated Beta-Peptides Are Resistant to Degradation by Glycoamidase A". *Chem. Biodiv.,* 1005, *2*, 1624-1634.

88 I. Neundorf, R. Rennert, J. Franke, I. Közle and R. Bergmann. "Detailed Analysis Concerning the Biodistribution and Metabolism of Human Calcitonin-Derived Cell-Penetrating Peptides". *Bioconjugate Chem.,* 2008, *19*, 1596-1603.

89 L. Gentilucci, R. De Marco and L. Cerisoli. "Chemical Modifications Designed to Improve Peptide Stability: Incorporation of Non-Natural Amino Acids, Pseudo-Peptide Bonds, and Cyclization". *Curr. Pharm. Design,* 2010, *16*, 3185-3203.

90 J. W. Jorgenson and K. D. Lukacs. "Zone electrophoresis in open-tubular glass capillaries". *Anal. Chem.,* 1981, *53*, 1298-1302.

91 R. P. Oda and J. P. Landers. "Introduction to Capillary Electrophoresis" in *Handbook of Capillary Electrophoresis,* ed. J. P. Landers, CRC Press, Inc., Boca Raton, FL, 1994, pp.9-42.

92 J. W. Jorgenson and K. D. Lukacs. "Capillary Zone Electrophoresis". *Science,* 1983, *222*, 266-272.

93 C. Lee, J. Linton, J. S. Soughayer, C. E. Sims and N. L. Allbritton. "Localized measurement of kinase activation in oocytes of *Xenopus laevis*". *Nat. Biotechnol.,* 1999, *17*, 759-762.

94 J. S. Soughayer, Y. Wang, H. Li, S. Cheung, F. M. Rossi, E. J. Stanbridge, C. E. Sims and N. L. Allbritton. "Characterization of TAT-Mediated Transport of Detachable Kinase Substrates". *Biochemistry,* 2004, *43*, 8528-8540.

95 S. L. Petoney and J. V. Sweedler. "Optical Detection Techniques for Capillary Electrophoresis" in *Handbook of Capillary Electrophoresis,* ed. J. P. Landers, CRC Press, Inc., Boca Raton, FL, 1994, pp.147-183.

96 C. E. Sims and N. L. Allbritton. "Single-cell kinase assays: opening a window onto cell behavior". *Curr. Opin. Biotech.,* 2003, *14*, 23-28.

97 N. J. Dovichi. "Origin, Current Status, and Future Perspectives of Chemical Cytometry" in *Chemical Cytometry: Ultrasensitive Analysis of Single Cells,* ed. C. Lu, Wiley-VCH, Weinheim, 2010, pp.1-19.

98 J. Edström, "Nucleotide Analysis on the Cyto-Scale". *Nature,* 1953, *4382*, 809.

99 N. J. Dovichi and S. Hu. "Chemical Cytometry". *Curr. Op. Chem. Biol.,* 2003, *7*, 603-608.

100 L. M. Borland, S. Kottegoda, K. S. Phillips and N. L. Allbritton. "Chemical Analysis of Single Cells". *Annu. Rev. Anal. Chem.,* 2008, *1*, 191-227.

101 M. L. Kovarik and N. L. Allbritton. "Measuring enzyme activity in single cells". *Trend. Biotechnol.,* 2011, *29*, 222-230.

102 S. J. Altschuler and L. F. Wu. "Cellular Heterogeneity: Do Differences Make a Difference?". *Cell,* 2010, *141*, 559-563.

103 S. S. Rubakhin and E. Romanova. "Profiling metabolites and peptides in single cells". *Nat. Med.,* 2011, *8*, S20-S29.

104 D. Wang and S. Bodovitz. "Single cell analysis: the new frontier in 'omics'". *Trends. Biotechnol.,* 2010, *28*, 281-290.

105 P. E. Ross, G. R. Ehring and M. D. Cahalan. "Dynamics of ATP-induced Calcium Signaling in Single Mouse Thymocytes". *J. Cell Biol.,* 1997, *138*, 987-998.

106 J. E. Ferrell Jr. and E. M. Machleder. "The Biochemical Basis of an All-or-None Cell Fate Switch in *Xenopus* Oocytes". *Science,* 1998, *280*, 895-898.

107 Q. Xue and E. S. Yeung. "Variability of Intracellular Lactate Dehydrogenase Isoenzymes in Single Human Erythrocytes". *Anal. Chem.,* 1994, *66*, 1175-1178.

108 M. Leslie, "The Power of One". *Science,* 2011, *331*, 24-26.

109 M. Saji and M. D. Ringel. "The PI3K-Akt-mTOR pathway in initiation and progression of thyroid tumors". *Mol. Cell Endocrinol.,* 2010, *321*, 20-28.

110 B. D. Manning and L. C. Cantley. "AKT/PKB Signaling: Navigating Downstream". *Cell,* 2007, *129*, 1261-1274.

CHAPTER 2

DESIGN, CONSTRUCTION AND VALIDATION OF A SINGLE-CELL CE-LIF INSTRUMENT

2.1 Introduction

2.1.1 Capillary Electrophoresis for Single-Cell Analysis

A discussion of the benefits of single-cell analysis is presented in Chapter 1. Capillary electrophoresis was chosen as the analytical tool for this work for many reasons, outlined below. CE is fast, efficient, and quantitative, with sensitive detection of very small sample sizes, a requirement when assaying single cells that are approximately 1 pL in volume.[1-8] In addition, CE has very high resolution with a large peak capacity, giving the option of simultaneous measurements of multiple analytes. The relative speed of CE affords high temporal resolution, and can be coupled with rapid lysis techniques to allow for fast analysis of enzymatic activity in single cells.[9-11] CE coupled with laser-induced fluorescence detection has very low detection limits, on the order of 10^{-20} moles, which is excellent for analysis of extremely low amounts of analyte, precisely that found in single cells.[12, 13] These benefits taken together with the amenability to incorporating higher throughput designs[10, 11, 14] are the reason CE was selected as the analytical measurement technique utilized in this work.

2.1.2 Single-Cell CE Instrument Designs

Multiple types of instruments for utilizing CE to analyze singe cells have already been described in the literature with many detection strategies.[4, 15] Several of these different designs are described below. The earliest work on single-cell CE appears in the late 1980s and early 1990s. An early design utilized micromanipulation to remove single neurons from land snails to a nanoliter-sized "test tube" generated by sealing one end of a glass capillary.[16] The contents of the single cell were homogenized and a finely pulled tip from a glass micropipette was attached to a pressure source and utilized to microinject the single cell homogenate directly into the capillary used for electrophoresis. Utilization of this sample injection method provided enough material for multiple samplings from the same cellular homogenate, giving the option of replicate studies with identical electrophoretic conditions or additional studies utilizing different conditions to probe alternate queries from the same cell. An LIF detection method was utilized to monitor naphthalene-2,3-dicarboxyaldehyde-labeled phenylalanine with a detection limit of 2×10^{-9} M. Benefits of this setup include the LIF detection for fluorescent compounds because of the increase in detection limits and the ability to sample the cellular homogenate multiple times. Difficulties of this design include the early lysis of the single cell and the tedious manipulation required to inject the contents into the capillary. The lysis of the single cell causes a loss of intracellular compartmentalization and could potentially damage analytes by making them more susceptible to proteolysis and could change signaling as requisite components are no longer in proper locations after lysis.

An alternate system also sampled the cytoplasm of a large neuronal cell, this time isolated from pond snails.[17] However, it differed from the previously described system in

both sample injection into the capillary and method of detection. The 5-μm inner diameter capillary used for electrophoresis was etched on the inlet side with hydrofluoric acid (HF) to create a very fine point. This tip was directly inserted into the neuron and a voltage applied across the capillary to electrokinetically load the compounds. This setup utilized a carbon fiber electrode for sub-attomole detection limits of electroactive compounds. This system was the first to describe sub-cellular sampling and detection, with the HF-etched capillary allowing for very small spatial resolution within the neuron. The main drawback of this design lies with the electrochemical detection setup, limiting the detectable analytes to electroactive compounds. However, this particular setup was designed for analysis of neurotransmitters in single cells, many of which are electroactive, so it remains a drawback only when the designated analyte is not compatible with this detection scheme.

Another early single cell CE system design was used to analyze contents in single human erythrocytes, a much smaller cell than the snail neurons previously described.[18-21] Single erythrocytes were loaded when the electrophoretic capillary was positioned over a single cell in a small drop of a dilute cell suspension. Vacuum was applied to the outlet to aspirate the cell and was halted when the cell was visually observed to enter the capillary lumen. The cell was lysed with a small plug of detergent loaded immediately after cell injection or via contact with the electrophoretic buffer. LIF was utilized for direct detection of native fluorescent compounds, on-column derivatized compounds or for indirect detection by monitoring the formation of a non-target analyte proportional to analyte concentration. This system was the earliest system described to sample the much smaller mammalian blood cells and opened the door for single cell analysis of alternative cells much smaller in size. A main drawback of the loading method is the uncontrollable and variable size of the sample

plug. Time required, and therefore amount injected, almost certainly varied from cell to cell. This could lead to different lengths of time to achieve cell lysis as the diffusion of the lysis solution through a larger plug would be slower than through a shorter plug. Additionally, injection plug volume can alter the separation if the background solution is different from the electrophoretic buffer. Band broadening can occur if destacking results from these differences or a localized region of elevated heat can occur if Joule heating in the higher ionic strength, cell-compatible buffer is not dissipated rapidly enough, also leading to band broadening.

As the technology progressed into the later 1990s and 2000s, other system designs began to emerge, combining the older strategies with new methods for cell lysis, sample loading and detection designs. The Dovichi group first introduced an off-column quartz sheath flow detector that utilized a helium/neon (HeNe) laser focused just beyond the capillary outlet.[22] The sheath flow detector is beneficial in that it provides a flat surface for the excitation laser to be focused and emission to be collected, as opposed to the curved surface of on-capillary detection windows. The flat surfaces result in less optical scatter, allowing for more sensitive detection techniques. A drawback of the sheath flow design is the complexity that arises from balancing the sheath flow rate and capillary flow rate while simultaneously ensuring appropriate seals to prevent fluid leakage. This sheath flow detector has been combined with many different sample injection and lysis strategies, discussed below. A chemically etched capillary tip was positioned just above the cell and suction applied to the outlet until the cell was aspirated into the capillary, where the cell was lysed when it came into contact with the non-physiologic electrophoretic buffer or when a strong electric field was applied with a Tesla coil.[5, 23-27] This injection and detection strategy has

also been combined for two-dimensional (2D) CE analysis of single cells when the eluent from one capillary is transferred to a second capillary using orthogonal electrophoretic separation strategy. For example, when capillary sieving electrophoresis in the first dimension is followed by micellar electrokinetic chromatography.[28-30]

More recent work from the Dovichi lab attempts parallel CE analysis of single cells using microfabricated microwell arrays to trap formalin-fixed cells in known positions so an array of capillaries can be lowered over the individual cells. These cells are then loaded when a vacuum is applied to the outlet.[14, 31] The design of the 5-capillary array[14] affords the potential to analyze single cells in parallel, but it is difficult to execute. Often, no cells or multiple cells settle into the wells over which the capillary was aligned, limiting the effectiveness of the parallel capillaries. In addition, the cells were fixed with formalin prior to experimental analysis. Formalin cross-links with itself and with amine groups while also making the membrane permeable.[32] Anything not cross-linked will leak out of the cell, so small molecule reporters such as peptides will not be present. Additionally, cross-linking of proteins generally renders them inactive, as they no longer have the dynamic range of motion available prior to fixation, so protein activity cannot be measured after formalin fixation.

More recent single cell CE on neurons has come from the Sweedler lab. The design of the systems in this lab combine many setups already described above. Cells or sub-cellular regions are loaded into the capillary tip electrokinetically when a voltage is applied.[33-35] Detection strategies have varied, with use of the same sheath flow detector as described above,[34] online absorbance detection utilizing an ultraviolet (UV) light source[33] and online LIF detection of fluorescent compounds.[35] The benefits and drawbacks of these injection and detection strategies are discussed in the above paragraphs, with the exception of

the absorbance detector. Absorbance depends on the detection pathlength through the sample, which is inherently small inside the fused silica capillaries, and leads to poor detection limits.

Finally, the Allbritton lab has utilized single cell CE-LIF instruments for various analyses of single cells. Early work focused on *Xenopus laevis* oocytes, where a piezo-driven, HF-etched capillary was used to obtain a plug of cytoplasm before the inlet was transferred to electrophoretic buffer for CE.[36-40] LIF detection was utilized to detect fluorescent analytes. An alternative design was introduced by Sims *et al.* in the late 1990s that utilized a focused pulse from an Nd:YAG laser to lyse an individual cell, halting cellular reactions within milliseconds.[41] The contents were then electrokinetically loaded into the capillary when a voltage was applied across the capillary. Many uses of this system have been described in the literature,[9, 42-45] mostly in the analysis of kinase activity in single cells. Additional usage of this system design has recently been described by the Audet lab.[3, 46, 47] An alternative lysis strategy has also been used by the Allbritton lab, where electroactive coverslips were used to apply an electrical pulse to cells, lysing them prior to loading into the capillary for separation.[10, 11, 48] Recent improvements to these system designs include replacement of the open beam excitation pathway by fiber optics[49] and similar conversion of the open emission pathway to fiber optics.[50, 51] The fiber optic design reduces the overall footprint of the instrument by moving the excitation and emission components to the microscope stage. This more compact design permits for shorter capillaries, yielding faster separations as the electrophoretic voltage can be increased and the distance traveled by samples is shorter. The main drawback to these systems is the cost of the pulsed laser

utilized for cell lysis, making this system more expensive than other designs lacking the Nd:YAG laser.

2.1.3 Instrument Design Rationale

Design of the instrument described in this chapter was based on previous designs of systems utilized in the Allbritton lab. Laser-based cell lysis was chosen because it lyses cells on sub-millisecond time scales, causing turbulent mixing of the contents, rapidly terminating cellular reactions. Laser-based lysis gives excellent temporal resolution of enzymatic reactions as the cell remains unperturbed until the moment of lysis. This is in contrast to the seconds or minutes required to lyse cells with detergents or buffers, times too long to allow for accurate assessment of enzymatic activity. As an example, PKB can be activated in response to cellular stress and has been found to be activated within one minute of cell stimulation.[52] Addition of a stressful stimulus such as detergent in a lysis buffer might activate PKB, causing substrate phosphorylation during the lysis step. Measurement of substrate phosphorylation after lysis with detergent could yield higher values than were present before the detergent was added and could lead to false assessment of PKB activity. The short timescales of lysis by the Nd:YAG laser greatly reduces this time lag, resulting in a measurement of kinase activity with little or no artifacts related to lysis-induced enzymatic stimulation. Finally, laser-based lysis is easily coupled to electrokinetic injection of the cellular contents and both functions are easily programmed and controlled with the chosen software.

Laser-induced fluorescence detection was chosen because of its exquisite sensitivity, on the order of atto- and zeptomoles,[13] and the peptide substrates utilized in these studies are easily synthesized to contain a fluorescent tag such as carboxyfluorescein. The conversion to

the fiber optics in this design versus earlier systems made the system more compact with a smaller footprint so both the excitation and emission optics were placed on the microscope stage. This instrument was also designed and constructed to facilitate incorporation of a commercial microinjection system that could be used to microinject cells with the reporter of choice prior to cell lysis and CE. While similar to previous designs of single cell CE-LIF systems constructed in this lab, the instrument described in this chapter consists of upgrades in the software and instrumentation to fit with the work described in this dissertation and in future work anticipated by the Allbritton lab.

2.2 Experimental Design

2.2.1 Instrument Parts

Appendix A contains the blueprints for the custom parts described below. The parts were machined by the UNC Physics Machine Shop (Chapel Hill, NC). The following components were machined from aluminum: two (2) microscope stage adapters and the CE-LIF base bottom, front and top. The remaining components were constructed of black delrin: photomultiplier tube (PMT) shutter, PMT shutter plate, PMT filter drawer, PMT housing, CE-LIF detector housing and the collection lens holder. Two (2) plate adapters (07 RPC521, Melles Griot, Albuquerque, NM) were adapted by the Physics Machine Shop by counterboring 2 screw locations and removing the lip in the slots on either side, indicated in Appendix A.

The following optical components were purchased from OZ Optics (Ontario, Canada): excitation fiber optic cable for 473 nm light with focusing optic, spot size of 40 μm at a distance of 3.9 cm (LPF-04-473-3.5/125-S-9.5-39-3.9AS-40-3AF3-2); fiber collimator

and collection lens (HPUCO-23-400/700-M-50AC-30OD); fiber patchcord for emission pathway (QMMJ-33-IRVIS-200/300-3-1); and a fiber collimator (HPUCO-23-400/700-M-3.5AC-SP). The following optical filters were purchased from Semrock (Rochester, NY): single band bandpass filter centered around 525 nm, 50 nm bandwidth (FF01-525/50-25); ultrasteep long-pass edge filter at 488 nm (LP02-488RS-25); and a single notch filter at 532 nm, 17 nm bandwidth (NF01-532U-25). Both the photomultiplier tube (H7732-10) and the PMT power supply (Mode C7169) were purchased from Hamamatsu (Bridgewater, NJ). The following data acquisition components were purchased from National Instruments (Austin, TX): connector block (SCB-68 shielded connector block); shielded cable (SHC68-68-EPM shielded cable); and the data acquisition (DAQ) card and board (NI-PCI-6229, M-Series DAQ, 32 analog inputs, 48 digital I/O, 4 analog outputs.)

Additional parts were purchased from the following companies, as listed below: computer (Optiplex 980, Dell, Round Rock, TX); 473 nm excitation laser (BML-473-10F0-A1-FC9) and power supply (DPSSL, Lasermate Group Inc., Pomona, CA); pre-amplifier (PMT-5 amplifier) and power supply (F-100PS, Advanced Research Instruments Corporation, Golden, CO); two (2) x, y translational stages (07-TMS512) and two (2) z translational stages (07-TEZ701, Melles Griot, Albuquerque, NM); capillary x, y, z translational stage (custom order, World Precision Instruments, Sarasota, FL); objective for gathering emission (PlanFluor. 40X/numerical aperture of 0.75); microscope (Axiovert 135, Zeiss, Thornwood, NY); high voltage power supply (CZE 1000R) and cable (105719-034, Spellman High Voltage Corporation, Hauppauge, NY); Nd:YAG pulsed laser and power supply (Minilite, Continuum, Santa Clara, CA); CMOS camera (MCN-B013-U, Mightex Systems, Pleasanton, CA); beam expander (Model 15900), two (2) high-energy mirrors

(10QM20HDM.15) and optical breadboard (LW3048B-OPT, Newport Corporation, Irvine, CA); dry bath incubator (Isotemp, Fisher Scientific, Waltham, MA); and microinjector (Transjector 5246, Eppendorf, Hamburg, Germany). Other mounting components and brackets were purchased from Newport or Melles Griot. Tubing used in the buffer flow system was purchased from Fisher Scientific (Waltham, MA). Data was collected with custom software (Appendix B) made with LabVIEW (Version 9.0.1, National Instruments, Austin, TX) and analyzed using Origin Software (Version 7.5, OriginLab Corporation, Northampton, MA).

2.2.2 Instrument Validation

2.2.2.1 Chemicals and Materials

Chemicals used in the validation of the instrument were purchased from the following companies: Fluorescein Reference Standard was procured from Invitrogen (Carlsbad, CA); trizma base and tricine were obtained from Sigma (St. Louis, MO); sodium hydroxide (NaOH) and hydrochloric acid (HCl) were bought from Fisher Scientific (Waltham, MA). Fused silica capillaries [50 μm inner diameter, 360 μm outer diameter (Polymicro Technologies, Phoenix, AZ)] had a total length of 38 cm and an effective length of 21.5 cm. Capillaries were conditioned prior to use with 0.1 M NaOH for 12 h, H_2O for 1 h, 0.1 M HCl for 6 h, and H_2O again for 12 h. After each sample, the capillary was sequentially washed with 1 M NaOH, H_2O and buffer for 10 min (approximately 10 column volumes) by applying pressure with nitrogen to the capillary outlet. A sample plug was injected by elevating the capillary inlet 3 cm relative to the outlet for 10 s. The volume injected was estimated with Poiseuille's equation (Eq 2.1) and was determined to be 0.13 nL s^{-1}.

Equation 2.1:[53]

$$\frac{V}{t} = \frac{\rho g h d^4 \pi}{128 \eta L}$$

V = volume

t = time sample is applied

ρ = density (assumed 1 g mL^{-1})

g = acceleration due to gravity (9.8 m s^{-2})

h = height difference between inlet and outlet

d = inner diameter of capillary

η = viscosity (assumed 8.9 x 10-3 g cm^{-1} s^{-1})

L = total capillary length

2.2.2.2 Optimum Electrophoretic Voltage

To determine the optimal electrophoretic voltage, an Ohm's Plot was generated by filling the capillary with and immersing both ends in a 100 mM tris/100 mM tricine, pH 8.1 buffer. A negative voltage was applied to the outlet electrode and the current was recorded for 30 s. The voltage was tested in 2 kV increments from 0 - 18 kV. The current as a function of voltage was plotted and a line with a slope corresponding to 1/R was generated utilizing the data. The optimum running voltage was determined to be the highest voltage that still obeyed a linear relationship between current and voltage.

2.2.2.3 Limit of Detection

In order to determine the limit of detection (LOD) of the CE system, successively higher concentrations of a fluorescein reference standard were gravity loaded into the

capillary as described above in section 2.2.2.1 and a voltage of -12 kV was applied to the outlet. On the resulting electropherogram, the height of the baseline and the height of the corresponding fluorescein peak were measured. The signal to noise (S/N) ratio was determined by dividing the height of the fluorescein reference standard peak by the average height of the baseline. The LOD was chosen as the amount of fluorescein required to achieve an S/N value of 3.

2.2.2.4 Cell Lysis

A focused pulse from an Nd:YAG laser was utilized to lyse cells. Individual cell chambers were prepared by using poly(dimethyl siloxane) (PDMS, Sylgard 184) to glue a silicon O-ring (McMaster-Carr, Cleveland, OH) to a #1 glass coverslip (Fisher). The location of the laser was determined by visual identification of ink ablation from the surface of the coverslip. Adherent HeLa cells were used to determine the laser energy setting appropriate for cell lysis. A single cell was positioned adjacent to the previously determined location of laser position and the laser was fired once. The cell was visually observed for signs of lysis. Lysis was considered achieved when the plasma membrane of the cell was compromised based on visual identification. The laser energy was chosen based on the amount of energy required to lyse >95% of cells with a single pulse.

2.2.2.5 Buffer Flow System

Gravity was utilized to drive the flow of ECB over the cells and vacuum was used to remove fluid from the cell chamber. The temperature in the cell chamber needed to be approximately 37 ^{o}C, meaning the temperature of the sand bath heating the fluid had to be significantly higher. To determine the required sand temperature, a thermometer was placed in the sand and a second thermometer was located in the cell chamber. Both temperatures

were recorded as the sand temperature was increased. The appropriate sand temperature was defined as the temperature required to hold the ECB in the cell chamber between 34 – 37 ^{o}C while the buffer was flowing.

2.3 Results and Discussion

2.3.1 Instrument Description

The single cell CE instrument possessed the following features or components, which are indicated in Figures 2.1 and 2.2. To load analyte directly into single cells, a commercialized microinjection system was installed on the instrument. To achieve lysis on sub-millisecond timescales, a pulsed Nd:YAG laser was incorporated into the system. Detection limits in the range of attomoles was desired, so the highly sensitive laser-induced fluorescence detection was chosen as the detection method used for this system. Fiber optic cables were utilized in the excitation and emission pathways so that all optical components were located on the microscope stage. Electrophoresis was driven through a fused silica capillary positioned over the microscope stage to allow for introduction of a single cell into the capillary. Construction of the instrument is described in the following sections.

2.3.2 Instrument Construction

2.3.2.1 Excitation Pathway

The primary step in preparing the excitation pathway was to center the laser beam in the 3.5 μm-diameter single-mode fiber core by optimizing the power output from the fiber to 2 mW. As demonstrated by Peck *et al*. in a systematic study of optimal laser power for laser-induced fluorescence detection, there is a maximum output signal reached for each fluorophore.[54] To obtain the maximum fluorescence signal, the excitation laser power must

be high enough for the fluorophores to emit as much as possible, yet not so high that the fluorophores photobleach at an unacceptably rapid rate, which would result in lower signal. For this system and fluorophore, 2 mW was determined to be the most acceptable power. Adjustments were made until a steady output from the fiber of 2.1 mW was achieved.

Once the desired power output was attained, the excitation fiber was positioned above the capillary. The most frequent capillary utilized in this system has an inner diameter of 50 μm, so the excitation fiber was purchased with a pigtail style lens to focus the laser to a spot size of 40 μm at a working distance of 3.9 cm. When properly aligned, the excitation laser spot fills the majority of the inner diameter of the capillary while minimizing light scatter from the curved fused silica walls. The x,y, z translational stage holding the excitation fiber was mounted to the CE-LIF base which was mounted directly to the microscope stage (Figure 2.3) and the emitting end of the excitation fiber was fixed to a z position 3.9 cm above the capillary detection window. The y position was determined by monitoring the diffraction pattern produced on the opposite side of the fluid-filled capillary. In the desired position where the 40 μm laser spot was centered in the capillary lumen, the diffraction pattern was symmetrical. The x position of the capillary was determined in conjunction with alignment of the emission pathway (described in section 2.3.2.2).

2.3.2.2 Emission Pathway

A 40X objective lens with a numerical aperture (NA) of 0.75 was positioned at a right angle from the excitation laser and was fit into the custom-made CE-LIF Detector Housing attached to an x, y, z translation stage using the custom-modified plate adapter (Figure 2.4). The focal length of this objective was just long enough to reach the center of the capillary lumen, where the location of maximum fluorescence was located. Positioning of the

objective to the precise focal length of the lens permitted maximum fluorescence signal collection by the objective lens.[55] A larger collection lens was attached to the opposite side of the Detector Housing to focus the emission light from the objective lens into the 200 μm core of the multimode emission fiber. The multimode emission fiber is capable of transmitting both infrared and visible light, a range containing the 520 nm wavelength of fluorescein emission. A collimator was placed at the terminus of the emission fiber to reduce the spread of emission light directed into the PMT entrance. The collimator was directly attached to the custom-designed PMT Housing. Prior to passing into the PMT entrance slit, the emission light was filtered through two spectral filters to reduce detection of emission not due to the fluorophore. An ultrasteep long-pass edge filter at 488 nm was utilized to eliminate wavelengths below 488 nm, including any radiation from the excitation laser. A single band bandpass filter centered at 525 nm (± 25 nm) was used to collect emission from the fluorophore and attenuate all wavelengths below and above the range of the bandpass filter. A custom-designed shutter was inserted to protect the PMT when data collection was not in process. Incident light entering the PMT strikes the first photocathode, which generates electrons. These electrons are steered to additional dynodes within the PMT, releasing a cascade of electrons at each dynode and generating a current at the anode of the PMT. Thus, the PMT converts photons into a current. The PMT was connected to a pre-amplifier utilized to amplify the current from the PMT, convert it to a positive voltage, and step the voltage to a range readable by the DAQ board. The pre-amplifier was positioned as closely as possible to the PMT to minimize the amount of noise introduced into the signal prior to amplification.

The x, y and z position of the Detector Housing, and therefore the position of the microscope objective, was determined by filling the capillary with a 10 μM solution of fluorescein reference standard in water and monitoring fluorescence as the x, y and z positions of the Detector Housing were adjusted. Additionally, the x position of the excitation laser was also adjusted as needed. These four positions were altered until a maximum signal was observed. Optimal positioning of the Detector Housing is key for obtaining the desired detection limit because as much emission light as possible needs to enter the PMT to maximize the amount of signal recorded. When the maximum signal was seen after adjustments to the four positions, each position was locked into place.

2.3.2.3 Laser-Based Cell Lysis

The Nd:YAG laser used for achieving cell lysis was steered at a right angle and elevated to the appropriate height with 2 mirrors adjusted with thumbscrews to direct the beam into the microscope. The pulsed laser beam alignment was adjusted until it filled the entire back aperture of the microscope objective. Filling the back aperture of the objective lens maximized the radiant flux focused at the focal point of the lens, delivering the maximum amount of energy. When the beam was properly aligned, the laser light was focused with the microscope objective to a location at the interface of the cell chamber surface and fluid, determined as described above (Section 2.2.2.4). Laser energy was adjusted and measured with an energy meter at the location of the cell chamber, with the microscope objective removed to protect the energy meter, as focusing of the beam by the objective results in energies higher than the upper limit of detection of the energy meter. The pulse was focused by the objective to a point just below the interface of the coverslip and the fluid in the cell chamber. Upon firing at this location, the pulse generated a plasma which

created a cavitation bubble. Collapse of the cavitation bubble generated a shock wave originating from the bubble and propagating outward.[56, 57] This cavitation bubble was responsible for disruption of the plasma membrane of the cells, with higher energies resulting in more complete disruption. On some occasions, the coverslip was cracked and a small bubble generated in the fluid above this location. This was an indication of sub-optimal focusing and was an indication of the laser being focused in the coverslip rather than at the interface between the coverslip and the fluid. All of these results are similar to what has been previously described for Nd:YAG laser-based lysis.[41, 57] To determine the energy required to reproducibly lyse cells, a cell was positioned approximately 10 μm laterally from the laser pulse location and was visually inspected for lysis after a single pulse from the laser. A laser energy of 30 μJ was found to lyse more than 95% of cells with a single pulse and was selected as the working energy.

2.3.2.4 Temperature Controlled Buffer Flow System

The main reservoir of ECB was located approximately 1 m above the CE system to provide gravity flow to bathe cells in the culture dish in a continuous stream of buffer. Continuous buffer flow allowed for maintenance of culture temperature at 37^{o}C, solution pH, and a means to remove excess analyte from the cell chamber prior to analysis. 1/4 inch diameter tubing was connected to a 3-way valve, with one end connected to a Luer-lock 30 mL syringe and the other end to a 1/16 inch inner diameter tubing that was wound around a metal rod and immersed in sand in a dry bath incubator. As this smaller tubing exited the sand, it was insulated with weather stripping and directed to the cell chamber to minimize heat loss from the solution. Effluent ECB was removed from the cell chamber via vacuum. The vacuum line was positioned slightly above the influent line so that approximately 500 μL

of fluid remained in the cell chamber at all times. A sand temperature between 70 – 75 ^{o}C provided an ECB temperature between 34 – 37 ^{o}C in the cell chamber with an approximate flow rate of 3 mL min^{-1}. This resulted in a fluid velocity of 0.2 mm s^{-1} experienced by the cells. This velocity is approximately 10X less than a previously reported velocity utilized for calculating shear stress experienced by cells in a microfluidic device, which was determined to be well below the acceptable limits for mammalian cells.[10, 58] Based on these measurements and comparisons to past calculations of shear stress, it was determined that the flow rate experienced by the cells in the chamber did not adversely affect the cells.

2.3.2.5 Capillary Electrophoresis

The voltage was supplied by a Spellman High Voltage Power Supply connected to a platinum electrode at the outlet end of the capillary (Figure 2.5). This high voltage outlet electrode was encased in a custom-made chamber as a safety precaution to protect the user from exposure to the electrode. The ground electrode was located on the microscope stage. For additional safety reasons, the entire optical table was grounded to prevent excess charge buildup around the system. The capillary inlet was mounted to a custom-made capillary holder with 3 cm movement in the z direction. The x and y position of the capillary inlet in this system was fixed over the location of cell lysis, determined as described in Section 2.2.2.4. Movement in the z direction allowed the capillary to be raised and lowered into the cell chamber or inlet buffer reservoir as needed. Gravity injections were performed with the capillary at the highest position relative to the microscope stage and outlet buffer reservoir, a 3-cm height difference that initiated hydrodynamic fluid flow into the capillary inlet.

The capillary was threaded through a custom-designed capillary holder that positioned the capillary window in front of the objective through which emission light was

collected. The holder cell was anchored to the CE-LIF Base to hold the capillary in a fixed position relative to the emission objective lens to provide maximum collection stability. The holder cell was designed with a V-groove for precise capillary positioning so that when a new capillary was installed, the detection window remained in the same location each time, reducing the likelihood of having to realign the emission pathway with each new capillary installment. The outlet of the capillary was inserted into the chamber containing the high voltage electrode. In addition to providing a barrier between the user and the high voltage electrode, this chamber was also designed to be completely sealed when a fluid-filled glass vial (03-338A, Fisher) was screwed into position. To wash the capillary, a nitrogen line at 20 psi was attached to the chamber with a simple on/off value to pressurize the chamber and force fluid from the vial through the capillary. An inlet reservoir was created by inverting the cap of a 15 mL centrifuge tube and the microscope stage was positioned with this inlet buffer reservoir below the capillary. When the capillary inlet and ground electrode were immersed in the buffer, electrophoresis could commence by application of a voltage to the outlet electrode. Voltage and data acquisition were controlled through the software described in Section 2.3.2.6.

2.3.2.6 Software and Hardware Interfacing

There were four components linked to the DAQ card through modified BNC cables. The pulsed Nd:YAG laser and the CE power supply were connected to the digital to analog (D/A) converter in the DAQ card and were controlled by user-input values. A 100 ms digital pulse was utilized to trigger the laser when indicated by the user. A sustained voltage specified by the user was applied to the CE power supply to drive electrophoresis. Analog data was converted to digital input by the analog to digital (A/D) converter in the DAQ card.

The analog voltage from the pre-amplifier was converted to a 32 bit digital signal by the A/D converter and recorded by the computer. Additionally, the current readout from the CE power supply across the electrodes was digitized by the A/D converter and recorded by the personal computer.

All hardware control, software data acquisition, and software filtering was performed with a custom-made program in LabVIEW. The code to initialize all hardware was adapted from a program constructed by Alexandra J. Dickinson. A copy of the front panel and select portions of the block diagram can be found in Appendix B. The program utilizes event-based programming to permit the program to remain idle while not in use, allowing the program to remain on and the hardware to remain initialized for immediate use when needed, yet does not slow the computer by running continuously in the background. When a task is requested, the task executes exactly once and then returns the program to idle mode. Tasks included in this event code are: voltage control for an electrokinetic injection of a specified voltage and duration; control of the lysis laser; sequential firing of the laser and an electrokinetic injection; starting a CE run with a specified voltage; and stopping a CE run.

The code executed when the "Start CE" case is called is shown in the block diagram in Appendix B. This code controls the voltage on the HV power supply, initializes the PMT, power supply and DAQ card for sample acquisition, generates a unique file for writing data and collects and displays the data. The user can specify a name or the program will auto-increment a number to identify each separate file. The DAQ collects data from the PMT at 12 kHz and averages this data so that 3,000 data points are averaged for a single output value every 0.25 s. Signal averaging was chosen to reduce the baseline noise and increase the S/N ratio for the system. Signal averaging works by assuming that noise is random with a mean

centered around an average and is not related to signal, while the signal is assumed to be a non-random, positive value. Signal averaging reduces the noise by averaging these random noise values, resulting in a value closer to the average. Because the signal is non-random and positive in value, signal averaging only partially attenuates the signal. The combination of reduced noise and minimal decrease of signal increases the S/N ratio. The S/N ratio increases in proportion to the square root of the number of measurements, so the more measurements taken yields a better S/N ratio, which is directly correlated to the LOD for the system. This unfiltered, averaged data is written directly to an ASCII file where a user can further filter with software if desired. Additionally, to further reduce the noise and enhance the S/N ratio, the collected data is filtered through a 2^{nd} order Butterworth filter (with a frequency of 10 Hz and a low cutoff frequency of 0.5 Hz) and is displayed in real-time on the front panel while also being saved in a separate ASCII file. All data presented in this dissertation utilizing this system was the data filtered through the Butterworth filter, unless specified otherwise.

2.3.3 Instrument Validation

2.3.3.1 CE Optimal Electrophoretic Voltage

Prior to using any new CE system or a new CE buffer, the working voltage ranges must be determined. The van Deemter equation for the open tubular column utilized in CE reduces down to Equation 2.2, indicating that a higher voltage results in smaller plate heights, giving a higher plate count and a better theoretical sensitivity.

Equation 2.2:[59]

$$H = \frac{B}{u}$$

H = theoretical plate height

B = longitudinal diffusion

u = linear velocity

However, in each capillary-buffer system, there is an upper limit to the voltage that can be applied. This upper limit is defined as the voltage at which Joule heat can no longer be effectively dissipated from the solution in the capillary and depends on the size of the capillary, the amount of current-carrying species in the buffer, and the ability to dissipate any heat generated.[59-61] The limit should be determined for each capillary-buffer system utilized as running too far below this limit means the system is not as efficient as it could be and running above this limit causes thermal band-broadening, unstable current and irreproducible results.

In order to determine the optimum running voltage for a 50-μm ID capillary on this system, a 100 mM tris/100 mM tricine, pH 8.1 buffer was loaded into the capillary and the inlet and outlet reservoirs. Varying voltages were applied across the capillary and the resulting current was measured. The current was plotted as a function of voltage (Figure 2.6) and deviation from linearity began just above 12 kV. Above this voltage, the current increased more than theory predicted, indicating Joule heating and ineffective heat dissipation. Based on these results, a run voltage of 12 kV was selected for this particular capillary-buffer system.

2.3.3.2 CE Limit of Detection

Determination of the LOD for this system was important to ensure that the system was aligned properly and achieved an LOD sufficient to detect analytes from single cells. It was also important to establish the LOD measurement as a benchmark for future comparison – a dramatically different LOD would result in sub-optimal performance and indicate system misalignment or capillary compromise. To determine the limit of detection, a known amount of successively higher concentrations of a fluorescein reference standard were electrophoresed and detected with laser-induced fluorescence. The resulting electropherogram was inspected and two values obtained: the height of the baseline noise (an average of three measurements) and the height of the signal peak. The signal to noise ratio was calculated by dividing the signal height by the average height of the noise and the LOD was defined as the amount of fluorescein reference standard required to give a signal to noise ratio of 3. The buffer utilized in this determination was 100 mM tris and 100 mM tricine, pH 8.1 with a voltage of -12 kV applied to the outlet reservoir. A 100 pM solution of fluorescein reference standard was gravity injected at the capillary inlet (0.6 nL, calculated with Eq 2.1) prior to initiation of electrophoresis. The resulting electropherogram and sample measurements can be found in Figure 2.7. The LOD for this system was determined to be 3 x 10^{-20} moles, approximately 10 times higher than the best detection limits of previous systems in this lab, but acceptable for most experiments. The robustness of this system has been tested several times throughout its lifetime, and the LOD remains the same from month to month, indicating acceptable instrument performance.

2.4 Conclusions

The design and construction of a CE-LIF instrument for single cell analysis was presented. The instrument has an excellent limit of detection, as measured using a fluorescent reference standard and compared to similar instrument designs. This instrument converted both the excitation and emission pathways to fiber optics, extending on previous single-cell CE instruments in this lab by eliminating ambient light from the detection pathway and reducing instrument footprint. Cells in custom made chambers can be incubated in warm extracellular buffer, which serves to keep the cells from becoming hypertonic as the solution evaporates. Additionally, this system was constructed to run entirely with LabVIEW software and was utilized for all single cell work presented in this dissertation.

2.5 Figures

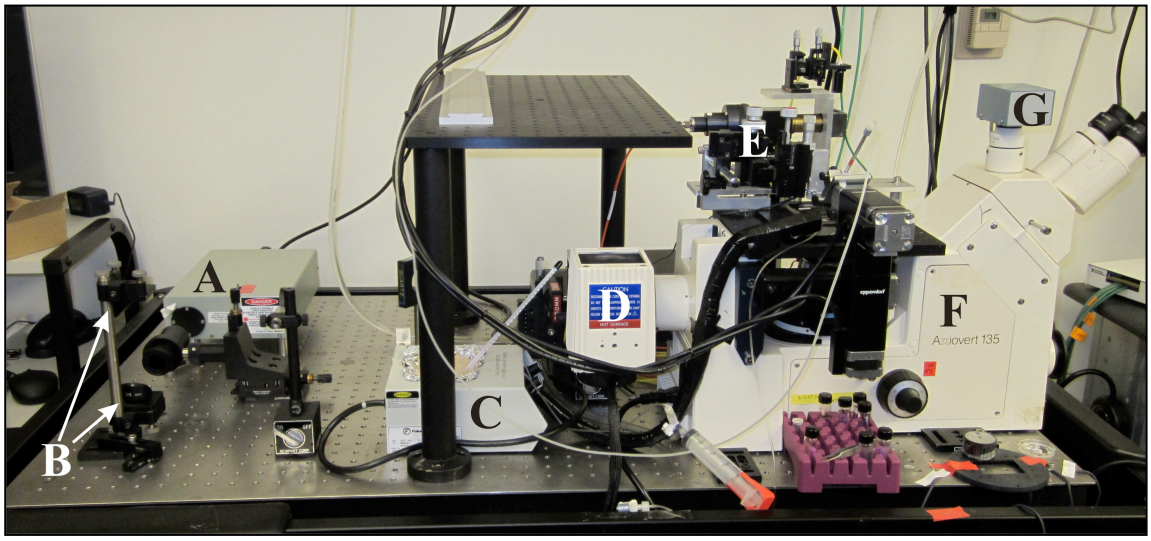

Figure 2.1: The single cell CE-LIF instrument described in this chapter. (A) The laser head for the Nd:YAG laser utilized for cell lysis; (B) the two mirrors used to steer the beam into the back of the microscope; (C) dry bath incubator to keep the ECB flow at approximately 37 ^{o}C; (D) arc lamp; (E) CE system, described in detail in Figure 2.2; (F) Zeiss Axiovert 135 microscope; and (G) CMOS camera connected to computer monitor.

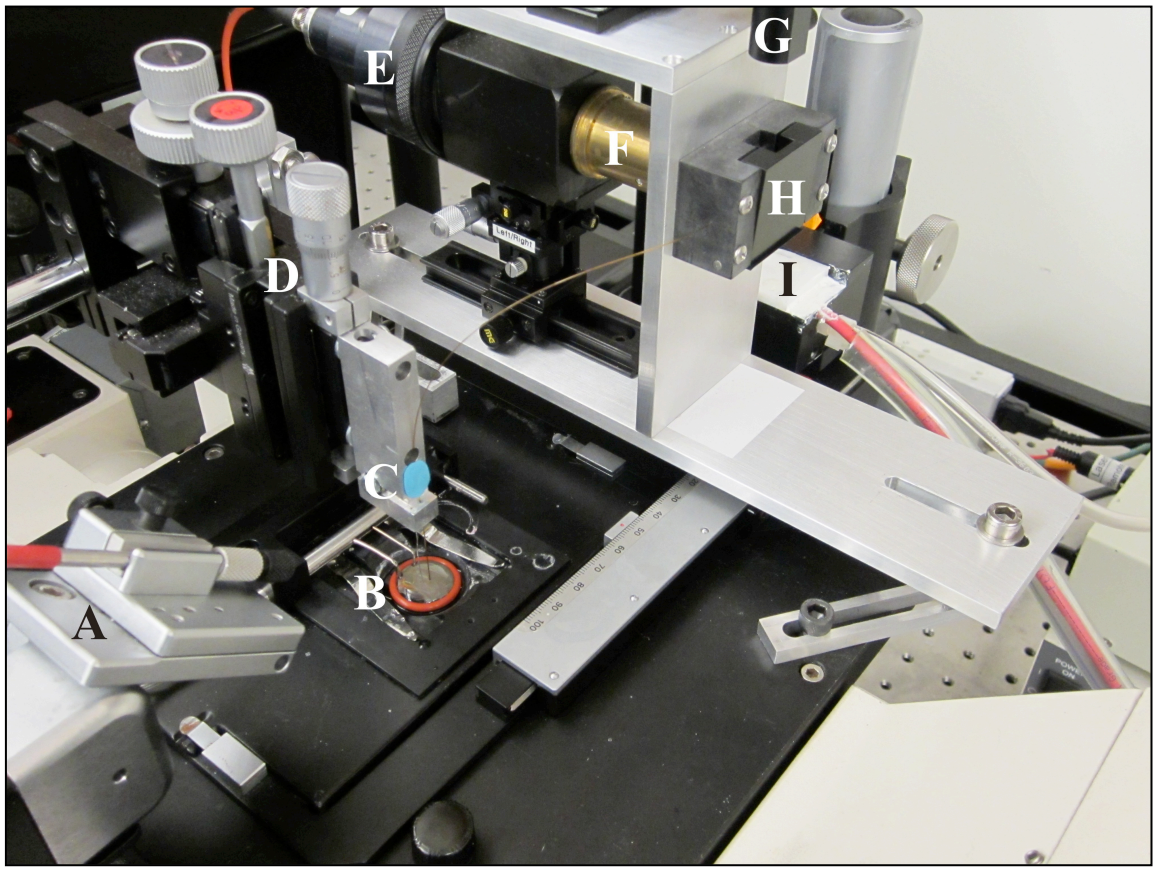

Figure 2.2: The CE portion of the CE-LIF instrument. (A) Microinjector connection; (B) cell chamber and ECB buffer flow inlet and outlet; (C) capillary holder and ground electrode; (D) x, y, and z translation knobs for capillary positioning; (E) collection lens for emission light; (F) microscope objective to collect fluorescence emission at the capillary window; (G) excitation fiber optic holder; (H) capillary holder cell; (I) outlet reservoir, the pink wire is the high voltage line from the CE power supply and the clear tubing is the nitrogen line for pressure driven capillary washing.

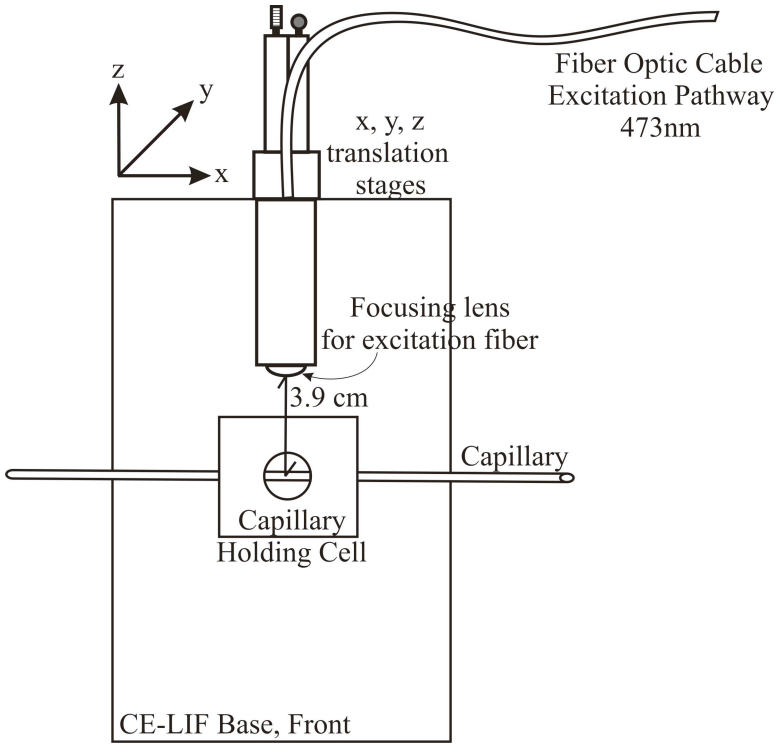

Figure 2.3: Schematic of the excitation pathway for the CE-LIF system. The fiber optic focusing lens is positioned 3.9 cm from the middle of the capillary detection window.

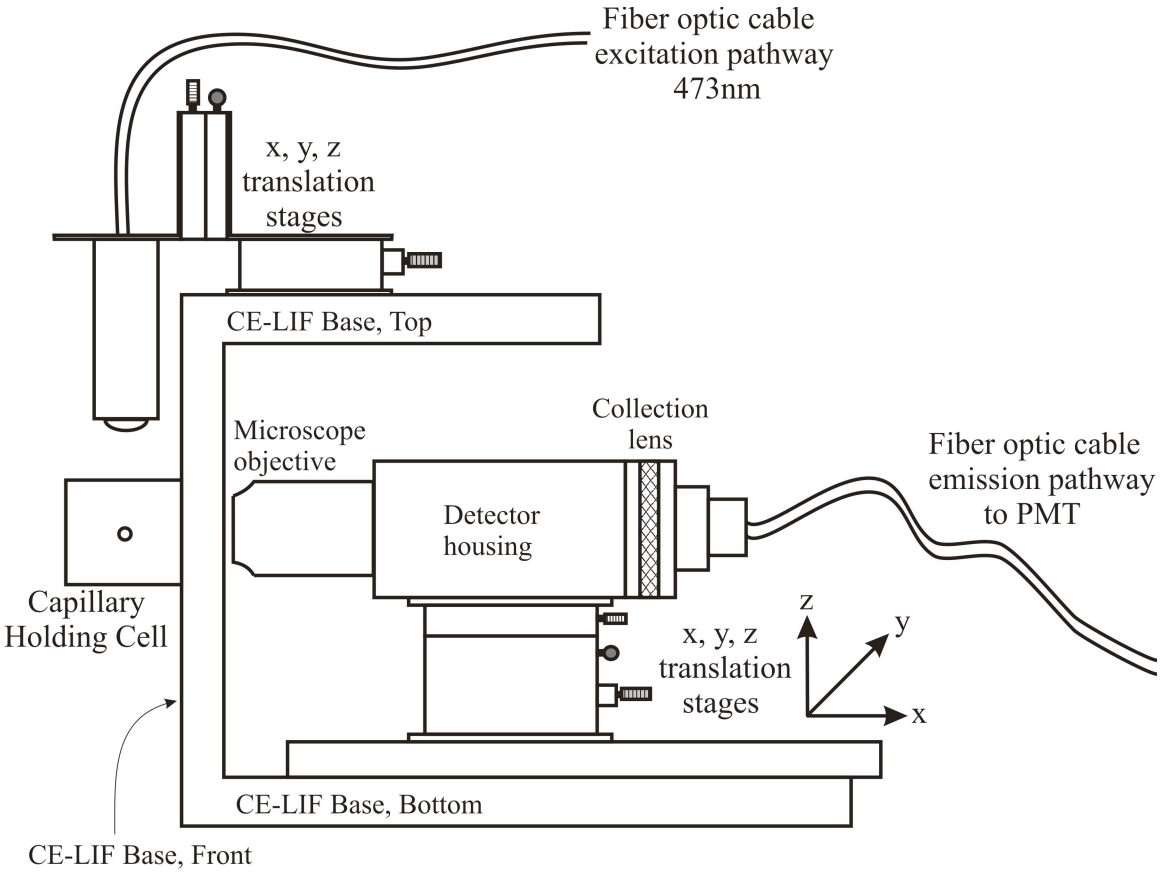

Figure 2.4: Schematic of the emission pathway for the CE-LIF system. The x, y, and z translation stages are adjusted to bring the microscope objective to the correct location for maximum collection of fluorescence emission.

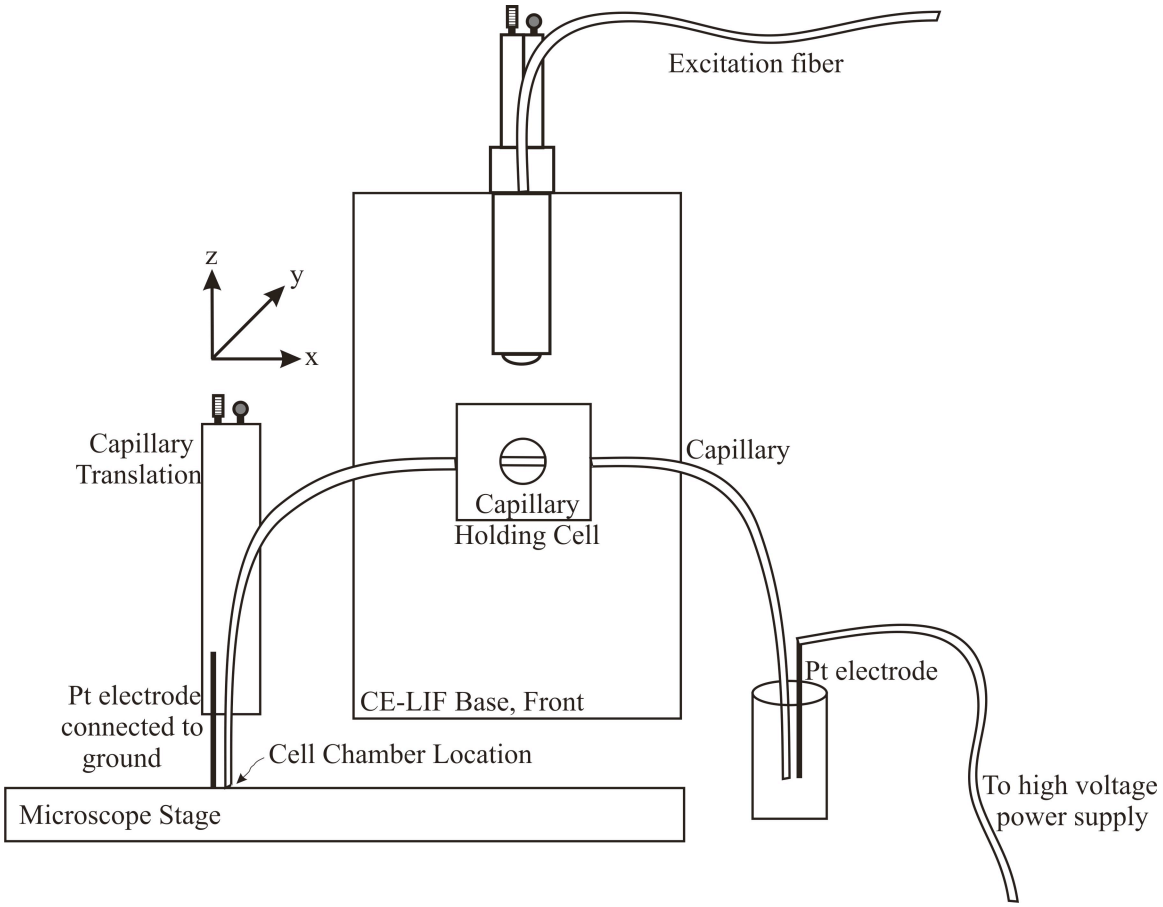

Figure 2.5: Schematic of the capillary electrophoresis portion of the CE-LIF system.

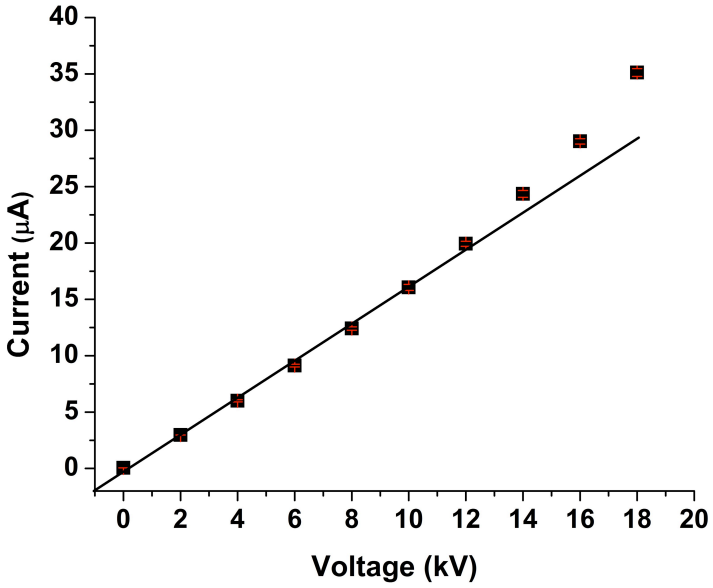

Figure 2.6: An Ohm's plot generated for a 100 mM tris and 100 mM tricine, pH 8.1 buffer on the single cell CE-LIF instrument. The data points are an average of three replicates and the error bars (shown in red) are the standard deviation of three replicates. The line represents theoretical current and voltage relationship.

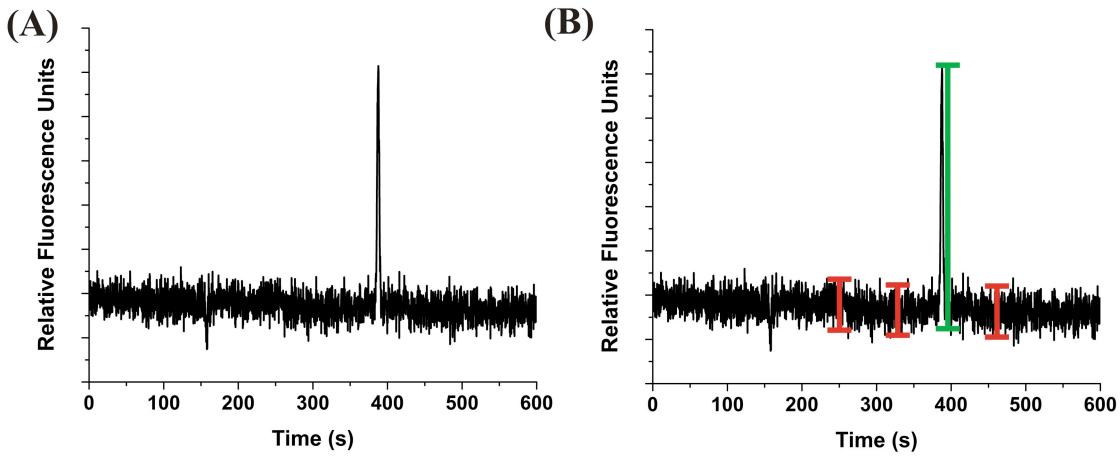

Figure 2.7: Limit of detection calculations for the CE-LIF system. (A) Electropherogram of 100 pM fluorescein reference standard. (B) The red bars show three locations for measuring the height of the noise and the green bar shows the measurement of the signal height.

2.6 References

1 I. G. Arcibal, M. F. Santillo and A. G. Ewing. "Recent Advances in Capillary Electrophoretic Analysis of Individual Cells". *Anal. Bioanal. Chem.,* 2007, *387*, 51-57.

2 L. M. Borland, S. Kottegoda, K. S. Phillips and N. L. Allbritton. "Chemical Analysis of Single Cells". *Annu. Rev. Anal. Chem.,* 2008, *1*, 191-227.

3 R. B. Brown and J. Audet. "Sampling Efficiency of a Single-Cell Capillary Electrophoresis System". *Cytom. Part A,* 2007, *71A*, 882-888.

4 J. A. Jankowski, S. Tracht and J. V. Sweedler. "Assaying single cells with capillary electrophoresis". *Trend. Anal. Chem.,* 1995, *14*, 170-176.

5 S. N. Krylov, D. A. Starke, E. A. Arriaga, Z. Zhang, N. W. C. Chan, M. M. Palcic and N. J. Dovichi. "Instrumentation for Chemical Cytometry". *Anal. Chem.,* 2000, *72*, 872-877.

6 T. Lapainis, S. S. Rubakhin and J. V. Sweedler. "Capillary Electrophoresis with Electrospray Ionization Mass Spectrometric Detection for Single-Cell Metabolomics". *Anal. Chem.,* 2009, *81*, 5858-5864.

7 T. Lapainis and J. V. Sweedler. "Contributions of capillary electrophoresis to neuroscience". *J. Chromatogr. A,* 2008, *1184*, 144-158.

8 J. N. Stuart and J. V. Sweedler. "Single-cell anaylsis by capillary electrophoresis". *Anal. Bioanal. Chem.,* 2003, *375*, 28-29.

9 G. D. Meredith, C. E. Sims, J. S. Soughayer and N. L. Allbritton. "Measurement of kinase activation in single mammalian cells". *Nat. Biotechnol.,* 2000, *18*, 309-312.

10 P. J. Marc, C. E. Sims and N. L. Allbritton. "Coaxial Flow System for Chemical Cytometry". *Anal. Chem.,* 2007, *79*, 9054-9059.

11 P. J. Marc, C. E. Sims, M. Bachman, G. P. Li and N. L. Allbritton. "Fast-lysis cell traps for chemical cytometry". *Lab Chip,* 2008, *8*, 710-716.

12 C. E. Sims and N. L. Allbritton. "Single-cell kinase assays: opening a window onto cell behavior". *Curr. Opin. Biotech.,* 2003, *14*, 23-28.

13 S. L. Petoney and J. V. Sweedler, “Optical Detection Techniques for Capillary Electrophoresis” in *Handbook of Capillary Electrophoresis,* ed. J. P. Landers, CRC Press, Boca Raton, FL, 1994, pp.147-183.

14 A. K. Boardman, S. C. McQuaide, C. Zhu, C. D. Whitmore, M. E. Lidstrom and N. J. Dovichi. "Interface of an Array of Five Capillaries with an Array of One-Nanoliter

Wells for High-Resolution Electrophoretic Analysis as an Approach to High-Throughput Chemical Cytometry". *Anal. Chem.,* 2008, *80*, 7634.

15 S. S. Rubakhin and E. Romanova. "Profiling metabolites and peptides in single cells". *Nat. Med.,* 2011, *8*, S20-S29.

16 R. T. Kennedy, M. D. Oates, B. R. Cooper, B. Nickerson and J. W. Jorgenson. "Microcolumn Separations and the Analysis of Single Cells". *Science,* 1989, *246*, 57-63.

17 T. M. Olefirowicz and A. G. Ewing. "Capillary Electrophoresis in 2 and 5 μm Diameter Capillaries: Application to Cytoplasmic Analysis". *Anal. Chem.,* 1990, *62*, 1872-1876.

18 B. L. Hogan and E. S. Yeung. "Determination of Intracellular Species at the Level of a Single Erythrocyte via Capillary Electrophoresis with Direct and Indirect Fluorescence Detection". *Anal. Chem.,* 1992, *64*, 2841-2845.

19 T. T. Lee and E. S. Yeung. "Quantitative Determination of Native Proteins in Individual Human Erythrocytes by Capillary Zone Electrophoresis with Laser-Induced Fluorescence Detection". *Anal. Chem.,* 1992, *64*, 3045-3051.

20 Q. Xue and E. S. Yeung. "Indirect fluorescence determination of lactate and pyruvate in single erythrocytes by capillary electrophoresis". *J. Chromatogr. A,* 1994, *661*, 287-295.

21 Q. Xue and E. S. Yeung. "Variability of Intracellular Lactate Dehydrogenase Isoenzymes in Single Human Erythrocytes". *Anal. Chem.,* 1994, *66*, 1175-1178.

22 J. Zhao, D. Chen and N. J. Dovichi. "Low-cost laser-induced fluorescence detector for micellar capillary zone electrophoresis". *J. Chromatogr.,* 1992, *608*, 117-120.

23 X. C. Le, W. Tan, C. H. Scaman, A. Szpacenko, E. Arriaga, Y. Zhang, N. J. Dovichi, O. Hindsgaul and M. M. Palcic. "Single cell studies of enzymatic hydrolysis of a tetramethylrhodamine labeled triglucoside in yeast". *Glycobiology,* 1999, *9*, 219-225.

24 S. N. Krylov and N. J. Dovichi. "Single-cell analysis using capillary electrophoresis: Influence of surface support properties on cell injection into the capillary". *Electrophoresis,* 2000, *21*, 767-773.

25 S. Hu, L. Zhang, S. Krylov and N. J. Dovichi. "Cell Cycle-Dependent Protein Fingerprint from a Single Cancer Cell: Image Cytometry Coupled with Single-Cell Capillary Sieving Electrophoresis". *Anal. Chem.,* 2003, *75*, 3495-3501.

26 E. H. Turner, K. Lauterbach, H. R. Pugsley, V. R. Palmer and N. J. Dovichi. "Detection of Green Fluorescent Protein in a Single Bacterium by Capillary Electrophoresis with Laser-Induced Fluorescence". *Anal. Chem.,* 2007, *79*, 778-781.

27 C. D. Whitmore, O. Hindsgaul, M. M. Palcic, R. L. Schnaar and N. J. Dovichi. "Metabolic Cytometry. Glycosphingolipid Metabolism in Single Cells". *Anal. Chem.,* 2007, *79*, 5139-5142.

28 K. Sobhani, S. L. Fink, B. T. Cookson and N. J. Dovichi. "Repeatability of chemical cytometry: 2-DE analysis of single RAW 264.7 macrophage cells". *Electrophoresis,* 2007, *28*, 2308-2313.

29 M. M. Harwood, J. V. Bleecker, P. S. Rabinovitch and N. J. Dovichi. "Cell cycle-dependent characterization of single MCF-7 breast cancer cells by 2-D CE". *Electrophoresis,* 2007, *28*, 932-937.

30 M. M. Harwood, E. S. Christians, M. A. Fazal and N. J. Dovichi. "Single-cell protein analysis of a single mouse embryo by two-dimensional capillary electrophoresis". *J. Chromatogr A,* 2006, *1130*, 190-194.

31 A. Boardman, T. Chang, A. Folch and N. J. Dovichi. "Indium-Tin Oxide Coated Microfabricated Device for the Injection of a Single Cell into a Fused Silica Capillary for Chemical Cytometry". *Anal. Chem.,* 2010, *82*, 9959-9961.

32 R. W. Dapson, "Macromolecular changes caused by formalin fixation and antigen retrieval". *Biotech. Histochem.,* 2007, *82*, 133-140.

33 L. Cruz, L. L. Moroz, R. Gillette and J. V. Sweedler. "Nitrite and Nitrate Levels in Individual Molluscan Neurons: Single-Cell Capillary Electrophoresis Analysis". *J. Neurochem.,* 1997, *69*, 110-115.

34 R. R. Fuller, L. L. Moroz, R. Gillette and J. V. Sweedler. "Single Neuron Analysis by Capillary Electrophoresis with Fluorescence Spectroscopy". *Neuron,* 1998, *20*, 173-181.

35 W. Kim, X. Ye, S. S. Rubakhin and J. V. Sweedler. "Measuring Nitric Oxide in Single Neurons by Capillary Electrophoresis with Laser-Induced Fluorescence: Use of Ascorbate Oxidase in Diaminofluorescein Measurements". *Anal. Chem.,* 2006, *78*, 1859-1865.

36 V. Luzzi, C. Lee and N. L. Allbritton. "Localized Sampling of Cytoplasm from *Xenopus* Oocytes for Capillary Electrophoresis". *Anal. Chem.,* 1997, *69*, 4761-4767.

37 V. Luzzi, C. E. Sims, J. S. Soughayer and N. L. Allbritton. "The Physiologic Concentration of Inositol 1,4,5-Trisphosphate in the Oocytes of *Xenopus laevis*". *J. Biol. Chem.,* 1998, *273*, 28657-28662.

38 V. Luzzi, D. Murtazina and N. L. Allbritton. "Characterization of a Biological Detector Cell for Quantitation of Inositol 1,4,5-Trisphosphate". *Anal. Biochem.,* 2000, *277*, 221-227.

39 C. Lee, J. Linton, J. S. Soughayer, C. E. Sims and N. L. Allbritton. "Localized measurement of kinase activation in oocytes of *Xenopus laevis*". *Nat. Biotechnol.,* 1999, *17*, 759-762.

40 J. Wagner, C. P. Fall, F. Hong, C. E. Sims, N. L. Allbritton, R. A. Fontanilla, I. I. Moraru, L. M. Loew and R. Nuccitelli. "A wave of IP_3 production accompanies the fertilization Ca^{2+} wave in the egg of the frog, *Xenopus laevis*: theoretical and experimental support". *Cell Calcium,* 2004, *35*, 433-447.

41 C. E. Sims, G. D. Meredith, T. B. Krasieva, M. W. Berns, B. J. Tromberg and N. L. Allbritton. "Laser-Micropipet Combination for Single-Cell Analysis". *Anal. Chem.,* 1998, *70*, 4570-4577.

42 H. Li, C. E. Sims, M. Kaluzova, E. J. Stanbridge and N. L. Allbritton. "A Quantitative Single-Cell Assay for Protein Kinase B Reveals Important Insights into the Biochemical Behavior of an Intracellular Substrate Peptide". *Biochemistry,* 2004, *43*, 1599-1608.

43 H. Li, C. E. Sims, H. Y. Wu and N. L. Allbritton. "Spatial Control of Cellular Measurements with the Laser Micropipet". *Anal. Chem.,* 2001, *73*, 4625-4631.

44 J. S. Soughayer, Y. Wang, H. Li, S. Cheung, F. M. Rossi, E. J. Stanbridge, C. E. Sims and N. L. Allbritton. "Characterization of TAT-Mediated Transport of Detachable Kinase Substrates". *Biochemistry,* 2004, *43*, 8528-8540.

45 D. Jiang, C. E. Sims and N. L. Allbritton. "Single-cell analysis of phosphoinositide 3-kinase and phosphatase and tensin homolog activation". *Farday Discuss,* 2011, *149*, 187-200.

46 R. B. Brown, J. A. Hewel, A. Emili and J. Audet. "Single Amino Acid Resolution of Proteolytic Fragments Generated in Individual Cells". *Cytom. Part A,* 2010, *77A*, 347-355.

47 R. B. Brown and J. Audet. "Current techniques for single-cell lysis". *J. R. Soc. Interface,* 2008, *5*, S131-S138.

48 F. Han, Y. Wang, C. E. Sims, M. Bachman, R. Chang, G. P. Li and N. L. Allbritton. "Fast Electrical Lysis of Cells for Capillary Electrophoresis". *Anal. Chem.,* 2003, *75*, 3688-3696.

49 S. Kottegoda, P. C. Aoto, C. E. Sims and N. L. Allbritton. "Biarsenical-Tetracysteine Motif as a Fluorescent Tag for Detection in Capillary Electrophoresis". *Anal. Chem.,* 2008, *80*, 5358-5366.

50 J. K. Grohman, S. Kottegoda, R. J. Gorelick, N. L. Allbritton and K. M. Weeks. "Femtomole SHAPE Reveals Regulatory Structures in the Authentic XMRV RNA Genome". *JACS,* 2011, *133*, 20326-20334.

51 A. Proctor, Q. Wang, D. S. Lawrence and N. L. Allbritton. "Metabolism of peptide reporters in cell lysates and single cells". *Analyst,* 2012, *137*, 3028-3038.

52 D. R. Alessi and P. Cohen. "Mechanism of activation and function of protein kinase B". *Curr. Opin. Genet. Dev.,* 1998, *8*, 55-62.

53 R. Weinberger, *Practical Capillary Electrophoresis*, Academic Press, London, 1993.

54 K. Peck, L. Stryer, A. N. Glazer and R. A. Mathies. "Single-molecule fluorescence detection: Autocorrelation criterion and experimental realization with phycoerythrin". *PNAS,* 1989, *86*, 4087-4091.

55 S. Nie, R. Dadoo and R. N. Zare. "Ultrasensitive Fluorescence Detection of Polycyclic Aromatic Hydrocarbons in Capillary Electrophoresis". *Anal. Chem.,* 1993, *65*, 3571-3575.

56 K. R. Rau, P. A. Quinto-Su, A. N. Hellman and V. Venugopalan. "Pulsed Laser Microbeam-Induced Cell Lysis: Time-Resolved Imaging and Analysis of Hydrodynamic Effects". *Biophys. J.,* 2006, *91*, 317-329.

57 K. R. Rau, A. Guerra III, A. Vogel and V. Venugopalan. "Investigation of laser-induced cell lysis using time-resolved imaging". *Appl. Phys. Lett.,* 2004, *84*, 2940-2942.

58 H. Yin, X. Zhang, N. Pattrick, N. Klauke, H. C. Cordingley, S. J. Haswell and J. M. Cooper. "Influence of Hydrodynamic Conditions on Quantitative Cellular Assays in Microfluidic Systems". *Anal. Chem.,* 2007, *79*, 7139-7144.

59 R. P. Oda and J. P. Landers. “Introduction to Capillary Electrophoresis” in *Handbook of Capillary Electrophoresis,* ed. J. P. Landers, CRC Press, Inc., Boca Raton, FL, 1994, pp. 9-42.

60 E. Grushka, R. M. McCormick and J. J. Kirkland. "Effect of Temperature Gradients on the Efficiency of Capillary Zone Electrophoresis Separations". *Anal. Chem.,* 1989, *61*, 241-246.

61 C. J. Evenhuis, R. M. Guijt, M. Macka, P. J. Marriott and P. R. Haddad. "Temperature Profiles and Heat Dissipation in Capillary Electrophoresis". *Anal. Chem.,* 2006, *78*, 2684-2693.

CHAPTER 3

METABOLISM OF PEPTIDE REPORTERS IN CELL LYSATES AND SINGLE CELLS

3.1 Introduction

3.1.1 Synthetic Peptides as Kinase Substrates and Inhibitors

Synthetic peptides have found widespread use in biomedical research particularly as substrates and inhibitors of kinases and peptidases. The chemistry of solid-phase peptide synthesis is well-defined, permitting relatively straightforward construction of large quantities of peptides comprised of native and non-native amino acids. Peptides have a long shelf life and are readily derivatized with labels such as fluorophores and targeting elements (e.g. biotin). Peptides are an attractive alternative to proteins in a variety of applications (e.g. enzyme assays) due to their chemical simplicity and ease of handling. Furthermore, the substrate preference of many protein kinases is largely determined by the amino acid sequence surrounding the phosphoryl-accepting residue. Consequently, consensus peptide sequences have been defined for large numbers of these enzymes.[1-4] In many cases, these short peptide sequences mimic the kinetic properties of the native protein substrates for the enzyme. For kinases, replacement of the residue that undergoes phosphorylation (serine, threonine, or tyrosine) with a non-phosphorylatable analogue (alanine or phenylalanine) often yields a peptide with excellent inhibitory properties for the targeted kinase.[5, 6] Modifications of a peptide substrate with non-native residues can lead to effective and stable

inhibitors when the inhibitor peptide binds tightly to the substrate binding domain of the kinase and prevents docking of the target substrate.[5, 7] For these reasons, a wide array of substrate and inhibitor peptides are commercially available to manipulate or monitor a plethora of kinase activities in *in vitro* systems.

3.1.2 Peptides as Reporters in Cell Lysates and Single Cells

In addition to their use in assays with purified kinases, peptides are often used to assay kinase activity in cell lysates and also increasingly in intact cells.[8-15] Cell lysates offer a native enzyme in an environment which retains many of the co-factors and other regulatory elements of the cell. Cell lysates can be prepared in large volumes to meet the sensitivity needs of almost any detection strategy. Manipulation of the reaction environment by addition or removal of modifiers or inhibitors is also relatively trivial in a cell lysate compared to intact cells. However, lysates do not recapitulate the environment of an intact cell in a variety of ways. For example, the contents of a cell lysate are diluted and intermixed when intracellular compartments are fragmented during lysis, resulting in a loss of protein compartmentalization as well as normal spatial relationships found in intact cells. Additionally, the heterogeneity of single cell populations has been well documented[16, 17] and cell lysates eliminate this heterogeneity when samples are pooled. For these reasons, intact cells are also used as an assay format in which peptides act as inhibitors or substrates for enzymes.[18-20] The low molecular weight of peptides offers the advantage of efficient loading into cells relative to intact proteins.[21] The loading of substrate peptides into cells followed by lysis and separation of substrate and product by electrophoresis has been performed to track a variety of enzymatic reactions including those of kinases, acyl transferases, and proteases.[22-

[24] This strategy offers direct quantification of the substrate and product quantities as well as the identification of the products of competing reactions with zeptomole detection limits.

3.1.3 Limitations of Peptide Reporters

Despite their benefits as substrates and inhibitors in biomedical research, the use of peptides in the presence of cellular constituents is plagued by unwanted and rapid proteolysis. Exo- and endo-peptidases are an integral part of the protein recycling and antigen processing machinery of cells and ensure that most peptides are rapidly hydrolyzed to their amino acid constituents.[25] While peptidase inhibitors can be used to slow these reactions, they are generally insufficient to eliminate peptide hydrolysis, are often not specific to a single protease, and have significant other off-target effects. Furthermore, many peptidase inhibitors are poorly soluble in aqueous solutions necessitating the use of organic solvents that may interfere with cellular reactions. To prevent peptide bond hydrolysis, a number of alternative strategies have been utilized to impart stability to peptides. Peptide cyclization reduces degradation by creating a fixed secondary structure preventing protease access to the peptide bond.[26-29] Although circularized peptides are excellent at resisting peptidase actions, peptide cyclization can be difficult and is often of low yield due to competing intermolecular reactions. More importantly, cyclization often reduces or eliminates the ability of kinases to phosphorylate the peptide. Another method frequently utilized to impart stability to peptides is the addition of a polyethylene glycol moiety (PEGylation); shorter PEG chains (average molecular weight of approximately 6,000 Da) attached to peptides show better affinity for the targeted enzyme yet less ability to resist degradation than PEGylated peptides with average molecular weights near 25,000 Da.[30-32] The addition of a PEG group greatly increases substrate molecular weight and diminishes the

chemical differences of the substrate and product, making detection and quantification of the substrate and product challenging. The polydispersity of molecular weights in PEG formulations also yields unacceptably broad electrophoretic peaks. Introduction of non-native residues into peptides, which can be achieved with standard solid phase synthesis strategies, has been shown to block unwanted proteolytic reactions. This strategy has been particularly successful in stabilizing inhibitor peptides.[30, 33-38] Extensive libraries of non-native amino acids provide numerous possibilities for the construction of selective inhibitors or substrates, as demonstrated by Lee *et al*. in 2004.[14] However, design of peptides that act as substrates for specific enzymes yet are peptidase resistant has been challenging.

3.1.4 Reporter Peptide Design and Evaluation

A strategy was developed to rationally design a kinase-substrate peptide with increased stability in cell lysates and intact cells. A consensus substrate sequence was selected for Abl kinase and used as the starting point for the design modifications. Abl kinase was chosen because of its role in chronic myelogenous leukemia (CML), where a constitutively active Abl enzyme results from the fusion of the Bcr to Abl protein in a majority of patients with CML.[39] The average rate and locations of lysate-induced cleavage sites in an Abl peptide substrate were identified by capillary electrophoresis. The starting peptide was then modified by replacement of residues adjacent to the identified cleavage site with non-native amino acids and then re-evaluated for peptidase resistance in the cell lysate. The modified peptides were also evaluated for Abl substrate suitability. Multiple cycles of peptide modification and assessment of protease resistance and kinase substrate efficacy generated a final modified peptide that was characterized in a cell lysate. The substrate was also assessed for phosphorylation by Abl relative to the starting sequence. Proteolytic

sensitivity of both the starting peptide sequence as well as the final modified peptide was also assessed in intact single cells.

3.2 Experimental Design

3.2.1 Chemicals

Peptide synthesis reagents were purchased from Aldrich or Fisher except for the following: 2-(6-Chloro-1H-benzotriazole-1-yl)-1,1,3,3-tetramethylaminium hexafluorophosphate (HCTU), 1-(Mesitylene-2-sulfonyl)-3-nitro-1,2,4-triazole (MSNT), 9-Fluorenylmethoxycarbonyl (Fmoc) amino acids, 5-carboxyfluorescien (5-FAM) and resins were received from ChemPep or NovaBiochem; N-Hydroxybenzotriazole (HOBt) was obtained from AnaSpec; and Fmoc-3-(2-Naphthyl)-L-Alanine was purchased from Peptides International. All other chemicals used in the assays were procured from Fisher or Sigma except for the following: Active Abl-1 enzyme was purchased from Invitrogen; bovine serum albumin (BSA) was received from Calbiochem; Roswell Park Memorial Institute Media (RPMI-1640) and Dulbecco's Modified Eagle's Medium (DMEM) were obtained from Cellgro; Penicillin/streptomycin was procured from Gibco; and fetal bovine serum (FBS) was purchased from Atlanta Biologicals.

3.2.2 Peptide Synthesis and Preparation

3.2.2.1 Synthesis of Full-Length Peptides Amidated on the C-Terminus

All peptides were synthesized by collaborator Dr. Qunzhao Wang in the Lawrence Lab unless specified otherwise. A detailed table of all peptides prepared and utilized in this dissertation can be found in Appendix C. Full-length substrate peptides with an amidated C terminus were synthesized via standard Fmoc peptide synthesis (Prelude Peptide Synthesizer, Protein Technologies, Tucson, AZ) utilizing TGR resin. Coupling was performed with two 5

min incubations in dimethylformamide (DMF) with 5 equivalents (eq) amino acid, 5 eq HCTU, and 10 eq N,N-Diisopropylethylamine (DIPEA). Fmoc deprotection was achieved with two 2.5 min incubations with 20% piperidine in DMF. The free N-terminus was reacted with 5 eq 5-FAM, 5 eq diisopropylcarbodiimide (DIC), and 5 eq HOBt in DMF overnight, then treated with 30% piperidine in DMF for 30 min. The peptide was cleaved with trifluoroacetic acid:water:triisopropylsilane (TFA:H_2O:TIS) in a ratio of 95:2.5:2.5, precipitated with ether, and dried in air. Peptide purity was assessed with HPLC-MS and further purification via HPLC was performed if needed. Peptides were dissolved in Tris buffer, pH 7.5, aliquoted, and stored at -80 ^{o}C.

3.2.2.2 Alternative Coupling for Difficult Amino Acids

In some instances, amino acids were coupled overnight in N-Methyl-2-pyrrolidone (NMP) with 5 eq amino acid, 5 eq bromo-tris-pyrrolidino phosphonium hexafluorophosphate (PyBrop), and 10 eq DIPEA. Capping with acetic anhydride was performed if necessary based on a ninhydrin test. Remaining amino acids were coupled as described in section 3.2.2.1. Product formation was assessed using HPLC-MS.

3.2.2.3 Synthesis of Peptide Fragment Standards

Peptide fragment standards with a free carboxylic acid at the peptide C terminus were synthesized using either a Wang or 2-Chlorotrityl resin. When using the Wang resin, 10 eq of the first Fmoc amino acid in CH_2Cl_2 was reacted with 7.5 eq 1-methylimidazole and 10 eq MSNT for 15 minutes in a dry glass vial on a shaker. The reaction mixture was transferred to another dry glass vial containing the Wang resin and incubated for 1 h. For the 2-Chlorotrityl resin, 1 eq of the first Fmoc amino acid and 4 eq DIPEA in dry CH_2Cl_2 was

reacted with the 2-Chlorotrityl resin for 2 h in a dry glass vial on a shaker. The remaining amino acids were attached as described in section 3.2.2.1 or 3.2.2.2.

3.2.3 Cell Culture

Baf/BCR-ABL cells are a mouse B-cell lymphoma line that was stably transfected with and overexpress Bcr-Abl.[40] HeLa cells were obtained from the American Type Culture Collection. Baf/BCR-ABL cells were cultured in RPMI-1640 medium supplemented with 10% FBS, penicillin (100 units/mL) and streptomycin (100 μg/mL). HeLa cells were cultured in DMEM medium supplemented with 10% FBS, penicillin (100 units/mL) and streptomycin (100 μg/mL). All cells were maintained in a humidified atmosphere of 37 ^{o}C in 5% CO_2 and passaged into fresh media every 2 – 3 days. HeLa cells used for single cell-CE experiments were plated the day before onto custom chambers, prepared by using poly(dimethyl siloxane) (PDMS, Sylgard 184) to glue a silicon O-ring (McMaster-Carr) to a #1 glass coverslip (Fisher). A dilute cell suspension was added to 500 μL of DMEM media in the chamber and the chambers were placed in the humidified incubator until use in the experiments.

3.2.4 Measurement of Peptide Degradation in a Cell Lysate

Baf/BCR-ABL cells were collected from two confluent 75 cm^2 flasks and were washed with and resuspended in phosphate buffered saline (PBS; 137 mM NaCl, 10 mM Na_2HPO_4, 27 mM KCl, 1.75 mM KH_2PO_4, pH 7.4). The cells were submerged in liquid nitrogen for 1 min and rapidly thawed at 37 ^{o}C for a total of three cycles. The mixture was centrifuged at 14,000 x g for 5 min at 4 ^{o}C. The supernatant was transferred to a clean centrifuge tube and maintained on ice until use in the assay. Total protein concentration in the supernatant was measured using fluorescamine.[41] Briefly, fluorescamine (10 μL, 3

mg/mL in acetone) was added to a cell lysate (30 μL) and incubated for 5 min at 25 ^{o}C. Fluorescence was measured with a fluorescence plate reader (SpectraMax M5, Molecular Devices, Sunnyvale, CA) with an excitation of 390 nm (bandwidth of 9 nm) and emission of 475 nm (bandwidth of 15 nm).

Assay of peptide degradation was performed by mixing peptide (1 μM) with the Baf/BCR-ABL cell lysate (3 mg/mL total cell protein) and incubating at 37 ^{o}C for 1 h. Aliquots were removed from the reaction mixture at various time intervals. The reactions were stopped by adding HCl to a final concentration of 100 mM. A 0 min timepoint was prepared by adding the HCl to the lysate prior to addition of the substrate peptide. Reaction mixtures were then separated by capillary electrophoresis and detected by LIF. Peptide fragments were identified by adding standards (250 nM) to the HCl-terminated aliquots and comparing the electropherograms with and without the added standard. The average initial degradation and fragmentation rates were calculated using the first two time points by monitoring the change in peptide amount divided by the change in time per amount cytosolic protein. The units are defined as zmol of peptide per pg of cytosolic protein per s, or zmol pg^{-1} s^{-1}.

3.2.5 *in vitro* Kinase Assay

Protein kinase assays were performed at 30 ^{o}C in assay buffer [50 mM Tris (pH 7.4), 5 mM $MgCl_2$, 1 mM $MnCl_2$, 2 mM DTT, 1 mM ATP] with Abl-1 kinase (12 nM) and substrate (29 μM). Aliquots were then removed from the reaction mixture at varying times. The reactions were stopped by heating at 90 ^{o}C for 4 min. Additionally, a negative control with no ATP was simultaneously assayed and sampled. The amount of peptide phosphorylation was measured using capillary electrophoresis coupled with laser-induced

fluorescence to separate the substrates and products and quantify peak areas. The samples with and without ATP were compared to identify the phosphorylated product and the non-phosphorylated precursor (Figure 3.1).

3.2.6 Measurement of Kinetic Parameters

Protein kinase assays were performed as described in section 3.2.5 with the following exceptions: substrate concentration ranged from 10 to 100 μM; Abl-1 (Invitrogen, Carlsbad, CA) enzyme concentration was 12 nM for QW-III-67B and 6 nM for QW-V-48B. The immobilized metal ion affinity-based fluorescent polarization (IMAP) assay (Molecular Devices Corp., Sunnyvale, CA) was used to measure the amount of phosphorylated peptide in reaction mixtures (http://www.moleculardevices.com/pages/reagents/imap.html). A calibration curve was constructed by measuring the anisotropy of solutions with known ratios of phosphorylated to non-phosphorylated peptide. The standard with 100% phosphorylated peptide was prepared using Abl-1 kinase and the percentage phosphorylation was verified with capillary electrophoresis. Anisotropy was measured using a fluorescence plate reader (SpectraMax M5, Molecular Devices, Sunnyvale, CA) with an excitation of 485 nm (bandwidth of 9 nm) and emission of 525 nm (bandwidth of 15 nm). Samples were diluted to the working concentration of 100 nM for the IMAP assay with a buffer containing 10 mM Tris-HCl (pH 7.2), 10 mM $MgCl_2$, and 0.01% Tween-20.

3.2.7 Capillary Electrophoresis

Laser-induced fluorescence (LIF, 488 nm) was used for peptide detection during capillary electrophoresis (ProteomeLab PA800, Beckman Coulter, Fullerton, CA). Fused-silica capillaries [50 μm inner diameter, 360 μm outer diameter, (Polymicro Technologies, Phoenix, AZ)] had a total length of 30 cm with an effective length of 20 cm. Capillaries

were conditioned prior to use with 0.1 M NaOH for 12 h, H_2O for 1 h, 0.1 M HCl for 6 h, and H_2O again for 12 h. After each sample, the capillary was sequentially rinsed with 1 M NaOH, H_2O, and buffer for 2 min by applying a pressure of 20 psi to the capillary inlet. A sample plug was hydrodynamically loaded into the capillary by applying 0.5 psi to the inlet for 5 s. Electrophoresis was initiated by application of a negative voltage to the outlet. For the assays employing a cell lysate, the electrophoretic buffer was 100 mM Tris and 100 mM Tricine, pH 8.1 and the field strength was 500 V/cm. For the *in vitro* kinase assay samples, the electrophoretic buffer was 100 mM Tris, 100 mM Tricine and 5 mM SDS, pH 8.1 and field strength was 600 V/cm. The data was analyzed using commercial software (32 Karat, version 8.0, Beckman Coulter, Fullerton, CA).

3.2.8 Single Cell Capillary Electrophoresis

Single cell capillary electrophoresis was performed using the custom-made CE system with LIF detection as described in detail in Chapter 2 of this dissertation. Fused-silica capillaries [30 μm inner diameter, 360 μm outer diameter, (Polymicro Technologies, Phoenix, AZ)] with a total length of 38 cm and an effective length of 21.5 cm were conditioned as described above. A negative voltage of 14 kV was applied to the outlet reservoir while the inlet reservoir was held at ground. The electrophoretic buffer was 100 mM Tris and 100 mM Tricine, pH 8.1. Cells were perfused with extracellular buffer (ECB; 135 mM NaCl, 5 mM KCl, 1 mM $MgCl_2$, 1 mM $CaCl_2$, and 10 mM HEPES, pH 7.4, 25 ^oC) during experiments, with the flow turned off immediately prior to cell lysis and loading into the capillary. Laser-based cell lysis was achieved with a focused Nd:YAG laser as previously described in Chapter 2. To identify peptide fragments formed in cells, standards of peptide fragments (100 nM) were hydrodynamically loaded into the capillary immediately

following loading of a single HeLa cell into the capillary. The HeLa cell was not loaded with peptide prior to loading into the capillary. The lysed HeLa cell provided a milieu for the subsequently loaded standards similar to that for peptide obtained from a lysed cell. To calibrate the amount of peptide on the electropherograms, a known concentration of a standard of each intact peptide was hydrodynamically loaded into the capillary, electrophoresed, and the area under the peak calculated. Poiseuille's equation (Equation 2.1) was utilized to estimate the amount of peptide injected, as demonstrated by Meredith *et al*.[22] Data was collected with the custom software described in Chapter 2 (LabVIEW 9.0.1, National Instruments, Austin, TX) and analyzed utilizing Origin software (version 7.5, OriginLab Corporation, Northampton, MA).

3.3 Results and Discussion

3.3.1 Selection of the Starting Peptide

The starting peptide QW-III-67B (5FAM-GGAYAAPFKKKA) is based on a related sequence obtained from an oriented peptide library by Songyang *et al.* directed at determining tyrosine kinase specificity.[42] The Songyang substrate was phosphorylated with good efficiency by Abl and was minimally phosphorylated by Src, a close relative of Abl that shares a similar consensus sequence. Another similar sequence has been shown to have good efficiency for both Abl and Bcr-Abl.[43] Based on these favorable properties and the good specificity for Abl kinase, peptide QW-III-67B was chosen as the starting peptide for this work.

3.3.2 Characterization of Peptide QW-III-67B Degradation in Cytosolic Lysates

To determine whether the peptide QW-III-67B is degraded by cytosolic peptidases, the peptide was incubated in a Baf/BCR-ABL cell lysate. After varying times, aliquots were removed and separated by electrophoresis followed by detection of all fluorescent peptides (Figure 3.2A-3.2C). At time zero, a single peak with a migration time identical to that of the standard intact peptide QW-III-67B was present. Within one minute, three peaks were seen, the intact peptide and two peaks with longer migration times. Under these conditions, the starting peptide possessed a half-life of 1.3 ± 0.4 min in the cytosolic lysate. The average rate of peptide breakdown in the cell lysate over 5 min was 1.7 ± 0.3 zmol pg^{-1} s^{-1} and approximately 6.2 ± 2.7 % of the intact peptide remained after 5 min. After 30 min, the initial peak was no longer identified and five additional peaks had formed, all with migration times slower than the intact peptide. Given the presence of peptidases in a cytosolic lysate, it was likely that these peaks were proteolytic fragments of the intact starting substrate. In order to determine the temporal pattern of fragment formation, the percentage of each fragment with respect to total peptide was plotted as a function of time (Figure 3.2D). The initial fragment was generated nearly as fast as the intact peptide was degraded, with an average initial rate of 1.2 ± 0.1 zmol pg^{-1} s^{-1}. It is possible that the later appearing fragments were formed as a consequence of further peptidase action on the first fragment. Phosphorylated product was not observed since neither ATP nor phosphatase inhibitors were present in the assay.

To compare the breakdown of QW-III-67B in lysates generated with different cells, the peptide was incubated in a HeLa cell lysate. During various times, aliquots were removed and separated by capillary electrophoresis. A peptide-fragment pattern similar to

that observed in the Baf/BCR-ABL lysate was present (Figure 3.2E). The initial rate of breakdown in the HeLa cell lysate was 1.3 zmol pg^{-1} s^{-1}, similar to that in the Baf/BCR-ABL lysate. Additionally, the major fragment that formed over time possessed a migration time identical to the major peak formed in the Baf/BCR-ABL lysate. This product formed at a rate of 1 zmol pg^{-1} s^{-1}, nearly identical to the result in the Baf/BCR-ABL lysate. Two additional peaks formed on slower time scales and the migration times of these peaks matched the two secondary peaks formed in the Baf/BCR-ABL lysate. The pattern and rate of breakdown in HeLa and Baf/BCR-ABL lysates was very similar despite the difference in species and tumor type. For this reason, subsequent lysate experiments utilized only the Baf/BCR-ABL cells.

3.3.3 Characterization of Peptides Following Lysine Replacement

Since trypsin-like proteases are common in cells and favor positively charged residues, the initial cleavage site was thought to be at one of the lysine residues near the carboxy terminus of the peptide.[44] Ornithine, a lysine analog, possesses a positively charged side chain but with one less carbon (Figure 3.3). Replacement of lysine with ornithine has been shown to limit the ability of trypsin to act on lysine-containing substrates.[45] Peptides with ornithine inserted into the peptide in place of one, two, or all three lysine residues (peptides QW-III-90A through QW-III-90G in Table 3.1) were synthesized, purified, and then incubated in the Baf/BCR-ABL cytosolic lysate for varying times. Aliquots were removed and electrophoresed to assess the formation of fluorescent fragments. The resulting traces were very similar to that of the control peptide, with the initial timepoint for each peptide showing a single peak that migrated at the same time as the intact parent. Subsequent time points demonstrated the disappearance of the initial peak and the

appearance of multiple peaks with slower migration times, presumably fragment peptides of the lysine-substituted peptides. To determine the pattern of fragment formation, the fraction of peptide present as each fragment was plotted as a function of time, with results for each of the seven modified peptides appearing very similar to that of the starting peptide QW-III-67B (Figure 3.4). Irrespective of the number or location, ornithine-for-lysine substitution provided only a modest enhancement in stability relative to that of the starting peptide, with the peptide half-lives ($t_{1/2}$) in the lysate ranging from 4.3 to 6.0 min compared to the 1.3 min for the starting peptide (Table 3.1).

To determine whether the ornithine-for-lysine-substituted peptides retain the ability to be phosphorylated by Abl kinase, each modified peptide was incubated with Abl kinase *in vitro* and aliquots were removed over time and separated. The relative peak areas of the phosphorylated and non-phosphorylated peptides were used as a measure of the Abl substrate efficacy. Half of the ornithine-containing peptides were phosphorylated at a faster rate than that of the QW-III-67B peptide. When the time for 50% peptide phosphorylation ($t_{50\%P}$) was measured, three of the double-ornithine peptides and one of the single-ornithine peptides achieved a 1.7-6X shorter $t_{50\%P}$ than that of QW-III-67B. The remaining single and triple-ornithine peptides were phosphorylated more slowly than QW-III-67B with a 3-4X greater $t_{50\%P}$. While peptidase resistance was slightly improved and kinase substrate suitability was acceptable, the ornithine-containing peptides did not possess dramatically improved proteolytic resistance relative to the starting peptide, suggesting that the lysine residues might not be the initial site of cleavage.

3.3.4 Identification of the Peptide Fragments

To identify the primary site of peptide-bond hydrolysis, standards consisting of all possible fluorescent peptide fragments formed from QW-III-67B were synthesized and characterized by electrophoresis. Under the electrophoretic conditions used, each peptide fragment migrated at a unique time and was present as a single major peak. Thus, the fragments formed and peptide cleavage sites targeted by the cytosolic lysate should be readily identifiable. The starting peptide, QW-III-67B, was incubated in a cell lysate and after the reaction was stopped, each of the possible fluorescent peptide standards was sequentially added to the lysate mixture to identify the lysate peaks. Each peak present in the cytosolic lysate matched to a fragment peak suggesting that the additional peaks on the electropherogram were indeed fragments of the original peptide (Figure 3.2). A 7-residue fragment (peptide f) generated by cleavage at the proline-phenylalanine bond formed initially and in the greatest quantity. 3, 4, and 5-residue fragments also formed over time but with a delay relative to that of the 7-mer. Since the proline-phenylalanine bond appeared to be the site of initial peptide cleavage, these residues were targeted for modification to enhance stability.

3.3.5 Characterization of Peptides with Proline Replacement

The proline and phenylalanine in QW-III-67B were replaced with native and non-native residues (Figure 3.3) and peptide stability assessed. Proline has a structure unique to the native residues in that the backbone nitrogen is linked via a ring to the side chain, creating a bend in the peptide backbone. Three strategies were attempted to replace the proline with a goal of diminishing peptidase rather than kinase action: *i)* an alanine was inserted in place of the proline to eliminate the bend in the peptide backbone; *ii)* native

residues with a side chain ring were substituted to maintain a similar side chain character while still eliminating the backbone bend; and *iii)* the non-native residue sarcosine (N-methylglycine) was used to maintain the backbone kink yet eliminate the closed-ring structure.[46] Peptides QW-IV-74A to QW-V-74E (Table 3.1) were synthesized, purified, incubated in a cytosolic lysate and then separated by CE to determine whether fluorescent fragments were formed. In each case, approximately eight fluorescent fragments were seen within 5 min of incubation in the lysate. Although these fragment peaks grew larger over time, additional peaks were not observed. To compare the peptidase resistance of these peptides to that of the prior peptides, the percentage of peptide fragment over time was measured and the $t_{1/2}$ calculated. The $t_{1/2}$ of all of the proline-substituted peptides was improved relative to that of the starting peptide QW-III-67B and the ornithine-containing peptides (Table 3.1). The peptide possessing a sarcosine displayed the most dramatic increase in stability with a $t_{1/2}$ of 24.0 min compared to the 1.3 min of the starting peptide (Figure 3.5A).

To determine whether the proline-substituted peptides also retained the ability to be phosphorylated by Abl kinase, each modified peptide was incubated with Abl kinase *in vitro* and phosphorylation measured over time. Minimal phosphorylation was observed for each of the five peptides over the assay period. Based on the measured phosphorylation rate, $t_{50\%P}$ for all of these peptides was estimated to be $>10^5$ min or >650-times longer than the 150 min of the starting peptide (Figure 3.5B). Despite the increased peptidase resistance, the poor substrate efficacy of the proline-substituted peptides rendered these modifications unsuitable for the creation of protease-resistant Abl kinase substrates.

3.3.6 Characterization of Peptides with Phenylalanine Replacement

Phenylalanine possesses a bulky hydrophobic side group, and therefore non-native residues with similar features, including β-(2-naphthyl)-L-alanine and 3-nitrotyrosine, were substituted in place of phenylalanine (Figure 3.3). Since both N-methylated and D-amino acids have been shown to impart stability to inhibitor peptides, D-phenylalanine and (N-methyl)phenylalanine were also incorporated as replacements for phenylalanine.[27, 35, 36, 38] Peptides QW-IV-85B through QW-V-23E (Table 3.1) were synthesized, purified, and then incubated in the Baf/BCR-ABL cytosolic lysate for varying times. Aliquots were removed and electrophoresed to assess the formation of fluorescent fragments. Within 1 min, the β-(2-naphthyl)-L-alanine-substituted peptide showed the appearance of a second peak in the electropherogram with a migration time slower than the intact peptide. This second peak grew larger over the course of the assay, and a much smaller, slower migrating peak first appeared after 30 min incubation. The intact peptide disappeared between 15 and 30 min. A similar pattern and time course was also observed for the 3-nitrotyrosine-substituted peptide. The electropherogram of the lysate-incubated, D-phenylalanine peptide did not show additional peaks until after 5 min of incubation. Unlike the prior two peptides, 30% of the D-phenylalanine peptide remained intact at 60 min. The (N-methyl)phenylalanine-substituted peptide showed results similar to that of the D-phenylalanine-substituted peptide but had an even slower rate of fragment formation with 70% of the peptide co-migrating with that of the starting peptide after 60 min (Figure 3.6). At this time, 5 additional peaks were present on the electropherogram of the (N-methyl)phenylalanine-substituted peptide. To compare cytosolic peptidase resistance among these peptides, the amount of intact peptide was plotted as a function of time and $t_{1/2}$ was calculated. As expected, the (N-methyl)phenylalanine-

substituted peptide showed the most dramatic increase in lifetime, with a 40-fold increase relative to that of the starting peptide QW-III-67B (Figure 3.5A). The D-phenylalanine-substituted peptide was also longer lived with a 30-fold increase in $t_{1/2}$. The remaining two peptides showed more modest results, with a 4- to 7-fold increase in peptide lifetime (Figure 3.5A).

The ability of each phenylalanine-modified peptide to be phosphorylated *in vitro* by Abl kinase was also assessed as described above. Two of the peptides, the (N-methyl) phenylalanine- and the 3-nitrotyrosine-substituted peptides, showed minimal phosphorylation, with $t_{50\%P} > 10^5$ min (Figure 3.5B). The β-(2-naphthyl)-L-alanine- and the D-phenylalanine-substituted peptides were phosphorylated at similar rates to the parent peptide with a $t_{50\%P}$ of 190 and 82 min, respectively (Figure 3.5B).

3.3.7 Design and Characterization of an (N-methyl)phenylalanine-substituted Lead Peptide

The (N-methyl)phenylalanine-substituted peptide QW-IV-85B was the most promising peptide with respect to peptidase resistance but performed poorly as an Abl substrate. Placement of an isoleucine in the position immediately upstream of the phosphorylatable tyrosine has been shown to improve Abl phosphorylation efficiency of some substrates, but can make the peptide more suitable for phosphorylation by Src.[4, 42] To improve the substrate behavior of the (N-methyl)phenylalanine-substituted peptide, the alanine adjacent to the tyrosine was replaced with an isoleucine. This new peptide (QW-V-48B in Table 3.1) was characterized for peptidase resistance as well as Abl- and Src-substrate performance. After a 3 min incubation in the cytosolic lysate, a small peak in addition to QW-V-48B appeared. Over a 5 min time, the average rate of breakdown was 0.20 ± 0.03 zmol pg^{-1} s^{-1} and 79.6 ± 2.5% remained intact in the lysate. By 10 min, the second peak had

increased and was accompanied by two additional peaks. The $t_{1/2}$ of this peptide was 19.1 ± 3.3 min or 15-fold longer than that of the starting peptide yet >2 fold less than that of the peptide without isoleucine (Table 3.1, Figure 3.5A). To determine whether this peptide was a substrate for Src, the peptide was incubated with various concentrations of Src kinase and the amount of phosphorylation measured. At all concentrations, no phosphorylation by Src was observed (Figure 3.7). To determine whether the isoleucine improved Abl-substrate performance, the QW-V-48B peptide was incubated with Abl kinase and the amount of phosphorylation measured. Incorporation of the isoleucine decreased the $t_{50\%P}$ by >2000-fold relative to that of the peptide with only the (N-methyl)phenylalanine-substitution (Figure 3.5B). The isoleucine peptide also possessed a 3.5X lower $t_{50\%P}$ than the original starting peptide. Based on the combined ability of this peptide to resist degradation, resist Src phosphorylation yet remain a substrate for Abl, peptide QW-V-48B was chosen for further characterization and evaluation.

3.3.8 Characterization of the Lead Peptide QW-V-48B in a Cytosolic Lysate

Although the lead peptide QW-V-48B possessed a substantially increased lifetime relative to that of the starting peptide QW-III-67B, QW-V-48B was still degraded into multiple different fragments over time. In order to understand which residues were the preferred sites of cleavage, all possible fluorescent fragments were synthesized and characterized by electrophoresis. Under the electrophoretic conditions used, all of these fragment peptides were resolved from each other and from the parent peptide. The lead peptide, QW-V-48B, was incubated in a Baf/BCR-ABL cell lysate and each of the possible fluorescent peptide standards were sequentially added to the mixture to identify the unknown peaks in the electropherogram. Each of the peaks present in the cytosolic lysate was matched

to a fragment peak (Figure 3.8). The first fragment formed was a 5-residue peptide cleaved at the alanine-alanine bond (peptide t) (Figure 3.8B, E). The amount of each fragment graphed as a function of time (Figure 3.8D) demonstrated that the 5-mer formed at an initial average rate of 0.11 ± 0.02 zmol pg^{-1} s^{-1} and accounted for approximately 50% of all peptide present by 60 min (Figure 3.8D). Other peptides that formed over time were the 3, 4, and 11-residue fragments, but they formed on longer time scales relative to that of the 5-mer (Figure 3.8C). Significantly, there was no evidence of the 7-mer fragment that would be generated from cleavage between the proline and (N-methyl)phenylalanine. Thus the substitution of (N-methyl)phenylalanine for phenylalanine greatly enhanced resistance to proteolysis.

The kinetic parameters of K_M and k_{cat} were determined for both peptides in order to quantitatively compare the ability of the starting peptide and lead peptide to act as substrates for Abl. Varying concentrations of each peptide were incubated with Abl kinase and the initial reaction velocity calculated. Peptide QW-V-48B had a lower K_M than QW-III-67B (20 μM compared to 58 μM) and also a higher turnover number, (k_{cat} = 3,000 min^{-1} compared to 2,100 min^{-1}). The lead peptide QW-V-48B was both a better Abl substrate and possessed greater peptidase resistance than the starting peptide QW-III-67B.

3.3.9 Characterization of Peptides in Single HeLa Cells

Although use of cytosolic lysates enables facile optimization of substrate peptide properties, most cellular processes are dramatically altered in this homogenous, diluted environment. In particular, peptidases located within organelles are expected to be released upon cell lysis. Thus a peptide in a cell lysate may encounter a different repertoire of peptidases relative to a peptide in the cytosol of an intact cell and it is important to understand whether the peptide fragments and fragmentation rates from a lysate faithfully

mimic that formed in intact cells. In order to assess and quantify the peptide fragments generated in single cells, peptide QW-III-67B was microinjected into a single HeLa cell (24 ± 8 amol, n = 4 cells). HeLa cells were utilized for single cell studies since they were more easily microinjected than non-adherent cells and possessed a similar fragmentation profile to that of Baf/BCR-ABL cell lysates (Figure 3.2E). After a 5 min incubation, cells were lysed and loaded into an overlying capillary and the different fluorescent peptides detected and quantified.[47] The peptide was nearly completely metabolized, with only 10 ± 2 % remaining intact (Table 3.2). Under the conditions used, the average rate of QW-III-67B degradation was calculated to be 0.7 ± 0.2 zmol pg^{-1} s^{-1} assuming a cellular protein concentration of 100 mg/mL and a cell volume of 1 pL.[48] Nine different peaks were observed on the electropherogram (Figure 3.9A), compared to the six peaks seen in the lysate samples (Figure 3.2C). The peptide fragment standards were utilized to identify the source of the peaks obtained from the single cells and each fragment generated in the single cells co-migrated with a standard fragment (Figure 3.9A). The most abundant fragment generated was the 5-mer (peptide h) that amounted to 36 ± 6 % of all peptides. This same 5-mer was also generated in the lysate studies but at approximately half the amount observed in single cells at 5 min. The 7-mer fragment (peptide f) that was generated the fastest in the lysate studies was present, but to a lesser extent (5 ± 2 %) in the intact cells. In single cells, the 4, 6, and 11-residue fragments were also seen at amounts greater than 10% (Table 3.2) while of these, only the 4-mer was seen in the lysate studies (Figure 3.2). The 2-mer seen in small amounts in the lysate studies was not seen at all in the intact cell studies.

Although the pattern of peptide fragmentation was similar in single cells compared to lysates, there were important differences. While the peptide concentration incubated in the

cell lysate was roughly 25-times lower than that loaded into single cells and the lysate protein was 30-times more dilute than a single cell, the rate of peptide metabolism in the cell lysate still remained significantly greater than that of peptide in an intact cell over the same time period. Thus the peptidase activity in cell lysates was considerably greater than that in the cytosol of an intact cell most likely due to the release of sequestered peptidases from ruptured organelles in the lysate. A second significant difference is the predominance of peptide h (representing Ala-Ala bond cleavage) in the single cells relative to other peptide fragments suggesting that the Ala-Ala bond may be the dominant cleavage site in single cells and not the Pro-Phe which dominated in the lysate. No phosphorylated product was detected or expected since HeLa cells do not express Bcr-Abl.

The lead peptide QW-V-48B was microinjected into a single HeLa cell, incubated for 5 min, and then the cellular contents were electrophoretically separated. On average, 28 ± 6 amol (n = 4 cells) of QW-V-48B was loaded into the cells. The peptide was degraded at an average rate of 0.6 ± 0.1 zmol pg^{-1} s^{-1} with 33 ± 14% remaining intact after 5 min (Table 3.2). Thus the average rate of metabolism in single cells was similar for the starting and lead peptides. Five peaks were observed on the electropherogram (Figure 3.9B) and the migration time of each of these peaks matched to that of a QW-V-48B fragment standard (Figure 3.9B, D). The 7-residue fragment representing cleavage between the proline and (N-methyl)phenylalanine was not present in the single cells. This bond was effectively stabilized by replacement with a non-native amino acid. However, 4, 5, and 11-residue peptide fragments were present with the 5-mer (peptide t), representing the Ala-Ala bond cleavage, being the most abundant with 22 ± 10 % present after 5 min. The 2-mer observed in cell lysates (Figure 3.8C) was absent from the single cells; however, the single cells

possessed a 6-amino acid fragment not observed in the lysates. As with QW-III-67B, peptide metabolism in the single cell was similar to that in a lysate but with some key differences. Since the rate of metabolism of QW-V-48B and QW-III-67B in single cells was nearly identical, replacement of the Pro-Phe bond did not stabilize the peptide in the single cells. The predominance of peptide h and t for both QW-III-67B and QW-V-48B in single cells suggests that the Ala-Ala bond is the preferred location for bond cleavage in the intact cytosol where disruption of the organelles has not occurred. No phosphorylated product was detected in any single cells.

3.4 Conclusions

Identification of the exact cleavage locations within a peptide permitted rational peptide redesign by placement of non-native residues at hydrolysis sites, resulting in increased peptide lifetimes in a cytosolic lysate. By contrast, both the starting and lead peptides showed similar degradation rates in intact cells suggesting that the cell lysate system may not be a good model for estimating intracellular rates and patterns of peptide proteolysis. It is likely that different peptidases acted on the substrates in single cells compared to that in lysates, leading to differences in primary cleavage sites and rates of proteolysis. One caveat is that only a single time point was sampled for the single cells and formation of the fragments over time was not determined. Assay of single cells loaded with peptide and incubated for other times would lead to a more complete picture of peptide fragmentation and permit further analysis of substrate lifetime in intact cells.

3.5 Figures and Tables

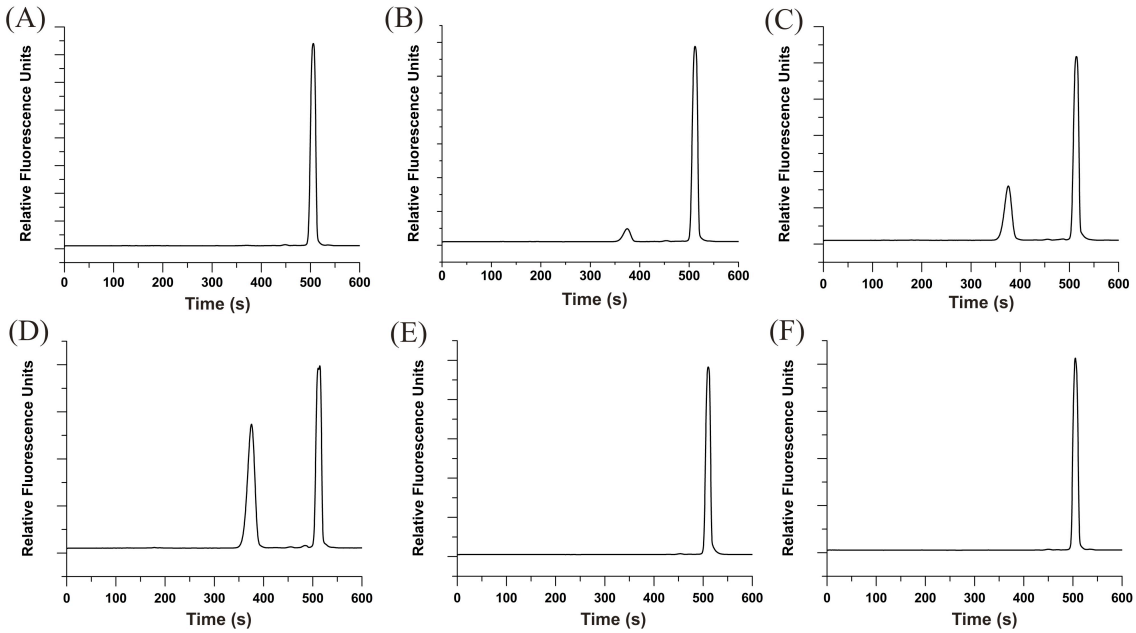

Figure 3.1: *in vitro* phosphorylation of the starting peptide (QW-III-67B) by recombinant Abl kinase. (A) – (D) Electropherograms of the peptide after incubation with Abl kinase in the presence of ATP for 0 (A), 15 (B), 60 (C) and 120 (D) min. (E) – (F) Electropherograms of the peptide with Abl kinase without ATP present for 0 (E) and 120 (F) min. The peak eluting at ~380 s is the phosphorylated counterpart of the non-phosphorylated peptide migrating at ~500 s.

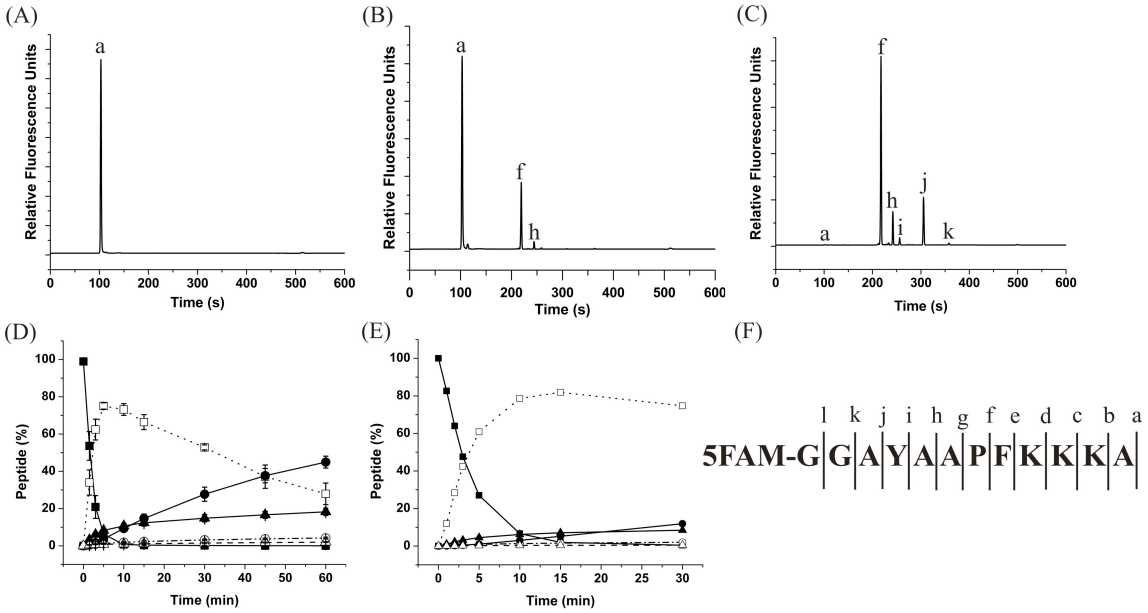

Figure 3.2: Degradation profile of the starting peptide (QW-III-67B) in a cell lysate. (A) – (C) Electropherograms of the peptide after incubation in the Baf/BCR-ABL lysate for 0 (A), 1 (B), or 30 (C) min. (D) Formation of peptide fragments over time in the Baf/BCR-ABL lysate. (E) Formation of peptide fragments over time in a HeLa cell lysate. Shown on the y-axis is the percentage of peptide present as a fragment. The symbols are defined as: filled square (peptide a or starting peptide), open square (peptide f), closed triangle (peptide h), open circle (peptide i), closed circle (peptide j) and open triangle (peptide k). The symbols and error bars represent the average and standard deviation of the data points. (F) The uppercase letters are the single amino acid abbreviations for the starting peptide sequence. The lowercase letters indicate the cleavage locations that generate the indicated peptide fragments.

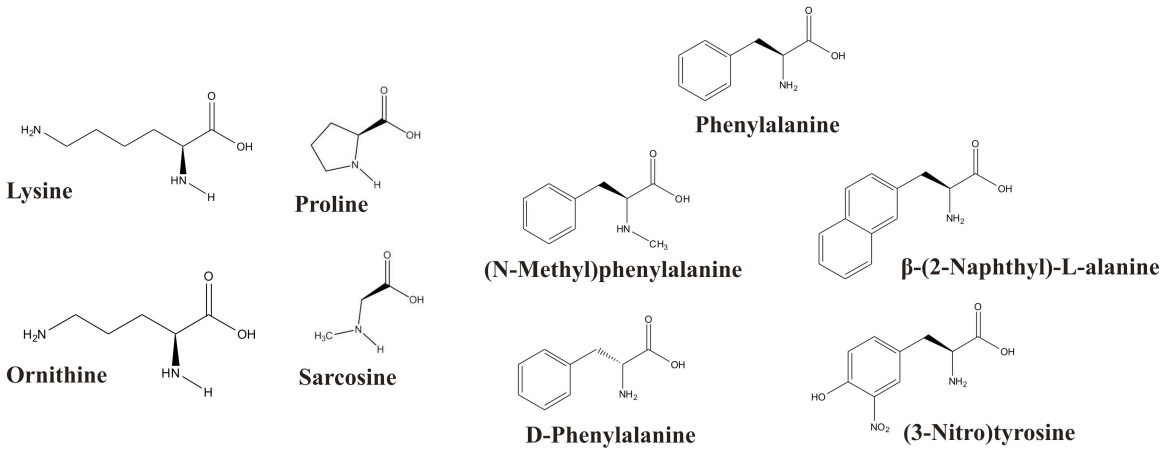

Figure 3.3: The native residues and the non-native residues that were inserted into the peptide to stabilize the peptide against hydrolysis.

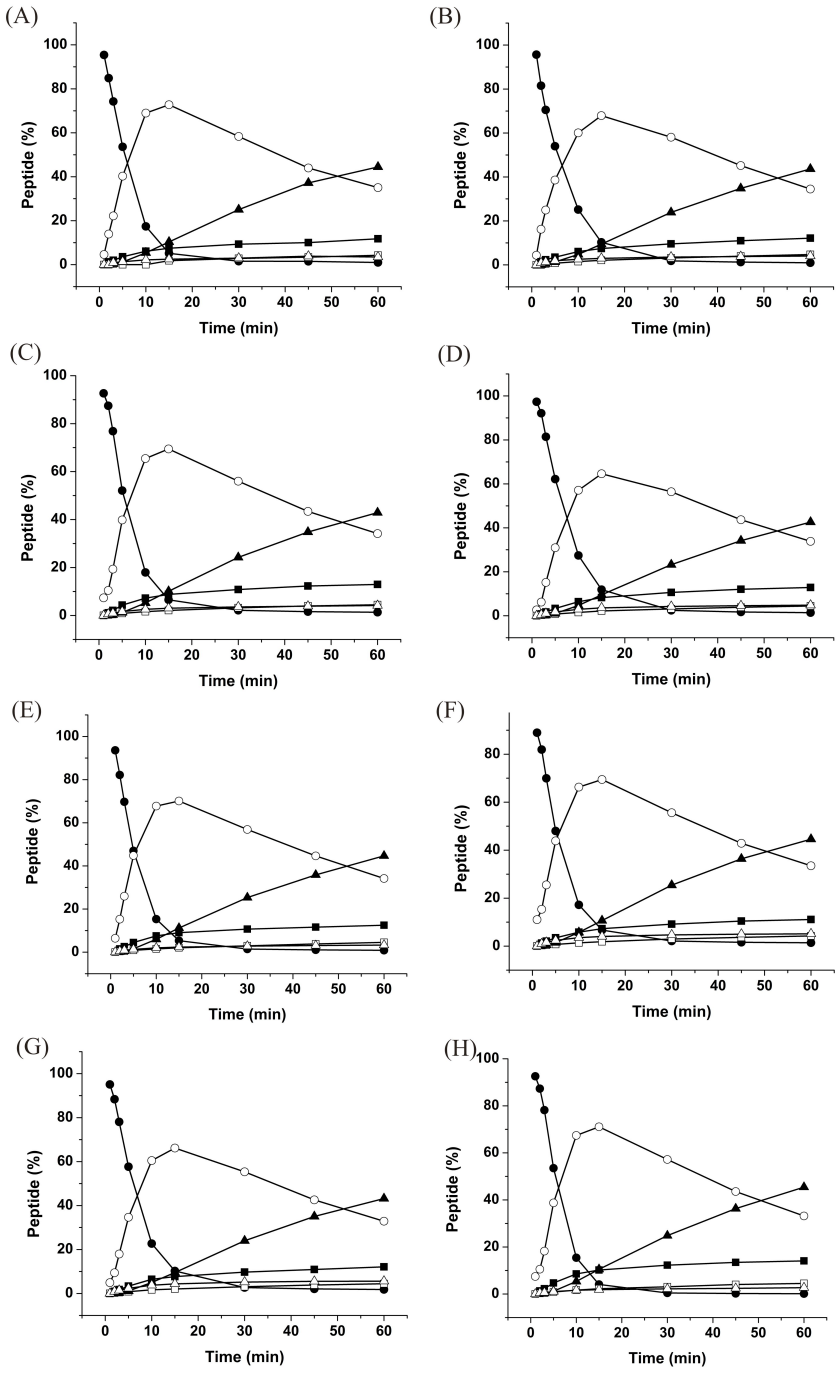

Figure 3.4: Formation of peptide fragments in the Baf/BCR-ABL lysate over time for the ornithine-substituted peptides. Degradation of peptide QW-III-90A (A), QW-III-90B (B), QW-III-90C (C), QW-III-90D (D), QW-III-90E (E), QW-III-90F (F), QW-III-90G (G), and QW-III-67B (H). The symbols are defined as: closed circle (intact parent); open circle (fragment migrating at 210 s); closed square (fragment migrating at 240 s); open square (fragment migrating at 260 s); closed triangle (fragment migrating at 305 s); and open triangle (fragment migrating at 360 s).

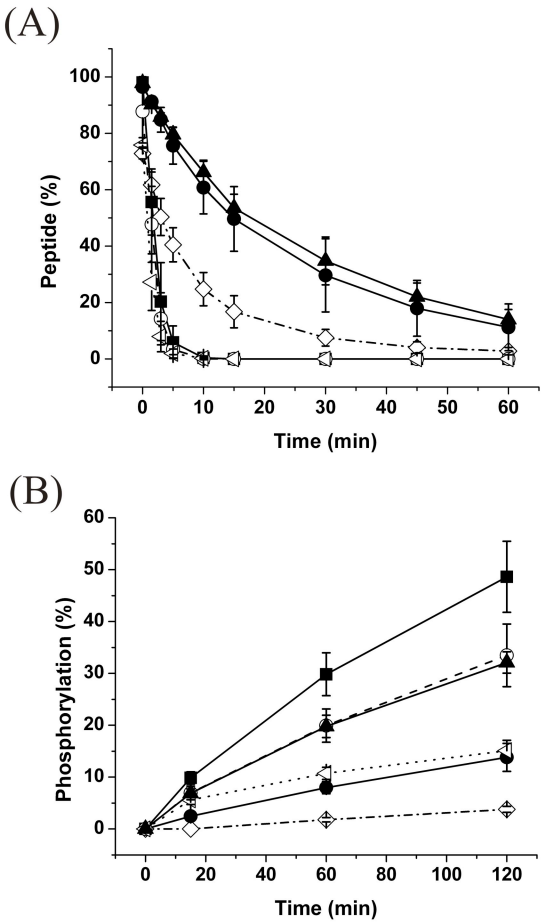

Figure 3.5: Baf/BCR-ABL cytosolic lysate degradation (A) and *in vitro* phosphorylation (B) of modified peptides. Filled square (QW-III-67B, starting peptide); open diamond (QW-IV-74D, sarcosine-substituted peptide); closed circle (QW-IV-85B, (N-methyl)phenylalanine-substituted peptide); open circle (QW-V-23C, β-(2-naphthyl)-L-alanine-substituted peptide); open triangle (QW-V-23E, 3-nitro tyrosine-substituted peptide); and closed triangle (QW-V-48B, isoleucine and N-methylated phenylalanine-substituted peptide). The symbols and error bars represent the average and standard deviation of the data points.

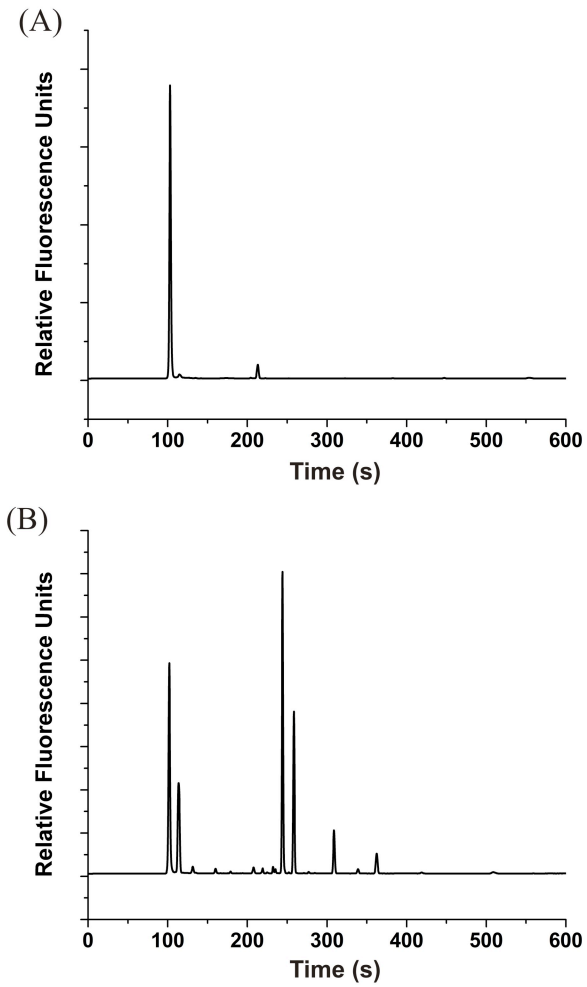

Figure 3.6: Electropherograms of peptide QW-IV-85B incubated in a Baf/BCR-ABL cytosolic lysate after 0 (A) and 60 (B) min. The intact parent peptide is identified as the major peak seen in (A) migrating at 100 s.

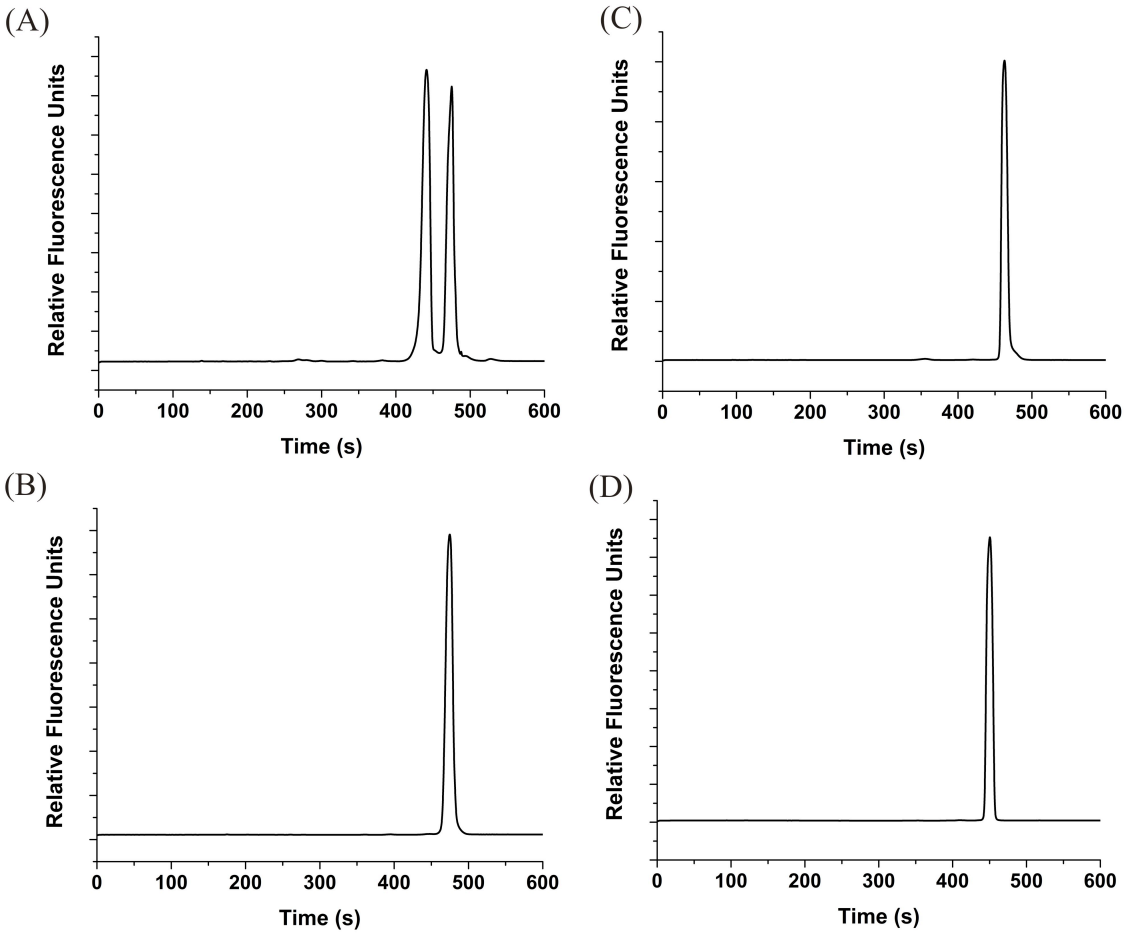

Figure 3.7: Electropherograms of QW-V-48B incubated with recombinant Abl kinase for 60 min with ATP (A) and without ATP (B) and incubated with recombinant Src kinase for 60 min with ATP (C) and without ATP (D).

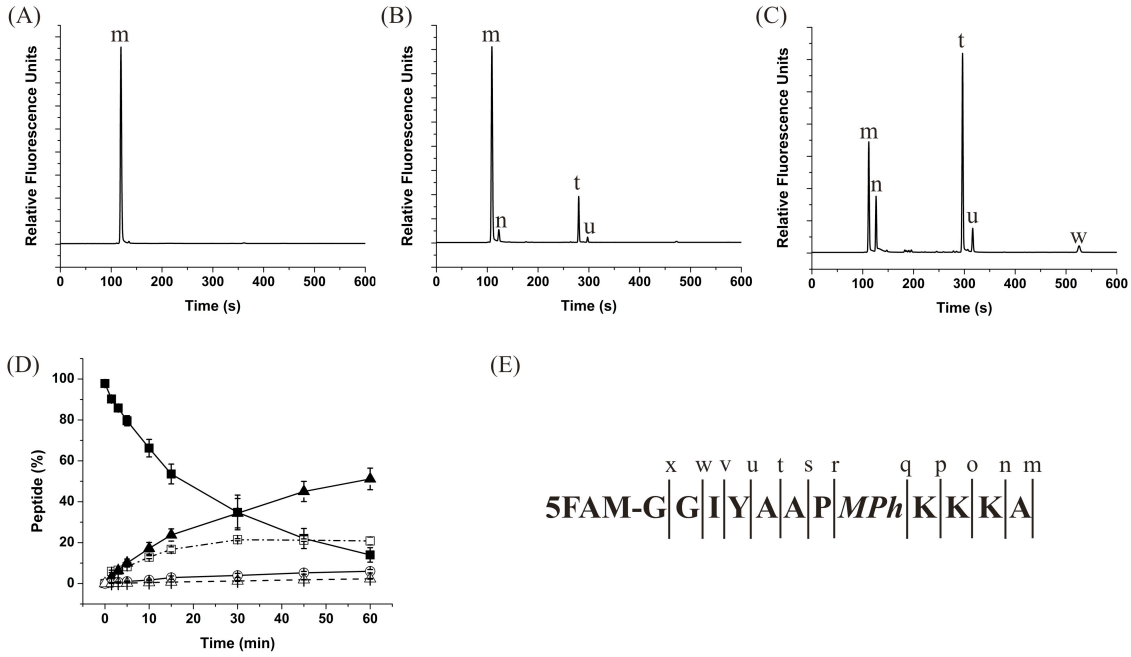

Figure 3.8: Degradation profile of the lead peptide (QW-V-48B) in a Baf/BCR-ABL cell lysate. (A) – (C) Electropherograms of the peptide after incubation in the lysate for 0 (A), 1 (B), or 30 (C) min. (D) Formation of peptide fragments over time. Shown on the y-axis is the percentage of peptide present as a fragment. The symbols are defined as: filled square (peptide m), open square (peptide n), closed triangle (peptide t), open circle (peptide u), open triangle (peptide w). The symbols and error bars represent the average and standard deviation of the data points. (E) The uppercase letters are the single amino acid abbreviations for the lead peptide sequence and *MPh* represents (N-methyl) phenylalanine. The lowercase letters indicate the cleavage locations that generate the indicated peptide fragments.

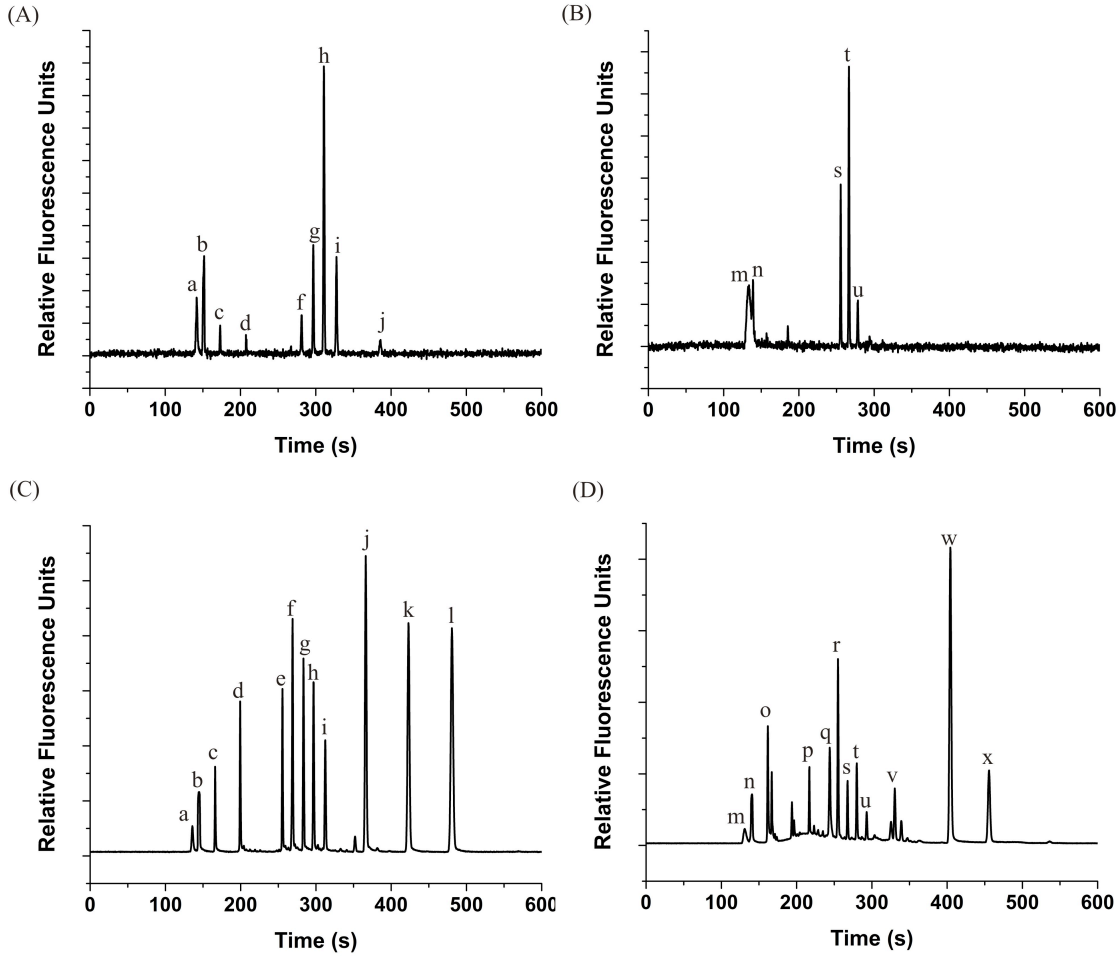

Figure 3.9: Degradation of peptides in single HeLa cells. Cells were microinjected with QW-III-67B (A,C) or the lead peptide QW-V-48B (B,D). (A,B) Electropherogram of a single cell 5 min after microinjection. The lowercase letters label the peptide fragments as defined in Figures 3.2F and 3.5E. (C,D) Identification of fragments formed in single cells. Single cell contents were loaded into a capillary 5 min after starting or lead peptide microinjection into the cell. Immediately after loading the cell contents into the capillary, the fragments of the starting peptide QW-III-67B (C) or lead peptide QW-V-48B (D) were loaded into the capillary. A voltage was then applied to the capillary to initiate simultaneous electrophoresis of the cellular contents and fragment standards.

Table 3.1: Properties of the modified peptides derived from the starting peptide (QW-III-67B).

Peptide Name	Sequence	$t_{1/2}$[a](min)	$t_{50\%\ P}$[b](min)
QW-III-67B	FAM-GGAYAAPFKKKA	1.3	150
QW-III-90A	FAM-GGAYAAPFKKOA	4.6	580
QW-III-90B	FAM-GGAYAAPFKOKA	5.3	500
QW-III-90C	FAM-GGAYAAPFOKKA	4.3	86
QW-III-90D	FAM-GGAYAAPFKOOA	4.9	44
QW-III-90E	FAM-GGAYAAPFOKOA	5.0	25
QW-III-90F	FAM-GGAYAAPFOOKA	6.0	90
QW-III-90G	FAM-GGAYAAPFOOOA	5.7	650
QW-IV-74A	FAM-GGAYAAAFKKKA	15.1	$> 10^5$
QW-IV-74B	FAM-GGAYAAWFKKKA	8.9	$> 10^5$
QW-IV-74C	FAM-GGAYAATKKKKA	10.6	$> 10^5$
QW-IV-74D	FAM-GGAYAA-Sarc-FKKKA	24.0	$> 10^5$
QW-IV-74E	FAM-GGAYAAFFKKKA	9.5	$> 10^5$
QW-IV-85B	FAM-GGAYAAP-MPh-KKKA	52.6	$> 10^5$
QW-V-23B	FAM-GGAYAAP-DPh-KKKA	36.3	82
QW-V-23C	FAM-GGAYAAP-Nal-KKKA	5.7	190
QW-V-23E	FAM-GGAYAAP-Tyr(3-NO_2)-KKKA	4.6	$> 10^5$
QW-V-48B	FAM-GGIYAAP-MPh-KKKA	19.4	42

[a]$t_{1/2}$ is the time at which 50% of the peptide was degraded by the cell lysate.
[b]$t_{50\%\ P}$ is the time required for 50% of the peptide to be phosphorylated by Abl-1 kinase under the conditions employed. Abbreviations are the standard single letter amino acids, except for the following: O (ornithine), Sarc (sarcosine), MPh [(N-methyl)phenylalanine], DPh (D-phenylalanine), Nal (β-(2-Naphthyl)-L-alanine), and Tyr(3-NO_2) (3-Nitro tyrosine).

Table 3.2: Percentage of each fragment formed following a 5 min incubation of the peptides in a single cell. The average and standard deviation are given (n = 4). The lowercase letters represent the peptide fragments defined in Figures 3.2F and 3.5E.

Starting Peptide QW-III-67B	Peptide (%)	Lead Peptide QW-V-48B	Peptide (%)
a	10 ± 2	m	33 ± 14
b	15 ± 8	n	15 ± 9
c	2 ± 0.6	s	13 ± 4
d	0.7 ± 0.5	t	22 ± 10
f	5 ± 2	u	17 ± 15
g	13 ± 4		
h	36 ± 6		
i	15 ± 5		
j	3 ± 2		

3.6 References

1 P. P. Pungaliya, Y. Bai, K. Lipinski, V. S. Anand, S. Sen, E. L. Brown, B. Bates, P. H. Reinhart, A. B. West, W. D. Hirst and S. P. Braithwaite. "Identification and Characterization of a Leucine-Rich Repeat Kinase 2 (LRRK2) Consensus Phosphorylation Motif". *PLoS ONE,* 2010, *5*, 1-13.

2 D. R. Alessi, F. B. Caudwell, M. Andjelkovic, B. A. Hemmings and P. Cohen. "Molecular basis for the substrate specificity of protein kinase B; comparison with MAPKAP kinase-1 and p70 S6 kinase". *FEBS Lett.,* 1996, *399*, 333-338.

3 K. Nishikawa, A. Toker, F. Johannes, Z. Songyang and L. C. Cantley. "Determination of the Specific Substrate Sequence Motifs of Protein Kinase C Isozymes". *J. Biol. Chem.,* 1997, *272*, 952-960.

4 J. Wu J., D. E. H. Afar, H. Phan, O. Witte N. and K. S. Lam. "Recognition of Multiple Substrate Motifs by the c-ABL Protein Tyrosine Kinase". *Com. Chem. High T. Scr.,* 2002, *5*, 83-91.

5 D. S. Lawrence, "Signaling protein inhibitors via the combinatorial modification of peptide scaffolds". *Biochim. Biophys. Acta,* 2005, *1754*, 50-57.

6 P. Litman, O. Ohne, S. Ben-Yaakov, L. Shemesh-Darvish, T. Yechezkel, Y. Salitra, S. Rubnov, I. Cohen, H. Senderowitz, D. Kidron, O. Livnah, A. Levitzki and N. Livnah. "A Novel Substrate Mimetic Inhibitor of PKB/Akt Inhibits Prostrate Cancer Tumor Growth in Mice by Blocking the PKB Pathway". *Biochemistry,* 2007, *46*, 4716-4724.

7 K. R. W. Ngoei, B. Catimel, N. Church, D. S. Lio, C. Dogovski, M. A. Perugini, P. M. Watt, H. Cheng, D. C. H. Ng and M. A. Bogoyevitch. "Characterization of a novel JNK (c-Jun N-terminal kinase) inhibitory peptide". *Biochem. J.,* 2011, *434*, 399-413.

8 D. Wu, J. E. Sylvester, L. J. Parker, G. Zhou and S. J. Kron. "Peptide reporters of kinase activity in whole cell lysates". *Biopolymers,* 2010, *94*, 475-486.

9 X. Xu, X. Liu, Z. Nie, Y. Pan, M. Guo and S. Yao. "Label-Free Fluorescent Detection of Protein Kinase Activity Based on the Aggregation Behavior of Unmodified Quantum Dots". *Anal. Chem.,* 2011, *83*, 52-59.

10 D. Wu, M. R. Mand, D. R. Veach, L. L. Parker, B. Clarkson and S. J. Kron. "A solid-phase Bcr-Abl kinase assay in 96-well hydrogel plates". *Anal. Biochem.,* 2008, *375*, 18-26.

11 X. Han, G. Yamanouchi, T. Mori, J. Kang, T. Niidome and Y. Katayama. "Monitoring Protein Kinase Activity in Cell Lysates Using a High-Density Peptide Microarray". *J. Biomol. Screen,* 2009, *14*, 262.

12 M. D. Shults, K. A. Janes, D. A. Lauffenburger and B. Imperiali. "A multiplexed homogenous fluorescence-based assay for protein kinase activity in cell lysates". *Nat. Methods,* 2005, *2*, 277-283.

13 Q. Wang, E. I. Zimmerman, A. Toutchkine, T. D. Martin, L. M. Graves and D. S. Lawrence. "Multicolor Monitoring of Dysregulated Protein Kinases in Chronic Myelogenous Leukemia". *ACS Chem. Biol.,* 2010, *5*, 887-895.

14 J. H. Lee, S. K. Nandy and D. S. Lawrence. "A Highly Potent and Selective PKCα Inhibitor Generated via Combinatorial Modification of a Peptide Scaffold". *J. Am. Chem. Soc,* 2004, *126*, 3395.

15 M. Stawikowski, R. Stowikowska, A. Jaśkiewicz, E. Zabłotna and K. Rolka. "Examples of Peptide-Peptoid Hybrid Serine Protease Inhibitors Based on the Trypsin Inhibitor SFTI-1 with Complete Protease Resistance at the P1-P1' Reactive Site". *ChemBioChem,* 2005, *6*, 1057-1061.

16 C. E. Sims and N. L. Allbritton. "Single-cell kinase assays: opening a window onto cell behavior". *Curr. Opin. Biotech.,* 2003, *14*, 23-28.

17 M. L. Kovarik and N. L. Allbritton. "Measuring enzyme activity in single cells". *Trend. Biotechnol.,* 2011, *29*, 222-230.

18 Q. Wang, Z. Dai, S. M. Cahill, M. Blumenstein and D. S. Lawrence. "Light-Regulated Sampling of Protein Tyrosine Kinase Activity". *J. Am. Chem. Soc.,* 2006, *128*, 14016-14017.

19 D. S. Lawrence and Q. Wang. "Seeing Is Believing: Peptide-Based Fluorescent Sensors of Protein Tyrosine Kinase Activity". *ChemBioChem,* 2007, *8*, 373-378.

20 M. A. Priestman and D. S. Lawrence. "Light-mediated remote control of signaling pathways". *Biochm. Biophys. Acta,* 2010, *1804*, 547-558.

21 S. Lee, E. Kim, K. Suk and W. Lee. "Synthetic peptides containing ITIM-like sequences of IREM-1 inhibit BAFF-mediated regulation of interleukin-8 expression and phagocytosis through SHP-1 and/or PI3K". *Immunology,* 2011, *134*, 224-233.

22 G. D. Meredith, C. E. Sims, J. S. Soughayer and N. L. Allbritton. "Measurement of kinase activation in single mammalian cells". *Nat. Biotechnol.,* 2000, *18*, 309-312.

23 S. N. Arkhipov, M. Berezovski, J. Jitkova and S. N. Krylov. "Chemical Cytometry for Monitoring Metabolism of a Ras-Mimicking Substrate in Single Cells". *Cytom. Part A,* 2005, *63A*, 41-47.

24 R. B. Brown, J. A. Hewel, A. Emili and J. Audet. "Single Amino Acid Resolution of Proteolytic Fragments Generated in Individual Cells". *Cytom. Part A,* 2010, *77A*, 347-355.

25 E. Reits, A. Griekspoor, J. Neijssen, T. Groothuis, K. Jalink, P. van Veelen, H. Janssen, J. Calafat, J. W. Drijfhout and J. Neefjes. "Peptide Diffusion, Protection, and Degradation in Nuclear and Cytoplasmic Compartments before Antigen Presentation by MHC Class I". *Immunity,* 2003, *18*, 97-108.

26 Y. Tal-Gan, M. Hurevich, S. Klein, A. Ben-Shimon, D. Rosenthal, C. Hazan, D. E. Shalev, M. Y. Niv, A. Levitzki and C. Gilon. "Backbone Cyclic Peptide Inhibitors of Protein Kinase B (PKB/Akt)". *J. Med. Chem.,* 2011, *54*, 5154-5164.

27 E. M. Molhoek, A. van Dijk, E. J. A. Veldhuizen, H. P. Haagsman and F. J. Bikker. "Improved proteolytic stability of chicken cathelicidin-2 derived peptides by D-amino acid substitutions and cyclization". *Peptides,* 2011, *32*, 875-880.

28 O. Ovadia, Y. Linde, C. Haskell-Leuvano, M. L. Dirain, T. Sheynis, R. Jelinek, C. Gilon and A. Hoffman. "The effect of backbone cyclization on PK/PD properties of bioactive peptide-peptoid hybrids: The melanocortin agonist paradigm". *Bioorgan. Med. Chem.,* 2010, *18*, 580-589.

29 L. T. Nguyen, J. K. Chau, N. A. Perry, L. de Boer, S. A. J. Zaat and H. J. Vogel. "Serum Stabilities of Short Tryptophan- and Arginine-Rich Antimicrobial Peptide Analogs". *PLoS ONE,* 2010, *5*, 1-8.

30 L. H. Brinckerhoff, V. V. Kalashnikov, L. W. Thompson, G. Yamshchikov, R. A. Pierce, H. S. Galavotti, V. H. Engelhard and C. L. Slingluff Jr. "Terminal Modifications Inhibit Proteolytic Degradation of an Immunogenic Mart-1_{27-35} Peptide: Implications for Peptide Vaccines". *Int. J. Cancer,* 1999, *83*, 326-334.

31 K. Bellmann-Sickert, C. E. Elling, A. N. Madsen, P. B. Little, K. Lundgren, L. Gerlach, R. Bergmann, B. Holst, T. W. Schwartz and A. G. Beck-Sickinger. "Long-Acting Lipidated Analogue of Human Pancreatic Polypeptide Is Slowly Released into Circulation". *J. Med. Chem.,* 2011, *54*, 2658-2667.

32 G. Pasut and F. M. Veronese. "PEG conjugates in clinical development or use as anticancer agents: An overview". *Adv. Drug Delivery Rev.,* 2009, *61*, 1177-1188.

33 Y. Koda, M. T. Liang, J. T. Blanchfield and I. Toth. "*In vitro* stability and permeability studies of lipsomal delivery systems for a novel lipophilic endomorphin 1 analogue". *Int. J. Pharm.,* 2008, *356*, 37-43.

34 C. D. Cros, I. Toth and J. T. Blanchfield. "Lipophilic derivatives of leu-enkephalinamide: In vitro permeability, stability and in vivo nasal delivery". *Bioorgan. Med. Chem.,* 2011, *19*, 1528-1534.

35 I. Neundorf, R. Rennert, J. Franke, I. Közle and R. Bergmann. "Detailed Analysis Concerning the Biodistribution and Metabolism of Human Calcitonin-Derived Cell-Penetrating Peptides". *Bioconjugate Chem,* 2008, *19*, 1596-1603.

36 R. Tugyi, K. Uray, D. Iván, E. Fellinger, A. Perkins and F. Hudecz. "Partial D-amino acid substitution: Improved enzymatic stability and preserved Ab recognition of a MUC2 epitope peptide". *PNAS,* 2005, *102*, 413-418.

37 L. Gentilucci, R. De Marco and L. Cerisoli. "Chemical Modifications Designed to Improve Peptide Stability: Incorporation of Non-Natural Amino Acids, Pseudo-Peptide Bonds, and Cyclization". *Curr. Pharm. Design,* 2010, *16*, 3185-3203.

38 E. V. Pappa, A. A. Zompra, Z. Spyranti, Z. Diamantopoulou, G. Pairas, F. N. Lamari, P. Katsoris, G. A. Spyroulias and P. Cordopatis. "Enzymatic Stability, Solution Structure, and Antiproliferative Effect on Prostate Cancer Cells of Leuprolide and New Gonadotropin-Releasing Hormone Peptide Analogs". *Biopolymers* 2010*, 96*, 260-272.

39 C. R. Bartram, A. de Klein, A. Hagemeijer, T. van Agthoven, A. G. van Kessel, D. Bootsma, G. Grosveld, M. A. Ferguson-Smith, T. Davies, M. Stone, N. Heisterkamp, J. R. Stephenson and J. Groffen. "Translocation of c-*abl* oncogene correlates with the presence of a Philadelphia chromosome in chronic myelocytic leukemia". *Nature,* 1983, *306*, 277-280.

40 F. X. Mahon, M. W. N. Deininger, B. Schultheis, J. Chabrol, J. Reiffers, J. M. Goldman and J. V. Melo. "Selection and characterization of *BCR-ABL* positive cell lines with differential sensitivity to the tyrosine kinase inhibitor STI571: diverse mechanisms of resistance". *Blood,* 2000, *96*, 1070-1079.

41 G. M. Funk, C. E. Hunt, D. E. Epps and P. K. Brown. "Use of a rapid and highly sensitive fluorescamine-based procedure for the assay of plasma lipoprotiens". *J. Lipid Res.,* 1986, *27*, 792-795.

42 Z. Songyang, K. L. Carraway III, M. J. Eck, S. C. Harrison, R. A. Feldman, M. Mohammadi, J. Schlessinger, S. R. Hubbard, D. P. Smith, C. Eng, M. J. Lorenzo, B. A. J. Ponder, B. J. Mayer and L. C. Cantley. "Catalytic specificity of protein-tyrosine kinases is critical for selective signalling". *Nature,* 1995, *373*, 536-539.

43 I. J. Griswold, M. MacPartlin, T. Bumm, V. L. Goss, T. O'Hare, K. A. Lee, A. S. Corbin, E. P. Stoffregen, C. Smith, K. Johnson, E. M. Moseson, L. J. Wood, R. D. Polakiewicz, B. J. Druker and M. W. Deininger. "Kinase Domain Mutants of Bcr-Abl Exhibit Altered Transformation Potency, Kinase Activity, and Substrate Utilization, Irrespective of Sensitivity to Imatinib". *Mol. Cell Biol.,* 2006, *26*, 6082-6093.

44 R. M. Stroud, "A Family of Protein-Cutting Proteins". *Sci. Am.,* 1974, *231*, 74-88.

45 J. H. Seely and N. L. Benoiton. "Effect of N-methylation and chain length on kinetic constants of trypsin substrates. ε-N-Methyllysine and homolysine derivative as substrates". *Can. J. Biochem. Cell B,* 1970, *48*, 1122-1131.

46 T. T. Tran, H. Treutlein and A. W. Burgess. "Designing amino acid residues with single-conformations". *Protein Eng. Des. Sel.,* 2006, *19*, 401-408.

47 C. E. Sims, G. D. Meredith, T. B. Krasieva, M. W. Berns, B. J. Tromberg and N. L. Allbritton. "Laser-Micropipet Combination for Single-Cell Analysis". *Anal. Chem.,* 1998, *70*, 4570-4577.

48 N. J. Dovichi and S. Hu. "Chemical Cytometry". *Curr. Op. Chem. Biol.,* 2003, *7*, 603-608.

CHAPTER 4

DEVELOPMENT OF A PEPTIDASE-RESISTANT SUBSTRATE FOR SINGLE-CELL MEASUREMENT OF PROTEIN KINASE B ACTIVATION

4.1 Introduction

4.1.1 Protein Kinase B Activation and Function

Protein kinase B (PKB, also known as Akt) is responsible for regulation of many cell functions, such as survival under stress, cell proliferation, and apoptosis.[1-3] When a cell is stimulated, activation of phosphatidylinositol 3-kinase (PI3-K) leads to generation of phosphatidylinositol-3,4,5-trisphosphate (PIP_3). PIP_3 recruits PKB to the plasma membrane, where it is phosphorylated by phosphoinositide-dependent kinase-1 (PDK-1) on a threonine residue at position 308. Phosphorylation at Thr308 by PDK-1 then triggers phosphorylation of a serine residue at position 473 by the protein complex mTORC2 (mammalian target of rapamycin complex 2), a complex that contains the kinase mTOR and rictor.[1-11] PKB is most active when it is phosphorylated at both Thr308 and Ser473.[2, 10] After activation at the plasma membrane, PKB moves throughout the cell to phosphorylate its substrates which go on to regulate the functions mentioned above. Interest in PKB and the PI3-K cascade has steadily increased due to their role in enabling cells to survive stressful conditions, namely in preventing apoptosis in cells normally targeted for programmed cell death.[4] The PI3-K cascade and its constituents have been implicated in tumor progression and survival in a wide

array of cancers, including pancreatic, breast, and prostate tumors.[10, 12] In particular, increase PKB activity is often the result of increased upstream activity in the PI3-K pathway, over expression of PKB, PKB mutations leading to constitutive activity, and decreased activity of the phosphatases dephosphorylating PKB.[2-5, 12, 13] Increased PKB of any origin appears to enable tumor cells to survive and proliferate in a stressful environment.[7, 12, 14] Inhibition of the PI3-K pathway and in particular PKB are current targets for drug development for cancer therapeutics.

4.1.2 Methods for Measuring PKB

Strategies to monitor PKB activity in tumor cells are needed to identify which patients would benefit from inhibitors of the PI3-K pathway as well as in identifying optimal therapeutic concentrations. Analysis of PKB activation can be performed on cell lysates using Western blots in which one or both phosphorylated residues are probed with phosphospecific antibodies to infer PKB activity.[5] A new technology incorporating isolelectric focusing within a capillary followed by immunoblotting permits the analysis of smaller cell numbers than a Western blot.[15] However, neither of these techniques enable measurement of PKB activation at the single-cell level. Alternative methods that use phosphospecific antibodies against Thr308/Ser473 to probe PKB activity at the single cell level include immunocytochemistry,[16] phosphoflow,[17-21] and cytometry by time of flight (CyTOF).[22-24] The latter two methods are designed for non-adherent cells and all require cell fixation and permeabilization prior to measurement. Additionally, immunocytochemistry staining of adherent cells identifies the presence of phosphorylated PKB but is generally considered to be non-quantitative.[25] Indicators employing fluorescent proteins have been developed to measure PKB activity at the single-cell level by monitoring fluorescence

resonance energy transfer between two fluorescent proteins.[26, 27] However, these indicators require the transfection of DNA into cells, making their use in primary cells challenging. Capillary electrophoresis has also been used to measure PKB activity in single cells; however, this strategy requires use of a fluorescently-tagged substrate peptide which can have a very short lifetime in cells, substantially limiting the technique's utility.[28-30]

4.1.3 Peptides as Kinase Substrates

Peptide substrates have been used extensively in biomedical research to assay kinase activity due to the ease of peptide design and synthesis and the ability to construct extensive peptide libraries for screening and optimization. As part of these endeavors, peptides serve as assay substrates for kinases obtained in pure form,[31, 32] from cell lysates,[33-36] and even in single cells.[37-40] However, peptides often possess limited lifetimes in the cellular milieu due to the presence of peptidases which can degrade them. Multiple strategies have been employed to stabilize peptides against degradation, including cyclization, terminus modifications, and inclusion of non-native amino acids. Peptide cyclization yields degradation-resistant peptides, but this often results in poor substrate recognition by the kinase and these constructs can be synthetically challenging.[41-44] Modifications to the C- and N-terminus are relatively simple to accomplish and provide protection against amino- and carboxy-peptidases, but not endopeptidases.[45-47] Terminal modifications can be used in combination with non-native residues, including N-methylated and D-amino acids, to impart additional stability to peptide bonds.[29, 48-51] These non-native residues are readily available commercially and are simply incorporated into peptides utilizing standard solid phase peptide synthesis. Peptides with non-native residues generally suffer greatly diminished kinase-substrate properties and the design of kinase substrates with non-native amino acids remains

challenging.[51] However, peptidase-resistant substrates should be of wide utility throughout biomedical research in assays of kinase activity in the presence of cellular constituents.

4.1.4 Iterative Strategy for Design of Peptidase-Resistant Kinase Substrates

The work described in this chapter develops an iterative strategy to screen rationally designed peptides for their suitability to act as a kinase substrate in a cell lysate. Three criteria, time to 50% phosphorylation, half-life within a lysate, and appearance of a dominant fragment over time, were utilized to screen small libraries to design a degradation-resistant peptide substrate for PKB activity. Cytosolic lysates and purified kinase assays were utilized to rapidly assess synthetic peptides for their peptidase resistance as well as their ability to act as a substrate. Cleavage sites of peptides incubated in a cell lysate were characterized using capillary electrophoresis. Fluorescent peptide fragments were identified by comparison of their migration times with those of synthesized standards while the amount of each fragment was quantified from its fluorescence. Identification of cleavage sites permitted iterative replacement of amino acids with either non-native residues or more suitable native residues. Substitution success was then reassessed using the three criteria above and new substitutions incorporated based on these results until a peptidase-resistant PKB substrate was identified. This designed substrate was used to assay PKB activity in single prostate cancer cells in the presence and absence of a PKB inhibitor. The heterogeneity of substrate phosphorylation, kinase inhibitor performance, and peptidase activity in single cells was also evaluated.

4.2 Experimental Design

4.2.1 Chemicals

2-(6-chloro-1*H*-benzotriazole-1-yl)-1,1,3,3-tetramethylaminium hexafluorophosphate (HCTU), 1-(mesitylene-2-sulfonyl)-3-nitro-1,2,4-triazole (MSNT), 9-

fluorenylmethoxycarbonyl (Fmoc) amino acids and resins were obtained from ChemPep or Novabiochem and 6-carboxyfluorescein (6FAM), N-Hydroxybenzotriazole (HOBt), Fmoc-Nα-Me-Arg(Mtr)-OH and were purchased from AnaSpec. Fmoc-β-HArg(Pbf)-OH was received from Aapptec. Fmoc-α-MeAla-OH, and Fmoc-Phe(F5)-OH were purchased from Advanced ChemTech. All other peptide synthesis reagents were purchased from Aldrich or Fisher. Active PKBα enzyme was purchased from Millipore. Wortmannin was obtained from LC Laboratories. Bovine serum albumin was procured from Calbiochem. Roswell Park Memorial Institute Media (RPMI-1640) and Dulbecco's Modified Eagle Medium (DMEM) were purchased from Cellgro. Penicillin/streptomycin was obtained from Gibco and fetal bovine serum (FBS) was purchased from Atlanta Biologicals. All other chemicals used in assays were purchased from Fisher or Sigma.

4.2.2 Peptide Synthesis and Preparation

4.2.2.1 Synthesis of Full-Length Peptides Amidated on the C-Terminus

All peptides were synthesized by collaborator Dr. Qunzhao Wang unless specified otherwise. A complete list of all peptides utilized in this dissertation can be found in Appendix C. Full-length substrate peptides amidated on the C-terminus were synthesized via standard Fmoc peptide synthesis (Prelude Peptide Synthesizer, Protein Technologies, Tucson, AZ) on TGR resin. Coupling was achieved with two 5-min incubations in dimethylformamide (DMF) with 5 equivalents (eq) Fmoc amino acid, 5 eq HCTU, and 10 eq N,N-Diisopropylethylamine (DIPEA). For couplings of amino acids next to N-methylated amino acids, three 60-min incubations in N-Methyl-2-pyrrolidone (NMP) was applied prior to capping with acetic anhydride. Fmoc deprotection was performed with two 2.5-min incubations with 20% piperidine in DMF. The N-terminus of all peptides was reacted with 5

eq 6FAM, 5 eq diisopropylcarbodiimide (DIC), and 5 eq HOBt in DMF overnight, then treated with 30% piperidine in DMF for 30 min. Generally, the peptide was cleaved with trifluoroacetic acid : water : triisopropylsilane (TFA : H_2O : TIS) in a ratio of 95 : 2.5 : 2.5, except for N-MeArg containing peptides, where the side chain was protected with Mtr. In these cases, the cleavage occurred overnight in a solution of TFA : Phenol : H_2O : TIS in a ratio of 88 : 5 : 5 : 2. All cleaved peptides were precipitated with ether, and dried in air. Peptide purity was analyzed with HPLC-MS and further purification via HPLC was performed if needed.

4.2.2.2 Alternative Coupling for Difficult Amino Acids

In some cases, amino acids required coupling with 5 eq of Fmoc amino acid, 5 eq HCTU, and 10 eq DIPEA in N-methyl-2-pyrrolidone (NMP) for 3 h, repeated for a total of 3 couplings. Finally, capping with acetic anhydride was performed and product formation was measured using HPLC-MS. Peptides were dissolved in Tris buffer, pH 7.5, aliquoted, and stored at – 80 ^{o}C.

4.2.2.3 Synthesis of Peptide Fragment Standards

Peptide fragment standards with a free carboxylic acid on the C-terminus were synthesized using either a Wang or 2-chlorotrityl resin. When using the Wang resin, 10 eq of the first Fmoc amino acid in CH_2Cl_2 was reacted with 7.5 eq 1-methyl-imidazole and 10 eq MSNT for 15 min in a dry glass vial on a shaker. The reaction mixture was transferred to another dry glass vial containing the Wang resin and incubated for 1 h. For the 2-chlorotrityl resin, 1 eq of the first Fmoc amino acid and 4 eq DIPEA in dry CH_2Cl_2 was reacted with the 2-chlorotrityl resin for 2 h in a dry glass vial on a shaker. The remaining amino acids were

attached as described for the amidated peptides above and the N-terminus of all peptides was labeled with 6FAM as described above.

4.2.3 Cell Culture

HeLa cells, a human cervical adenocarcinoma cell line, and LNCaP cells, a human prostate carcinoma cell line, were obtained from the American Type Culture Collection. HeLa cells were cultured in DMEM medium supplemented with 10% FBS, penicillin (100 units/mL) and streptomycin (100 μg/mL). LNCaP cells were cultured in RPMI medium supplemented with 10% FBS, penicillin (100 units/mL) and streptomycin (100 μg/mL). All cells were maintained in a humidified atmosphere of 37 ^{o}C in 5% CO_2 and passaged into fresh media every 2 – 3 days. LNCaP cells used for single-cell CE experiments were plated the day before onto custom chambers prepared by gluing a silicon O-ring (McMaster-Carr) to a #1 glass coverslip (Fisher) using poly(dimethyl siloxane) (PDMS, Sylgard 184). A dilute cell suspension was added to 500 μL of RPMI-1640 media in the chamber and the chambers were placed in the humidified incubator until use in the experiments. Cells treated with inhibitor were incubated with 500 nM Wortmannin in RPMI-1640 for 10 min prior to experiments.

4.2.4 Measurement of Peptide Degradation in a Cell Lysate

A HeLa or LNCaP cell pellet was washed with and resuspended in phosphate buffered saline (PBS; 137 mM NaCl, 10 mM Na_2HPO_4, 27 mM KCl, 1.75 mM KH_2PO_4, pH 7.4). The cells were submerged in liquid nitrogen for 1 min and thawed at 37 ^{o}C for a total of three cycles. The mixture was centrifuged at 14,000 x g for 5 min at 4 ^{o}C and the supernatant was transferred to a clean centrifuge tube and maintained on ice until use in the assay. Total protein concentration in the supernatant was measured using fluorescamine.[52] A standard

curve was created utilizing BSA concentrations ranging from 0 – 100 μg mL^{-1}. Briefly, fluorescamine (10 μL, 3 mg/mL in acetone) was added to a cell lysate (30 μL) and incubated for 5 min at 25 ^{o}C. Fluorescence was measured with a fluorescence plate reader (SpectraMax M5, Molecular Devices, Sunnyvale, CA) with an excitation of 390 nm (bandwidth of 9 nm) and emission of 475 nm (bandwidth of 15 nm).

Assessment of peptide degradation was performed by mixing peptide substrate (1 μM) with cell lysate (3 mg mL^{-1} total cell protein) and incubating at 37 ^{o}C. Aliquots were removed and stopped by adding HCl to a final concentration of 100 mM. A 0 min timepoint was prepared by adding the HCl to the lysate prior to the addition of the peptide. Reaction mixtures were then separated and detected with CE-LIF. Peptide fragments were identified by adding standards (250 nM) to the HCl-terminated aliquots and comparing the electropherograms with and without the added standard. The average initial degradation and fragmentation rates were calculated using the initial and 5 min time points by monitoring the change in peptide quantity divided by the change in time per amount of cytosolic protein. The units are defined as zmol of peptide per pg of total cytosolic protein per s (zmol pg^{-1} s^{-1}).

4.2.5 *in vitro* Kinase Assay

Protein kinase assays were performed at 30 ^{o}C in assay buffer [8 mM MOPS (3-(N-morpholino)propanesulfonic acid), pH 7.0, 0.2 mM EDTA, 4 mM $MgCl_2$, 1 mM ATP] with PKBα kinase (6 nM) and substrate (25 μM). Aliquots were removed from the reaction mixture at various times and the reaction was halted by heating at 90 ^{o}C for 4 min. The amount of peptide phosphorylation was measured using capillary electrophoresis coupled with laser-induced fluorescence detection (CE-LIF).

4.2.6 Measurement of Kinetic Parameters

Protein kinase assays were performed as described in the *in vitro* kinase assay section with the following exceptions: substrate concentrations ranged from 0.5 to 30 μM; and PKBα enzyme concentration was 1 nM for peptide I and 6 nM for peptide VI-B. The immobilized metal ion affinity-based fluorescent polarization (IMAP) assay (Molecular Devices Corporation, Sunnyvale, CA) was used to measure the amount of phosphorylated peptide in reaction mixtures. A calibration curve was constructed by measuring the anisotropy of solutions with known ratios of phosphorylated to non-phosphorylated peptide. The standard with 100% phosphorylated peptide was prepared using purified PKB and the percentage phosphorylation was verified with capillary electrophoresis. Anisotropy was measured using a fluorescence plate reader (SpectraMax M5, Molecular Devices, Sunnyvale, CA) with an excitation of 485 nm (bandwidth of 9 nm) and emission of 525 nm (bandwidth of 15 nm). Samples were diluted to the working concentration of 100 nM for the IMAP assay with a buffer containing 10 mM Tris-HCl (pH 7.2), 10 mM $MgCl_2$, and 0.01% Tween-20.

4.2.7 Capillary Electrophoresis

Laser-induced fluorescence (excitation of 488 nm and emission at 525 nm) was used for peptide detection during capillary electrophoresis (ProteomeLab PA800, Beckman Coulter, Fullerton, CA). Fused silica capillaries [50 μm inner diameter, 360 μm outer diameter (Polymicro Technologies, Phoenix, AZ)] had a total length of 30 cm with an effective length of 20 cm. Capillaries were conditioned prior to use with 0.1 M NaOH for 12 h, H_2O for 1 h, 0.1 M HCl for 6 h, and H_2O again for 12 h. After each sample, the capillary was sequentially rinsed with 1 M NaOH, H_2O, and buffer for 2 min by applying a pressure of 20 psi to the capillary inlet. A sample plug was hydrodynamically loaded into the capillary

by applying 0.5 psi to the inlet for 5 s. Electrophoresis was initiated by application of a negative voltage to the outlet. For most peptides, the electrophoretic buffer was 100 mM borate and 100 mM SDS, pH 7.7, with a field strength of 400 V cm^{-1}. For the remaining peptides, the electrophoretic buffer was 100 mM borate and 7 mM SDS, pH 9.5, with a field strength of 333 V cm^{-1}.

4.2.8 Single-Cell Capillary Electrophoresis

Single-cell CE was performed using a custom made CE system with LIF detection, as described previously.[29] Fused silica capillaries [30 μm inner diameter, 360 μm outer diameter, (Polymicro Technologies, Phoenix, AZ)] with a total length of 38 cm and an effective length of 21.5 cm were conditioned as described above. For peptide I, the electrophoretic buffer was 100 mM borate and 100 mM SDS, pH 7.7 and a field strength of 315 V cm^{-1} was applied. For peptide VI-B, the electrophoretic buffer was either 300 mM borate, pH 7.5 or 100 mM borate and 7 mM SDS, pH 7.7, with a field strength of 260 V cm^{-1}. In all instances, electrophoresis was initiated by application of a negative voltage to the outlet while the inlet reservoir was held at ground. Cells were perfused with extracellular buffer (ECB; 135 mM NaCl, 5 mM KCl, 1 mM $MgCl_2$, 1 mM $CaCl_2$, and 10 mM HEPES, pH 7.4, 37 ^oC) during experiments, with the flow turned off immediately prior to lysis and loading into the capillary. Laser-based lysis was achieved with a focused Nd:YAG laser as previously described[53] and the cell contents were electrokinetically loaded into the capillary by applying -3 kV to the capillary outlet while holding the inlet at ground. To identify the peptide fragments formed in a cell, standards of peptide fragments (100 nM) were hydrodynamically loaded into the capillary following the contents of a cell previously microinjected with the full-length peptide. A voltage was then applied across the capillary to

initiate electrophoretic separation. These electropherograms were compared to electropherograms with no standard co-injected to determine if that peptide fragment was formed. To calibrate the amount of peptide on the electropherograms, a known concentration of standard of each intact peptide was hydrodynamically loaded into the capillary, electrophoresed, and the area under the peak calculated. Poiseuille's equation was utilized to estimate the amount of peptide injected.[37]

4.3 Results and Discussion

4.3.1 Selection of the Starting Peptide and Screening Lysates

The starting peptide I (*6FAM*-GRPRAATFAEG) was based on the consensus sequence RPRAATF, determined in a library screen to be phosphorylated by PKB, but not phosphorylated by two other closely-related kinases, p70 S6 Kinase and MAP kinase activated protein kinase-1, the only peptide screened in the library with these properties.[54] Furthermore, in a large multiplexed assay to analyze substrate specificity of 26 kinases, peptide I was found to be relatively selective for PKB.[55] Peptide I was efficiently phosphorylated by purified PKB *in vitro* (Figure 4.1). Two cell types with upregulated PKB activity were chosen for this proof-of-principle work. LNCaP cells, a line derived from a human metastatic prostate adenocarcinoma, have decreased PTEN (phosphatase and tensin homolog) activity resulting in elevated PKB activity.[56] PTEN is a phosphatase that dephosphorylates the lipid messenger PIP_3, leading to a decrease in the association of PKB to the membrane and a decrease in additional PKB activation[2, 5, 57] HeLa cells, a line derived from a human cervical adenocarcinoma, overexpress PI3-K, also resulting in increased PKB activity.[58]

In order to identify the initial peptide bond hydrolyzed in a cellular environment, peptide I was incubated in a HeLa or LNCaP cell lysate. Aliquots were removed over time and CE-LIF was utilized to quantify the peak area of fluorescent species over time. At time zero in both the HeLa and LNCaP cytosolic lysates, a single peak with a migration time identical to that of the intact substrate was seen (Figure 4.2A). However as the incubation time was increased, peptide I was rapidly metabolized with a lifetime of 20 ± 2 and 6 ± 0.9 min in the HeLa and LNCaP lysate, respectively (Figure 4.2-4.4). Under these conditions and when normalized for total cytosolic protein, peptide I was broken down at an average initial rate of 0.12 ± 0.01 and 0.4 ± 0.06 zmol pg^{-1} s^{-1} in the HeLa and LNCaP lysates, respectively. In both the HeLa and LNCaP lysate, multiple additional peaks formed over time with similar initial rates. This suggested that in these lysates, several different peptide bonds could be utilized as the initial site of hydrolysis. By 60 min, six peaks other than that due to the starting peptide were present in the lysate and the original peptide had decreased to approximately 10% and 0% of all species present in the HeLa and LNCaP lysate, respectively. Since the cytosolic lysates did not possess peptidase or phosphatase inhibitors or added ATP, it was likely that the six additional peaks were proteolytic fragments of the starting peptides. The significantly shorter lifetime of the peptide in the LNCaP lysate relative to the HeLa lysate was most likely due to the large amounts of proteases synthesized by cells of the prostate lineage.[59]

To identify which peptide fragments were formed in the cell lysates, standards of all possible fluorescent fragments of peptide I were synthesized and the migration time of each standard compared to that resulting from the cell lysates. Under the electrophoretic conditions utilized, all fragment standards were present as a single major peak and each

migrated at a unique time. Each of the peaks generated in the HeLa and LNCaP lysates matched to a single standard fragment (Figure 4.2B, C, F). After incubation in the HeLa lysate for 60 min, two peptide fragments (peptides k and i, Figure 4.2F) each totaled approximately 20% of all species present, while the remaining four peptide fragments (peptides h, g, f, and e) each comprised less than 10% of all species present. After 60 min in the LNCaP lysate, the same 6 peptide fragments were present although in different amounts and peptide k was present as the dominant species. From these data, no clear initial bond was identified as a primary site of hydrolysis in either cell lysate.

4.3.2 Strategy for Design of a Peptidase-Resistant PKB Substrate

Since there was no clear initial peptidase cleavage site on peptide I for either cell lysate, a strategy to repeatedly generate a small library incorporating altered peptide residues followed by screening was utilized. Each library targeted a single residue for modification and was screened for the time for 50% phosphorylation by PKB ($t_{50\%P}$) as well as for the peptide lifetime ($t_{1/2}$) and the appearance of a dominant fragment in a HeLa cell lysate (Figure 4.5). The appearance of a dominant hydrolysis site narrowed the choice of residues for targeted modifications and offered a rational next step in peptide modification. After identification of the optimal peptide sequence in the library, all possible fluorescent fragments were synthesized to identify cleavage sites to target for subsequent alterations. A second small library was generated followed by rescreening for $t_{50\%P}$ and $t_{1/2}$ and dominant fragment formation. Successive iterations of this process led to identification of multiple cleavage locations that were stabilized to yield a longer-lived substrate for PKB.

4.3.3 Characterization of Peptides Following Replacement of the Amino-Terminal Alanine

The alanine residue on the amino-terminal side of the alanine-alanine bond was selected at random for initial residue modification. Cleavage of this peptide bond yielded peptide g, a five-residue fragment. Peptide I was synthesized with the amino-terminal alanine replaced by one of the alanine derivatives: β-, N-methylated, or D-alanine (Figure 4.6) all of which have been demonstrated to impart resistance to peptidase activity in peptide substrates.[49-51] $t_{50\%P}$ and $t_{1/2}$ for peptides II-A through II-C (Table 4.1) were measured. None of the peptides showed an increased resistance to degradation when compared to peptide I, with $t_{1/2}$ values equal to or much less than peptide I (20, 11, and 3 min compared to 20 min). No phosphorylation was detected for any of these peptides either. As none of these peptide modifications resulted in a substrate peptide with any improved properties, these peptides were not pursued further.

4.3.4 Characterization of Peptides Following Arginine Replacement

The next site targeted for modification was the arginine carboxy-terminal to the proline since cleavage at this site yielded peptide i, a three-residue peptide and the most abundant fragment formed in the HeLa lysate after 45 min of incubation with peptide I. Mono- and di-methyl-substituted, β-, and D-arginine are readily available derivatives that can impart stability against proteolysis.[50] These modified arginine residues were utilized to synthesize peptides III-A through III-D (Table 4.1) and $t_{1/2}$ and $t_{50\%\,P}$ were measured for each peptide. These peptides showed no improvement in $t_{1/2}$ over peptide I, with values ranging from 2 to 17 min. Three of the four peptides showed no evidence of phosphorylation, while the N-methylated arginine-substituted peptide (III-B) possessed a $t_{50\%\,P}$ of 1013 min, more than 50X longer than peptide I. When the fragment standards of peptide III-B were generated and utilized to identify the fragments formed in the lysate, the cleavage at the 3-

mer site or Arg-Pro bond was eliminated. After 60 min, the 4- and 5-mer fragments accounted for a small percentage of the total peptide, while the 6-residue fragment generated by hydrolysis of the alanine-threonine bond was the dominant fragment, comprising 92% of all peptide present within 15 min. Although III-B possessed poorer properties than the starting substrate, it did yield a dominant fragment upon incubation with a cell lysate and a single preferred hydrolysis site that could be targeted for modification. For this reason, peptide III-B was used as the template in all subsequent optimization rounds.

4.3.5 Characterization of Peptides Following the Replacement of the Carboxy-Terminal Alanine

The alanine residue located at the alanine-threonine cleavage site of III-B was targeted for modification since hydrolysis of this peptide bond yielded the dominant fragment when III-B was incubated in a HeLa cell lysate. Non-native derivatives of alanine, β- and D-alanine, were substituted for the alanine (peptides IV-A and IV-B, Table 4.1). Furthermore, since the active site of PKB possesses a hydrophobic pocket near the phosphorylatable threonine and is adjacent to a localized region of positive potential,[60] two hydrophobic residues (peptides IV-D and IV-E) and a glutamic acid (peptides IV-F) were also inserted in place of the alanine (Table 4.1). The $t_{1/2}$ and $t_{50\%\ P}$ were measured for each of the peptides IV-A through IV-E. Peptide IV-E showed no resistance to degradation ($t_{1/2}$ of 2 min). Two peptides, IV-A and IV-D, displayed a $t_{1/2}$ of 14 min, 7X longer than peptide III-B. Peptides IV-B and IV-C exhibited even longer $t_{1/2}$ values, 32 and 37 min, respectively. Three peptides, IV-A, IV-B and IV-C, possessed a $t_{50\%\ P}$ more than 30X greater than the starting peptide I. Peptide IV-E demonstrated a $t_{50\%\ P}$ of 125 min, 7X longer than peptide I, but 8X better than that of peptide III-B. The final peptide, IV-D, demonstrated a $t_{50\%\ P}$ of 30 min, on the same order of magnitude as that for peptide I and over 30X faster than that of peptide III-

B. Additionally, when the fragments of peptide IV-D were analyzed, the dominant initial fragment in the HeLa lysate was the 8-residue fragment generated when the phenylalanine-alanine bond was hydrolyzed. Thus peptide IV-D was selected as the next lead peptide.

4.3.6 Characterization of Peptides Following Phenylalanine or Alanine Replacement

The next residues targeted for modification were the two amino acids flanking the cleavage site of the most abundant fragment of peptide IV-D. Pentafluorophenylalanine (Figure 4.6) was substituted in place of the phenylalanine to impart additional hydrophobicity to the position (peptide V-A).[61] In addition, the non-native derivatives D-alanine and sarcosine (Figure 4.6) were inserted in place of the alanine to investigate substrate suitability (peptides V-B and V-C). Peptides V-A and V-C possessed $t_{1/2}$ values 5X greater than that of peptide IV-D. However, peptide V-B displayed the greatest resistance to proteolysis, with a $t_{1/2}$ of nearly 900 min, over 60X greater than that of IV-D. Although V-A and V-B were phosphorylated more slowly than peptide IV-D ($t_{50\%\ P}$ values more than 6X larger than that of IV-D), peptide V-C was phosphorylated at a rate ($t_{50\%\ P}$ of 21 min) similar to that of IV-D. Furthermore, V-C displayed upon lysate incubation a single fragment which formed over time, the 9-mer peptide generated by hydrolysis of the sarcosine-glutamic acid bond (40% of the total peptide present after 60 min). Based on this single hydrolysis position, peptide V-C was selected for further modifications.

4.3.7 Characterization of Peptides Following Truncation of the Substrate

As illustrated by the consensus sequence, RPRAATF (where T is the site of phosphorylation), the amino terminal sites play the predominant role in PKB substrate recognition. Thus removal of the two carboxy-terminal residues from the lead peptide V-C might not significantly alter the suitability of the substrate for PKB. Since the only fragment

formed when peptide V-C was incubated in the cytosolic lysate was the 9-residue fragment, this truncated peptide (peptide VI-A) was assessed for its stability over time in a HeLa cell lysate. Additionally $t_{1/2}$ and $t_{50\%\ P}$ for a methyl-alanine substituted 9-mer (peptide VI-B) was also measured. The $t_{1/2}$ of peptide VI-A was 13 min, indicating that this peptide was significantly less stable than the parent peptide V-C. However, peptide VI-B possessed a $t_{1/2}$ of 92 ± 7 min, similar to that of peptide V-C. When the peptides were incubated with PKBα, $t_{50\%\ P}$ for both VI-A and VI-B was similar to that of peptide V-C. Based on these combined properties, peptide VI-B was selected for further characterization.

4.3.8 Characterization of Lead Peptide VI-B in Cytosolic Lysates

Although the lead peptide VI-B was more stable than peptide I in a HeLa cell lysate, it was still hydrolyzed into four fragments. The latter were identified by synthesizing all possible fluorescent fragments. Under the electrophoretic conditions employed, all of the fragments were present as individual non-co-migrating peaks that also did not co-migrate with the intact non-phosphorylated or phosphorylated parent peptides (Figure 4.7). Each peak in the lysate mixture co-migrated with a single standard peak (Figure 4.8B). Peptide p, which was the fragment present in the highest amount, comprised 20% of all species after 60 min, and formed at an average initial rate of 0.02 ± 0.002 zmol pg^{-1} s^{-1} (Figure 4.8D). Three additional peaks also formed in the HeLa lysate, but on much slower timescales than peptide p (Figure 4.8D). The parent peptide was degraded at an average initial rate of 0.03 ± 0.004 zmol pg^{-1} s^{-1}, and approximately 60% remained after 60 min.

Peptide VI-B was also incubated in a LNCaP cytosolic lysate, a more aggressive proteolytic environment, and fragment formation over time was assessed (Figure 4.8E and 4.9). Only three fragments were seen in addition to the intact parent peptide, with peptide p

making up 90% of all peptide present after 60 min. The rate of breakdown of the intact parent in the LNCaP lysate was 0.16 ± 0.03 zmol pg^{-1} s^{-1}, over 5X faster than breakdown in the HeLa lysate. Peptide p formed at a rate essentially as fast as the parent was degraded, at 0.14 ± 0.02 zmol pg^{-1} s^{-1}. Two additional fragments, peptides o and n, formed at a much slower rate, similar to the result obtained in the HeLa lysate. As expected in the cell line with a more aggressive proteolytic environment, peptide bond hydrolysis proved to be much faster, although the primary cleavage location remained the same.

The kinetic parameters K_M and k_{cat} were determined for peptide I and the lead peptide VI-B in order to compare the substrate efficiency of these peptides. Varying concentrations of each peptide were incubated with PKB and the initial reaction velocity was calculated for each substrate concentration. Peptide I exhibited a better K_M than peptide VI-B (3 μM compared to 23 μM) but a poorer k_{cat} (3,400 min^{-1}) relative to that of VI-B (5,800 min^{-1}) leading to a 4.5-fold better efficiency for VI-B over peptide I.

4.3.9 Characterization of Peptide Degradation in Single LNCaP Cells

In order to assess the fate of the peptides when loaded into single cells, peptide I or VI-B was microinjected into a single LNCaP cell. Individual single cells were washed, briefly incubated, lysed with a single pulse from an Nd:YAG laser, and the cell contents separated and detected by CE-LIF. Eight peaks were observed on the electropherogram upon incubation of peptide I for 90 s in a single cell (n = 7 cells; Figure 4.10A). Fragment identification was achieved by injecting the fluorescent fragment standards immediately after the contents of a microinjected cell and electropherograms of samples with and without standards were compared. Under the electrophoretic conditions employed, all fragment standards were present as non-co-migrating individual single peaks, making positive

identification of all fragments possible. In addition, the phosphorylated peptide was detected and comprised between 0 – 22% of the total peptide in a cell (9 ± 8%). Finally, the intact peptide I constituted between 4 – 25% of all peptide present (11 ± 7%). Fragment peptides i (3-mer) and f, (6-mer), were present at the highest amounts, up to 26% and 27%, respectively, and a smaller amount of 1-, 4-, 5-, and 7-mer fragments were present. In short, peptide I was degraded too rapidly for use in intact LNCaP cells. By contrast, the lead peptide VI-B comprised 56 ± 13% (n = 30 cells) of all peptide species present and phosphorylated substrate 10 ± 9% (with a range from 0 – 37%; Figure 4.10B). Only two other species were observed, namely fragments corresponding to peptides m (8-mer) and p (5-mer).

Based on these preliminary results, peptide VI-B was selected for further study in single LNCaP cells. To quantify the amount of peptide degradation and phosphorylation over a longer time scale, peptide VI-B was microinjected into single LNCaP cells (n = 19) and incubated for 5 min prior to cell lysis and CE-LIF. Four peaks were observed, with intact, non-phosphoryated, parent peptide accounting for 15 ± 5% of all species present. The parent peptide was degraded into one of two fragment peaks (peptides m or p) or converted to phosphorylated product (Figure 4.11A). In addition, the major peptide fragment identified in single cells was peptide m (40% of total peptide present), the 8-residue fragment seen only in small amounts in the LNCaP lysate studies (Figure 4.8E). The major fragment seen in the LNCaP lysate studies, peptide p, was present only as a minor species in the single cells. Assuming a cell volume of 1 pL and a total protein concentration of 100 mg mL^{-1},[62] the intact peptide was eliminated at an average rate of 0.1 ± 0.2 zmol pg^{-1} s^{-1}, similar to the breakdown rate measured in LNCaP cytosolic lysates. The rate of degradation of the intact parent

peptide was linearly dependent on the peptide concentration (4 ± 8 μM) in the cell (Figure 4.11C), with a linear regression analysis yielding an R^2 value of 0.9899.

4.3.10 Phosphorylation of Peptide VI-B in Single LNCaP Cells

Five min after introduction of VI-B into single cells, the percentage of intact peptide that was phosphorylated ranged from 0 – 80% (58 ± 26%). The amount of phosphorylated peptide present varied linearly with respect to the amount of peptide microinjected into the cell (Figure 4.11D). A linear regression analysis of the rate of phosphorylation yielded an R^2 value of 0.9401, indicating greater cell-to-cell variability in amount of peptide phosphorylated relative to that degraded in cells even after correction for the amount of peptide loaded into cells. This may be due to a greater variation in the concentration of active kinase present in single cells relative to that of the peptidases. Flow cytometry-based measurements suggest that the numbers of protein molecules per cell for enzymes involved in proteolytic degradation are tightly regulated and thus have relatively little cell-to cell variation.[63] By contrast, the copy number for molecules acting as components of signaling cascades responsive to environmental stimuli generally have significant noise or much greater variation in the cell-to-cell copy numbers.

4.3.11 Inhibition of PKB Activity in Single Cells

Wortmannin is a selective inhibitor of PI3-K when used in nanomolar concentrations.[64] The decreased formation of PIP_3 resulting from wortamnnin-exposure leads to decreased PKB activation. LNCaP cells were pre-incubated with 500 nM wortmannin (10 min) and then loaded with VI-B (n = 10). After 5 min, cells were individually lysed and their contents separately electrophoresed. Four peaks (intact parent, phosphorylated substrate, and fragments m and p) were identified in these cells as with the

cells without wortmannin (Figure 4.11B). There was no statistical difference in the amount of degradation observed when compared to cells with no pre-treatment (p-value of 0.77) (Figure 4.11C). Formation of phosphorylated product was substantially decreased (13% ± 12%) compared that for cells not pretreated with wortmannin (p-value of 1.1×10^{-6}). Wortmannin also inhibits mTOR, myosin light chain kinase (MLCK), and phosphatidylinositol 4-kinase (PI4K) but at micromolar concentrations.[64] Thus, inhibition of phosphorylation by these low concentrations of wortmannin suggests that the peptide was predominantly acting as a substrate for PKB.

4.4 Conclusions

An iterative design and screening process was used to identify and stabilize locations susceptible to proteolysis in a kinase substrate peptide. Each round of redesign yielded a substrate with more favorable properties until a peptide resistant to lysate peptidases, yet suitable as a PKB substrate, was obtained. The optimized peptide displayed similar fragmentation patterns in lysates from cervical (HeLa) *vs* prostate (LNCaP) cancer cell lines, but the rates of hydrolysis were dramatically different. The relatively high proteolytic rates observed in the prostate-derived cells was likely due to the fact that normal prostate produce an abundance of proteases. The rate of proteolysis in the LNCaP lysate was similar to that seen in the single LNCaP cells. Remarkably, the primary cleavage locations differed between lysates and single cells, suggesting that different peptidases may access the peptide in these two conditions, thereby indicating that lysates do not always provide an accurate mimic of the intact cell. Although substantial variability existed in the percentage of peptide degraded in single cells, this variability was a consequence of the variation in the amount of

peptide loaded into cells *i.e.* the final intracellular peptide concentration. With regard to phosphorylation, substantial variability existed between single cells, indicating differing amounts of kinase activity in cells within the same population. These measurements are consistent with other measures of single cell variability, such as that seen in flow cytometry and microscopy.[18, 65-68]

4.5 Figures and Tables

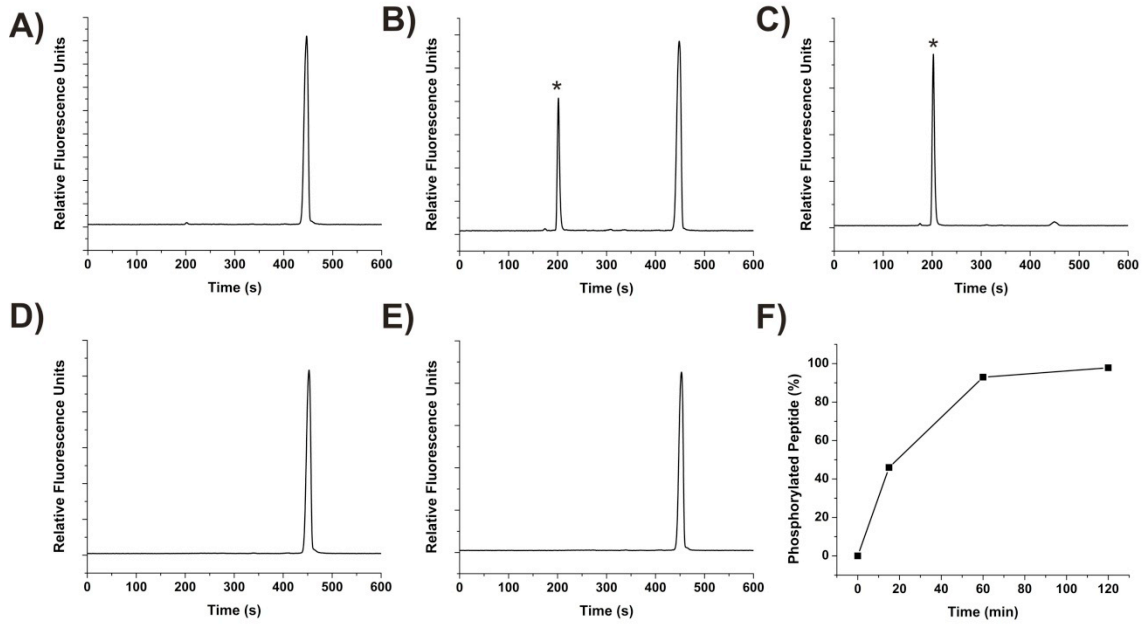

Figure 4.1: *in vitro* phosphorylation of starting peptide I over time. (A) – (C) Electropherograms of the reaction mixture with PKB after 0 (A), 15 (B), and 120 (C) min of incubation. The * represents phosphorylated product. (D) – (E) Electropherograms of peptide product after 0 (D) and 120 (E) min incubation with the reaction mixture with PKB but without ATP. (F) Peptide phosphorylation as a function of time.

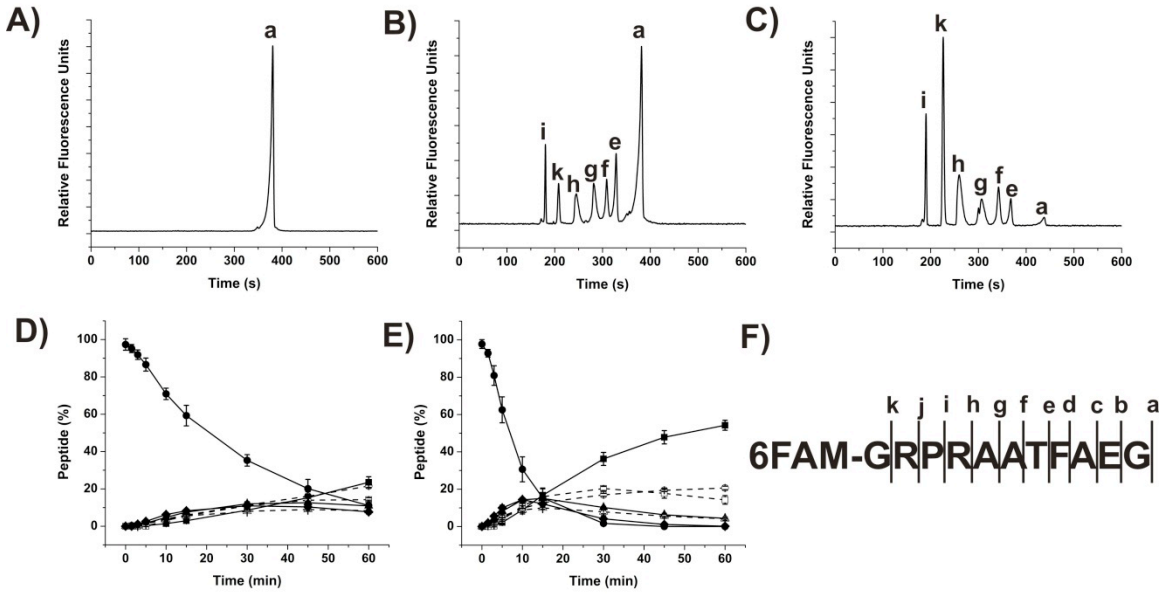

Figure 4.2: Degradation of the starting peptide I in cytosolic lysates. (A) - (C) Electropherograms of peptide I after incubation in a HeLa or LNCaP lysate for 0 min (A) for 30 min in HeLa (B) or for 30 min in LNCaP (C) cytosolic lysate. (D) Formation of peptide fragments over time in HeLa lysate. (E) Formation of peptide fragments over time in LNCaP lysate. The symbols are defined as: closed circle (peptide a or starting peptide); open circle (peptide i); closed square (peptide k); open square (peptide h); closed triangle (peptide g); open triangle (peptide f); and closed diamond (peptide e). (F) The uppercase letters are the single amino acid abbreviations for the starting peptide sequence. The lowercase letters represent cleavage locations that form the indicated fluorescent peptide fragments.

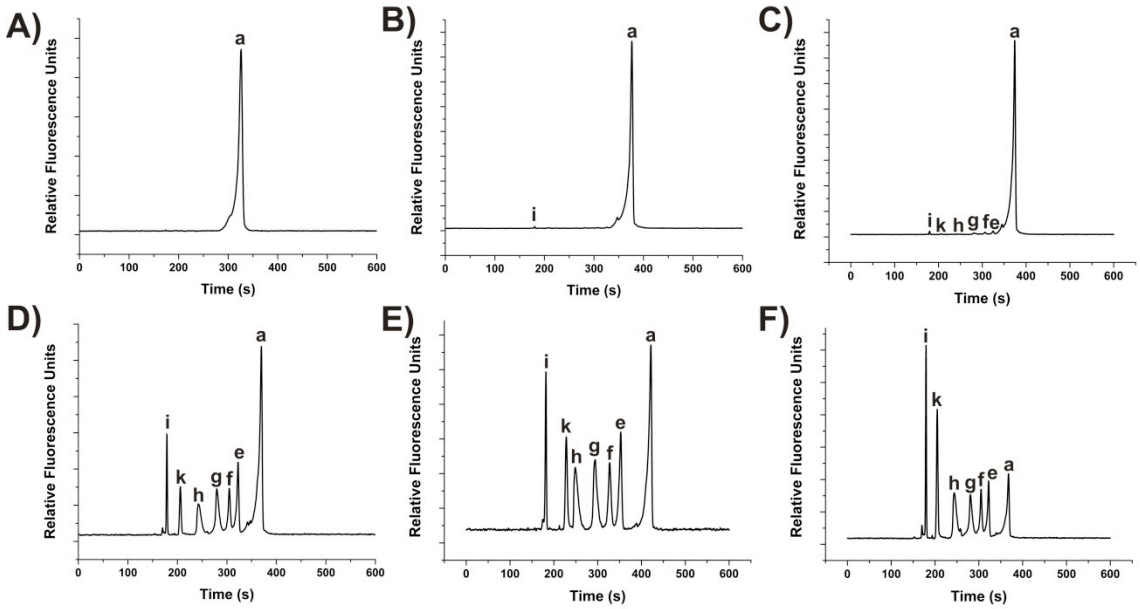

Figure 4.3: Electropherograms of the starting peptide I when incubated in HeLa cytosolic lysate for 0 (A), 1.5 (B), 3 (C), 30 (D), 45 (E), and 60 (F) min. The lowercase letters represent the intact peptide or fragment peptides as defined in Figure 4.2F.

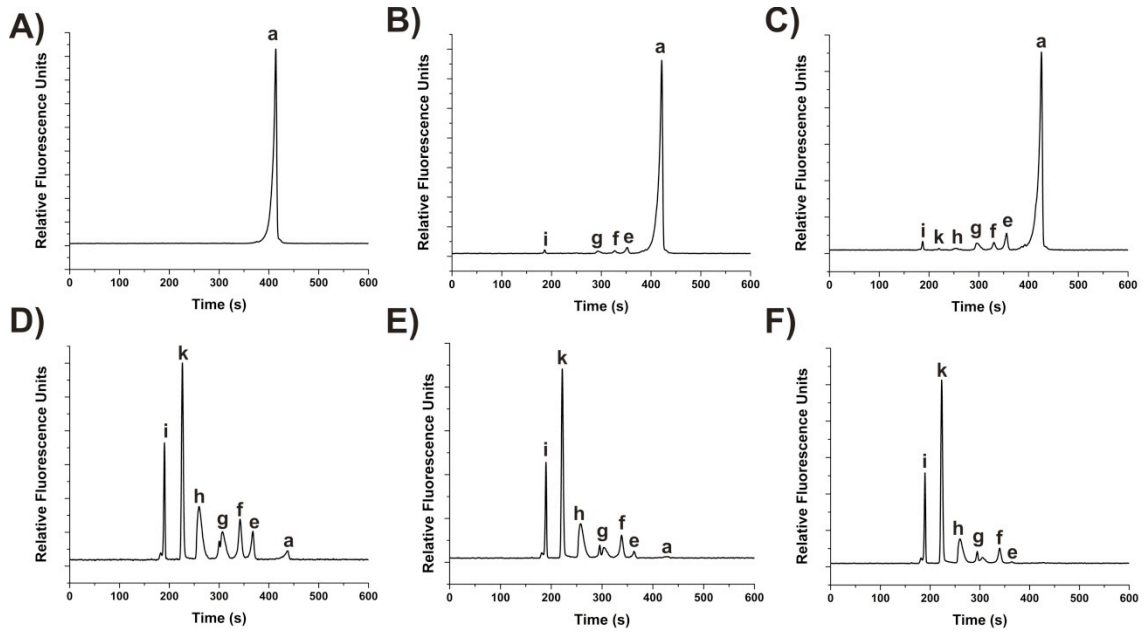

Figure 4.4: Electropherograms of the starting peptide I when incubated in LNCaP cytosolic lysate for 0 (A), 1.5 (B), 3 (C), 30 (D), 45 (E), and 60 (F) min. The lowercase letters represent the intact peptide or fragment peptides as defined in Figure 4.2F.

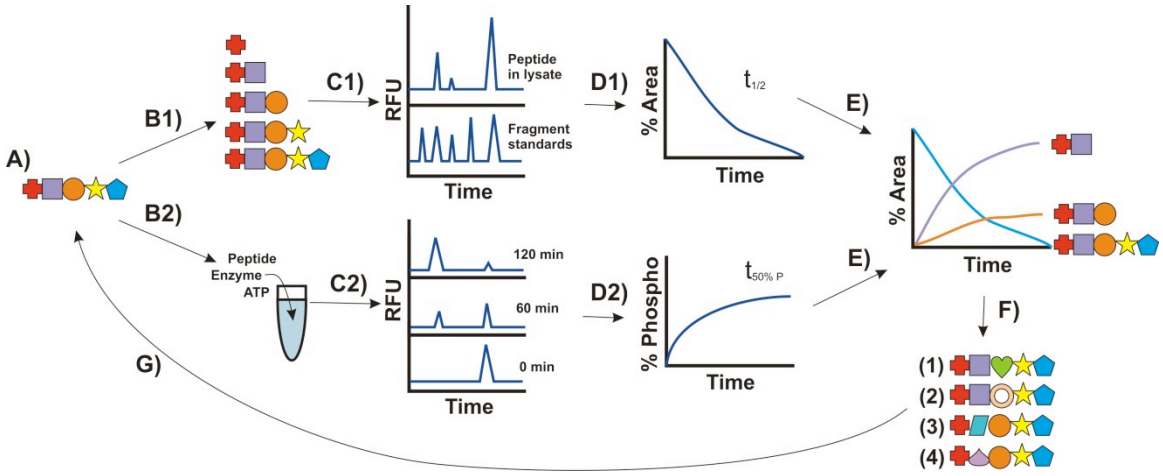

Figure 4.5: Schematic of rational peptide substrate design. (A) Synthesize starting peptide. The different geometrical shapes represent different amino acids. (B) Synthesize all possible peptide fragments of starting peptide (B1) and incubate starting peptide with active enzyme and ATP (B2). (C) Use CE-LIF to analyze degradation and identify peptide fragments formed (C1) and to assess phosphorylation over time (C2). (D) Determine the half-life of the peptide in the lysate (D1) and the time required for the peptide to reach 50% phosphorylation (D2). (E) Of the peptides showing favorable $t_{1/2}$ and $t_{50\% P}$ values, identify whether a preferred cleavage site exists in the peptide. (F) Synthesize a library of new peptide substrates with non-native amino acids adjacent to the most susceptible bond in the lead peptide. (G) Reiterate through steps (B) - (F) until a suitable, long-lived substrate is obtained.

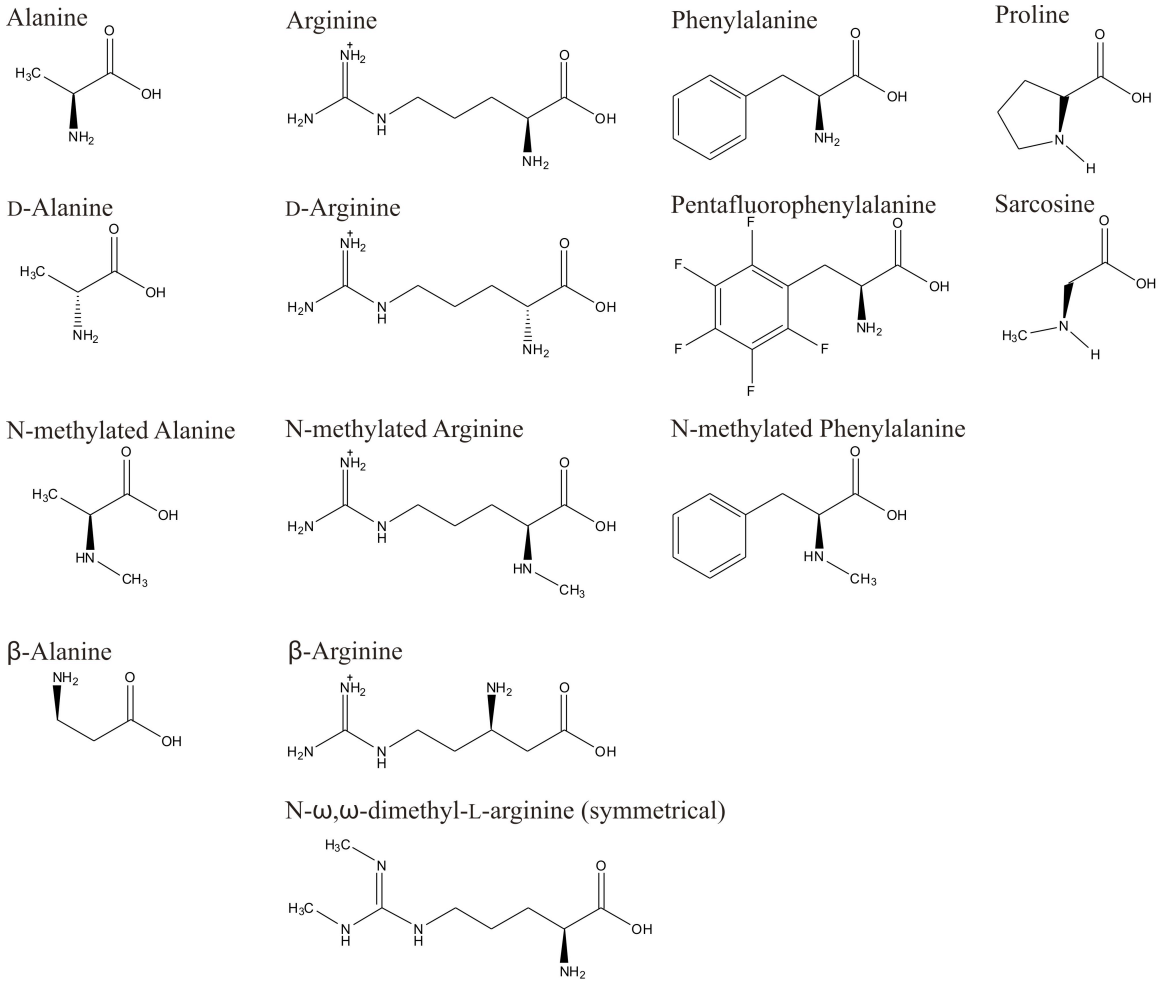

Figure 4.6: Line bond structures of native and non-native amino acids utilized in peptide construction.

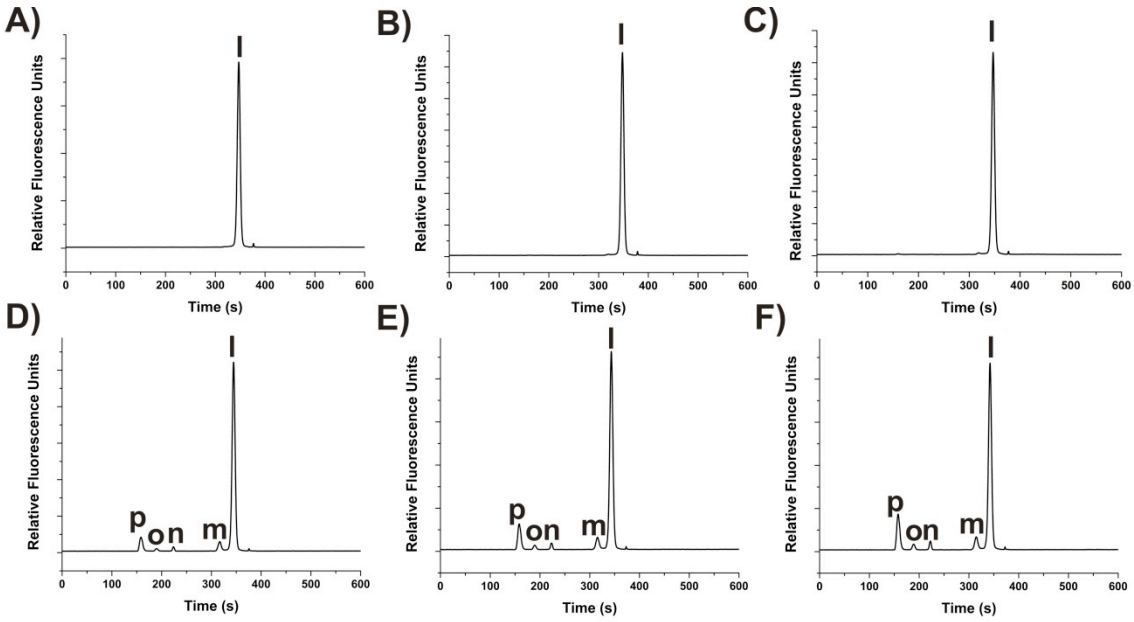

Figure 4.7: Electropherograms of the lead peptide VI-B when incubated in HeLa cytosolic lysate for 0 (A), 1.5 (B), 3 (C), 30 (D), 45 (E), and 60 (F) min. The lowercase letters represent the intact peptide or fragment peptides as defined in Figure 4.8F.

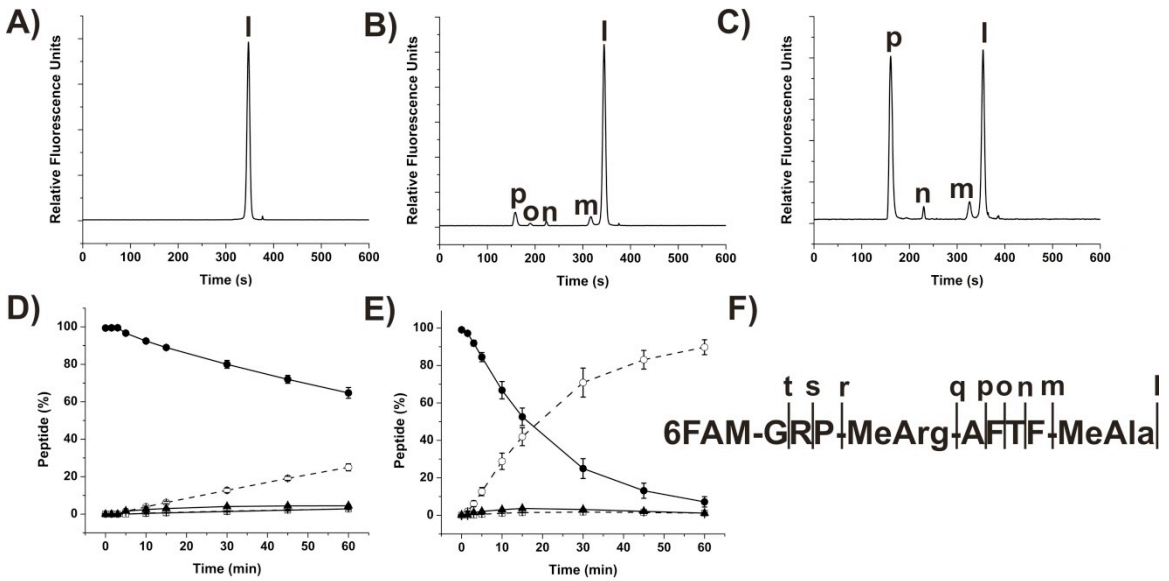

Figure 4.8: Degradation of the lead peptide VI-B in cytosolic lysates. (A) - (C) Electropherograms of peptide I after incubation in a HeLa or LNCaP lysate for 0 min (A) for 30 min in HeLa (B) or for 30 min in LNCaP (C) cytosolic lysate. (D) Formation of peptide fragments over time in HeLa cell lysate. (E) Formation of peptide fragments over time in LNCaP cell lysate. The symbols are defined as: closed circle (peptide l); open circle (peptide p); closed square (peptide o); open square (peptide n); and closed triangle (peptide m). (F) The uppercase letters are the single amino acid abbreviations for the lead peptide sequence, MeArg is N-methylated arginine, and MeAla is N-methylated alanine. The lowercase letters represent cleavage locations that form the indicated fluorescent peptide fragments.

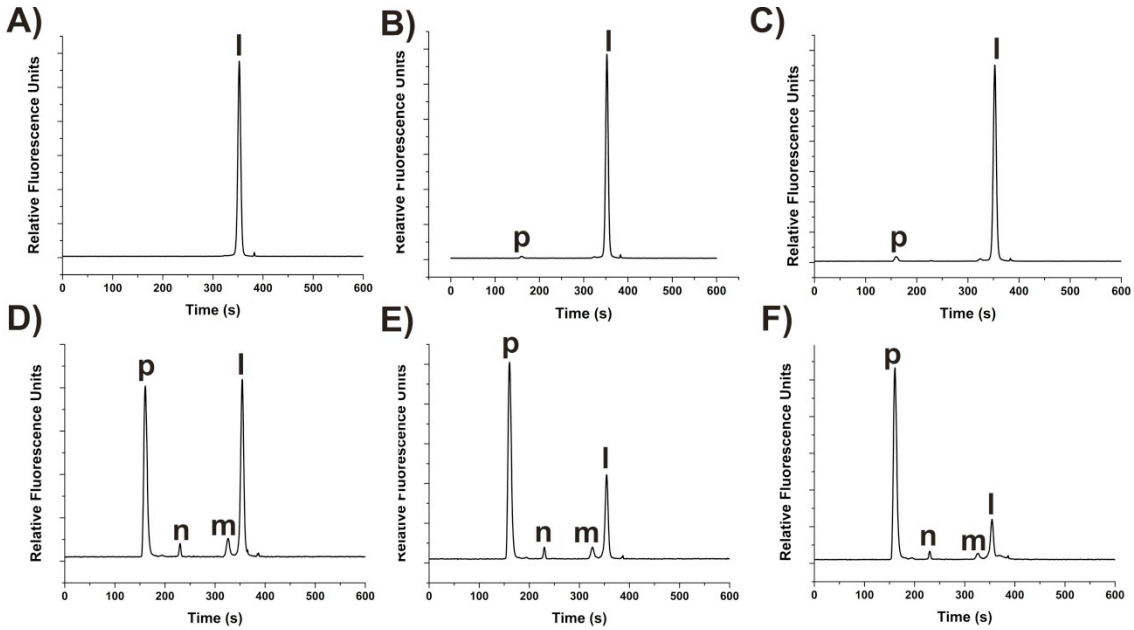

Figure 4.9: Electropherograms of the lead peptide VI-B when incubated in LNCaP cytosolic lysate for 0 (A), 1.5 (B), 3 (C), 30 (D), 45 (E), and 60 (F) min. The lowercase letters represent the intact peptide or fragment peptides as defined in Figure 4.8F.

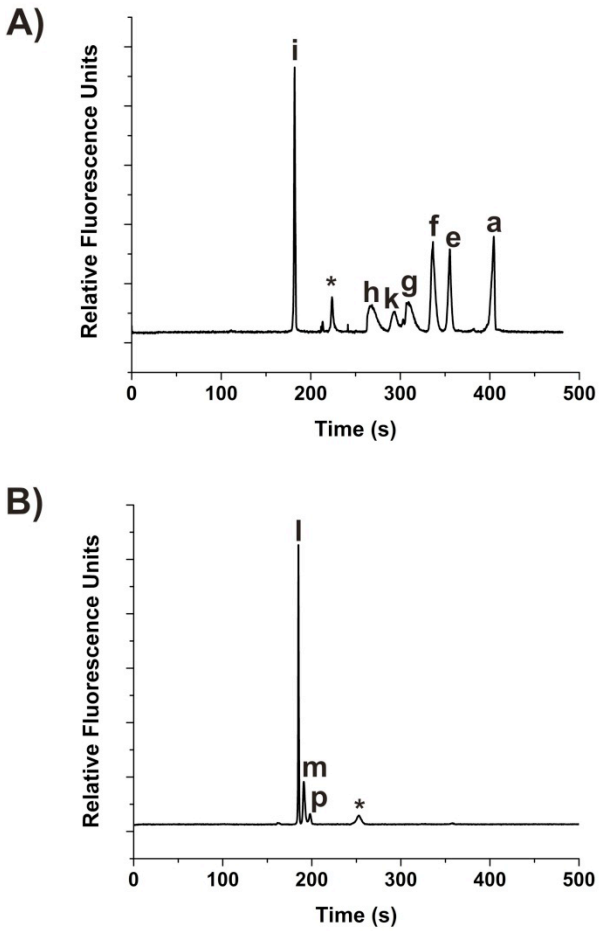

Figure 4.10: Electropherograms of single LNCaP cells 90 s after microinjection of the starting peptide I (A) or lead peptide VI-B (B). The lowercase letters represent the intact peptide or peptide fragments identified in Figures 4.2F and 4.8F and the * represents phosphorylated peptide product.

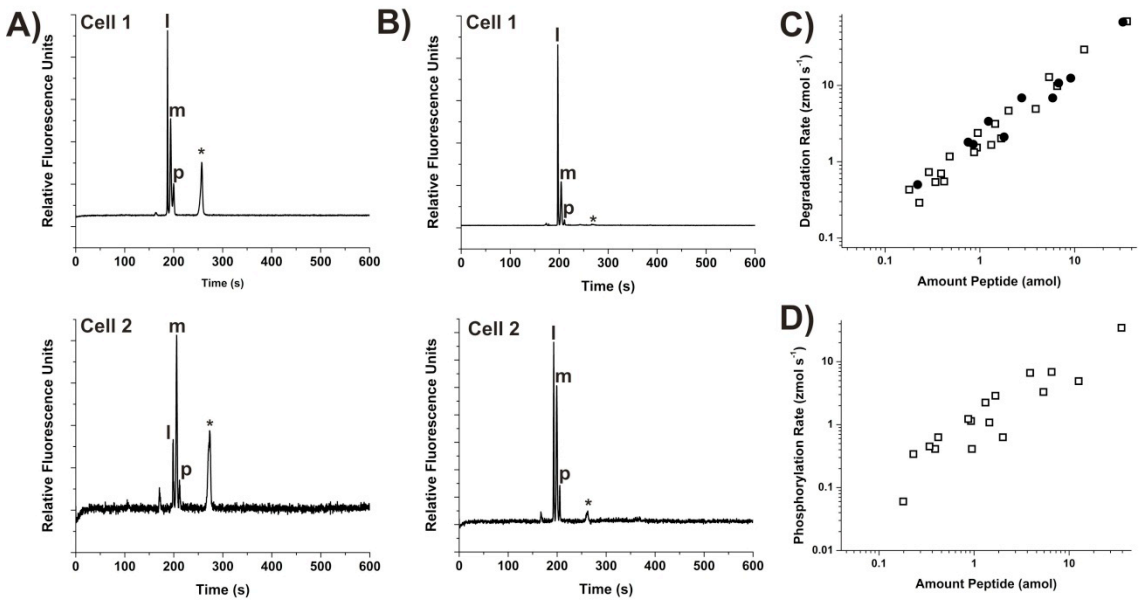

Figure 4.11: Electropherograms of single LNCaP cells 5 min after microinjecting the lead peptide QW-VII-48F without (A) or with pre-treatment with wortmannin (B). The lowercase letters mark the peaks due to the intact peptide or peptide fragments identified in Figure 4.8F and the * labels the peak due to the phosphorylated peptide product. Two representative cells are shown for (A) and for (B). (C) Rate of degradation of parent peptide as a function of amount microinjected in single cells with (open squares, n = 19) and without (closed circles, n = 10) pre-treatment with wortmannin. (D) Rate of phosphorylation as a function of amount microinjected in single cells.

Table 4.1: Properties of the modified peptides derived from starting peptide I.

Peptide	Sequence	$t_{50\%P}$ (min)	$t_{1/2}$ (min)	Initial Dominant Fragment
I	6FAM-GRPRAATFAEG	17	20	5-mer
II-A	6FAM-GRPR-βAla-ATFAEG	NP	20	ND
II-B	6FAM-GRPR-MeAla-ATFAEG	NP	3	ND
II-C	6FAM-GRPR-DAla- ATFAEG	NP	11	ND
III-A	6FAM-GRP-βArg-AATFAEG	NP	9	ND
III-B	6FAM-GRP-MeArg-AATFAEG	1013	2	6-mer
III-C	6FAM-GRP-Arg(Me2)-AATFAEG	NP	8	ND
III-D	6FAM-GRP-DArg-AATFAEG	NP	17	ND
IV-A	6FAM-GRP-MeArg-A-βAla-TFAEG	$>10^5$	14	ND
IV-B	6FAM-GRP-MeArg-A-DAla-TFAEG	$>10^5$	32	ND
IV-C	6FAM-GRP-MeArg-A-Glu-TFAEG	679	37	ND
IV-D	6FAM-GRP-MeArg-A-FTFAEG	30	14	8-mer
IV-E	6FAM-GRP-MeArg-A-MePhe-TFAEG	125	2	ND
V-A	6FAM-GRP-MeArg-AFT-Phe(F5)-AEG	174	88	ND
V-B	6FAM-GRP-MeArg-AFTF-DAla-EG	306	895	9-mer
V-C	6FAM-GRP-MeArg-AFTF-Sarc-EG	21	84	9-mer
VI-A	6FAM-GRP-MeArg-AFTF-Sarc-NH_2	36	13	ND
VI-B	6FAM-GRP-MeArg-AFTF-MeAla-NH_2	34	92	5-mer

[a]$t_{50\%\,P}$ is the time required for 50% of the peptide to be phosphorylated and [b]$t_{1/2}$ is the half-life of the intact peptide in a cytosolic lysate. NP = no phosphorylation. ND = not determined. The amino acids are represented by their standard one letter code except for the following, which are defined as: βAla (Beta-alanine), MeAla (N-methylated alanine), DAla (D-alanine), βArg (Beta-arginine), MeArg (N-methylated arginine), Arg(Me2) (N-ω,ω-dimethyl-L-arginine(symmetrical)), MePhe (N-methylated phenylalanine), Phe(F5) (pentafluorophenylalanine), and Sarc (sarcosine, or N-methyl glycine).

4.6 References

1 D. P. Brazil, J. Park and B. A. Hemmings. "PKB Binding Proteins: Getting in on the Akt". *Cell,* 2002, *111*, 293-303.

2 J. Brognard and A. C. Newton. "PHLiPPing the switch on Akt and protein kinase C signaling". *Trends Endocrin. Met.,* 2008, *19*, 223-230.

3 E. Fayard, L. A. Tintignac, A. Baudry and B. A. Hemmings. "Protein kinase B/Akt at a glance". *J. Cell Science,* 2005, *118*, 5675-5678.

4 D. R. Alessi and P. Cohen. "Mechanism of activation and function of protein kinase B". *Curr. Opin. Genet. Dev.,* 1998, *8*, 55-62.

5 D. P. Brazil and B. A. Hemmings. "Ten years of protein kinase B signalling: a hard Akt to follow". *Trends Biochem. Sci.,* 2001, *26*, 657-664.

6 S. R. Datta, A. Brunet and M. E. Greenberg. "Cellular survival: a play in three Akts". *Gene Dev.,* 1999, *13*, 2927.

7 C. Garcia-Echeverria and W. R. Sellers. "Drug discovery approaches targeting the PI3-K/Akt pathway in cancer". *Oncogene,* 2008, *27*, 5511-5526.

8 E. S. Kandel and N. Hay. "The Regulation and Activities of the Multifunctional Serine/Threonine Kinase Akt/PKB". *Exp. Cell Res.,* 1999, *253*, 210-229.

9 C. C. Kumar and V. Madison. "AKT crystal structure and AKT-specific inhibitors". *Oncogene,* 2005, *24*, 7493-7501.

10 K. M. Nicholson and N. G. Anderson. "The protein kinase B/Akt signalling pathway in human malignancy". *Cell. Signal.,* 2002, *14*, 381-393.

11 B. D. Manning and L. C. Cantley. "AKT/PKB Signaling: Navigating Downstream". *Cell,* 2007, *129*, 1261-1274.

12 X. Chen, H. Thakkar, F. Tyan, S. Gim, H. Robinson, C. Lee, S. K. Pandey, C. Nwokorie, N. Onwudiew and R. K. Srivastava. "Constitutively active Akt is an important regulator of TRAIL sensitivity in prostate cancer". *Oncogene,* 2001, *20*, 6073-6083.

13 D. Auguin, P. Barthe, M. Augé-Sénégas, M. Stern, M. Noguchi and C. Roumestand. "Solution structure and backbone dynamics of the pleckstrin homology domain of the human protein kinase B (PKB/Akt). Interaction with inositol phosphates". *J. Biomol. NMR,* 2004, *28*, 137-155.

14 M. A. Lawlor and D. R. Alessi. "PKB/Akt: a key mediator of cell proliferation, survival and insulin responses?". *J. Cell Sci.,* 2001, *114*, 2903-2910.

15 J. E. Knittle, D. Roach, P. B. Vander Horn and K. O. Voss. "Laser-Induced Fluorescence Detector for Capillary-Based Isoelectric Immunoblot Assay". *Anal. Chem.,* 2007, *79*, 9478-9483.

16 J. Ždychová, L. Kazdová, T. Pelikanová, J. N. Lindsley, S. Anderson and R. Komers. "Renal Activity of Akt Kinase in Obese Zucker Rats". *Exp. Biol. M.,* 2008, *233*, 1231-1241.

17 P. O. Krutzik, J. M. Crane, M. R. Clutter and G. P. Nolan. "High-content single-cell drug screening with phosphospecific flow cytometry". *Nat. Chem. Biol.,* 2008, *4*, 132-142.

18 P. O. Krutzik, J. Irish M., G. P. Nolan and O. D. Perez. "Analysis of protein phosphorylation and cellular signaling events by flow cytometry: techniques and clinical applications". *Cl. Immunol.,* 2004, *110*, 206-221.

19 O. D. Perez and G. N. Nolan. "Simultaneous measurement of multiple active kinase states using polychromatic flow cytometry". *Nat. Biotechnol.,* 2002, *20*, 155-162.

20 P. L. Tazzari, A. Cappellini, T. Grafone, I. Mantovani, F. Ricci, A. M. Bili, E. Ottaviani, R. Conte, G. Martinelli and A. M. Martelli. "Detection of serine 473 phosphorylated Akt in acute myeloid leukaemia blasts by flow cytometry". *Brit. J. Haematol.,* 2004, *126*, 675-681.

21 P. L. Tazzari, A. Cappellini, R. Bortul, F. Ricci, A. M. Billi, G. Tabellini, R. Conte and A. M. Martelli. "Flow Cytometric Detection of Total and Serine 473 Phosphorylated Akt". *J. Cell Biochem.,* 2002, *86*, 704-715.

22 E. Newell, S. Bendall, D. Hong, D. Lewis, G. Nolan and M. Davis. "Surveying the Influenza-specific Cytotoxic T Cell Response in Humans and Mice Using Mass-cytometry (CyTOF) and Combinatorial Tetramer Staining". *Cl. Immunol.,* 2010, *135*, S104.

23 R. K. Cheung and P. J. Utz. "CyTOF-the next generation of cell detection". *Nat. Rev. Rheumatol.,* 2011, *7*, 502-503.

24 S. C. Bendall, E. F. Simonds, P. Qiu, E. D. Amir, P. O. Krutzik, R. Finchk, R. V. Bruggner, R. Melamed, A. Trejo, O. I. Ornatsky, R. S. Balderas, S. K. Plevritis, K. Sachs, D. Pe'er, S. D. Tanner and G. P. Nolan. "Single-Cell Mass Cytometry of Differential Immune and Drug Responses Across a Human Hematopoietic Continuum". *Science,* 2011, *332*, 687-696.

25 J. Fritschy, "Is my antibody-staining specific? How to deal with pitfalls of immmunohistochemistry". *Eur. J. Neurosci.,* 2008, *28*, 2365-2370.

26 M. T. Kunkel, Q. Ni, R. Y. Tsien, J. Zhang and A. C. Newton. "Spatio-temporal Dynamics of Protein Kinase B/Akt Signaling Revealed by a Genetically Encoded Fluorescent Reporter". *J. Biol. Chem.,* 2005, *280*, 5581-5587.

27 L. Zhang, K. C. Lee, M. S. Bhojani, A. P. Khan, A. Shilman, E. C. Holland, B. D. Ross and A. Rehemtulla. "Molecular imaging of Akt kinase activity". *Nat. Med.,* 2007, *13*, 1114-1119.

28 H. Li, C. E. Sims, M. Kaluzova, E. J. Stanbridge and N. L. Allbritton. "A Quantitative Single-Cell Assay for Protein Kinase B Reveals Important Insights into the Biochemical Behavior of an Intracellular Substrate Peptide". *Biochemistry,* 2004, *43*, 1599-1608.

29 A. Proctor, Q. Wang, D. S. Lawrence and N. L. Allbritton. "Metabolism of peptide reporters in cell lysates and single cells". *Analyst,* 2012, *137*, 3028-3038.

30 J. W. Yewdell, E. Reits and J. Neefjes. "Making Sense of Mass Destruction: Quantitating MHC Class I Antigen Presentation". *Nat. Rev. Immunol.,* 2003, *3*, 952-961.

31 D. J. Bernsteel, D. L. Roman and R. R. Neubig. "In vitro protein kinase activity measurement by flow cytometry". *Anal. Biochem.,* 2008, *383*, 180-185.

32 L. L. Parker, S. B. Brueggemeier, W. J. Rhee, D. Wu, S. B. H. Kent, S. J. Kron and S. P. Palecek. "Photocleavable peptide hydrogel arrays for MALDI-TOF analysis of kinase activity". *Analyst,* 2006, *131*, 1097-1104.

33 Q. Wang, E. I. Zimmerman, A. Toutchkine, T. D. Martin, L. M. Graves and D. S. Lawrence. "Multicolor Monitoring of Dysregulated Protein Kinases in Chronic Myelogenous Leukemia". *ACS Chem. Biol.,* 2010, *5*, 887-895.

34 X. Xu, X. Liu, Z. Nie, Y. Pan, M. Guo and S. Yao. "Label-Free Fluorescent Detection of Protein Kinase Activity Based on the Aggregation Behavior of Unmodified Quantum Dots". *Anal. Chem.,* 2011, *83*, 52-59.

35 X. Han, G. Yamanouchi, T. Mori, J. Kang, T. Niidome and Y. Katayama. "Monitoring Protein Kinase Activity in Cell Lysates Using a High-Density Peptide Microarray". *J. Biomol. Screen,* 2009, *14*, 262.

36 D. Wu, J. E. Sylvester, L. J. Parker, G. Zhou and S. J. Kron. "Peptide reporters of kinase activity in whole cell lysates". *Biopolymers,* 2010, *94*, 475-486.

37 G. D. Meredith, C. E. Sims, J. S. Soughayer and N. L. Allbritton. "Measurement of kinase activation in single mammalian cells". *Nat. Biotechnol.,* 2000, *18*, 309-312.

38 S. Kottegoda, P. C. Aoto, C. E. Sims and N. L. Allbritton. "Biarsenical-Tetracysteine Motif as a Fluorescent Tag for Detection in Capillary Electrophoresis". *Anal. Chem.,* 2008, *80*, 5358-5366.

39 S. N. Arkhipov, M. Berezovski, J. Jitkova and S. N. Krylov. "Chemical Cytometry for Monitoring Metabolism of a Ras-Mimicking Substrate in Single Cells". *Cytom. Part A,* 2005, *63A*, 41-47.

40 R. B. Brown, J. A. Hewel, A. Emili and J. Audet. "Single Amino Acid Resolution of Proteolytic Fragments Generated in Individual Cells". *Cytom. Part A,* 2010, *77A*, 347-355.

41 Y. Tal-Gan, M. Hurevich, S. Klein, A. Ben-Shimon, D. Rosenthal, C. Hazan, D. E. Shalev, M. Y. Niv, A. Levitzki and C. Gilon. "Backbone Cyclic Peptide Inhibitors of Protein Kinase B (PKB/Akt)". *J. Med. Chem.,* 2011, *54*, 5154-5164.

42 E. M. Molhoek, A. van Dijk, E. J. A. Veldhuizen, H. P. Haagsman and F. J. Bikker. "Improved proteolytic stability of chicken cathelicidin-2 derived peptides by D-amino acid substitutions and cyclization". *Peptides,* 2011, *32*, 875-880.

43 O. Ovadia, Y. Linde, C. Haskell-Leuvano, M. L. Dirain, T. Sheynis, R. Jelinek, C. Gilon and A. Hoffman. "The effect of backbone cyclization on PK/PD properties of bioactive peptide-peptoid hybrids: The melanocortin agonist paradigm". *Bioorga.n Med. Chem.,* 2010, *18*, 580-589.

44 L. T. Nguyen, J. K. Chau, N. A. Perry, L. de Boer, S. A. J. Zaat and H. J. Vogel. "Serum Stabilities of Short Tryptophan- and Arginine-Rich Antimicrobial Peptide Analogs". *PLoS ONE,* 2010, *5*, 1-8.

45 Y. Koda, M. T. Liang, J. T. Blanchfield and I. Toth. "*In vitro* stability and permeability studies of lipsomal delivery systems for a novel lipophilic endomorphin 1 analogue". *Int. J. Pharm.,* 2008, *356*, 37-43.

46 C. D. Cros, I. Toth and J. T. Blanchfield. "Lipophilic derivatives of leu-enkephalinamide: In vitro permeability, stability and in vivo nasal delivery". *Bioorgan. Med. Chem.,* 2011, *19*, 1528-1534.

47 L. H. Brinckerhoff, V. V. Kalashnikov, L. W. Thompson, G. Yamshchikov, R. A. Pierce, H. S. Galavotti, V. H. Engelhard and C. L. Slingluff Jr. "Terminal Modifications Inhibit Proteolytic Degradation of an Immunogenic Mart-1_{27-35} Peptide: Implications for Peptide Vaccines". *Int. J. Cancer,* 1999, *83*, 326-334.

48 I. Neundorf, R. Rennert, J. Franke, I. Közle and R. Bergmann. "Detailed Analysis Concerning the Biodistribution and Metabolism of Human Calcitonin-Derived Cell-Penetrating Peptides". *Bioconjugate Chem.,* 2008, *19*, 1596-1603.

49 R. Tugyi, K. Uray, D. Iván, E. Fellinger, A. Perkins and F. Hudecz. "Partial D-amino acid substitution: Improved enzymatic stability and preserved Ab recognition of a MUC2 epitope peptide". *PNAS,* 2005, *102*, 413-418.

50 L. Gentilucci, R. De Marco and L. Cerisoli. "Chemical Modifications Designed to Improve Peptide Stability: Incorporation of Non-Natural Amino Acids, Pseudo-Peptide Bonds, and Cyclization". *Curr. Pharm. Design,* 2010, *16*, 3185-3203.

51 E. V. Pappa, A. A. Zompra, Z. Spyranti, Z. Diamantopoulou, G. Pairas, F. N. Lamari, P. Katsoris, G. A. Spyroulias and P. Cordopatis. "Enzymatic Stability, Solution Structure, and Antiproliferative Effect on Prostate Cancer Cells of Leuprolide and New Gonadotropin-Releasing Hormone Peptide Analogs". *Biopolymers,* 2010, *96*, 260-272.

52 G. M. Funk, C. E. Hunt, D. E. Epps and P. K. Brown. "Use of a rapid and highly sensitive fluorescamine-based procedure for the assay of plasma lipoprotiens". *J. Lipid Res.,* 1986, *27*, 792-795.

53 C. E. Sims, G. D. Meredith, T. B. Krasieva, M. W. Berns, B. J. Tromberg and N. L. Allbritton. "Laser-Micropipet Combination for Single-Cell Analysis". *Anal. Chem.,* 1998, *70*, 4570-4577.

54 D. R. Alessi, F. B. Caudwell, M. Andjelkovic, B. A. Hemmings and P. Cohen. "Molecular basis for the substrate specificity of protein kinase B; comparison with MAPKAP kinase-1 and p70 S6 kinase". *FEBS Lett.,* 1996, *399*, 333-338.

55 M. D. Shults, I. A. Kozlov, N. Nelson, B. G. Kermani, P. C. Melnyk, V. Shevchenko, A. Srinivasan, J. Musmacker, J. P. Hachmann, D. L. Barker, M. Lebl and C. Zhao. "A Multiplexed Protein Kinase Assay". *ChemBioChem,* 2007, *8*, 933-942.

56 H. Murillo, H. Huang, L. J. Schmidt, D. I. Smith and D. J. Tindall. "Role of PI3-K Signaling in Survival and Progression of LNCaP Prostate Cancer Cells to the Androgen Refractory State". *Endocrinology,* 2001, *142*, 4795-4805.

57 T. L. Yuan and L. C. Cantley. "PI3-K pathway alterations in cancer: variations on a theme". *Oncogene,* 2008, *27*, 5497-5510.

58 X. Zhang, H. Zhang, P. Zhang, X. Lu and H. Sun. "Elevated phosphatidylinositol 3-kinase activation and its clinicopathological significance in cervical cancer". *Eur. J. Obstet. Gyn. R. B.,* 2008, *139*, 237-244.

59 L. Santamaría, I. Ingelmo, L. Alonso, J. M. Pozuelo and R. Rodriguez, “Neuroendocrine Cells and Peptidergic Innervation” in *Advances in Anatomy Embryology and Cell Biology,* ed. F. F. Beck, F. Clasca, M. Frotscher, D. E. Haines, H. W. Korf, E. Marani, R. Putz, Y. Sano and T. H. Schiebler, 2007, pp.1-79.

60 T. Obata, M. B. Yaffe, G. G. Leparc, E. T. Piro, H. Maegawa, A. Kashiwagi, R. Kikkawa and L. C. Cantley. "Peptide and Protein Library Screening Defines Optimal Substrate Motifs for AKT/PKB". *J. Biol. Chem.,* 2000, *275*, 36108-36115.

61 D. M. Ryan, S. B. Anderson, F. T. Senguen, R. E. Youngman and B. L. Nilsson. "Self-assembly and hydrogelation promoted by F_5-phenylalanine". *Soft Matter,* 2010, *6*, 475-479.

62 A. Schmid, H. Kortmann, P. S. Dittrich and L. M. Blank. "Chemical and biological single cell analysis". *Curr. Opin. Biotech.,* 2010, *21*, 12-20.

63 J. R. S. Newman, S. Ghaemmaghami, J. Ihmels, D. K. Breslow, M. Noble, J. L. DeRisi and J. S. Weissman. "Single-cell proteomic analysis of S. cerevisiae reveals the architecture of biological noise". *Nature,* 2006, *441*, 840-846.

64 J. Bain, L. Plater, M. Elliott, N. Shpiro, C. J. Hastie, H. McLauchlan, I. Klevernic, J. S. C. Arthur, D. R. Alessi and P. Cohen. "The selectivity of protein kinase inhibitors: a further update". *Biochem. J.,* 2007, *408*, 297-315.

65 J. S. Rasey, J. R. Grierson, L. W. Wiens, P. D. Kolb and J. L. Schwartz. "Validation of FLT Uptake as a Measure of Thymidine Kinase-1 Activity in A549 Carcinoma Cells". *J. Nucl. Med.,* 2002, *43*, 1210-1217.

66 Q. Ni, D. V. Titov and J. Zhang. "Analyzing protein kinase dynamics in living cells with FRET reporters". *Methods,* 2006, *40*, 279-286.

67 M. Ouyang, H. Huang, N. C. Shaner, A. G. Remacle, S. A. Shiryaev, A. Y. Strongin, R. Y. Tsien and Y. Wang. "Simultaneous Visualizatoin of Protumorigenic Src and MT1-MMP Activities with Fluorescence Resonance Engery Transfer". *Cancer Res.,* 2010, *70*, 2204-2212.

68 Q. Xue and E. S. Yeung. "Variability of Intracellular Lactate Dehydrogenase Isoenzymes in Single Human Erythrocytes". *Anal. Chem.,* 1994, *66*, 1175-1178.

CHAPTER 5

MEASUREMENT OF PKB ACTIVITY IN SINGLE PANCREATIC CANCER CELLS

5.1 Introduction

5.1.1 Pancreatic Ductal Adenocarcinoma

Pancreatic ductal adenocarcinoma (PDA) accounts for greater than 90% of all types of pancreatic cancer and it is the 4th most common cause of cancer-related deaths in the United States.[1-4] PDA generally develops in adults over 60 in and around the pancreatic duct and can lead to a blockage of the pancreatic or bile ducts. PDA tumors can invade deep into the pancreas and into nearby organs and can also metastasize to the lymph nodes or other regions of the body often prior to diagnosis.[5, 6] The American Cancer Society estimates there will be approximately 44,000 new cases of PDA and 38,000 deaths from PDA in 2012, with equal mortality rates between men and women.[5] The 1-year survival rate after diagnosis with PDA is only 26%, with a 5-year survival rate around 6%. The facts are even more grim for individuals diagnosed with late-stage PDA, where the 5-year survival rate is only 2%.[5] As there are little to no early symptoms of PDA, greater than 50% of individuals are not diagnosed until the late stages, once the cancer has already metastasized, giving a median survival rate of 6 months. Treatment for patients with PDA can include surgical removal of the cancer as well as radiation therapy and chemotherapy, though these measures usually only relieve symptoms and may briefly extend survival, and rarely do they end in a cure.[5]

Two chemotherapeutic drugs often used are gemcitabine and erlotinib (Tarceva) and many new compounds are in clinical trials with hopes of identification of new and useful treatments for PDA.[5, 7]

5.1.2 Protein Kinase B and PDA

The PI3-K pathway, and specifically PKB, is responsible for multiple cellular functions such as transcription, proliferation, stress response, and apoptosis (section 1.1.2). The PI3-K/PKB pathway has been found to be mutated or overactive in greater than 50% of all human cancers, meaning this pathway is of intense interest to cancer researchers and clinicians working to understand and eliminate cancer.[8-10] PKB has been found to be constitutively active in PDA, both in tissue-cultured cell lines and human tumor samples, though actual activity varies between cell type.[2, 9, 11-15] No gene mutations of PKB have been found, meaning alterations to the pathway are likely occurring at the mRNA or protein levels through mechanisms not yet fully elucidated.[16]

Activation of PKB in tumors can occur by modulation of the upstream components of the PI3-K pathway. Expression of the phosphatase responsible for dephosphorylation of PIP_3 (PTEN) is often found to be low or missing in PDA cell lines and tumor specimens, with PTEN activity undetected in 5 of 8 cells lines and in 12 of 17 tumor specimens interrogated.[2] When PTEN expression and activity is low, PIP_3 remains phosphorylated with sustained recruitment of PKB to the membrane (section 1.1.2), resulting in sustained PKB activity. Furthermore, activation of PKB can be an indicator of the aggressiveness of the pancreatic cancer, with higher levels of PKB associated with decreased patient survival as PKB helps to prevent apoptosis and promote angiogenesis within the bulk PDA tumor.[9, 14, 15, 17, 18] In studies where PI3-K and PKB activity were inhibited with wortmannin or LY294002 (a

reversible PI3-K inhibitor), cells became sensitive to anti-cancer treatment, further demonstrating the role of the PI3-K/PKB pathway in cancer survival and progression.[1, 9, 12] As PKB gene copy number and protein levels do not always correlate with a measurable increase in PKB activity, a technique that can directly measure PKB activity would be of high utility in determination of PKB kinase activity in single PDA cells.

5.1.3 Xenografts of Human Cancer

A technique widely used in pharmaceutical testing of anticancer therapeutic compounds involves the transplantation of human cell lines into nude mice. Although these cell lines have been sustained in tissue culture for prolonged times, the cell lines retain the ability to form tumors *in vivo*. These tumors are known as xenografts and have long been used as a model of various human cancers such as breast, lung, ovarian, and pancreatic cancers.[19, 20] The mice are treated with therapeutics and the tumor response is characterized, with the hopes that the murine model will predict behavior of the corresponding tumor type in humans. However, in most cases, therapeutics that appear to work in the mouse tumors derived from tissue-cultured cell lines do not often work in the human form of the cancer.[19] However, first reported in the 1970s was the use of a direct-transfer xenograft (also known as a tumorgraft), where a section of a tumor removed from a human patient is directly transferred into a mouse model and allowed to grow. These types of xenografts show proliferation within the mouse, retain the heterogeneity and behaviors of the human tumor, and provide a model for drug discovery, therapy, or histological analysis of the human tumor.[7, 19, 20] A recent paper by Hidalgo *et al*. outlines the use of direct-transfer xenografts from 14 different cancer patients to determine likely therapeutic drugs for successful treatment of their respective cancers.[7] The authors reported likely treatment options for 12 of

the 14 patients, and showed treatment success in all but one of those patients (who died prior to treatment), demonstrating a potential use for direct-transfer xenografts. In the context of the work described in this chapter, these direct-transfer xenografts provide a means of obtaining primary human pancreatic cancer cells for analysis of PKB activity. Collaborator Dr. Jen Jen Yeh, of the UNC-CH Department of Pharmacology and UNC Hospitals Division of Surgical Oncology, provided all xenograft cells utilized in this work.

5.1.4 Single-cell Analysis of PKB Activity in Pancreatic Cancer Cells

The peptidase-resistant peptide substrate reporter developed in Chapter 4 was used to assay PKB activity in single tissue-cultured pancreatic cancer cells and in primary human pancreatic cancer cells derived from direct-transfer xenografts into mice. The immortalized tissue cultured cells were used to assess PKB activity in cell lines with varying amounts of PKB activity to demonstrate the feasibility of the technique, the heterogeneity of cells within a population, and to characterize the substrate breakdown and phosphorylation in single cells. Finally, this substrate was characterized in single primary pancreatic cells obtained from the direct-transfer xenografts and utilized to measure PKB activity in these cells

5.2 Materials and Methods

5.2.1 Chemicals

Peptide synthesis reagents were purchased as indicated in sections 3.2.1 and 4.2.1 of this dissertation. Dulbecco's Modified Eagle Medium (DMEM), was procured from Cellgro; Iscove's Modified Dulbecco's Medium (IMDM), Minimal Essential Medium (MEM), 0.25% trypsin, and penicillin/streptomycin were obtained from Gibco; fetal bovine serum (FBS) was

purchased from Atlanta Biologicals; and wortmannin was obtained from LC Laboratories. All other chemicals used in the assays were purchased from Sigma for Fisher.

5.2.2 Peptide Synthesis and Preparation

All peptides were synthesized by collaborator Dr. Qunzhao Wang in the Lawrence Lab unless specified otherwise. A detailed table of all peptides prepared and utilized in this dissertation can be found in Appendix C. Synthesis of the peptide used in this chapter is fully described in section 4.2.2.

5.2.3 Cell Culture

5.2.3.1 Immortalized Cell Lines

HPAF-II (human pancreatic adenocarcinoma), CFPAC-1 (human metastatic ductal pancreatic adenocarcinoma), and PANC-1 (human pancreatic carcinoma) were obtained from the American Type Culture Collection.[21-23] HPAF-II cells were cultured in MEM supplemented with 10% FBS, penicillin (100 units/mL), and streptomycin (100 μg/mL). CFPAC-1 cells were cultured in IMDM supplemented with 10% FBS, penicillin (100 units/mL), and streptomycin (100 μg/mL). PANC-1 cells were cultured in DMEM supplemented with 10% FBS, penicillin (100 units/mL), and streptomycin (100 μg/mL). All cells were maintained in a humidified atmosphere of 37^{o}C in 5% CO_2 and passaged into fresh media every 2-3 days. Cells used for single-cell CE experiments were plated the day before onto custom chambers, prepared by using poly(dimethyl siloxane) (PDMS, Sylguard 184) to glue a silicon O-ring (McMaster-Carr) to a #1 glass coverslip (Fisher). A dilute cell suspension was added to 500 μL of the appropriate media in the chamber. Chambers were placed in the humidified incubator until use in the experiments.

5.2.3.2 Xenograft Cells

In the Yeh lab, tumors were removed from each mouse, washed with PBS solution, and dissected into small fragments. Tumors were disaggregated by incubating at 37^{o}C for 20 min in 40 mg mL^{-1} collagenase D and Dispase II. After incubation, the mixture was centrifuged at 1,500 x g for 2 min prior to resuspension in fresh media. These direct-transfer xenograft cell solutions procured from the Yeh lab were immediately placed in standard tissue culture flasks or single cell chambers and were cultured in DMEM supplemented with 10% FBS, penicillin (100 units/mL), and streptomycin (100 μg/mL) and maintained in a humidified atmosphere of 37^{o}C in 5% CO_2. The chambers for single cell experiments were prepared by using PDMS to glue a silicon O-ring to a 22 mm^2 cellulose acetate coverslip. Chambers were plasma treated and either plated immediately with a dilute suspension of cells or were coated with a 0.1% gelatin solution prior to addition of cells.

5.2.4 Single Cell Analysis of PKB Activity

Chambers plated with cells the day before the experiment were placed on the microscope stage and rinsed with ECB at 37 ^{o}C to remove all traces of media. Cell volume was estimated by measuring the length and width of each cell and assuming a height of 3 μm. A single cell was microinjected with peptide VI-B and incubated for 5 min in ECB flowing at 3 mL min^{-1} at 37 ^{o}C. The cell was lysed with the Nd:YAG laser, loaded electrokinetically into the capillary, and the capillary was transferred to electrophoretic buffer prior to initiation of electrophoresis.

Cells pre-treated with the inhibitor wortmannin were treated as follows: prior to experiment start, the media was removed from the cell chamber and replaced with 500 μL of 500 nM wortmannin in the appropriate cell media. The cells were incubated for 10 min in a

37 ^{o}C humidified incubator. After this step, the cells were treated the same as the untreated cells described above.

5.2.5 Single-Cell Capillary Electrophoresis

Single-cell CE was performed using the custom built CE system with LIF detection described in Chapter 2 of this dissertation. Fused silica capillaries [30-µm inner diameter, 360-µm outer diameter, (Polymicro Technologies, Phoenix, AZ)] with a total length of 38 cm and an effective length of 21.5 cm were conditioned as described in section 3.2.7. A negative voltage of 10 kV was applied to the outlet reservoir while the inlet reservoir was held at ground. The electrophoretic buffer was 300 mM borate, pH 7.5. Cells were perfused with ECB during experiments, with the flow turned off immediately prior to cell lysis and loading into the capillary. Laser-based cell lysis was achieved with a focused Nd:YAG laser as previously described in Chapter 2.

To identify peptide fragments formed in cells, standards of peptide fragments (100 nM) were hydrodynamically loaded into the capillary immediately following loading of a single cell into the capillary. The cell was not loaded with peptide prior to loading into the capillary, it just provided a milieu for the subsequently loaded standards similar to that obtained from a lysed cell. To calibrate the amount of peptide on the electropherograms, a known concentration of standard of each intact peptide was hydrodynamically loaded into the capillary, electrophoresed, and the area under the peak calculated. Poiseuille's equation (Equation 2.1) was utilized to estimate the amount of peptide injected, as demonstrated by Meredith *et al*.[24] Data was collected with the custom software described in Chapter 2 (LabVIEW 9.0.1, National Instruments, Austin, TX) and analyzed using Origin Software (version 7.5, OriginLab Corporation, Northampton, MA).

5.3 Results and Discussion

5.3.1 Selection of the Substrate Peptide and Cell Lines

Peptide VI-B (*6FAM*-GRP-MeArg-AFTF-MeAla-NH_2) was selected as the peptide substrate for several reasons and the development of peptide VI-B is thoroughly discussed in Chapter 4. In brief, peptide VI-B was more resistant to peptidase degradation than a peptide substrate composed entirely of native amino acids when incubated in single cells. Peptide VI-B was also efficiently phosphorylated by purified PKB enzyme *in vitro* (K_M of 23 μM and k_{cat} of 5,800 min^{-1}), and was phosphorylated in single prostate cancer cells, most likely by PKB (Chapter 4).

Three representative pancreatic cancer cell lines were selected based on their variability in PKB activity, as determined by members of collaborator Dr. Jen Jen Yeh's lab, where PKB activity was determined by utilizing Western blot analysis to measure the amount of phosphorylated serine at position 473 with anti-Ser473 antibody.[25] Pancreatic cancer was chosen as the model for the reasons discussed in the introduction of this chapter (section 5.1). HPAF-II cells were derived from a human pancreatic carcinoma isolated from the peritoneal ascitic fluid of a 44-year old Caucasian male with primary pancreatic adenocarcinoma and metastases to the liver, diaphragm, and lymph nodes.[21] HPAF-II cells displayed very low amounts of active PKB as determined by the Western blot analysis in the Yeh lab. CFPAC-1 cells were derived from the liver of a 26-year old Caucasian male with cystic fibrosis and pancreatic cancer[22] and showed moderate amounts of active PKB in the Western blots performed by the Yeh lab. PANC-1 cells were derived from a 56-year old Caucasian male

with pancreatic cancer[23] and showed the highest amount of active PKB in the Yeh lab Western blot analysis.

5.3.2 Characterization of Peptide Degradation in Single Tissue-Cultured Cells

To assess the degradation of peptide VI-B in intact pancreatic cancer cell lines, the peptide was microinjected into a cell and incubated for 5 min prior to lysis and electrophoresis. Peaks corresponding to fragment peptides were identified based on co-migration with fragment standards, as described in Chapters 3 and 4. When peptide VI-B was incubated in HPAF-II cells (n = 10) for 5 min, four peaks were present in the electropherogram, corresponding to intact parent peptide, phosphorylated parent, and two fragment peptides (Figure 5.1A). The fragment peptides were the same fragments seen when peptide VI-B was incubated in LNCaP cells (Chapter 4), the 5- and 8-residue fragments. The 8-mer fragment formed in the highest amounts, comprising 41 ± 4% of all peptide present after 5 min. The 5-mer was less prevalent, making up only 10 ± 2% of total peptide. 45 ± 2% of the parent peptide was detected in the HPAF-II cells after 5 min. When the total amount of protein in each cell was assumed to be 100 pg,[26] the rate of degradation of the parent peptide was estimated as 0.3 ± 0.3 zmol pg^{-1} s^{-1}, with a range from 0.02 – 0.7 zmol pg^{-1} s^{-1}. Initial substrate concentration in each cell was determined by dividing the calculated number of moles microinjected into each cell (section 5.2.5) by the estimated cell volume (section 5.2.4). When the rate of degradation of intact VI-B was plotted as a function of initial substrate concentration, the rate increased linearly as the substrate concentration was increased (Figure 5.2A). This was the same trend that was seen in the prostate cancer cell line (LNCaP) described in Chapter 4.

When peptide VI-B was microinjected into CFPAC-1 cells (n = 11) and incubated for 5 min, the same four peaks were seen in the electropherograms as were seen in the HPAF-II cells, only at slightly different amounts (Figure 5.1B). The parent peptide was present in the highest amounts, accounting for 39 ± 13% of all peptide present after 5 min. The 8-mer fragment peptide was the next most abundant, at 36 ± 17% of all peptide. The 5-residue fragment was present as 9 ± 5% of all peptide after 5 min. When assuming a total protein concentration of 100 pg per cell, the rate of degradation of the parent peptide was 0.1 ± 0.2 zmol pg^{-1} s^{-1}, with a range of values similar to that seen in the HPAF-II cells, from 0.01 to 0.6 zmol pg^{-1} s^{-1}, indicating that there was no difference in the amount of degradation between CFPAC-1 and HPAF-II cells (p-value of 0.053). The same trend was also observed when degradation rate of intact VI-B was plotted as a function of initial substrate concentration, with the rate increasing linearly with an increase in concentration (Figure 5.2B).

When peptide VI-B was incubated in PANC-1 cells (n = 11) for 5 min, the same four peaks were seen as has been previously described for the HPAF-II and CFPAC-1 cells, just at varying amounts (Figure 5.1C). The 8-residue fragment was formed in the highest amounts after 5 min, accounting for 38 ± 10% of all peptide present after 5 min. The intact parent peptide was present as 23 ± 10% of all peptide after 5 min, and the 5-residue fragment comprised 12 ± 3% of all peptide. When the cells were assumed to contain 100 pg of total protein, the rate of degradation was found to be 0.08 ± 0.2 zmol pg^{-1} s^{-1}, with a range from 0.01 to 0.5 zmol pg^{-1} s^{-1}, not statistically different from that seen in CFPAC-1 cells (p-value of 0.24) or in HPAF-II cells (p-value of 0.81). The same linear trend of increased rate as the substrate concentration was increased was also observed in PANC-1 cells when degradation

rate of intact peptide VI-B was plotted as a function of initial substrate concentration (Figure 5.2C).

5.3.3 Phosphorylation of Peptide VI-B in Single Tissue-Cultured Cells

In addition to the two fragment peaks observed in single cells, phosphorylation of peptide VI-B was also seen in all 3 cell types. After a 5 min incubation of peptide VI-B in HPAF-II cells, 7 ± 6% of undegraded peptide was present as the phosphorylated product and ranged from 0 to 15% (Figure 5.3). When the total protein in each cell was taken to be 100 pg, the rate of phosphorylation was 0.01 ± 0.01 zmol pg^{-1} s^{-1}, with a range from 0 to 0.05 zmol pg^{-1} s^{-1}. The rate of phosphorylation was plotted as a function of initial substrate concentration (Figure 5.4A) and it was determined that the rate of phosphorylation increased linearly as substrate concentration was increased.

When peptide VI-B was incubated for 5 min in CFPAC-1 cells, phosphorylated substrate accounted for 29 ± 18% of undegraded peptide present in the electropherograms (Figure 5.3), ranging from a low of 8% to a high of 59% phosphorylation. It was also noted that the distribution of phosphorylated product appeared to be bimodal, with a cluster of 6 cells showing lower amounts of phosphorylation (8 – 20%) and a cluster of 5 cells showing higher amounts of phosphorylation (41 – 60%). A t-test analysis of these two groups of cells reveals that they are statistically different from each other (p-value of 3.6×10^{-5}). The percent phosphorylation plotted as a function of time was utilized to determine if a bimodal variation of concentration injected into the cells would explain the bimodal distribution of phosphorylation. However, no such relationship was observed, as there appeared to be no correlation between initial substrate concentration and percent phosphorylation. Perhaps

PKB is activated in an on/off fashion, though many more cells would need to be sampled prior to drawing this conclusion. When a cell was assumed to contain 100 pg total protein, the rate of phosphorylation of CFPAC-1 cells was found to be 0.03 ± 0.03 zmol pg^{-1} s^{-1}, with a range from 0.003 to 0.09 zmol pg^{-1} s^{-1}. When the rate of phosphorylation was plotted as a function of initial substrate concentration, the same linear trend as was seen in HPAF-II cells was also observed: as the concentration increased, the rate of phosphorylation also increased (Figure 5.4B).

When peptide VI-B was incubated for 5 min in PANC-1 cells, the amount of phosphorylated substrate ranged from 0 to 76% of undegraded peptide, with an average of 51 ± 25% (Figure 5.3). The amount of phosphorylation was skewed to the high end, with 7 cells showing greater than 50% phosphorylation, and only 4 cells with phosphorylation amounts more than 10% below the average. Once again, when substrate phosphorylation was plotted as a function of initial substrate concentration, there was no correlation between these two parameters and these populations were also statistically different when analyzed with a t-test (p-value of 0.01). This also caused the rate of phosphorylation rates to vary widely, from 0 to 0.09 zmol pg^{-1} s^{-1}, with an average of 0.02 ± 0.03 zmol pg^{-1} s^{-1}, if each cell was assumed to contain 100 pg of total protein. As was seen with both the HPAF-II and CFPAC-1 cells, the rate of phosphorylation increased linearly as a function of initial substrate concentration (Figure 5.4C).

Single cell analysis of substrate phosphorylation by PKB in HPAF-II, CFPAC-1, and PANC-1 cells revealed the difference in the PKB activity amongst the 3 lines. HPAF-II cells showed the lowest amount of substrate phosphorylation, CFPAC-1 cells demonstrated a moderate amount of substrate phosphorylation, and PANC-1 cells possessed the highest

amount of substrate phosphorylation (Figure 5.3), suggesting low, moderate, and high levels of active PKB in the cells, respectively. A non-parametric statistical analysis of variance of these three populations demonstrated a statistically significant difference between the populations (p-value of 4.4×10^{-4}). This was the same trend observed in the Western Blot analysis performed by the Yeh lab, where PKB activity was determined by measurement of the amount of phosphorylated serine at position 473 with anti-Ser473 antibody.[25] However, the single-cell work presented here offers information on cell-to-cell heterogeneity that is not available via Western blot. While HPAF-II cells demonstrated the lowest amount of substrate phosphorylation, a range of nearly 20% was observed. As discussed briefly above, the CFPAC-1 cells appeared to be bi-modally distributed about the mean, while the PANC-1 cells appeared skewed, with a higher number of cells demonstrating phosphorylation greater than the mean, and tailing off toward lower amounts, with one cell even demonstrating no phosphorylation. None of these results are resolvable in Western blot analyses.

Western blot analysis required hundreds of thousands of cells and can only reveal the average of a population, while single cell interrogation can give a wider understanding of what is happening on an individual basis and in the population as a whole. However, the measurement technique utilized in this work is low throughput, with only 7 – 10 cells successfully analyzed in a single day, much too slow for analysis of statistically significant numbers of cells. While tentative conclusions can be drawn about variability within and between each cell population from these results, there is not enough data to draw over-reaching conclusions. Ideally, hundreds to thousands of cells need to be analyzed to further demonstrate the heterogeneity within and among cell populations. However, even with these small sample numbers, differences between cells in the same population did exist. These

differences could have arisen from the cells being at different stages in the cell cycle, where PKB and regulatory enzyme activity could vary dramatically. As was determined by Hu *et al*., protein expression varied in a cell cycle-dependent manner, though PKB was not one of the proteins analyzed.[27] It is possible that PKB could vary depending on cell cycle, accounting for the differences seen among cells of the same type. In each case, while the rate of phosphorylation varied linearly with respect to initial substrate concentration, it did not appear as if there was a correlation between phosphorylation percent and the initial substrate concentration.

Another indication of the variability in these cells is when the rates of phosphorylation were plotted as a function of initial substrate concentration (Figure 5.4). In all 3 cells lines, these plots were linear, with the rate increasing as the concentration was increased. However, there was a large variability in these plots, more than what was seen when rate of degradation of the parent peptide was calculated (Figure 5.2). This same trend was also observed in the LNCaP cells (Chapter 4). Perhaps the kinases and phosphatases are tightly regulated, but are active during some parts of the cell cycle and inactive during other parts.[27] Cells sampled at different stages of the cell cycle could yield large differences in PKB activity. It could also indicate that the peptidases are simply more tightly regulated than the kinase and phosphatases are. Protein degradation is a destructive process that can irreparably damage cell function when not tightly controlled, while regulations on the variability of kinase and phosphatase activity can be less stringent. This was demonstrated by Newman *et al*. in *S. cerevisiae*, where potentially destructive processes varied less than expected while other processes not inherently destructive to the cell varied more than expected.[28] As was postulated by Newman *et al*., variability in kinase function imparts

phenotypic differences in a population that provide the variations in function that can lead a population to survive selective pressures by ensuring that some, if not all, of the population can survive under various stresses. But the evolutionary cost versus benefit is too high for potentially destructive processes, and so more energy likely goes into regulation of the potentially detrimental functions such as peptide degradation.[28]

5.3.4 Inhibition of PKB Activity in Single Tissue-Cultured Cells

Wortmannin, an irreversible inhibitor of PI3-K at nanomolar levels, can also inhibit mTOR, myosin light chain kinaes, and PI4K when used in micromolar concentrations.[29] Wortmannin prevents the phosphorylation of PIP_2 to PIP_3, which is needed for PKB recruitment to, and activation at, the cell membrane. To provide evidence that PKB was at least partially responsible for phosphorylation of peptide VI-B in the single cells, HPAF-II (n = 10), CFPAC-1 (n = 11), and PANC-1 (n = 11) cells were pre-treated with 500 nM wortmannin prior to microinjection of VI-B into single cells. In all three cell lines, pre-treatment with wortmannin essentially eliminated any phosphorylation seen in the single cells, with phosphorylation averaging 0.4 ± 0.7% in HPAF-II cells, 0.1 ± 0.3% in CFPAC-1 cells, and 1 ± 3% in PANC-1 cells (Figure 5.3). In all cases, there was a statistical difference in the amount of phosphorylation seen in treated and non-treated cells (p-values of 0.0033, 2.8×10^{-6}, and 4.8×10^{-5}, respectively). Inhibition of phosphorylation by these low concentrations of wortmannin suggests that the peptide was predominantly acting as a substrate for PKB, as the concentration of wortmannin was an order of magnitude less than that reported for efficient inhibition of MLCK, the next kinase most susceptible to wortmannin. Degradation of peptide VI-B was also observed in all wortmannin-treated cells, and evidence of both the 8- and 5-residue fragments were observed in most of the

wortmannin-treated cells (Figure 5.5). When the rate of degradation of the parent peptide was plotted as a function of initial substrate concentration (Figure 5.2), a linear correlation with a positive slope was observed, no different than that seen in untreated cells (p-values of 0.27, 0.078, and 0.26 for HPAF-II, CFPAC-1, and PANC-1 cells, respectively).

5.3.5 Characterization of VI-B in Pancreatic Tumor Xenografts

Behavior of peptide VI-B in single cells obtained from primary human pancreatic cancer xenografts was assessed next. Peptide VI-B was microinjected into a single xenograft cell and incubated for 90 s or 5 min prior to electrophoresis and detection of fluorescent products. When the peptide was incubated for 90 s (n = 2), intact parent peptide and the 8-mer fragment were detected (Figure 5.6A-B). When the amount of protein in the cell was taken to be 100 pg, the parent peptide was degraded at a rate of 0.003 and 0.1 zmol pg^{-1} s^{-1} in the two cells. No phosphorylated product was detected in these two cells. This could be due to the very short incubation time or could be because these cells were stromal cells and not epithelial cells. At this point, there have not been been efforts to distinguish between the fibroblast and epithelial cells in these xenograft samples, though this will be done in the future. When the peptide was incubated for 5 min (n = 1), four products were detected: intact parent peptide, the 8-mer and 5-mer fragments, and phosphorylated product (Figure 5.6C). The parent peptide was degraded at a rate of 0.04 zmol pg^{-1} s^{-1}, in the same range as the degradation rate for the shorter incubation time. The phosphorylated product accounted for 31% of intact peptide after 5 min, and formed at a rate of 0.006 zmol pg^{-1} s^{-1}. This result indicates that phosphorylation of peptide VI-B can be accomplished in primary samples and demonstrates the feasibility of using this peptide for analysis of PKB activity in single primary cells. However, many more cells would need to be analyzed prior to drawing

conclusions regarding the amount of PKB activity in these cells. This work is currently underway.

5.4 Conclusions

Single cell analysis of PKB activity in three different cell lines showed differences between cells of different lineage, with some possessing greater amounts of PKB, such as PANC-1, when compared to others, such as HPAF-II. The variability of PKB activity in cells from the same population points to potential differences in cell cycle as well as to kinase variability due to biological noise. The variability in kinase and phosphatase activity could provide the phenotypic variety to enable these cell lines to survive certain selective pressures. Peptide VI-B was also phosphorylated in a single primary cell obtained from a human pancreatic cancer xenograft, demonstrating the feasibility of this method for primary cells. Future work includes extended characterization of peptide degradation and phosphorylation in mouse xenograft cells derived from human pancreatic cancer tumors as well as in primary cells from human tumors. Further stabilization of peptide substrate VI-B is also underway, using the iterative design strategy described in Chapter 4 to render the peptide more proteolytically stable in single cells. Analysis of substrate specificity for PKB is also desired in order to ensure proper interpretation of enzyme activity in single tissue-cultured and primary cells.

5.5 Figures

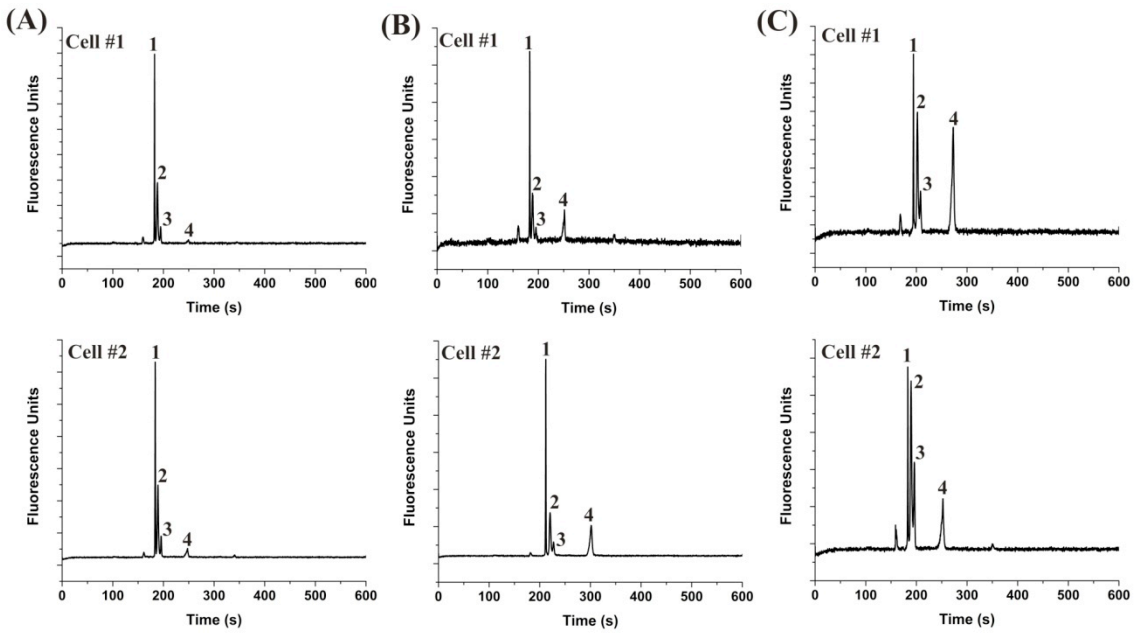

Figure 5.1: Select electropherograms from HPAF-II (A), CFPAC-1 (B), and PANC-1 (C) cells with no inhibitor treatment. Two representative cells are shown for each cell line. Peak 1 is the intact parent peptide; peak 2 is the 8-residue fragment; peak 3 is the 5-residue fragment; and peak 4 is phosphorylated product.

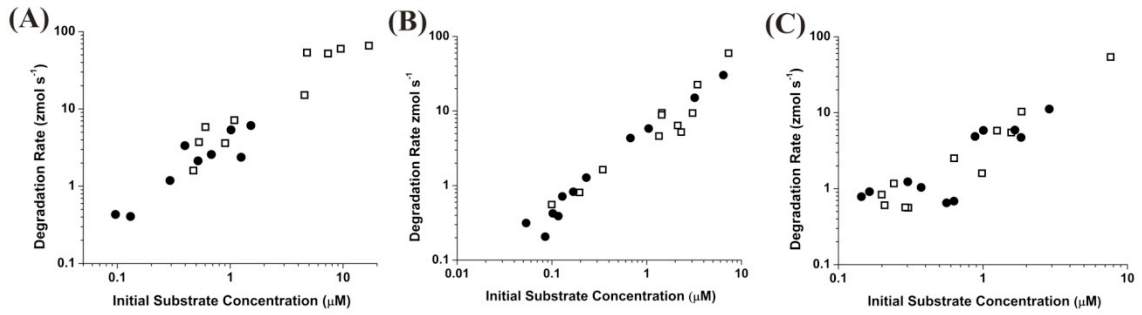

Figure 5.2: The rate of degradation of intact peptide VI-B as a function of initial substrate concentration in HPAF-II (A), CFPAC-1 (B), and PANC-1 (C) cells with no treatment (open squares) or pre-treatment with wortmannin (closed circles).

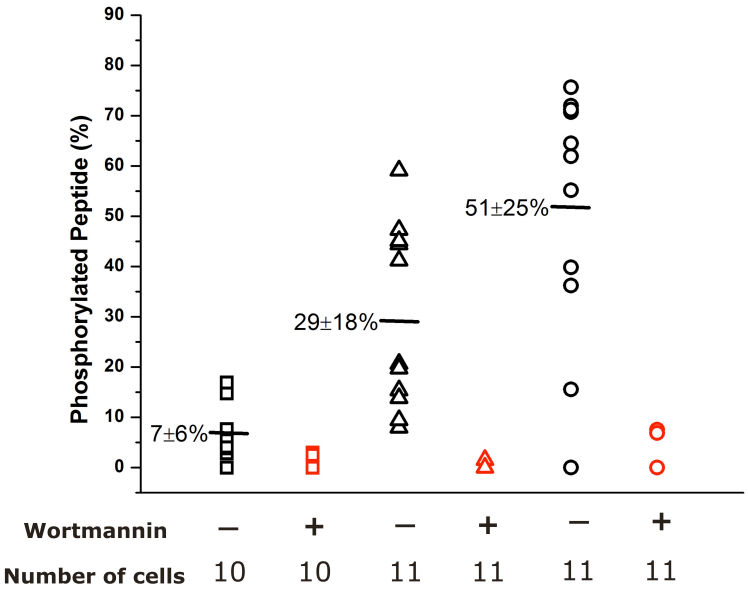

Figure 5.3: Percent phosphorylation in HPAF-II (open squares), CFPAC-1 (open triangles), and PANC-1 (open circles) cells with and without pre-treatment with wortmannin. Percent phosphorylated peptide is calculated for undegraded peptide only. The average and standard deviation are indicated for each untreated cell line.

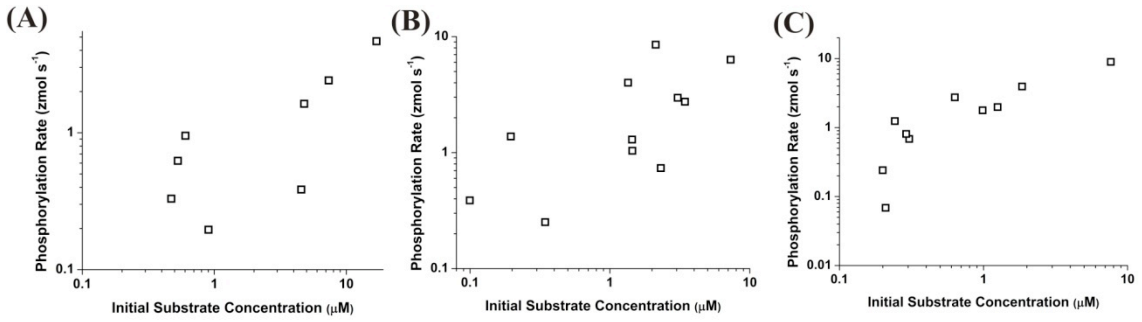

Figure 5.4: The rate of phosphorylation of intact peptide VI-B as a function of initial substrate concentration in HPAF-II (A), CFPAC-1 (B), and PANC-1 (C) cells.

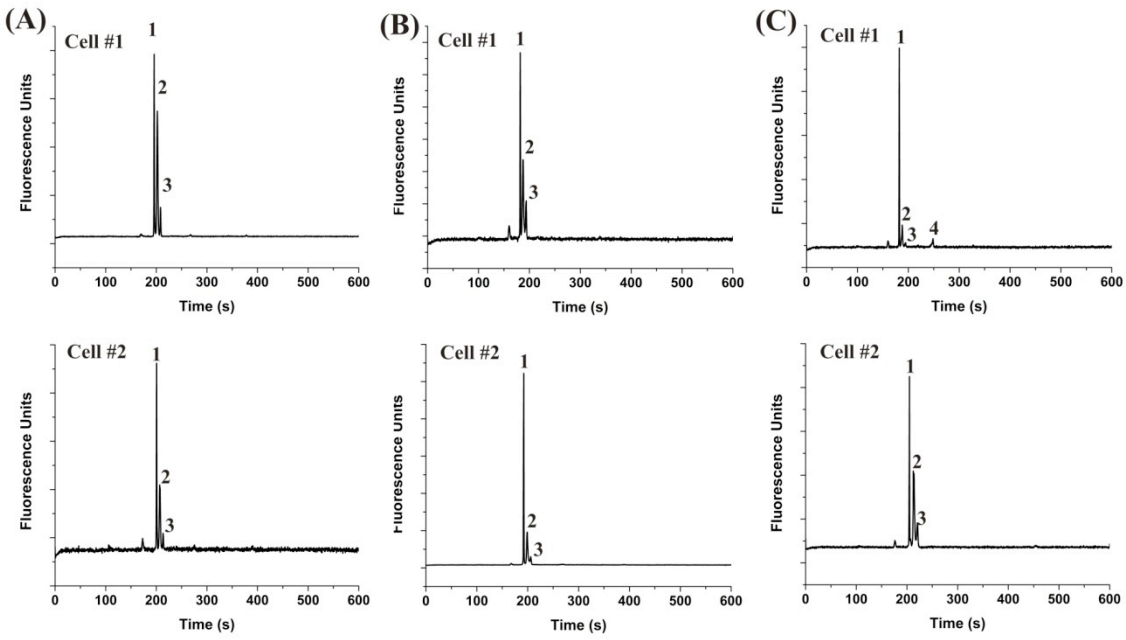

Figure 5.5: Select electropherograms from HPAF-II (A), CFPAC-1 (B), and PANC-1 (C) cells pre-incubated with wortmannin. Two representative cells are shown for each cell line. Peak 1 is the intact parent peptide; peak 2 is the 8-residue fragment; peak 3 is the 5-residue fragment; and peak 4 is phosphorylated product.

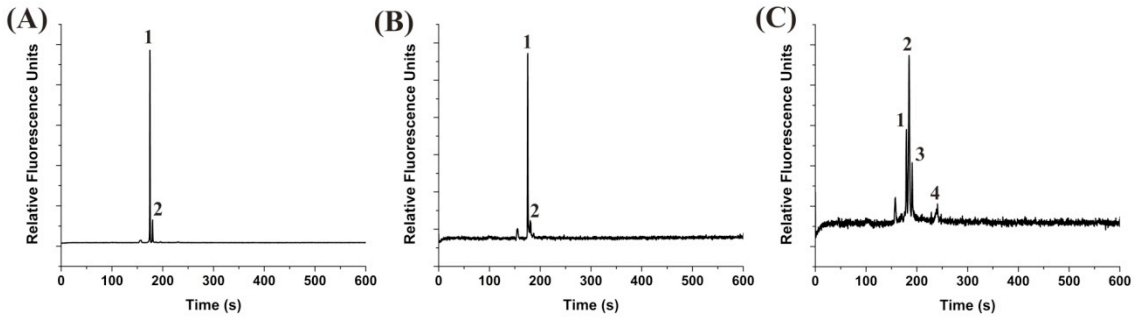

Figure 5.6: Electropherograms from incubation of peptide 48F in human pancreatic cancer xenograft cells for 90 s (A and B) and 5 min (C). Two representative cells are shown for the 90 s incubation time. Peak 1 is the intact parent peptide; peak 2 is the 8-residue fragment; peak 3 is the 5-residue fragment; and peak 4 is phosphorylated product.

5.6 References

1 C. Agbunag and D. Bar-Sagi. "Oncogenic K-ras Drives Cell Cycle Progression and Phenotypic Conversion of Primary Pancreatic Duct Epithelial Cells". *Cancer Res.,* 2004, *64*, 5659-5663.

2 T. Asano, Y. Yao, J. Zhu, D. Li, J. L. Abbruzzese and S. A. G. Reddy. "The PI 3-kinase/Akt signaling pathway is activated due to aberrant Pten expression and targets trasncription factors NF-jB and c-Myc in pancreatic cancer cells". *Oncogene,* 2004, *23*, 8571-8589.

3 N. Bardessy and R. A. DePinho. "Pancreatic cancer biology and genetics". *Nat. Rev. Cancer,* 2002, *2*, 897-909.

4 T. R. Donahue, L. M. Tran, R. Hill, Y. Li, A. Kovochich, J. H. Calvopina, S. G. Patel, N. Wu, A. Hindoyan, J. J. Farrell, X. Li, D. W. Dawson and H. Wu. "Integrative Survival-Based Molecular Profiling of Human Pancreatic Cancer". *Clin. Cancer Res.,* 2012, *18*, 1352-1363.

5 Cancer Facts and Figures 2012, American Cancer Society, Atlanta, 2012.

6 A. F. Hezel, A. C. Kimmelman, B. Z. Stanger, N. Bardeesy and R. A. DePinho. "Genetics and biology of pancreatic ductal adenocarcinoma". *Gene. Dev.,* 2006, *20*, 1218-1249.

7 M. Hidalgo, E. Bruckheimer, N. V. Rajeshkumar, I. Garrido-Laguna, E. De Oliveira, B. Rubio-Viqueira, S. Strawn, M. J. Wick, J. Martell and D. Sidransky. "A Pilot Clinical Study of Treatment Guided by Personalized Tumorgrafts in Patients with Advanced Cancer". *Mol. Cancer Ther.,* 2011, *10*, 1311-1316.

8 T. L. Yuan and L. C. Cantley. "PI3K pathway alterations in cancer: variations on a theme". *Oncogene,* 2008, *27*, 5497-5510.

9 C. E. Edling, F. Selvaggi, R. Buus, T. Maffucci, P. Di Sebastiano, H. Friess, P. Innocenti, H. M. Kocher and M. Falasca. "Key Role of Phosphoinositide 3-Kinase Class IB in Pancreatic Cancer". *Clin. Cancer Res.,* 2010, *16*, 4928-4937.

10 A. M. Martelli, C. Evangelisti, M. Y. Follo, G. Ramazzotti, M. Fini, R. Giardino, L. Manzoli, J. A. McCubrey and L. Cocco. "Targeting the Phosphatidylinositol 3-Kinase/Akt/Mammalian Target of Rapamycin Signaling Network in Cancer Stem Cells". *Curr. Med. Chem.,* 2011, *18*, 2715-2726.

11 C. Nitsche, M. Edderkaoui, R. M. Moore, G. Eibl, N. Kasahara, J. Treger, P. J. Grippo, J. Mayerle, M. M. Lerch and A. S. Gukovskaya. "The Phosphatase PHLPP1 Regulates Akt2, Promotes Pancreatic Cancer Cell Death, and Inhibits Tumor Formation". *Gastroenterology,* 2012, *142*, 377-387.

12 S. R. Boreddy, K. C. Pramanik and S. K. Srivastava. "Pancreatic Tumor Suppression by Benzyl Isothiocyanate Is Associated with Inhibition of PI3K/AKT/FOXO Pathway". *Clin. Cancer Res.,* 2001, *17*, 1784-1795.

13 B. N. Fahy, M. Schlieman, S. Virudachalam and R. J. Bold. "AKT inhibition is associated with chemosensitisation in the pancreatic cancer cell line MIA-PaCa-2". *Brit. J. Cancer,* 2003, *89*, 391-397.

14 C. M. Parsons, D. Muilenburg, T. L. Bowles, S. Mirudachalam and R. J. Bold. "The Role of Akt Activation in the Response to Chemotherapy in Pancreatic Cancer". *Anticancer Res.,* 2010, *30*, 3279-3290.

15 M. G. Schlieman, B. N. Fahy, R. Ramsamooj, L. Beckett and R. J. Bold. "Incidence, mechanism and prognostic value of activated AKT in pancreas cancer". *Brit. J. Cancer,* 2003, *89*, 2110-2115.

16 M. Osaki, M. Oshimura and H. Ito. "PI3K-Akt pathway: Its functions and alterations in human cancer". *Apoptosis,* 2004, *9*, 667-676.

17 S. Yamamoto, Y. Tomita, Y. Hoshida, T. Morooka, H. Nagano, K. Dono, K. Umeshita, M. Sakon and O. Ishikawa. "Prognostic Significance of Activated Akt Expression in Pancreatic Ductal Adenocarcinoma". *Clin. Cancer Res.,* 2004, *10*, 2846-2850.

18 M. Zavoral, P. Minarikova, F. Zavada, C. Salek and M. Minarik. "Molecular biology of pancreatic cancer". *World J. Gastroenterol.,* 2001, *17*, 2897-2908.

19 K. Garber, "From Human to Mouse and Back: "Tumorgraft" Models Surge in Popularity". *J. Natl. Cancer Inst.,* 2009, *101*, 6-8.

20 D. Decaudin, "Primary human tumor xenografted models ('tumorgrafts') for good management of patients with cancer". *Anti-Cancer Drugs,* 2011, *22*, 827-841.

21 R. S. Metzgar, M. T. Gaillard, S. J. Levine, F. L. Tuck, E. H. Bossen and M. J. Borowitz. "Antigens of Human Pancreatic Adenocarcinoma Cells Defined by Murine Monoclonal Antibodies". *Cancer Res.,* 1982, *42*, 601-608.

22 R. A. Schoumacher, J. Ram, M. C. Iannuzzi, N. A. Bradbury, R. W. Wallace, C. Tom Hon, D. R. Kelly, S. M. Schmid, F. B. Gelder, T. A. Rado and R. A. Frizzell. "A cystic fibrosis pancreatic adenocarcinoma cell line". *PNAS,* 1990, *87*, 4012-4016.

23 M. Lieber, J. Mazzetta, W. Nelson-Rees, M. Kaplan and G. Todaro. "Establishment of a continuous tumor-cell line (PANC-1) from a human carcinoma of the exocrine pancreas". *Int. J. Cancer,* 1975, *15*, 741-747.

24 G. D. Meredith, C. E. Sims, J. S. Soughayer and N. L. Allbritton. "Measurement of kinase activation in single mammalian cells". *Nat. Biotechnol.,* 2000, *18*, 309-312.

25 Personal communication with J. J. Yeh, Chapel Hill, NC, 2012.

26 A. Schmid, H. Kortmann, P. S. Dittrich and L. M. Blank. "Chemical and biological single cell analysis". *Curr. Opin. Biotech.,* 2010, *21*, 12-20.

27 S. Hu, L. Zhang, S. Krylov and N. J. Dovichi. "Cell Cycle-Dependent Protein Fingerprint from a Single Cancer Cell: Image Cytometry Coupled with Single-Cell Capillary Sieving Electrophoresis". *Anal. Chem.,* 2003, *75*, 3495-3501.

28 J. R. S. Newman, S. Ghaemmaghami, J. Ihmels, D. K. Breslow, M. Noble, J. L. DeRisi and J. S. Weissman. "Single-cell proteomic analysis of S. cerevisiae reveals the architecture of biological noise". *Nature,* 2006, *441*, 840-846.

29 J. Bain, L. Plater, M. Elliott, N. Shpiro, C. J. Hastie, H. McLauchlan, I. Klevernic, J. S. C. Arthur, D. R. Alessi and P. Cohen. "The selectivity of protein kinase inhibitors: a further update". *Biochem. J.,* 2007, *408*, 297-315.

CHAPTER 6

FURTHER STABILIZATION OF A BCR-ABL KINASE SUBSTRATE REPORTER

6.1 Introduction

As was discussed in Chapter 3, the lead peptide developed as a substrate for Abl kinase was QW-V-48B (5FAM-GGIYAAP-MePh-KKKA), derived from the native amino acid substrate QW-III-67B (5FAM-GGAYAAPFKKKA).[1] Peptide QW-V-48B was more stable than QW-III-67B in a cytosolic lysate, but the two peptides were degraded at nearly identical rates in single HeLa cells. Also determined in Chapter 3, the major cleavage location of QW-V-48B in single cells was between the two alanine residues, leaving a 5-residue fragment in single cells. In order to render the peptide even more resistant to peptidase degradation, the strategy outlined in Chapter 4 was applied to peptide QW-V-48B, where this susceptible cleavage location between the alanine residues was targeted for stabilization. This was accomplished by inserting non-native amino acids into the positions adjacent to the susceptible bond and re-evaluating each resulting peptide for resistance to degradation and suitability as a Bcr-Abl substrate.

6.2 Experimental Design

6.2.1 Chemicals

Peptide synthesis reagents were purchased from Aldrich or Fisher except for the following: 2-(6-Chloro-1H-benzotriazole-1-yl)-1,1,3,3-tetramethylaminium

hexafluorophosphate (HCTU), 1-(Mesitylene-2-sulfonyl)-3-nitro-1,2,4-triazole (MSNT), 9-Fluorenylmethoxycarbonyl (Fmoc) amino acids, 5-carboxyfluorescien (5-FAM) and resins were received from ChemPep or NovaBiochem; N-Hydroxybenzotriazole (HOBt) was obtained from AnaSpec. All other chemicals used in the assays were procured from Fisher or Sigma except for the following: Active Abl-1 enzyme was purchased from Invitrogen; bovine serum albumin (BSA) was received from Calbiochem; Roswell Park Memorial Institute Media (RPMI-1640) was obtained from Cellgro; Penicillin/streptomycin was procured from Gibco; and fetal bovine serum (FBS) was purchased from Atlanta Biologicals.

6.2.2 Peptide Synthesis and Preparation

6.2.2.1 Synthesis of Full-Length Peptides Amidated on the C-Terminus

All peptides were synthesized by collaborator Dr. Qunzhao Wang in the Lawrence Lab unless specified otherwise. A detailed table of all peptides prepared and utilized in this dissertation can be found in Appendix C. Full-length substrate peptides with an amidated C terminus were synthesized via standard Fmoc peptide synthesis (Prelude Peptide Synthesizer, Protein Technologies, Tucson, AZ) utilizing TGR resin. Coupling was performed with two 5 min incubations in dimethylformamide (DMF) with 5 equivalents (eq) amino acid, 5 eq HCTU, and 10 eq N,N-Diisopropylethylamine (DIPEA). Fmoc deprotection was achieved with two 2.5 min incubations with 20% piperidine in DMF. The free N-terminus was reacted with 5 eq 5-FAM, 5 eq diisopropylcarbodiimide (DIC), and 5 eq HOBt in DMF overnight, then treated with 30% piperidine in DMF for 30 min. The peptide was cleaved with trifluoroacetic acid:water:triisopropylsilane (TFA:H_2O:TIS) in a ratio of 95:2.5:2.5, precipitated with ether, and dried in air. Peptide purity was assessed with HPLC-MS and

further purification via HPLC was performed if needed. Peptides were dissolved in Tris buffer, pH 7.5, aliquoted, and stored at -80 ^{o}C.

6.2.2.2 Alternative Coupling for Difficult Amino Acids

In some instances, amino acids were coupled overnight in N-Methyl-2-pyrrolidone (NMP) with 5 eq amino acid, 5 eq bromo-tris-pyrrolidino phosphonium hexafluorophosphate (PyBrop), and 10 eq DIPEA. Capping with acetic anhydride was performed if necessary based on a ninhydrin test. Remaining amino acids were coupled as described in section 6.2.2.1. Product formation was assessed using HPLC-MS.

6.2.2.3 Synthesis of Peptide Fragment Standards

Peptide fragment standards with a free carboxylic acid at the peptide C terminus were synthesized using a 2-Chlorotrityl chloride resin. To couple the first amino acid, 1 eq of the first Fmoc amino acid and 4 eq DIPEA in dry CH_2Cl_2 was reacted with the 2-Chlorotrityl chloride resin for 2 h in a dry glass vial on a shaker. The remaining amino acids were attached as described in section 6.2.2.1 or 6.2.2.2.

6.2.3 Cell Culture

Baf/BCR-ABL cells were cultured in RPMI-1640 medium supplemented with 10% FBS, penicillin (100 units/mL) and streptomycin (100 μg/mL) and were maintained in a humidified atmosphere of 37 ^{o}C in 5% CO_2. Cells were passaged into fresh media every 2 – 3 days.

6.2.4 Measurement of Peptide Degradation in a Cell Lysate

Baf/BCR-ABL cells were collected from two confluent 75 cm^2 flasks and were washed with and resuspended in phosphate buffered saline (PBS; 137 mM NaCl, 10 mM Na_2HPO_4, 27 mM KCl, 1.75 mM KH_2PO_4, pH 7.4). The cells were submerged in liquid

nitrogen for 1 min and rapidly thawed at 37 ^{o}C for a total of three cycles. The mixture was centrifuged at 14,000 x g for 5 min at 4 ^{o}C. The supernatant was transferred to a clean centrifuge tube and maintained on ice until use in the assay. Total protein concentration in the supernatant was measured using fluorescamine.[2] Briefly, fluorescamine (10 μL, 3 mg/mL in acetone) was added to a cell lysate (30 μL) and incubated for 5 min at 25 ^{o}C. Fluorescence was measured with a fluorescence plate reader (SpectraMax M5, Molecular Devices, Sunnyvale, CA) with an excitation of 390 nm (bandwidth of 9 nm) and emission of 475 nm (bandwidth of 15 nm).

Assay of peptide degradation was performed by mixing peptide (1 μM) with the Baf/BCR-ABL cell lysate (3 mg/mL total cell protein) and incubating at 37 ^{o}C for 1 h. Aliquots were removed from the reaction mixture at various time intervals. The reactions were stopped by adding HCl to a final concentration of 100 mM. A 0 min timepoint was prepared by adding the HCl to the lysate prior to addition of the substrate peptide. Reaction mixtures were then separated by capillary electrophoresis and detected by LIF. Peptide fragments were identified by adding standards (250 nM) to the HCl-terminated aliquots and comparing the electropherograms with and without the added standard. The average initial degradation and fragmentation rates were calculated using the 0 and 5 min time points by monitoring the change in peptide amount divided by the change in time per amount cytosolic protein. The units are defined as zmol of peptide per pg of cytosolic protein per s, or zmol pg^{-1} s^{-1}.

6.2.5 *in vitro* Kinase Assay

Protein kinase assays were performed at 30 ^{o}C in assay buffer [50 mM Tris (pH 7.4), 5 mM $MgCl_2$, 1 mM $MnCl_2$, 2 mM DTT, 1 mM ATP] with Abl-1 kinase (12 nM) and

substrate (29 μM). Aliquots were then removed from the reaction mixture at varying times. The reactions were stopped by heating at 90 ^{o}C for 4 min. Additionally, a negative control with no ATP was simultaneously assayed and sampled. The amount of peptide phosphorylation was measured using capillary electrophoresis coupled with laser-induced fluorescence to separate the substrates and products and quantify peak areas. The samples with and without ATP were compared to identify the phosphorylated product and the non-phosphorylated precursor.

6.2.6 Capillary Electrophoresis

Laser-induced fluorescence (488 nm) was used for peptide detection during capillary electrophoresis (ProteomeLab PA800, Beckman Coulter, Fullerton, CA). Fused-silica capillaries [50 μm inner diameter, 360 μm outer diameter, (Polymicro Technologies, Phoenix, AZ)] had a total length of 30 cm with an effective length of 20 cm. Capillaries were conditioned prior to use with 0.1 M NaOH for 12 h, H_2O for 1 h, 0.1 M HCl for 6 h, and H_2O again for 12 h. After each sample, the capillary was sequentially rinsed with 1 M NaOH, H_2O, and buffer for 2 min by applying a pressure of 20 psi to the capillary inlet. A sample plug was hydrodynamically loaded into the capillary by applying 0.5 psi to the inlet for 5 s. Electrophoresis was initiated by application of a negative voltage to the outlet. For the assays employing a cell lysate, the electrophoretic buffer was 100 mM Tris and 100 mM Tricine, pH 8.1 and the field strength was 500 V/cm. For the *in vitro* kinase assay samples, the electrophoretic buffer was 100 mM Tris, 100 mM Tricine and 5 mM SDS, pH 8.1 and field strength was 600 V/cm. The data was analyzed using commercial software (32 Karat, version 8.0, Beckman Coulter, Fullerton, CA).

6.3 Results and Discussion

6.3.1 Characterization of Peptides Following Replacement of the N-Terminal Alanine

To determine if substitution on the N-terminal side of the cleaved bond resulted in greater peptide stability, the alanine residue in this position was replaced by (N-methyl)alanine, sarcosine, or D-alanine (Figure 6.1). All of these residues have been known to impart stability to peptides when incorporated into sequences.[3-5] Peptides VII-A through VII-C (Table 6.1) were synthesized, purified, incubated in a Baf/BCR-ABL cytosolic lysate and then separated by CE to determine if fluorescent fragments were formed. Over the course of 60 min, peptides VII-A, VII-B, and VII-C were degraded into 3, 3, and 4 fragment peptides, respectively (Figure 6.2). In order to compare degradation resistance of each peptide, the percentage of intact parent peptide was plotted as a function of time and the half-life ($t_{1/2}$) was calculated (Figure 6.3A, Table 6.1). Peptide VII-A possessed a $t_{1/2}$ of 1.6 min, 12X less than that for QW-V-48B. Peptide VII-B had a $t_{1/2}$ of 5.5 min, 3.5X less than that for QW-V-48B, while peptide VII-C showed the greatest resistance to degradation with a $t_{1/2}$ of 17.9 min, approximately the same as that for QW-V-48B.

To determine whether these substituted peptides retained the ability to be phosphorylated by Abl kinase, each peptide was incubated with purified Abl kinase *in vitro* and phosphorylation was measured over time. In all cases, none of the modified peptides showed evidence of phosphorylation over the 120 min incubation, while both QW-III-67B and QW-48B demonstrated $t_{50\%\,P}$ (time to attain 50% phosphorylation) values of 190 and 400 min, respectively (Figure 6.3B). The poor substrate efficacy of these substituted peptides rendered these modifications unsuitable for follow up.

6.3.2 Characterization of Peptides Following Replacement of the C-Terminal Alanine

The next round of modifications involved replacement of the alanine on the C-terminal side of the susceptible bond with sarcosine, D-alanine, or (N-methyl)alanine (Figure 6.1) in an attempt to render the bond more peptidase-resistant. Peptides VIII-A through VIII-C (Table 6.1) were synthesized and assessed for stability in a Baf/BCR-ABL cytosolic lysate. After 60 min in the cytosolic lysate, peptides VIII-A and VIII-C were each metabolized into 5 fragment peptides and VIII-B was metabolized into 4 fragment peptides (Figure 6.4). Peptides VIII-A and VIII-B were more stable than previous peptides tested, with 22 ± 8% and 43 ± 10% of each parent peptide remaining after 60 min, respectively. When the $t_{1/2}$ values were calculated (Figure 6.5A) and used to compare peptide resistance to degradation, peptide VIII-C was found to have a $t_{1/2}$ of 5.1 min, approximately 4X less than that of QW-V-48B. Peptides VIII-A and VIII-B had $t_{1/2}$ values of 25.8 and 48.7 min, respectively, corresponding to a 1.3- and 2.5-fold increase over that of QW-V-48B.

The ability of each modified peptide to be phosphorylated *in vitro* by Abl kinase was also assessed and $t_{50\%\ P}$ was calculated (Figure 6.5B). Peptide VIII-C showed minimal phosphorylation, with a $t_{50\%\ P}$ greater than 10^5 min. Peptide VIII-A possessed a $t_{50\%\ P}$ of 68 min, approximately 6X faster than QW-V-48B, while VIII-B demonstrated a $t_{50\%\ P}$ of 650 min, approximately 1.5X slower than that of QW-V-48B. Based on the $t_{1/2}$ and $t_{50\%\ P}$ values calculated, it was determined that both peptides VIII-A and VIII-B were suitable candidates for further evaluation. And though it appeared to be a poorer substrate for Abl kinase, peptide VIII-B was selected for further evaluation based on its increased ability to resist degradation by peptidases, with the thought that a longer-lived substrate would be more

beneficial than a shorter-lived substrate with more favorable kinetic properties, if the longer-lived substrate could still act as a kinase substrate.

6.3.3 Characterization of VIII-B in a Baf/BCR-ABL Cytosolic Lysate

Although the sarcosine-containing VIII-B peptide possessed a much longer lifetime in the cytosolic lysate than QW-V-48B, it was still broken down into four additional fragments over time. To determine which locations were the preferred sites of cleavage, all possible fluorescent fragments were synthesized and characterized by electrophoresis, as described in Chapters 3 and 4. Under the electrophoretic conditions utilized, all of the fragment peptides were resolved from each other and from the parent peptide. Peptide VIII-B was incubated in a Baf/BCR-ABL lysate and each of the possible fluorescent peptide standards were sequentially added to the mixture to identify the unknown peaks in the electropherogram. Each of the peaks present in the cytosolic lysate was matched to a fragment peak (Figure 6.6). Percentage of peptide was plotted as a function of time to calculate the degradation and formation of each peptide over time (Figure 6.6D). The first fragment formed, and the one that formed in the highest abundance over time, was peptide a, the longest possible fragment. Peptide a formed at a rate nearly equal to that of the degradation of the parent peptide, or 0.04 zmol pg^{-1} s^{-1}. The remaining 3 fragments, 2-, 5-, and 9-residue peptides, formed at very low amounts compared to peptide a. While the replacement of the alanine with a sarcosine did not eliminate cleavage at the 5-mer bond, it did reduce bond hydrolysis significantly, with this 5-mer representing approximately 2% of all peptide present after 60 min (Figure 6.6C).

6.3.4 Characterization of Peptide Following Truncation of the Substrate

As the consensus sequence of many kinases usually involves those residues nearest to the phosphorylatable residue, removal of a single residue at the carboxy-terminus might not eliminate kinase suitability, but might impart stability to the substrate by eliminating the cleavage site. The most abundant fragment of peptide VIII-B was formed when the last residue was cleaved, so an alternate substrate was synthesized without this residue and the resistance to degradation and suitability as a substrate was assessed. Peptide IX-A (Table 6.1) was slowly degraded over time, and 4 small peaks in addition to the parent peptide were seen on the electropherogram (Figure 6.7A-C). After 60 min in the Baf/BCR-ABL cytosolic lysate, the parent peptide was 68% of all peptide present. One fragment peptide accounted for 18% of all peptide, with the remaining 3 fragments making up the remainder of peptides (Figure 6.7). The $t_{1/2}$ of peptide IX-A was 365 min, over 19X better than QW-V-48B and 7X better than precursor peptide VIII-B (Figure 6.8A). The identification of the fragment peptides was accomplished with the fragment standards (Figure 6.7). Remarkably, the data suggest that the fragment formed in largest amounts was peptide a (Figure 6.7E), which was formed by removing only the amidated terminus from the last amino acid. This type of cleavage has not been previously observed in any peptides examined and its formation was surprising. However, this bond is still a pseudo-peptide bond, meaning that it can theoretically be cleaved by peptidases. More investigations, including mass spectrometric analysis, need to be performed in order to confirm this result. Furthermore, two of the three additional fragments that formed were different from those formed when the precursor VIII-B peptide was incubated in the lysate, as a 3- and 6-mer fragment were seen in addition to the 5-mer seen previously.

Additionally, the substrate efficacy of peptide IX-A for purified Abl kinase was also examined. When incubated with purified kinase, the substrate was phosphorylated at a rate similar to that of the precursor peptide (Figure 6.8B), with a $t_{50\%\ P}$ of 610 min, compared to 650 min for the predecessor peptide VIII-B (Table 6.1). This $t_{50\%\ P}$ value is approximately 3X slower than that for the control peptide QW-III-67B. Further work needs to be performed to determine if peptide IX-A is a suitable substrate for Bcr-Abl *in vitro* and in intact cells.

6.4 Conclusions

Identification of susceptible cleavage locations in peptide QW-V-48B led to further stabilization by replacement of native amino acids with non-native residues. The location targeted was the most abundant fragment formed in single cells, the 5-residue peptide generated when QW-V-48B was incubated in single HeLa cells. The iterative design strategy demonstrated in Chapter 4 for a PKB substrate peptide was successfully utilized to render this Bcr-Abl substrate peptide more peptidase-resistant in cytosolic lysates. While not yet evaluated in single cells, peptide IX-A was much more stable in a cytosolic lysate than previous peptides tested, showing an increase in stability over 280X that of the original, unmodified peptide QW-III-67B. Future work includes extensive characterization of peptide stability and evaluation of substrate suitability of IX-A in single cells. Future work for all peptides evaluated in this dissertation also includes higher-throughput analyses of single cells as well as analysis of PKB and Bcr-Abl kinase activity in single primary cells obtained directly from human patients.

6.5 Figures and Tables

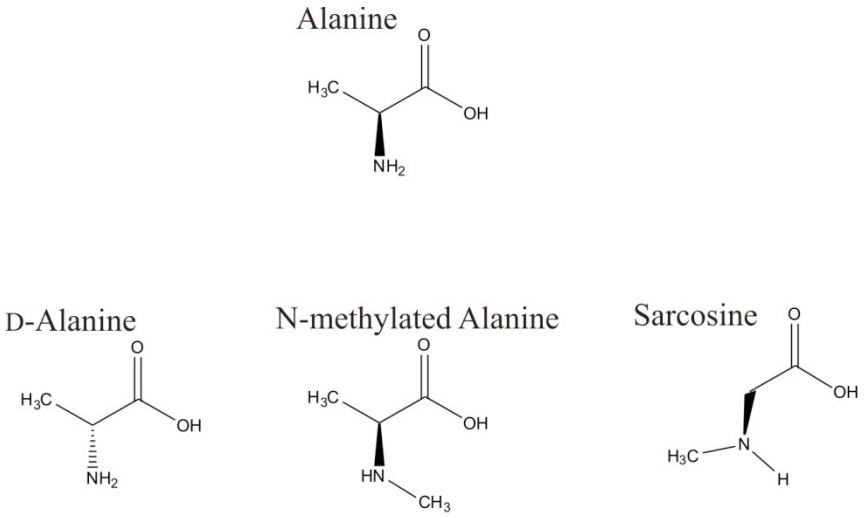

Figure 6.1: The non-native amino acids utilized in the construction of alternative peptides.

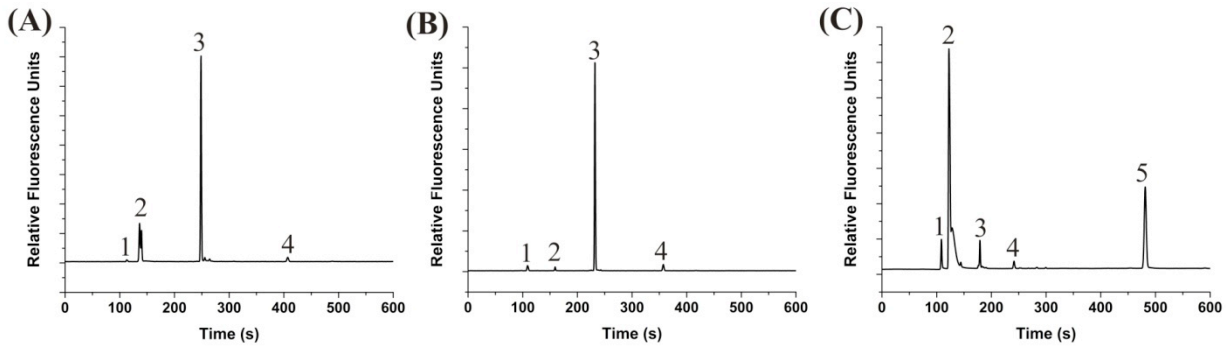

Figure 6.2: Select electropherograms of peptide VII-A (A), VII-B (B), and VII-C (C) incubated for 60 min in a Baf/BCR-ABL cytosolic lysate. Peak 1 in each case corresponds to the intact parent peptide or the location of migration of the intact parent peptide. The other numbers correspond to fragments of each peptide.

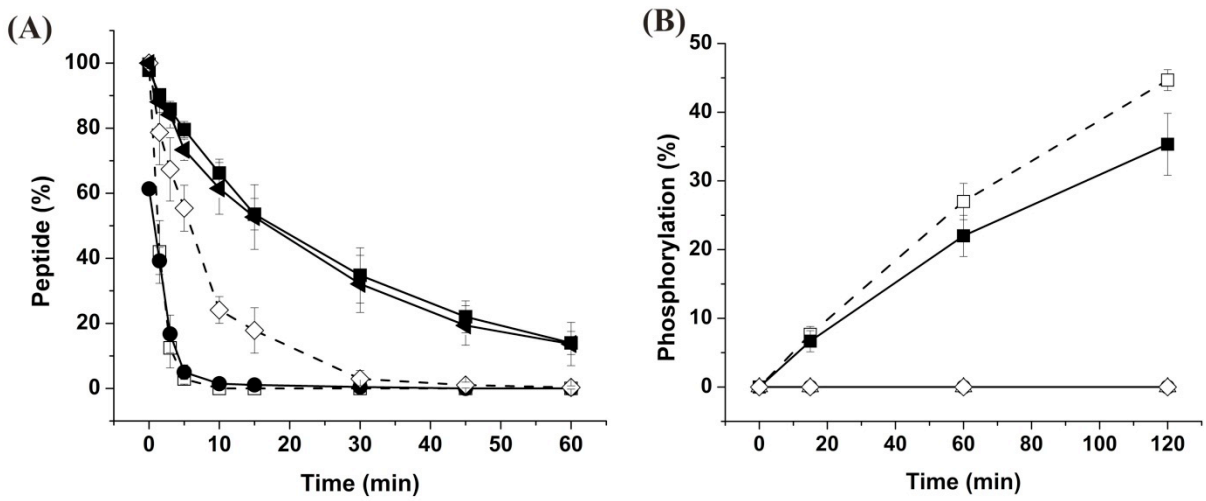

Figure 6.3: Baf/BCR-ABL cytosolic lysate degradation (A) and *in vitro* phosphorylation (B) of the series VII peptides. Open square (QW-III-67B), closed square (QW-V-48B), closed circle (VII-A), open triangle (VII-B), and open diamond (VII-C).

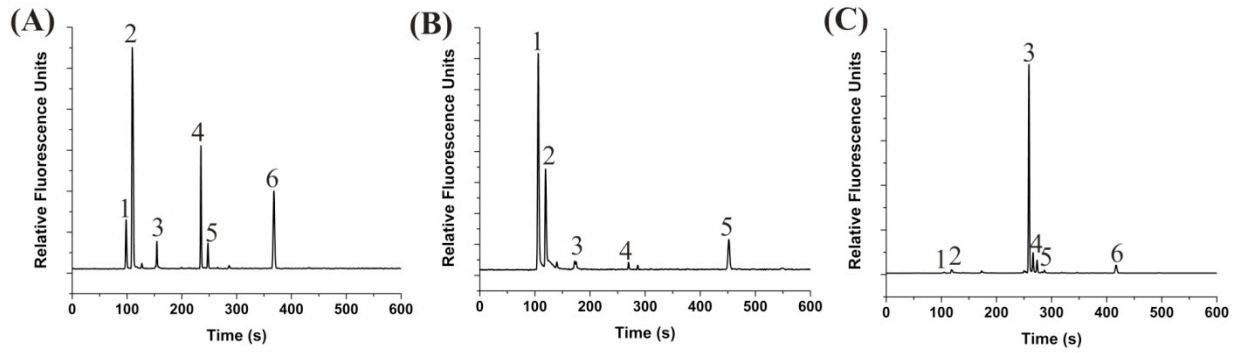

Figure 6.4: Select electropherograms of peptide VIII-A (A), VIII-B (B), and VIII-C (C) incubated for 60 min in a Baf/BCR-ABL cytosolic lysate. Peak 1 in each case corresponds to the intact parent peptide or the location of migration of the intact parent peptide. The other numbers correspond to fragments of each peptide.

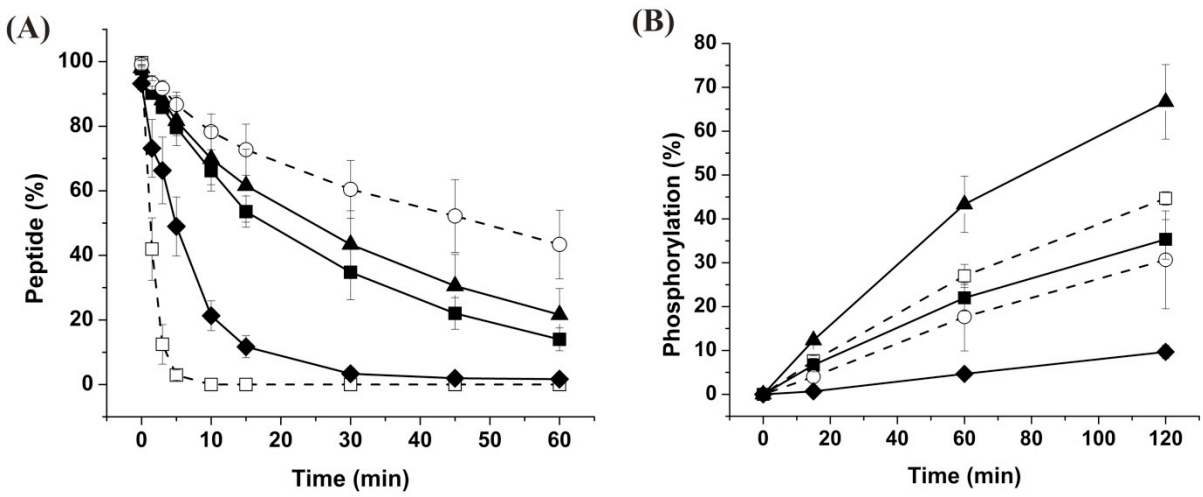

Figure 6.5: Baf/BCR-ABL cytosolic lysate degradation (A) and *in vitro* phosphorylation (B) of the series VIII peptides. Open square (QW-III-67B), closed square (QW-V-48B), closed triangle (VIII-A), open circle (VIII-B), and closed diamond (VIII-C).

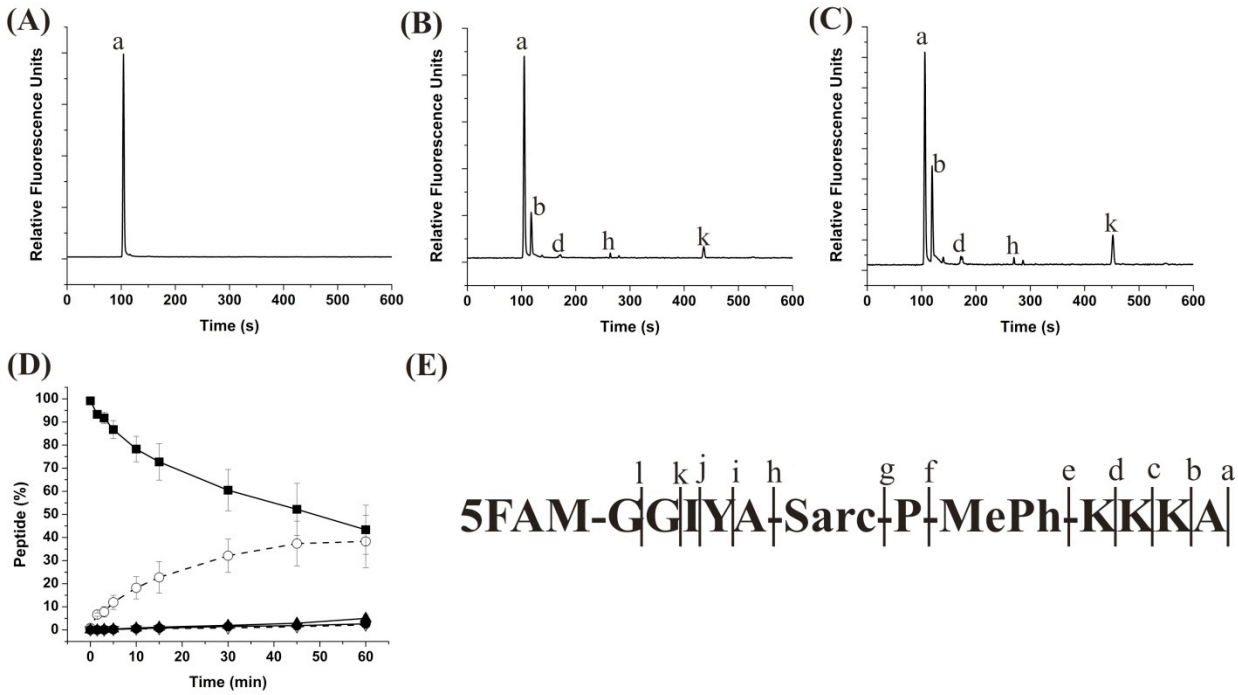

Figure 6.6: Degradation profile of peptide VIII-B in a Baf/BCR-ABL cell lysate. (A) – (C) Electropherograms of the peptide after incubation in the lysate for 0 (A), 30 (B), or 60 (C) min. (D) Formation of peptide fragments over time. Shown on the y-axis is the percentage of peptide present as a fragment. The symbols are defined as: closed square (peptide a), open circle (peptide b), closed triangle (peptide d), open triangle (peptide h), closed circle (peptide k). (E) The uppercase letters are the single amino acid abbreviations for the lead peptide sequence, Sarc represents sarcosine and MPh represents (N-methyl) phenylalanine. The lowercase letters indicate the cleavage locations that generate the indicated peptide fragments.

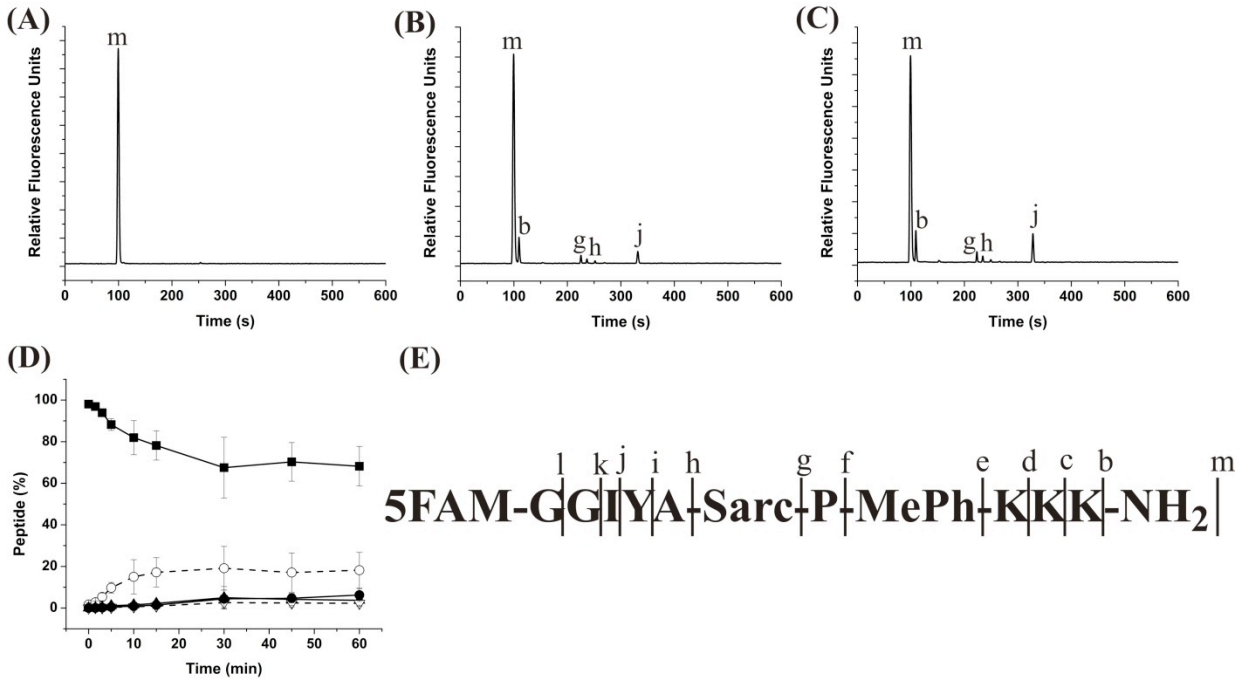

Figure 6.7: Degradation profile of peptide IX-A in a Baf/BCR-ABL cell lysate. (A) – (C) Electropherograms of the peptide after incubation in the lysate for 0 (A), 30 (B), or 60 (C) min. (D) Formation of peptide fragments over time. Shown on the y-axis is the percentage of peptide present as a fragment. The symbols are defined as: filled square (peptide m), open circle (peptide b), closed triangle (peptide g), open triangle (peptide h), closed circle (peptide j). (E) The uppercase letters are the single amino acid abbreviations for the lead peptide sequence, Sarc represents sarcosine and MPh represents (N-methyl) phenylalanine. The lowercase letters indicate the cleavage locations that generate the indicated peptide fragments.

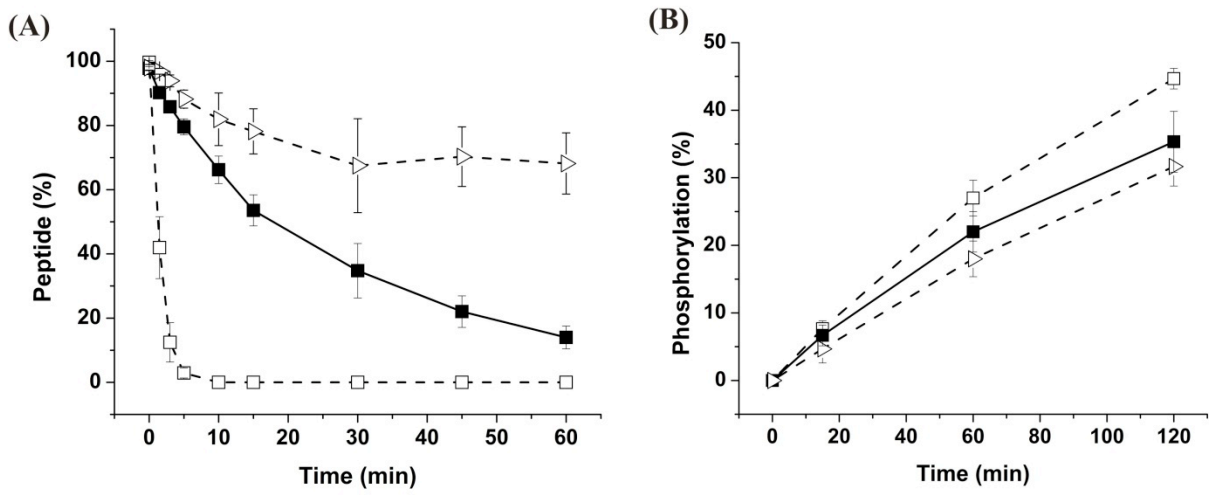

Figure 6.8: Baf/BCR-ABL cytosolic lysate degradation (A) and *in vitro* phosphorylation (B) of peptides. Open square (QW-III-67B), closed square (QW-V-48B), and open triangle (IX-A, truncated, sarcosine-containing peptide).

Table 6.1: Properties of the modified peptides.

Peptide Name	Sequence	$t_{1/2}$[a] (min)	$t_{50\%P}$[b] (min)
QW-III-67B	5FAM-GGAYAAPFKKKA	1.3	190
QW-V-48B	5FAM-GGIYAAP-MePh-KKKA	19.4	400
VII-A	5FAM-GGIY-MeAla-AP-MePh-KKKA	1.6	NP
VII-B	5FAM-GGIY-Sarc-AP-MePh-KKKA	5.5	NP
VII-C	5FAM-GGIY-DAla-AP-MePh-KKKA	17.9	NP
VIII-A	5FAM-GGIYA-MeAla-P-MePh-KKKA	25.8	68
VIII-B	5FAM-GGIYA-Sarc-P-MePh-KKKA	48.7	650
VIII-C	5FAM-GGIYA-DAla-P-MePh-KKKA	5.1	$>10^5$
IX-A	5FAM-GGIYA-Sarc-P-MePh-KKK	365	610

[a] $t_{1/2}$ is the time at which 50% of the peptide was degraded by the cell lysate.
[b] $t_{50\%\,P}$ is the time required for 50% of the peptide to be phosphorylated by Abl-1 kinase under the conditions employed. Abbreviations are the standard single letter amino acids, except for the following: Sarc (sarcosine), MPh [(N-methyl)phenylalanine], MeAla [(N-methyl)alanine], and DAla (D-alanine).

6.6 References

1 A. Proctor, Q. Wang, D. S. Lawrence and N. L. Allbritton. "Metabolism of peptide reporters in cell lysates and single cells". *Analyst,* 2012, *137*, 3028-3038.

2 G. M. Funk, C. E. Hunt, D. E. Epps and P. K. Brown. "Use of a rapid and highly sensitive fluorescamine-based procedure for the assay of plasma lipoprotiens". *J. Lipid Res.,* 1986, *27*, 792-795.

3 T. T. Tran, H. Treutlein and A. W. Burgess. "Designing amino acid residues with single-conformations". *Protein Eng. Des. Sel.,* 2006, *19*, 401-408.

4 R. Tugyi, K. Uray, D. Iván, E. Fellinger, A. Perkins and F. Hudecz. "Partial D-amino acid substitution: Improved enzymatic stability and preserved Ab recognition of a MUC2 epitope peptide". *PNAS,* 2005, *102*, 413-418.

5 L. Gentilucci, R. De Marco and L. Cerisoli. "Chemical Modifications Designed to Improve Peptide Stability: Incorporation of Non-Natural Amino Acids, Pseudo-Peptide Bonds, and Cyclization". *Curr. Pharm. Design,* 2010, *16*, 3185-3203.

APPENDIX A: SINGLE-CELL CE-LIF INSTRUMENT CUSTOM PARTS

This appendix contains the blueprints for the custom made machined parts for the single cell CE-LIF system described in Chapter 2. These blueprints can also be found on the hard drive of the single system CE-LIF computer in the following location: Desktop>>Users>>Angie>>Single Cell CE-LIF>>Blueprints. The blueprints were drafted by either Angela Proctor or Freddy Pinero, an employee of the UNC-CH Chemistry Machine Shop at the time of drafting. The parts drafted by Mr. Pinero were originally designed for a system built in collaboration between the Allbritton and Weeks labs, which shares similar features to the single cell system described here. Each figure has a brief legend detailing the name of the part, who drafted the part, what material should be used for construction and how many pieces are required for a single CE-LIF instrument. Figure A11 is the blueprint for the modification of a part purchased commercially from Melles Griot and contains the original part and dimensions as well as the modifications required. For the instrument described in Chapter 2 of this dissertation, all parts were machined or modified by the UNC-CH Physics Machine Shop. A detailed description of parts required and instrument design can be found in Notebook #6, Pages 103-114.

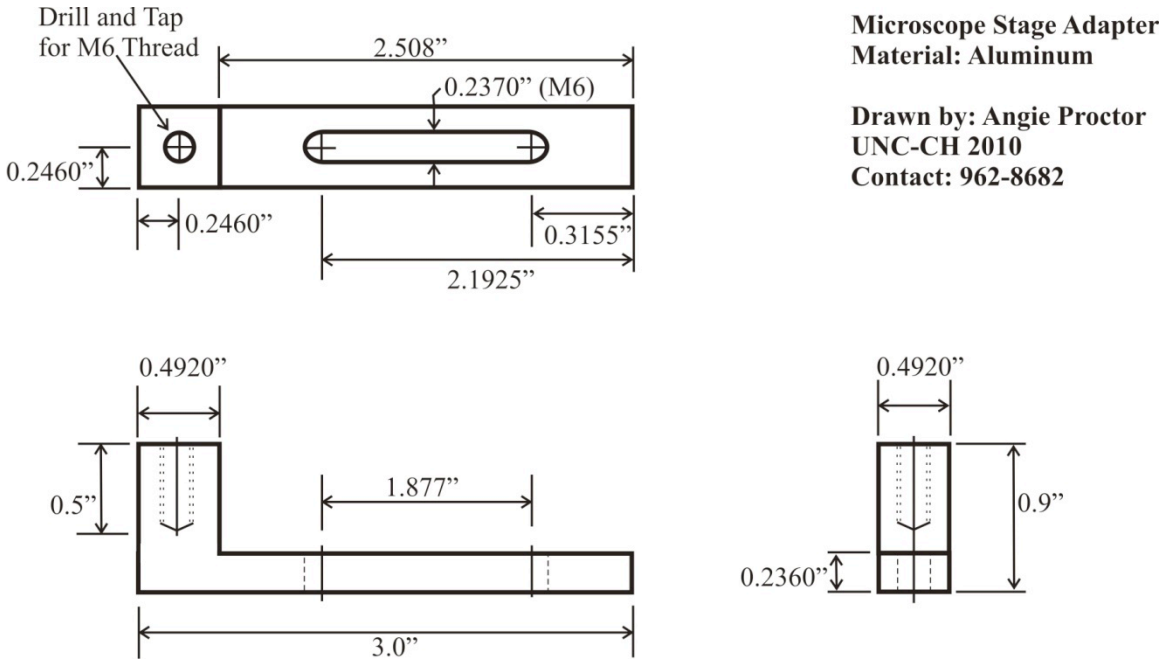

Figure A1: Blueprint for the CE-LIF microscope stage adapter, drawn by Angela Proctor. Two (2) pieces should be constructed out of aluminum for one CE-LIF system.

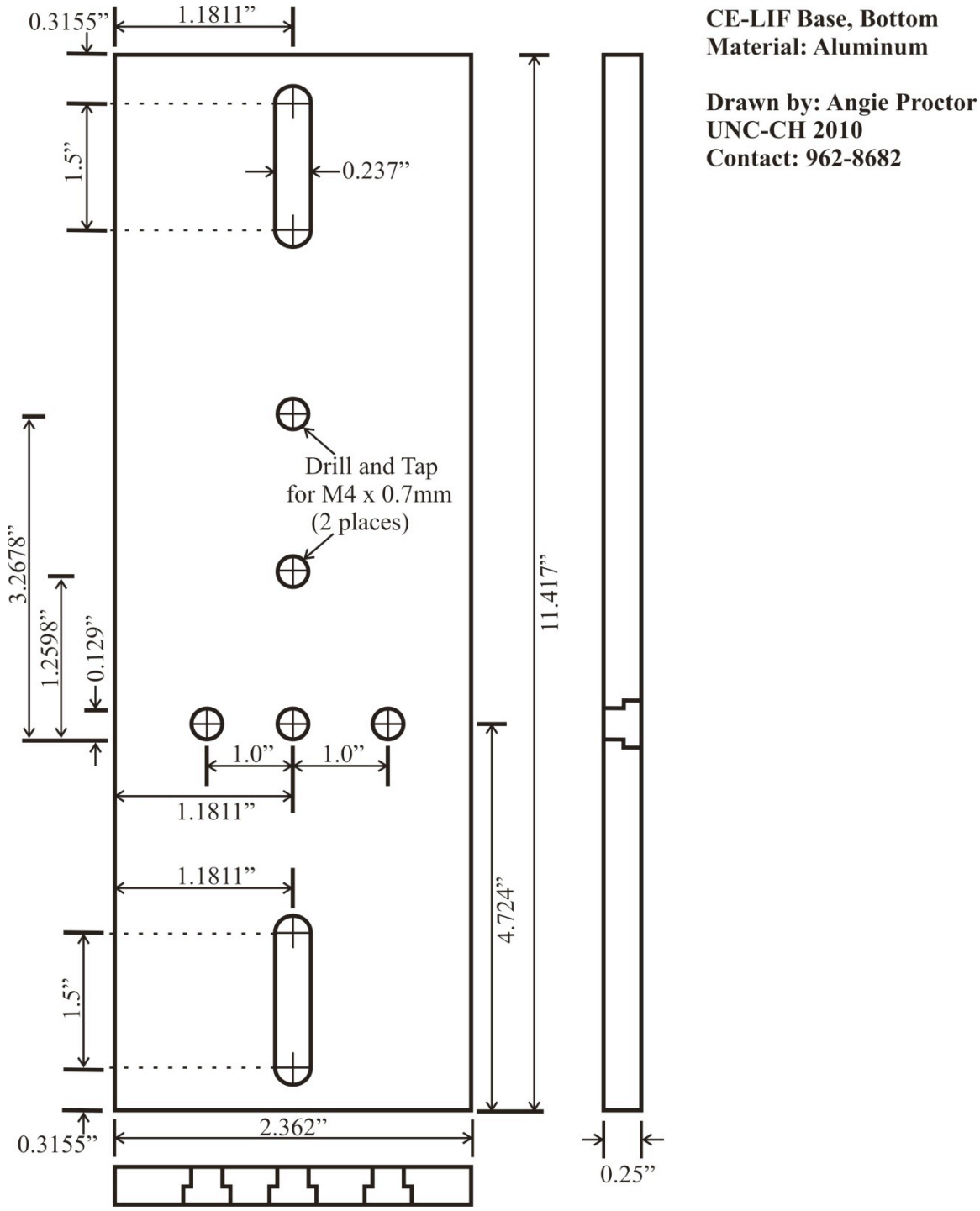

Figure A2: Blueprint for the CE-LIF base, bottom, drawn by Angela Proctor. One (1) piece should be constructed out of aluminum for one CE-LIF system.

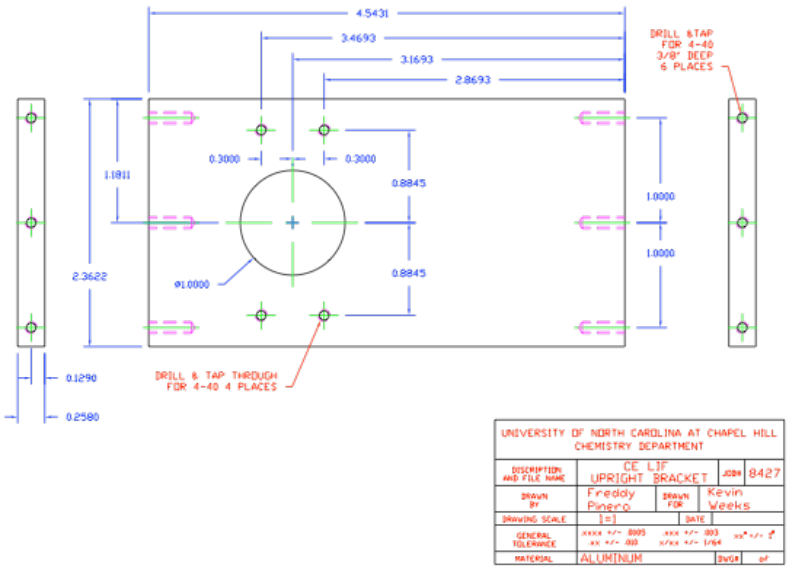

Figure A3: Blueprint for the CE-LIF base, front, drawn by Freddy Pinero. One (1) piece should be constructed out of aluminum for one CE-LIF system.

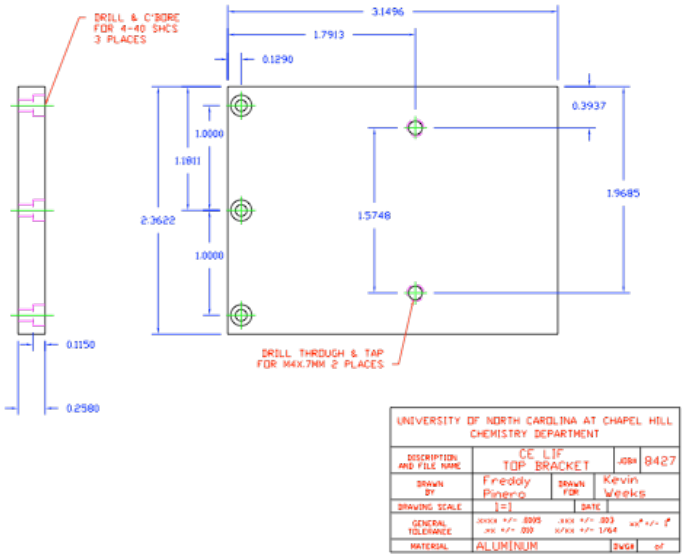

Figure A4: Blueprint for the CE-LIF base, top, drawn by Freddy Pinero. One (1) piece should be constructed out of aluminum for one CE-LIF system.

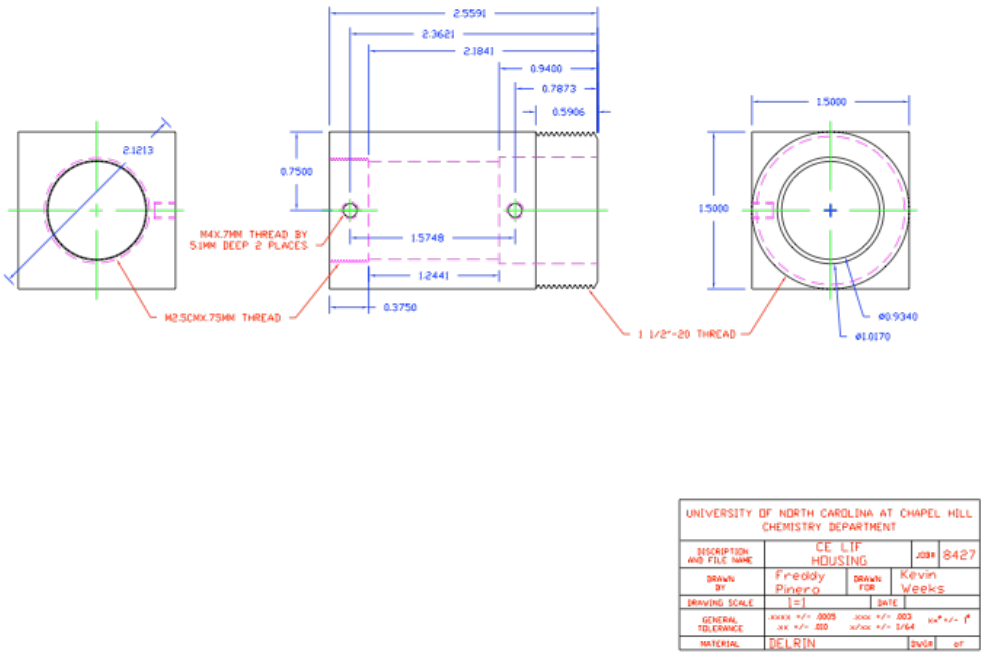

Figure A5: Blueprint for the CE-LIF detector housing, drawn by Freddy Pinero. One (1) piece should be constructed out of black delrin for one CE-LIF system.

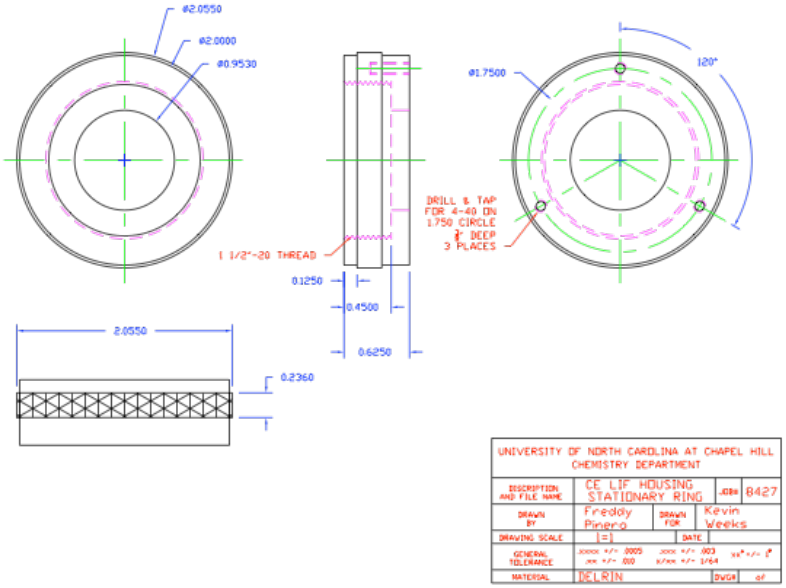

Figure A6: Blueprint for the Collection lens holder, drawn by Freddy Pinero. One (1) piece should be constructed out of black delrin for one CE-LIF system.

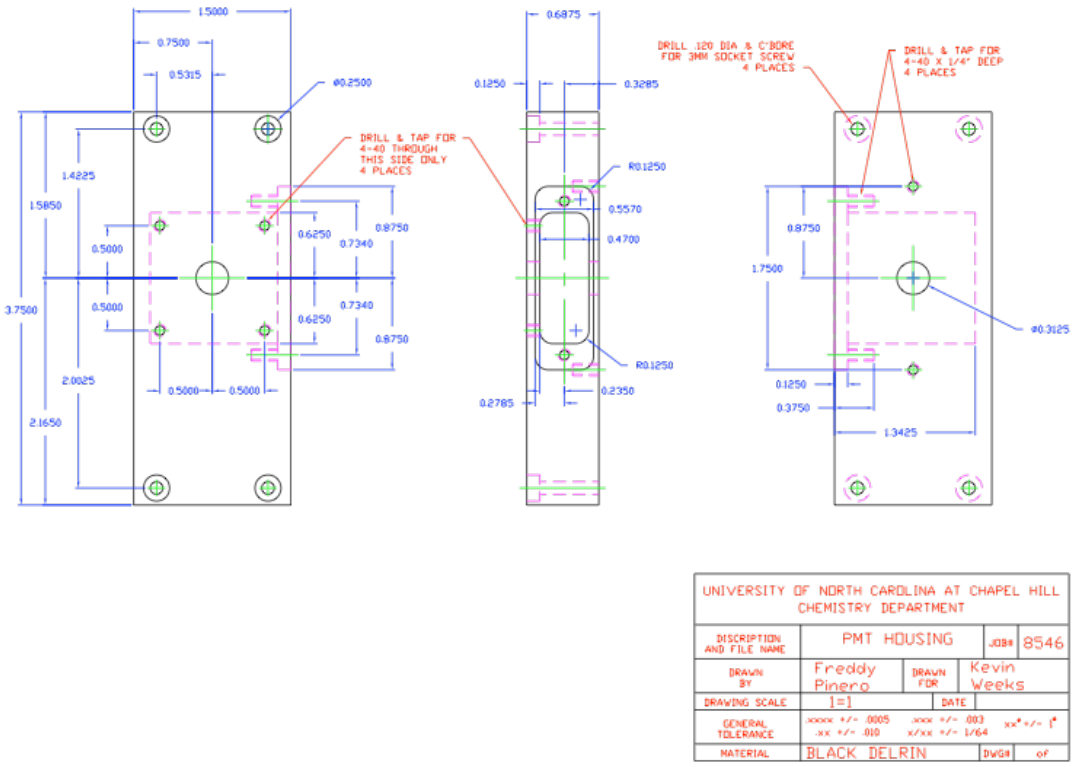

Figure A7: Blueprint for the PMT housing, drawn by Freddy Pinero. One (1) piece should be constructed out of black delrin for one CE-LIF system.

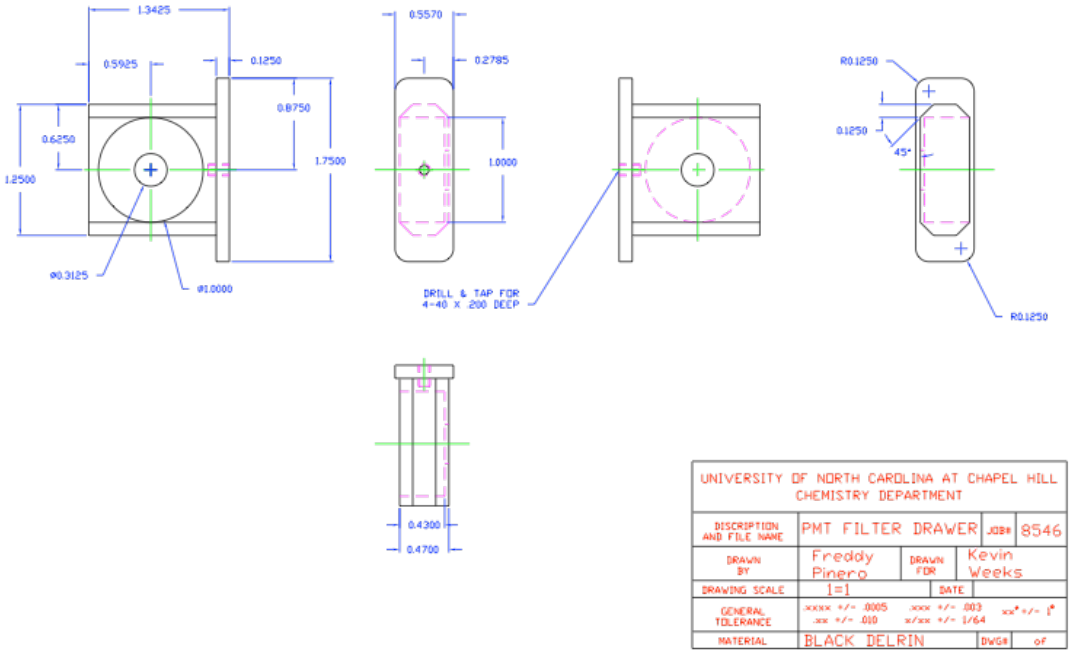

Figure A8: Blueprint for the PMT filter drawer, drawn by Freddy Pinero. One (1) piece should be constructed out of black delrin for one CE-LIF system.

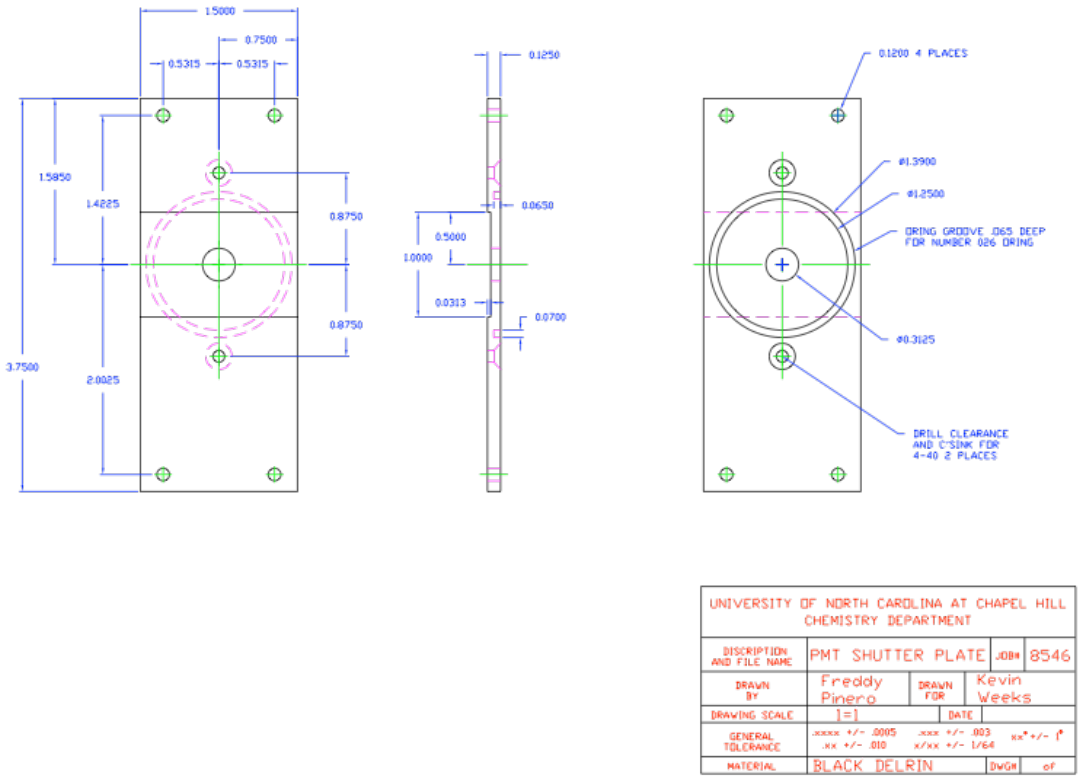

Figure A9: Blueprint for the PMT shutter plate, drawn by Freddy Pinero. One (1) piece should be constructed out of black delrin for one CE-LIF system.

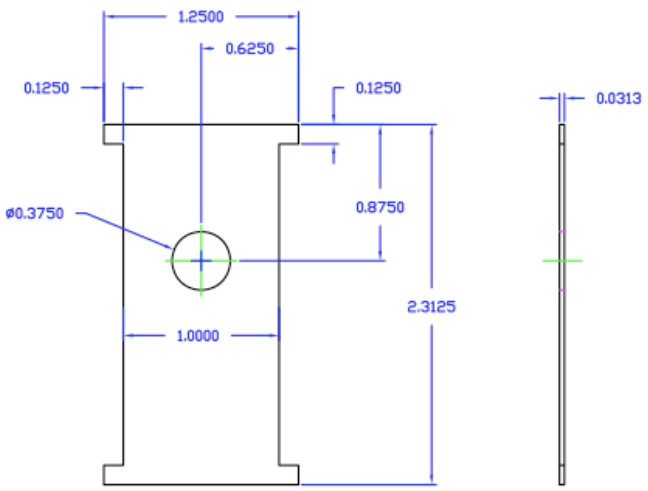

UNIVERSITY OF NORTH CAROLINA AT CHAPEL HILL CHEMISTRY DEPARTMENT			
DISCRIPTION AND FILE NAME	PMT SHUTTER	JOB#	8546
DRAWN BY	Freddy Pinero	DRAWN FOR	Kevin Weeks
DRAWING SCALE	1=1	DATE	
GENERAL TOLERANCE	.xxxx +/- .0005 .xx +/- .010	.xxx +/- .003 x/xx +/- 1/64	xx° +/- 1°
MATERIAL	BLACK DELRIN	DWG#	of

Figure A10: Blueprint for the PMT shutter, drawn by Freddy Pinero. One (1) piece should be constructed out of black delrin for one CE-LIF system.

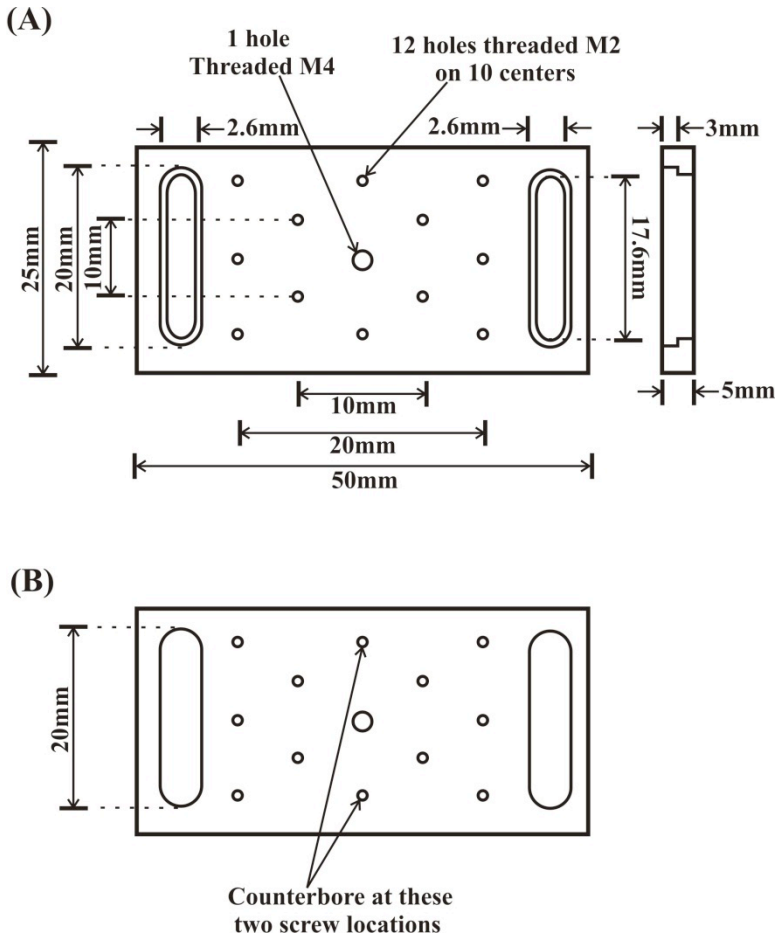

Figure A11: The modifications needed on the two (2) plate adapters (07 RPC521, Melles Griot, Albuquerque, NM), drawn by Angela Proctor (A) A blueprint of the original plate as purchased from Melles Griot and (B) the modifications required. The lip needs to be removed from both slots and the indicated screw holes need to be counterbored so the top of the plate adapter is flush. All other dimensions and features are the same as shown in (A).

APPENDIX B: SINGLE-CELL CE-LIF INSTRUMENT SOFTWARE PROGRAMMING

This appendix contains select portions of the LabVIEW program created to run the single cell CE-LIF system described in Chapter 2 of this dissertation. The program was written by Angela Proctor, with the instrument initialization steps (Figure B2) taken from a program written by Alexandra J. Dickinson, a graduate student in the Allbritton lab. A copy of the program can be found on the desktop of the CE-LIF system and a version is also being used on another single cell system in the Allbritton lab. Detailed programming notes can be found in Notebook #6, Pages 144-153.

Figure B1: The front panel of the LabVIEW program created for the single cell CE-LIF system. The user specifies a CE running voltage, the voltage and duration for an electrokinetic injection and the filename. The program autoincrements a file number before each file, indicates where the data is saved and displays fluorescence and current signals in real-time during a CE run.

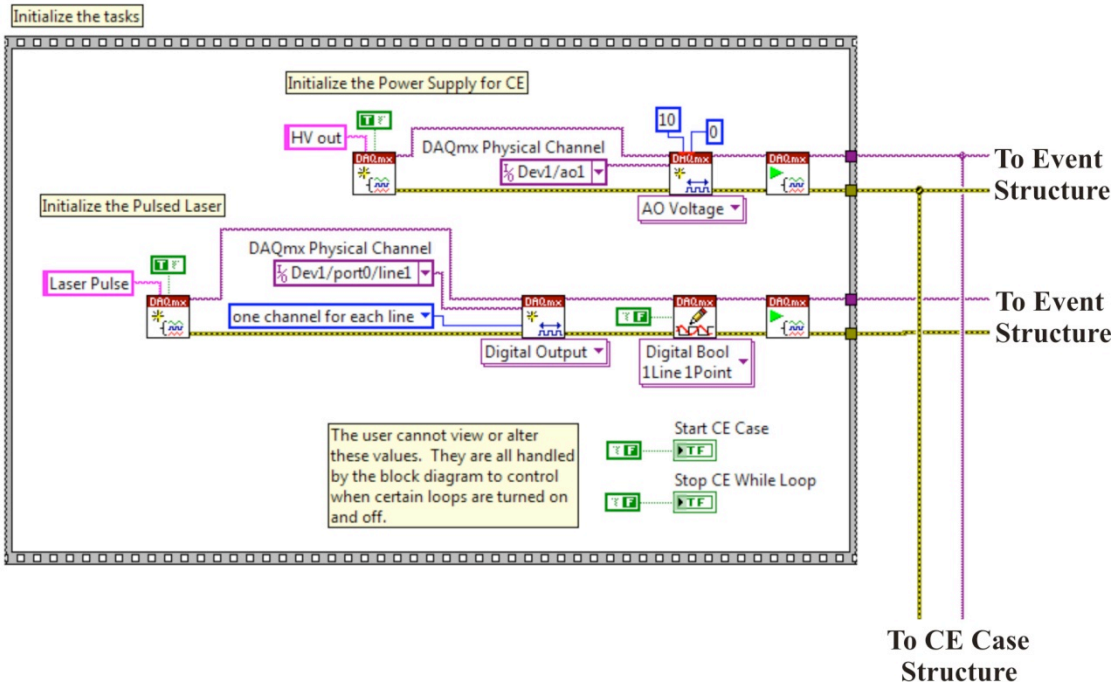

Figure B2: The first portion of the block diagram of the LabVIEW program created for the single cell CE-LIF system. This portion executes once when the program is started and then goes into the event structure (Figure B3) to wait until the user issues a command. The CE case structure (Figures B4-B5) executes only when called by a trigger in the event structure.

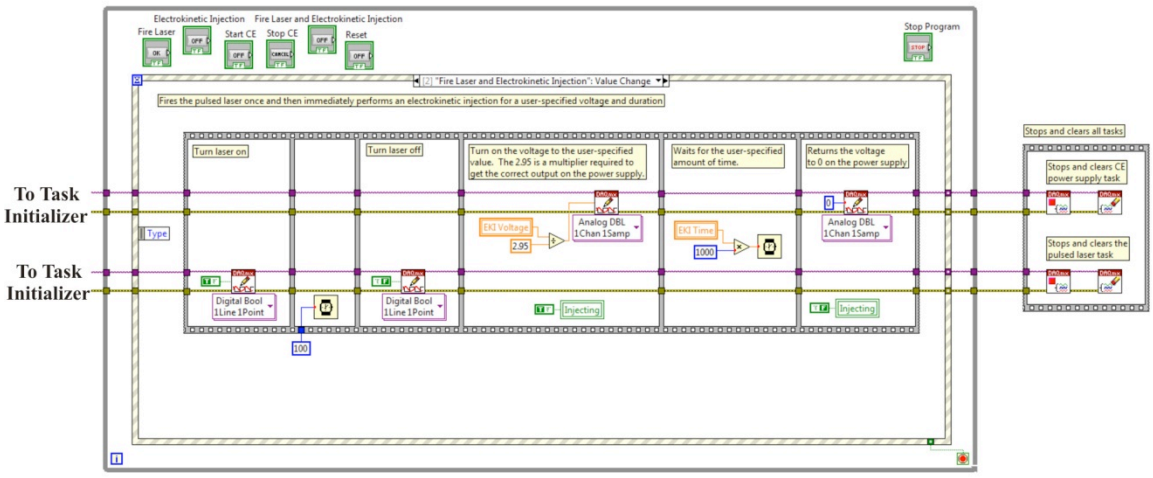

Figure B3: The event structure utilized in the block diagram of the LabVIEW program created for the single cell CE-LIF system. The event structure contains six cases, each of which executes exactly once when called. The code shown in this figure is the code that executes when the user wants to fire the Nd:YAG laser immediately followed by an electrokinetic injection. Note that the program waits at the event structure indefinitely and only exits this while loop when the user presses the "Stop Program" button on the front panel (Figure B1). When this occurs, the instruments are shut down and the program is turned off.

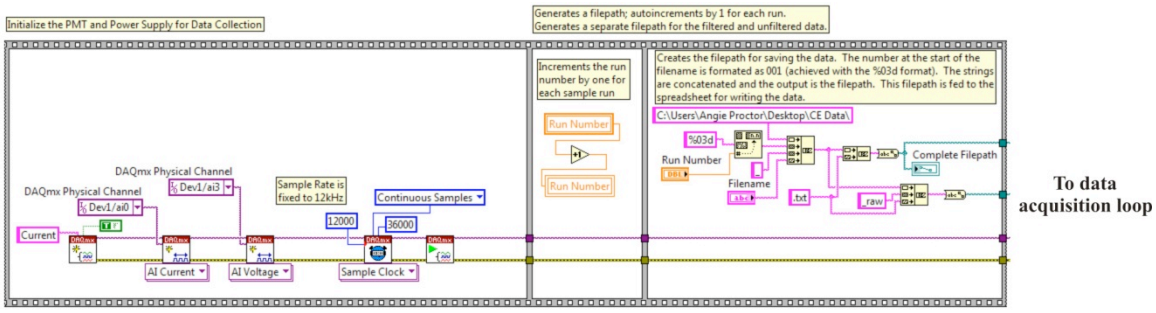

Figure B4: The code contained within the CE case structure which is executed once when the user presses the green "Start CE" button on the front panel (Figure B1). This prepares the DAQ for data collection and generates a filename where the data will be saved.

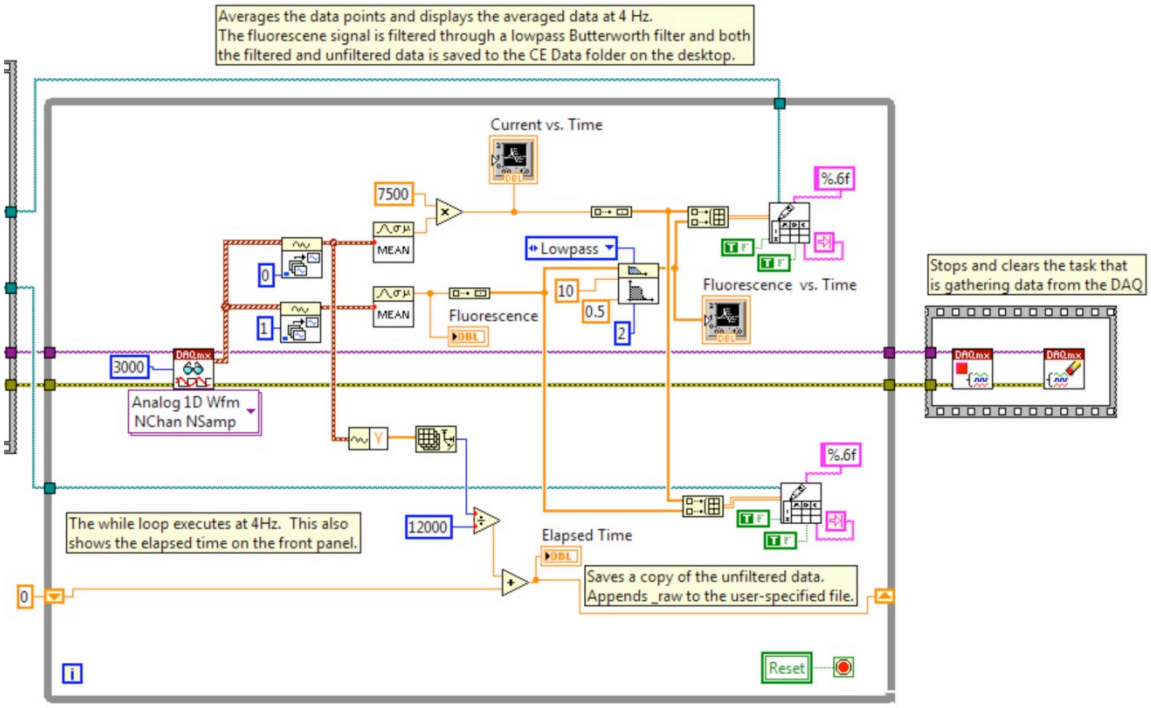

Figure B5: The data acquisition portion of the block diagram. The data is gathered at 12 kHz, averaged at 4 Hz, and is either passed through a lowpass Butterworth filter and written to a text file or directly written to a text file. This code is contained within the CE case structure and executes until the user presses the red "Stop CE" button on the front panel (Figure B1).

APPENDIX C: PEPTIDE SEQUENCES

This appendix contains the complete list of peptides utilized in this project, whether mentioned previously in this dissertation or not. Some of the peptides were called by an alternate name in papers submitted for publication; both names are listed in the tables below to minimize confusion. Peptides were synthesized by four different individuals and are indicated by the initials of the individual. The initials belong to the following individuals: QW is Dr. Qunzhao Wang; AP is Angela Proctor; AK is Ana Kamilaris; and WX is Weichen Xu. Each amino acid is represented by the standard one-letter code for amino acids, except when mentioned otherwise and clarified in Table C1.

Table C1: The non-standard abbreviations used in the peptide sequences.

Abbreviation	Meaning
5FAM	5-carboxyfluorescein
6FAM	6-carboxyfluorescein
Ac	Acetylated
Arg(Me2)	N-ω,ω-dimethyl-L-arginine (symmetrical)
DAla	D-alanine
Dap(Ac)	Acetylated diaminopropionic acid
DArg	D-arginine
DPhe	D-phenylalanine
hArg	Homoarginine
MeAla	(N-Methyl)-alanine
MeArg	(N-Methyl)-arginine
MePh	(N-Methyl)-phenylalanine
Myr	C14 (Myristate)
Nal	β-(2-Naphthyl)-L-alanine
O	Ornithine
PEG	Polyethylene glycol
Phe(F5)	Pentafluorophenylalanine
Sarc	Sarcosine
TetDec	Tetradecane
Tyr(3-NO_2)	(3-Nitro)-tyrosine
βAla	Beta-alanine
βArg	Beta-arginine

Table C2: Peptides intended as Abl kinase substrates (Part 1 of 2).

Peptide Name	Sequence	First Notebook Location	Date Obtained	Prepared By
QW-III-36A	*5FAM*-GEAYAAP-Dap(Ac)-EEE-NH_2	Book 1, Page 143	10.16.2008	QW
QW-III-36B	*5FAM*-GEAYAA-Dap(Ac)-FEEE-NH_2	Book 1, Page 143	10.16.2008	QW
QW-III-36C	*5FAM*-GEAYA-Dap(Ac)-PFEEE-NH_2	Book 1, Page 143	10.16.2008	QW
QW-III-36D	*5FAM*-GEAY-Dap(Ac)-APFEEE-NH_2	Book 1, Page 143	10.16.2008	QW
QW-III-36E	*5FAM*-GE-Dap(Ac)-YAAPFEEE-NH_2	Book 1, Page 143	10.16.2008	QW
QW-III-36F	*5FAM*-G-Dap(Ac)-AYAAPFEEE-NH_2	Book 1, Page 143	10.16.2008	QW
QW-III-36Z	*5FAM*-GEAYAAPFEEE-NH_2	Book 1, Page 143	10.16.2008	QW
QW-III-53A	*5FAM*-GEAYAAPFEEE~COSH	Book 2, Page 32	1.7.2009	QW
QW-III-53B	*5FAM*-GEAYAAPFKKKA~COSH	Book 2, Page 32	1.7.2009	QW
QW-III-67A	*5FAM*-GEAYAAPFEEE-NH_2	Book 2, Page 76	2.4.2009	QW
QW-III-67B	*5FAM*-GGAYAAPFKKKA-NH_2	Book 2, Page 76	2.4.2009	QW
QW-III-90A	*5FAM*-GGAYAAPFKKOA-NH_2	Book 2, Page 131	3.30.2009	QW
QW-III-90B	*5FAM*-GGAYAAPFKOKA-NH_2	Book 2, Page 131	3.30.2009	QW
QW-III-90C	*5FAM*-GGAYAAPFOKKA-NH_2	Book 2, Page 131	3.30.2009	QW
QW-III-90D	*5FAM*-GGAYAAPFKOOA-NH_2	Book 2, Page 131	3.30.2009	QW
QW-III-90E	*5FAM*-GGAYAAPFOKOA-NH_2	Book 2, Page 131	3.30.2009	QW
QW-III-90F	*5FAM*-GGAYAAPFOOKA-NH_2	Book 2, Page 131	3.30.2009	QW
QW-III-90G	*5FAM*-GGAYAAPFOOOA-NH_2	Book 2, Page 131	3.30.2009	QW
QW-IV-21A	*5FAM*-G-COOH	Book 2, Page 196	5.14.2009	QW
QW-IV-21B	*5FAM*-GG-COOH	Book 2, Page 196	5.14.2009	QW
QW-IV-21C	*5FAM*-GGA-COOH	Book 2, Page 196	5.14.2009	QW
QW-IV-21D	*5FAM*-GGAY-COOH	Book 2, Page 196	5.14.2009	QW
QW-IV-21E	*5FAM*-GGAYA-COOH	Book 2, Page 196	5.14.2009	QW
QW-IV-21F	*5FAM*-GGAYAA-COOH	Book 2, Page 196	5.14.2009	QW
QW-IV-36G	*5FAM*-GGAYAAP-COOH	Book 3, Page 78	7.6.2009	QW
QW-IV-36H	*5FAM*-GGAYAAPF-COOH	Book 3, Page 78	7.6.2009	QW
QW-IV-36I	*5FAM*-GGAYAAPFK-COOH	Book 3, Page 78	7.6.2009	QW
QW-IV-36J	*5FAM*-GGAYAAPFKK-COOH	Book 3, Page 78	7.6.2009	QW
QW-IV-36K	*5FAM*-GGAYAAPFKKK-COOH	Book 3, Page 78	7.6.2009	QW
QW-IV-54B	*5FAM*-GGAYAAP-COOH	Book 3, Page 112	7.21.2009	QW
QW-IV-74A	*5FAM*-GGAYAAAFKKKA-NH_2	Book 3, Page 162	8.28.2009	QW
QW-IV-74B	*5FAM*-GGAYAAWFKKKA-NH_2	Book 3, Page 162	8.28.2009	QW
QW-IV-74C	*5FAM*-GGAYAATKKKKA-NH_2	Book 3, Page 162	8.28.2009	QW
QW-IV-74D	*5FAM*-GGAYAA-Sarc-FKKKA-NH_2	Book 3, Page 162	8.28.2009	QW
QW-IV-74E	*5FAM*-GGAYAAFFKKKA-NH_2	Book 3, Page 162	8.28.2009	QW
QW-IV-85B	*5FAM*-GGAYAAP-MePh-KKKA-NH_2	Book 3, Page 191	9.14.2009	QW
QW-V-23A	*5FAM*-GGIYAAP-MePh-KKKA-NH_2	Book 4, Page 34	10.20.2009	QW
QW-V-23B	*5FAM*-GGAYAAP-DPhe-KKKA-NH_2	Book 4, Page 34	10.20.2009	QW
QW-V-23C	*5FAM*-GGAYAAP-Nal-KKKA-NH_2	Book 4, Page 34	10.20.2009	QW
QW-V-23D	*5FAM*-GGAYAAP-MePh-COOH	Book 4, Page 34	10.20.2009	QW
QW-V-23E	*5FAM*-GGAYAAP-Tyr(3-NO_2)-KKKA-NH_2	Book 4, Page 34	10.20.2009	QW

Table C3: Peptides intended as Abl kinase substrates (Part 2 of 2).

Peptide Name	Alt Name*	Sequence	First Notebook Location	Date Obtained	Prepared By
QW-V-41A		*5FAM*-GGAYAAP-MePh-K-COOH	Book 5, Page 3	02.10.2010	QW
QW-V-41B		*5FAM*-GGAYAAP-MePh-KK-COOH	Book 5, Page 3	02.10.2010	QW
QW-V-41C		*5FAM*-GGAYAAP-MePh-KKK-COOH	Book 5, Page 3	02.10.2010	QW
QW-V-48A		*5FAM*-GGIYAAPFEEE-NH_2	Book 5, Page 3	02.17.2010	QW
QW-V-48B		*5FAM*-GGIYAAP-MePh-KKKA-NH_2	Book 5, Page 3	02.17.2010	QW
QW-V-49A		*5FAM*-GGI-COOH	Book 5, Page 40	03.03.2010	QW
QW-V-49B		*5FAM*-GGIY-COOH	Book 5, Page 40	03.03.2010	QW
QW-V-49C		*5FAM*-GGIYA-COOH	Book 5, Page 40	03.03.2010	QW
QW-V-49D		*5FAM*-GGIYAA-COOH	Book 5, Page 40	03.03.2010	QW
QW-V-49E		*5FAM*-GGIYAAP-COOH	Book 5, Page 40	03.03.2010	QW
QW-V-49F		*5FAM*-GGIYAAP-MePh-COOH	Book 5, Page 40	03.03.2010	QW
QW-V-49G		*5FAM*-GGIYAAP-MePh-K-COOH	Book 5, Page 40	03.03.2010	QW
QW-V-49H		*5FAM*-GGIYAAP-MePh-KK-COOH	Book 5, Page 40	03.03.2010	QW
QW-V-49I		*5FAM*-GGIYAAP-MePh-KKK-COOH	Book 5, Page 40	03.03.2010	QW
QW-V-48Br		*5FAM*-GGIYAAP-MePh-KKKA-NH_2	Book 8, Page 34	07.13.2011	QW
QW-VII-76A	VII-A	*5FAM*-GGIY-MeAla-AP-MePh-KKKA-NH_2	Book 9, Page 50	01.10.2012	QW
QW-VII-76B	VIII-A	*5FAM*-GGIYA-MeAla-P-MePh-KKKA-NH_2	Book 9, Page 50	01.10.2012	QW
QW-VII-76C	VII-B	*5FAM*-GGIY-Sarc-AP-MePh-KKKA-NH_2	Book 9, Page 50	01.10.2012	QW
QW-VII-76D	VIII-B	*5FAM*-GGIYA-Sarc-P-MePh-KKKA-NH_2	Book 9, Page 50	01.10.2012	QW
QW-VII-76E	VII-C	*5FAM*-GGIY-DAla-AP-MePh-KKKA-NH_2	Book 9, Page 50	01.10.2012	QW
QW-VII-76F	VIII-C	*5FAM*-GGIYA-DAla-P-MePh-KKKA-NH_2	Book 9, Page 50	01.10.2012	QW
QW-VIII-18A		*5FAM*-GGIYA-Sarc-COOH	Book 9, Page 111	02.02.2012	QW
QW-VIII-18B		*5FAM*-GGIYA-Sarc-P-COOH	Book 9, Page 111	02.02.2012	QW
QW-VIII-18C		*5FAM*-GGIYA-Sarc-P-MePh-COOH	Book 9, Page 111	02.02.2012	QW
QW-VIII-18D		*5FAM*-GGIYA-Sarc-P-MePh-K-COOH	Book 9, Page 111	02.02.2012	QW
QW-VIII-18E		*5FAM*-GGIYA-Sarc-P-MePh-KK-COOH	Book 9, Page 111	02.02.2012	QW
QW-VIII-18F		*5FAM*-GGIYA-Sarc-P-MePh-KKK-COOH	Book 9, Page 111	02.02.2012	QW
QW-VIII-20A	IX-A	*5FAM*-GGIYA-Sarc-P-MePh-KKK-NH_2	Book 9, Page 142	02.20.2012	QW

*These are the names used for these peptides when they are mentioned in this dissertation in Chapter 6.

Table C4: Peptides intended as PKB substrates (Part 1 of 2).

Peptide Name	Alt Name*	Sequence	First Notebook Location	Date Obtained	Prepared By
API	I	*6FAM*-GRPRAATFAEG-NH_2	Book 1, Page 73	8.20.2008	AP
API-1A		*6FAM*-GRP-hArg-Dap(Ac)-ATFAEG-NH_2	Book 2, Page 168	5.4.2009	AP
API-1B		*6FAM*-GRP-hArg-Dap(Ac)-Dap(Ac)-TFAEG-NH_2	Book 2, Page 168	5.4.2009	AP
API-1C		*6FAM*-GRP-hArg-Dap(Ac)-ATF-Dap(Ac)-EG-NH_2	Book 2, Page 168	5.4.2009	AP
API-1D		*6FAM*-GRP-hArg-Dap(Ac)-Dap(Ac)-TF-Dap(Ac)-EG-NH_2	Book 2, Page 168	5.4.2009	AP
API-1E		*6FAM*-GR-Sarc-hArg-Dap(Ac)-ATFAEG-NH_2	Book 2, Page 168	5.4.2009	AP
API-2A		*6FAM*-GRPR-Dap(Ac)-ATFAEG-NH_2	Book 3, Page 132	8.3.2009	AP
API-3A		*6FAM*-GRPR-Dap(Ac)-ATFAEG-NH_2	Book 3, Page 159	8.24.2009	AP
API-4A		*6FAM*-GRPR-Dap(Ac)-ATFAEG-NH_2	Book 4, Page 18	10.4.2009	AP
API-5A		*6FAM*-GRP-hArg-AATFAEG-NH_2	Book 4, Page 51	10.28.2009	AP
API-6A		*6FAM*-G-COOH	Book 4, Page 142	01.07.2010	AK
API-6B		*6FAM*-GR-COOH	Book 4, Page 142	01.07.2010	AK
API-6C		*6FAM*-GRP-COOH	Book 4, Page 142	01.07.2010	AK
API-6D		*6FAM*-GRPR-COOH	Book 4, Page 142	01.07.2010	AK
API-6E		*6FAM*-GRPRA-COOH	Book 4, Page 142	01.07.2010	AK
API-6F		*6FAM*-GRPRAA-COOH	Book 4, Page 142	01.07.2010	AK
API-6G		*6FAM*-GRPRAAT-COOH	Book 4, Page 142	01.07.2010	AK
API-6H		*6FAM*-GRPRAATF-COOH	Book 4, Page 142	01.07.2010	AK
API-6I		*6FAM*-GRPRAATFA-COOH	Book 4, Page 142	01.07.2010	AK
API-6J		*6FAM*-GRPRAATFAE-COOH	Book 4, Page 142	01.07.2010	AK
API-7K		*6FAM*-GRPRAATFAE-COOH	Book 5, Page 3	02.17.2010	AK
AP-I-8A		*6FAM*-K(Myr)GRPRAATFAEG-NH_2	Book 5, Page 45	03.12.2010	AP
AP-I-9A		*6FAM*-KKKK(Myr)GRPRAATFAEG-NH_2	Book 5, Page 59	03.19.2010	AP
AP-II-1A		*6FAM*-RKRDRLGTLGI-NH_2	Book 4, Page 170	01.19.2010	AK
AP-III-1A		*6FAM*-ARKRARAYSFGHHA-NH_2	Book 4, Page 170	01.19.2010	AK
AP-III-2A		*6FAM*-ARKRARAYSFGHHA-NH_2	Book 5, Page 176	05.13.2010	AP
QW-V-84A		*5FAM*-NH_2RKRDRLGTLGI-NH_2	Book 6, Page 34	07.26.2010	QW
QW-V-84B		*5FAM*-NH_2K(Myr)-RKRDRLGTLGI-NH_2	Book 6, Page 34	07.26.2010	QW
QW-V-84C		*5FAM*-NH_2K(Myr)-*PEG*-RKRDRLGTLGI-NH_2	Book 6, Page 34	07.26.2010	QW
QW-V-84D		*5FAM*-NH_2C(SS-TetDec)-RKRDRLGTLGI-NH_2	Book 6, Page 34	07.26.2010	QW
QW-V-84E		*5FAM*-NH_2C(SS-TetDec)-*PEG*-RKRDRLGTLGI-NH_2	Book 6, Page 34	07.26.2010	QW
QW-VI-31A1	II-A	*6FAM*-GRPR-βAla-ATFAEG-NH_2	Book 6, Page 159	12.03.2010	QW
QW-VI-31A2	II-B	*6FAM*-GRPR-MeAla-ATFAEG-NH_2	Book 6, Page 159	12.03.2010	QW
QW-VI-31A3	II-C	*6FAM*-GRPR-DAla- ATFAEG-NH_2	Book 6, Page 159	12.03.2010	QW
QW-VI-31B1	III-A	*6FAM*-GRP-βArg-AATFAEG-NH_2	Book 6, Page 159	12.03.2010	QW
QW-VI-31B2	III-B	*6FAM*-GRP-MeArg-AATFAEG-NH_2	Book 6, Page 159	12.03.2010	QW
QW-VI-31B3	III-C	*6FAM*-GRP-Arg(Me2)-AATFAEG-NH_2	Book 6, Page 159	12.03.2010	QW
QW-VI-31B4	III-D	*6FAM*-GRP-DArg-AATFAEG-NH_2	Book 6, Page 159	12.03.2010	QW
QW-VI-51C		*6FAM*-Lys(Myr)-PEG-GRPRAATFAEG-NH_2	Book 6, Page 197	01.17.2011	QW
QW-VI-51D		*6FAM*-GRPRAATFAEG-PEG-Lys(Myr)-NH_2	Book 6, Page 197	01.17.2011	QW

*These are the names used for these peptides when they are mentioned in this dissertation as well as in the article(s) submitted for publication based on Chapters 4 and 5.

Table C5: Peptides intended as PKB substrates (Part 2 of 2).

Peptide Name	Alt Name*	Sequence	First Notebook Location	Date Obtained	Prepared By
QW-VI-57A		*6FAM*-GRP-MeArg-COOH	Book 7, Page 23	02.09.2011	QW
QW-VI-57B		*6FAM*-GRP-MeArg-A-COOH	Book 7, Page 23	02.09.2011	QW
QW-VI-57C		*6FAM*-GRP-MeArg-AA-COOH	Book 7, Page 23	02.09.2011	QW
QW-VI-57D		*6FAM*-GRP-MeArg-AAT-COOH	Book 7, Page 23	02.09.2011	QW
QW-VI-57E		*6FAM*-GRP-MeArg-AATF-COOH	Book 7, Page 23	02.09.2011	QW
QW-VI-57F		*6FAM*-GRP-MeArg-AATFA-COOH	Book 7, Page 23	02.09.2011	QW
QW-VI-57G		*6FAM*-GRP-MeArg-AATFAE-COOH	Book 7, Page 23	02.09.2011	QW
QW-VI-69A	IV-A	*6FAM*-GRP-MeArg-A-βAla-TFAEG-NH_2	Book 7, Page 67	03.23.2011	QW
QW-VI-69B	IV-B	*6FAM*-GRP-MeArg-A-DAla-TFAEG-NH_2	Book 7, Page 67	03.23.2011	QW
QW-VI-69E	IV-C	*6FAM*-GRP-MeArg-A-E-TFAEG-NH_2	Book 7, Page 67	03.23.2011	QW
QW-VI-69F	IV-D	*6FAM*-GRP-MeArg-A-F-TFAEG-NH_2	Book 7, Page 67	03.23.2011	QW
QW-VI-70C		*6FAM*-EFRERLETFG-NH_2	Book 7, Page 67	03.23.2011	QW
QW-VI-70D		*6FAM*-EFRERLESFG-NH_2	Book 7, Page 67	03.23.2011	QW
API-Orn		*5FAM*-O(Ac)-GRPRAATFAEG-O(Ac)-NH_2	Book 7, Page 72	03.31.2011	WX
QW-VII-10A		*6FAM*-GRP-MeArg-A-F-TFAE-NH_2	Book 7, Page 158	06.01.2011	QW
QW-VII-10B	IV-E	*6FAM*-GRP-MeArg-A-MePhe-TFAEG-NH_2	Book 7, Page 158	06.01.2011	QW
QW-VII-11C		*6FAM*-GRP-MeArg-A-F-TFA-COOH	Book 7, Page 158	06.01.2011	QW
QW-VII-11D		*6FAM*-GRP-MeArg-A-F-TF-COOH	Book 7, Page 158	06.01.2011	QW
QW-VII-11E		*6FAM*-GRP-MeArg-A-F-T-COOH	Book 7, Page 158	06.01.2011	QW
QW-VII-11F		*6FAM*-GRP-MeArg-A-F-COOH	Book 7, Page 158	06.01.2011	QW
QW-VII-23A		*6FAM*-GRP-MeArg-AFTFAE-COOH	Book 8, Page 34	07.13.2011	QW
QW-VII-23B		*6FAM*-GRP-MeArg-AFTAE-NH_2	Book 8, Page 34	07.13.2011	QW
QW-VII-23C		*6FAM*-ESRERTGTAG-NH_2	Book 8, Page 34	07.13.2011	QW
QW-VII-23D		*6FAM*-SMRERNETAM-NH_2	Book 8, Page 34	07.13.2011	QW
QW-VII-23E		*6FAM*-SMRERNETLQ-NH_2	Book 8, Page 34	07.13.2011	QW
QW-VII-23F		*6FAM*-EQRERNGTAQ-NH_2	Book 8, Page 34	07.13.2011	QW
QW-VII-32A	V-A	*6FAM*-GRP-MeArg-AFT-Phe(F5)-AEG-NH_2	Book 8, Page 70	08.08.2011	QW
QW-VII-32B	V-B	*6FAM*-GRP-MeArg-AFTF-DAla-EG-NH_2	Book 8, Page 70	08.08.2011	QW
QW-VII-32C	V-C	*6FAM*-GRP-MeArg-AFTF-Sarc-EG-NH_2	Book 8, Page 70	08.08.2011	QW
QW-VII-48A		*6FAM*-GRP-MeArg-AFTF-DAla-COOH	Book 8, Page 133	09.07.2011	QW
QW-VII-48B		*6FAM*-GRP-MeArg-AFTF-DAla-E-COOH	Book 8, Page 133	09.07.2011	QW
QW-VII-48C		*6FAM*-GRP-MeArg-AFTF-Sarc-COOH	Book 8, Page 133	09.07.2011	QW
QW-VII-48D		*6FAM*-GRP-MeArg-AFTF-Sarc-E-COOH	Book 8, Page 133	09.07.2011	QW
QW-VII-48E	VI-A	*6FAM*-GRP-MeArg-AFTF-Sarc-NH_2	Book 8, Page 133	09.07.2011	QW
QW-VII-48F	VI-B	*6FAM*-GRP-MeArg-AFTF-MeAla-NH_2	Book 8, Page 133	09.07.2011	QW

*These are the names used for these peptides when they are mentioned in this dissertation as well as in the article(s) submitted for publication based on Chapters 4 and 5.

References

1 A. Proctor, Q. Wang, D. S. Lawrence and N. L. Allbritton. "Metabolism of peptide reporters in cell lysates and single cells". *Analyst,* 2012, *137*, 3028-3038.

2 G. M. Funk, C. E. Hunt, D. E. Epps and P. K. Brown. "Use of a rapid and highly sensitive fluorescamine-based procedure for the assay of plasma lipoprotiens". *J. Lipid Res.,* 1986, *27*, 792-795.

3 T. T. Tran, H. Treutlein and A. W. Burgess. "Designing amino acid residues with single-conformations". *Protein Eng. Des. Sel.,* 2006, *19*, 401-408.

4 R. Tugyi, K. Uray, D. Iván, E. Fellinger, A. Perkins and F. Hudecz. "Partial D-amino acid substitution: Improved enzymatic stability and preserved Ab recognition of a MUC2 epitope peptide". *PNAS,* 2005, *102*, 413-418.

5 L. Gentilucci, R. De Marco and L. Cerisoli. "Chemical Modifications Designed to Improve Peptide Stability: Incorporation of Non-Natural Amino Acids, Pseudo-Peptide Bonds, and Cyclization". *Curr. Pharm. Design,* 2010, *16*, 3185-3203.